Schenley Park to C.R. Park: Exploring Air Pollution, Energy, and Climate in Pittsburgh and New Delhi

Submitted in partial fulfillment of the requirements for

the degree of

Doctor of Philosophy

in

Engineering and Public Policy

Shayak Sengupta

B.S., Civil & Environmental Engineering, Rice University
M.S., Engineering & Public Policy, Carnegie Mellon University

Carnegie Mellon University
Pittsburgh, PA

August, 2021

Acknowledgements

It's crazy to think how the past five years have flown by as I worked towards completing my Ph.D. I write this as a once-in-a-lifetime pandemic ravages the world. As I reflect, the pandemic has just been one of the several events that have punctuated my time in graduate school.

My journey towards developing as an independent scholar began with my time as an undergraduate at Rice University in Houston. I want to thank Dan Cohan my undergraduate research advisor and mentor who took a chance and hired me when a newly minted college sophomore asked if he could do research with his faculty advisor from freshman year. Dan's advice and guidance not only helped me cultivate my interest in air quality, climate and energy, but really hone exactly the kind of science I wanted to do: public policy relevant research grounded in quantitative, engineering rigor.

After finishing college with Dan's advice, and a bit of luck, I was awarded a Fulbright-Nehru scholarship to study energy and environment in India. The opportunity to go live and work in the country of my parents' birth as an American was both personally and professionally rewarding. The first several months were quite tough: from navigating daily life to understanding the complexities associated with India's energy and environmental challenges. During this time Josh Apte and Rahul Tongia were especially helpful. I want to thank Josh for being open to discussing challenges of doing research in India for the first time and providing advice on how to make the best of my time there. Likewise, I want to thank Rahul, who first answered the cold email of a motivated Fulbright scholar who did not know exactly what he was doing at the time. Since then, working with Josh as part of the network of collaborators at Carnegie Mellon has been fruitful. Rahul has continued to provide me constant support and advice, especially during my second stint in India when he hosted me at the Centre for Social and Economic Progress (formerly Brookings India). Rahul constantly challenges me to think beyond the obvious to the policy-relevance of my work.

Wrapping up Fulbright, I knew I wanted to continue working in the energy and environment space in India when I started graduate school. This brings me to my next

round of gratitude and thanks: Peter Adams and Inês Azevedo, my thesis committee co-chairs. Peter thank you for your flexibility, your openness to devoting time to help me through tough problems, and your emphasis on work/life balance. Likewise, Inês, you have provided unwavering support, flexibility, and I like that you constantly challenged me to think how my work fits in with the work of other scholars. Both of you are really the co-advisor pair every graduate student could dream of: intellectually invested, respectful of everyone's contributions, and striving to make research truly interdisciplinary combining your individual insights. You provided me the space to grow as a scholar, and even let me dash off to India and take intensive Hindi lessons while I was doing part of the research for this thesis!

Other professional thanks from me go to Allen Robinson, Albert Presto, Subu, and the rest of the CAPS team. There is always something new in aerosol science that I learn from you all. To the EPP admin staff: Debbie Kuntz, Debbie Scappatura, Patti Steranchak, Vicki Finney, Adam Loucks, and Kim Martin, thanks for always being there to make sure the trains run on time.

Personally, I'd like to thank the great friends, new and old, I've had in Pittsburgh: Prithvi Acharya, Nyla Khan, Stephanie Jennings, Carlos Hernandez, and Priyank Lathwal. They've kept me sane, laughing every day, and understanding what it was like to go through graduate school. Likewise thank you to my friends in Delhi: Aradhika Menokee, Ganesh Sivamani, Pratuysha Joshi, Maitriyi Menon, Sharang Shah, Saket Rajprohat, and Mike Benevenia. While the pandemic cut our time short, I know I've made memories in Delhi that I won't forget.

And lastly, thank you to my family: my sister Madhurita Sengupta, my brother-in-law Aaron Pierce, and my parents Mila and Sujit Sengupta. They've likewise provided me unwavering personal support during my Ph.D. The story of our family is a familiar one to many immigrant American families: leaving one's loved ones behind, coming to a strange new land in search of opportunities. I consider myself extremely fortunate for the sacrifices of previous generations that have been made on my behalf. Moreover, I find myself uniquely lucky to live in the time that we do, to able to help forge stronger ties with my work between the country of my birth, the United States, and the country of my parents' birth, India. Generations of Americans before me did not have this

opportunity I've had to make this country stronger and the world a better place, even if by a little bit. My story and my family's story are only possible in a country like the United States.

-Shayak Sengupta, May 2021

Doctoral Committee

Peter J. Adams (co-chair)
Thomas Lord Professor, Engineering and Public Policy, Carnegie Mellon University

Inês M.L. Azevedo (co-chair)
Associate Professor, Energy Resources Engineering, Stanford University

Rahul Tongia
Senior Fellow, Centre for Social and Economic Progress, New Delhi, India

Joshua S. Apte
Assistant Professor, Civil and Environmental Engineering, University of California, Berkeley

Allen L. Robinson
Distinguished University Professor, Mechanical Engineering, Carnegie Mellon University

This work is supported in part by a Carnegie Mellon University Presidential Fellowship in the College of Engineering and an American Meteorological Society Graduate Fellowship. This material is based upon work supported by the National Science Foundation Graduate Research Fellowship Program Grant No. DGE-1252522 and Grant No. DGE-1745016. Any opinions, findings, and conclusions or recommendations expressed in this material are those of the authors and do not necessarily reflect the views of the National Science Foundation. This publication was developed as part of the Center for Air, Climate, and Energy Solutions (CACES), which was supported under Assistance Agreement No. R835873 awarded by the U.S. Environmental Protection Agency. It has not been formally reviewed by EPA. The views expressed in this document are solely those of authors and do not necessarily reflect those of the Agency. EPA does not endorse any products or commercial services mentioned in this publication. This work was supported by the Center for Climate and Energy Decision

Making (SES-1463492), through a cooperative agreement between the National Science Foundation and Carnegie Mellon University. Any opinions, findings, and conclusions or recommendations expressed in this material are those of the authors and do not necessarily reflect the views of the National Science Foundation. Funding for this research was supported by the National Security Education Program's Boren Fellowship.

Abstract

High resolution, 1-km chemical transport modeling of ultrafine particulate matter over Pittsburgh

The lack of widespread ambient monitoring, their high spatial variability, and correlations with multiple co-emitted pollutants make long-term health impacts studies of ultrafine particles (UFPs), particles with diameters less than 100 nm (0.1 μm), difficult. Consequently, chemical transport models (CTMs) can help evaluate scientific understanding of UFPs and quantify human exposure.

In this work, we deploy a state-of-the-science CTM, PM-CAMx-UF at high resolution (1 km) over Pittsburgh in winter and summer to simulate UFP concentrations and explore the model's ability to resolve intraurban spatial and temporal variability in UFP concentrations. We evaluate model predictions against an extensive intraurban network of ~30 long-term UFP and ~50 other pollutant observations sites. Simulations quantify the sources of UFPs within an urban area, and we assess the value-added from increasing model resolution to 1 km. Model inputs include particle number emissions derived from source-specific particle size distributions. Moreover, for traffic sources, we derive spatially resolved emissions from a traffic model for Pittsburgh.

Baseline simulations for February and July 2017 indicate predicted particle number concentrations (PNC) in Pittsburgh vary by more than a factor of two at 1-km resolution, with similar levels of intraurban and urban-rural variability in both winter and summer. Comparisons to a network of 27 long-term (~1 month) winter observation sites in Pittsburgh show model spatial agreement with MFB = -42% and MFE = 42% with better agreement at local road or urban background sites than sites impacted by local sources or topography. Temporally, the model matches winter diurnal variability in PNC at 12 sites with r^2 values of monthly average observations and predictions exceeding 0.28 spread across all site types. While on-road traffic contributes to intraurban UFP concentrations in both seasons (~16% winter, ~4% summer), other primary sources such as off-road mobile sources and stationary combustion rival traffic's contribution.

Primary emissions largely govern the spatial variability in predicted UFP concentration at the 1-km scale. Modeling at 1-km resolution resolves similar human exposure as 4-km resolution, but more than 12-km and 36-km resolutions. The 1st-99th

percentiles of population were estimated to be exposed to 3,200-9,600 cm^{-3} at 1 km resolution and 3,200-9,700 cm^{-3} at 4 km resolution, but 3,300-8,100 cm^{-3} at 12 km resolution, and 3,400-5,500 cm^{-3} at 36 km resolution. However, coarser resolutions fail to capture intraurban variability at observation sites like 1-km resolution. Lastly, while higher resolution and 1 km CTM can resolve more variability in human exposure than coarser model resolutions, we see evidence of unresolved sub-1-km variability. Consequently, future efforts to resolve exposure for chronic UFP health impacts quantifications must account for this variability.

National policy interventions in current Indian power generation produce disparate, state-level carbon and sulfur emission impacts

Current, coal-heavy electricity generation contributes to India's greenhouse gas emissions and premature mortality from air pollution. Electricity generation and capacity vary by state in India. This implies heterogenous emissions impacts from policy interventions not captured by national, aggregate analyses. We develop a reduced-order dispatch model of Indian power generation to assess state-level, spatial CO_2 and SO_2 emission impacts of potential policy interventions. We present the first state-level consumption-based average annual CO_2 emission factors for today's Indian grid. Among states with 96% national electricity demand, emission factors vary between 521-879 kg CO_2/MWh, heterogeneity not reflected in a nationwide average of 711 kg/MWh. Carbon taxes up to $100/metric ton CO_2, without new investments in low-carbon infrastructure, cause CO_2 reductions of 3% in the current Indian grid due to a low-carbon capacity unable to fully displace coal. A carbon tax nonetheless spatially shifts SO_2 emissions, which increase at 47 plants and decrease at 95 plants. Simulating nationwide implementation of SO_2 control to meet upcoming regulations shows 88% of plants see changes in plant capacity factor less than 5%, informing SO_2 control investment decisions. Regional sulfur control may shift emissions away from target areas because of state-wise dispatch in India and plants with sulfur control penalized in the dispatch order. Lastly, regional dispatch, not state-wise, results in 3% and 2% increases in CO_2 and SO_2 emissions, respectively. Predicted emissions increase at 97 plants and decrease at 32 plants because regional dispatch incentivizes generation from cheaper, less efficient plants closer to coal mining areas with lower transportation

costs.

$PM_{2.5}$ mortality burden of power generation in India under current and future policies

There is spatial variability between electricity generation fuel mixes, electricity demand, and associated air pollution deaths among states in India, the world's third largest electricity generator. However, no study has quantified this variability in associated air pollution deaths within the context of power sector operations accounting for the exchange of electricity between states. Here we pair a reduced-form power dispatch model of Indian power generation with a reduced-form air quality model and associated risk-exposure relationships to quantify the mortality from $PM_{2.5}$ attributable to power generation in India. In addition to quantifying $PM_{2.5}$ mortality associated with electricity consumption and production in each Indian state, we also evaluate the impact on power sector operations and associated mortalities from a range of policy scenarios including greater sulfur emissions controls, carbon taxes ($10-$100/ton CO_2) and market integration.

We estimate ~71,000 deaths per year associated with $PM_{2.5}$ attributable to electricity generation in India. Furthermore, we find distinct differences in the net burden of electricity $PM_{2.5}$ deaths among states in India: coal-mining states in eastern India face a disproportionate higher burden of deaths than high renewable energy states in western and southern India which face a disproportionate lower burden. Enforcing sulfur control emission regulations at Indian power plants results in ~42,000 fewer annual deaths, spread across states through the country. Progressively increasing carbon taxes result in 9,400-14,000 fewer annual $PM_{2.5}$ deaths due to reductions in ambient $PM_{2.5}$ concentrations. Under carbon taxes, generation shifts and emissions reduce at more plants than at which they increase. Consequently, reductions in risk from ambient $PM_{2.5}$ concentration reductions are greater than increases in risk from ambient $PM_{2.5}$ concentration increases. Finally, coordinating power dispatch across states by dispatching plants at regional and national levels results in 1,800 and 6,900 fewer annual deaths, respectively, due to concentrations reducing at areas furthest away from coal mining areas, where plants with the most expensive electricity sit.

Current and future estimated marginal emission factors for Indian power generation

Emission factors from Indian power generation remain poorly characterized, despite known spatial and temporal variability. Lack of publicly available emissions and generation data at sufficient detail make quantification for the world's third largest power grid difficult. Here, we use reduced-form and full-form power scheduling and dispatch models to quantify current (2017-2018) and future (2030-2031) marginal CO_2, SO_2, NO_X, and $PM_{2.5}$ emission factors, which represent the Indian power system's emissions changes due to small demand changes. For 2017-2018, we find spatial variability in system-wide, all-source marginal CO_2 emission factors ranging three orders of magnitude across states in India. Moreover, there is limited seasonal variability or variability between times-of day in marginal emissions with coal generation likely to meet changes in demand most of the time (> 50%) in most (> 50%) states. For 2030-2031 greater renewable generation consistent with Government of India targets decreases median marginal CO_2 emission factors by approximately a factor of two, but emission factors still span three orders of magnitude across all states. Moreover, under these 2030-2031 assumptions there is greater seasonal (factor of ~2) and time-of-day (factor of ~4)S variability in marginal emissions. Greater shares of average zero-emission generation, the focus of policy efforts, are associated with lower marginal emission factors, indicating that increasing average renewable generation is more likely to fulfill new power demand in India. These estimates provide policymakers, analysts, and researchers representative emission factors useful to evaluate interventions that cause changes in power demand between seasons and times-of-day such as electric vehicles, increased air conditioning, and energy efficiency.

Table of Contents

Acknowledgements iii

Abstract vii

Table of Contents xi

List of Tables xiii

List of Figures xiii

1 Introduction 1

2 High resolution, 1-km chemical transport modeling of ultrafine particulate matter over Pittsburgh 4

2.1 Introduction 4

2.2 Methods 7

2.2.1 Model description 7

2.2.2 Simulation period, nested modeling domain, and model settings 8

2.2.3 Inputs 9

2.2.3.1 Meteorology 9

2.2.3.2 Emissions and particle size distributions 9

2.2.4 Sensitivity simulations 12

2.2.5 Observation Network 12

2.3 Results 14

2.3.1 Spatial and temporal comparisons to observation sites 15

2.3.2 Source apportionment 20

2.3.3 Evaluation of on-road traffic emissions 21

2.3.4 Modeling resolution and human exposure 24

2.4 Discussion and Conclusions 25

3 National policy interventions in current Indian power generation produce disparate,

state-level carbon and sulfur emission impacts 31
3.1 Introduction 31
3.2 Methods 35
3.3 Results 39
3.4 Discussion and Conclusions 47
4 $PM_{2.5}$ mortality burden of power generation in India under current and future policies 54
4.1 Introduction 54
4.2 Methods 55
4.3 Results 59
4.4 Discussion and Conclusions 69
5 Current and future estimated marginal emission factors for Indian power generation 74
5.1 Introduction 74
5.2 Methods 77
5.3 Results 80
5.4 Discussion and Conclusions 90
6 Conclusion 95
7 References 96
8 Appendix A 110
9 Appendix B 122
10 Appendix C 137
11 Appendix D 140

List of Tables

Table 1 38
Table 2 110
Table 3 127
Table 4 128
Table 5 139
Table 6 144
Table 7 149
Table 8 151
Table 9 153
Table 10 154

List of Figures

Figure 1 8
Figure 2 10
Figure 3 14
Figure 4 16
Figure 5 17
Figure 6 18
Figure 7 20
Figure 8 22
Figure 9 23
Figure 10 24
Figure 11 40
Figure 12 42
Figure 13 43
Figure 14 45
Figure 15 45
Figure 16 46
Figure 17 61

Figure 18 63
Figure 19 65
Figure 20 66
Figure 21 67
Figure 22 80
Figure 23 82
Figure 24 84
Figure 25 85
Figure 26 87
Figure 27 88
Figure 28 89
Figure 29 111
Figure 30 111
Figure 31 112
Figure 32 112
Figure 33 113
Figure 34 114
Figure 35 115
Figure 36 116
Figure 37 117
Figure 38 118
Figure 39 118
Figure 40 119
Figure 41 119
Figure 42 120
Figure 43 120
Figure 44 121
Figure 45 121
Figure 46 128
Figure 47 129
Figure 48 129

Figure 49 130
Figure 50 130
Figure 51 131
Figure 52 131
Figure 53 132
Figure 54 132
Figure 55 133
Figure 56 133
Figure 57 134
Figure 58 134
Figure 59 135
Figure 60 135
Figure 61 137
Figure 62 137
Figure 63 138
Figure 64 138
Figure 65 144
Figure 66 145
Figure 67 145
Figure 68 146
Figure 69 146
Figure 70 147
Figure 71 147
Figure 72 148
Figure 73 148
Figure 74 155
Figure 75 155
Figure 76 156
Figure 77 156
Figure 78 157
Figure 79 157

Figure 80 158
Figure 81 158
Figure 82 159

1 Introduction

Air pollution is largely a regional physical phenomenon, but a global societal problem. In 2017, nearly three million deaths worldwide (approximately 5% of all deaths) can be associated with ambient air pollution from solid or liquid particles with diameters less than 2.5 μm ($PM_{2.5}$) suspended in the atmosphere. While most of those deaths occur in India (~980,000 deaths) and China (~1.42 million deaths), they also occur in developed countries such as the United States (~47,800 deaths) (Abbafati et al., 2020; Institute, 2020; Pandey et al., 2021). The particles responsible for these health impacts largely come directly from the burning of fossil fuels or from reactions in the atmosphere of precursor gases emitted from fossil fuel use. Consequently, the burden of $PM_{2.5}$ and any public policy efforts to reduce this burden must consider both energy use and the physical and chemical processes governing $PM_{2.5}$ concentrations in the atmosphere.

Developed countries such as the United States have made strides in reducing $PM_{2.5}$ exposure (Cohen et al., 2017; Wang et al., 2017; Zhang et al., 2018). However, $PM_{2.5}$ is not homogenous but rather a complex mixture of particles composed of different chemical species and across size ranges as small as 1 nm. While the health impacts of $PM_{2.5}$ are well documented (Dockery et al., 1993; Hoek et al., 2013; Laden et al., 2006; Lipsett et al., 2011; Pope et al., 2002), the health effects of ultrafine particles (UFP), particles with diameters less than 100 nm (0.1 μm) are not as well understood (Baldauf et al., 2016; HEI Review Panel, 2013). Consequently, the first chapter of this thesis explores UFPs and the variability in their concentrations within cities using Pittsburgh as a case study. The aim of this section is to understand intraurban variability in concentrations to ultimately inform health effects studies of UFPs.

As opposed to the United States where $PM_{2.5}$ exposure has decreased and the focus of public policy-relevant scientific study has shifted to further exploring smaller classes of particles such as UFPs, $PM_{2.5}$ exposure has steadily increased in India since 1990 with average population-weighted concentrations to be approximately seven times that of the United States (Cohen et al., 2017; Pandey et al., 2021). Furthermore, if current trends under a “do-nothing” scenario continue, $PM_{2.5}$ exposure is estimated to increase 40% by 2050 (GBD MAPS Working Group, 2018).

$PM_{2.5}$ and associated greenhouse gas emissions have increased because India is a rapidly developing country with growing energy needs. It is the world's third largest economy (World Bank, 2018a), but per capita GDP remains a fraction of other large economies (World Bank, 2018b). As of 2019, while the Government of India has made considerable progress in delivering electricity to 26 million previously unelectrified households, there is potential to improve quality of electricity supply in the future (Ministry of Power, 2020c). Electricity demand from 2015 could roughly double or triple by 2030 depending on economic growth rates and demand sector composition (Ali, 2018; Spencer and Awasthy, 2019). As the Indian power grid grows, it could exacerbate both local and global environmental challenges: greenhouse gas (GHG) emissions and local and regional air pollution.

Indian power generation remains a significant source of GHG emissions and air pollution emissions which lead to premature deaths from $PM_{2.5}$ exposure. Coal-fired power stations form 74% of electricity generation and 55% of installed capacity (Central Electricity Authority, 2019b, 2020a; Centre for Social and Economic Progress, 2019). In addition to contributing to close to 40% of India's GHG emissions (Mohan et al., 2019), Indian coal power stations release uncontrolled $PM_{2.5}$ precursors. They are responsible for about 50% of sulfur dioxide (SO_2) and 40% of nitrogen oxides (NO_X) emissions, which lead to an estimated 7-21% of premature deaths (Apte and Pant, 2019; Conibear et al., 2018; GBD MAPS Working Group, 2018; Guo et al., 2018; Lelieveld et al., 2015).

However, coal power alone will not meet increased future demand; the Government of India plans to increase renewable generation so that it will constitute 40% of all capacity by 2030 (Government of India, 2015). Other policy efforts by the Government of India include stricter limits on SO_2 and NO_X emissions from power stations in 2015 (Ministry of Environment Forest and Climate Change, 2015), and planned market reforms to coordinate and economically dispatch power on a limited basis at the national level (Power System Operation Corporation Limited, 2020).

Future scenarios point to the power sector to remain an significant source of GHG emissions and air pollution in India (International Energy Agency, 2021; Peng et al., 2020; Venkataraman et al., 2018). Expected increases in electricity demand from economic growth may drive emissions increase due to expansions of coal generation

capacity even at lower rates than the past (Guttikunda and Jawahar, 2014, 2018; Sahu et al., 2017; Sehgal and Tongia, 2016). However, decarbonization efforts to reduce coal generation in favor of renewables may blunt those emissions increases. Consequently, even if emissions from the Indian power sector do not increase, they may plateau to remain a sizable portion of the country's total emissions.

Given the power sector's critical role in India's current and future energy system, climate and air pollution control policies for the Indian power sector remain an active area of research. In the remaining chapters of this thesis, we quantify at higher spatial and temporal resolution air pollution and climate impacts of Indian power generation under current and future policies. These efforts hope to address present shortcomings on the lack of detailed work that explores how these impacts vary by Indian state. This ultimately helps to inform policy by providing additional granularity at the subnational level.

2 High resolution, 1-km chemical transport modeling of ultrafine particulate matter over Pittsburgh

2.1 Introduction

While the health impacts of $PM_{2.5}$ are well documented (Dockery et al., 1993; Hoek et al., 2013; Laden et al., 2006; Lipsett et al., 2011; Pope et al., 2002), the health effects of ultrafine particles (UFP), generally defined as particles with diameters less than 100 nm (0.1 μm) are not as well understood (Baldauf et al., 2016; HEI Review Panel, 2013). Toxicological evidence suggests UFPs translocate from the lungs to other organs. UFPs also show cardiovascular and respiratory effects like those associated with $PM_{2.5.}$ (Kreyling et al. 2006; HEI Review Panel 2013). The lack of widespread ambient monitoring, their high spatial variability, and correlations between multiple co-emitted pollutants make long-term health impacts studies of UFPs difficult (Baldauf et al., 2016). Health impacts of UFPs may come with traffic pollution exposure, given elevated UFP concentrations near roadways (Karner et al. 2010). Several studies have linked traffic pollution exposure to health (Hoek et al., 2002; Hoffmann et al., 2007; Lanki et al., 2006; Laumbach et al., 2010; McCreanor et al., 2007; Peters et al., 2004; Weichenthal et al., 2011; Zuurbier et al., 2011). The modest increase in $PM_{2.5}$ concentrations near roadways explain only a portion of observed impacts (Hoek et al. 2002; Karner et al. 2010). UFPs along with other factors such as noise and demographic characteristics could also explain health effects observed with traffic pollution exposure. Co-emitted traffic pollutants also complicate a definitive association with UFPs. Coupled with this is the unresolved question of whether UFPs have any independent or additional health impacts beyond those associated with $PM_{2.5}$, especially if there is spatial correlation between $PM_{2.5}$ and UFP concentrations. Weichenthal et al. (2017) assigned UFP exposure to 1.1 million adults in Toronto using an empirical land-use regression (LUR) model to yield inconclusive results on the associations between UFPs and respiratory illness separate from those of other pollutants such as NO_2 or $PM_{2.5}$. Likewise, Downward et al. (2018) use a LUR model to assign UFP exposure to a much smaller cohort of approximately 34,000 adults in the Netherlands to find positive, statistically significant associations between UFPs and cardiovascular disease, heart attacks and heart failure, but insignificant positive

associations with stroke. These positive associations hold when accounting for both UFPs and $PM_{2.5}$. To date, studies have yet to reach sufficient conclusions on the long-term health impacts of UFPs (Ohlwein et al., 2019).

Given the spatial variability in observed UFP number concentrations, lack of widespread measurements, and the need to quantify any UFP health impacts separate from those of $PM_{2.5}$, chemical transport models (CTM) can help evaluate scientific understanding of UFPs and quantify human exposure. Previous CTM analyses at the regional scale to assess UFP scientific understanding have generally focused on source apportionment or the influence of microphysical processes, and not human exposure. Posner and Pandis (2015) conducted zero-out source apportionment CTM simulations for July 2001 over the eastern United States at 36 km resolution to find nucleation and gasoline and diesel combustion contribute significantly to domain-averaged UFP number concentrations. Jung et al. (2010) simulates a similar time period and domain at 36 km to find CTMs must accurately capture nucleation to reproduce observations of UFPs in July 2001 in Pittsburgh. Subsequent work by Fountoukis et al. (2012) and Patoulias et al. (2018) using CTMs to simulate UFPs over Europe at 36 km resolution confirm the importance of simulating nucleation as well as incorporating condensation of organic vapors into models.

To extend CTM capabilities to quantify UFP human exposure, several studies simulate UFP concentrations at higher spatial resolution and perform associated health analyses. Ostro et al. (2015) use a CTM to generate spatial and temporally resolved UFP exposure fields at the 4-km scale. Using predicted UFP mass concentrations along with multi-year demographic data, Ostro and colleagues estimate health impacts from both $PM_{2.5}$ and UFPs by chemical composition and source. Their results indicate a positive association between UFP mass and ischemic heart disease mortality, but few distinct differences between estimated effects of $PM_{2.5}$ and UFP mass concentrations. While the model used by Ostro et al. (2015) lacks nucleation, Ostro et al. (2015) illustrate that model-generated concentration exposure fields can reproduce estimated health impacts from previous methods which use observed $PM_{2.5}$ and UFP measurements.

Continued efforts to use CTMs to simulate UFPs at finer spatial resolutions

include Venecek et al. (2019) and Yu et al. (2019). Venecek et al. (2019) simulate UFPs at 4-km resolution in selected U.S. cities during peak ozone events in 2010 with a CTM capable of online source apportionment. They find as expected, on-road traffic to contribute significantly (~23%) to simulated, population-weighted UFP concentrations, but also the influence of natural gas combustion which contributes to 33% of population-weighted $PM_{0.1}$ concentrations in the United States. However, Venecek et al. (2019) do not simulate longer periods to quantify chronic UFP exposure and use measurements of ozone and $PM_{2.5}$, but not $PM_{0.1,}$ to evaluate their model. Yu et al. (2019) use the same CTM to simulate regions in California at 4-km resolution for selected months in 2012, 2015, and 2016. They find that nucleation followed by natural gas combustion are the largest contributors to particle number concentrations, and low spatial correlation (r^2 = 0.35) between particle number concentration and $PM_{2.5}$ mass concentration, which suggests future epidemiological studies may disentangle the health impacts of $PM_{2.5}$ and UFPs.

Previous analyses (Fountoukis et al., 2012; Jung et al., 2010; Ostro et al., 2015; Patoulias et al., 2018; Posner and Pandis, 2015; Venecek et al., 2019; Yu et al., 2019) to simulate UFPs with CTMs lack finer spatial resolution, leaving room for further development in deploying CTMs to evaluate UFP human exposure and source apportionment at intraurban resolutions. First, there is an outstanding question of the appropriate resolution to model UFPs. Several studies focus on coarse, 36-km resolution (Fountoukis et al., 2012; Jung et al., 2010; Patoulias et al., 2018; Posner and Pandis, 2015) while others go to the finer 4-km resolution (Ostro et al., 2015; Venecek et al., 2019; Yu et al., 2019), and 250-m resolution (limited simulations over Oakland, CA, by Yu et al., 2019). However, no analysis has systematically evaluated whether higher (e.g. 1 km) resolutions are required to capture intraurban spatial variability or compared exposure estimates from different resolutions to each other. Second, there has been limited evaluation of model predictions because of lack of data. Coupled with evaluation of spatial scales is the need to have an adequate number of intraurban observations sites to validate any spatial variability predicted by a CTM. Yu et al. (2019) evaluated the model with data from a network of ten sites to analyze interurban, not intraurban, differences in UFP concentrations. Lastly, while Venecek et al. (2019) and

Yu et al., (2019) conduct source apportionment and Yu et al., (2019) present limited intraurban source apportionment in Oakland, CA, no analysis has investigated UFP source apportionment at a finer, intraurban scale and whether previous conclusions about the contribution of natural gas to UFP number concentration extends to finer, sub 4-km resolution and to other locations.

In this work we apply a state-of-the-science CTM, PM-CAMx-UF at high, 1-km resolution over Pittsburgh in winter and summer to simulate UFP concentrations and investigate the model's ability to resolve intraurban spatial and temporal variability in UFP concentrations. We evaluate model predictions against an extensive intraurban network of long-term observations sites. Simulations quantify the sources of UFPs driving concentrations within an urban area, and we assess the value-added from increasing model resolution to 1 km.

2.2 Methods

2.2.1 Model description

Particulate Matter CAMx Ultrafine (PM-CAMx-UF) is a state-of-the-science CTM that explicitly simulates mass and number concentration of particles across diameters, D_p, from 0.8 nm to 10 μm. Like its predecessor models CAMx (Environ, 2003) and PM-CAMx (Gaydos et al., 2007; Karydis et al., 2007), PM-CAMx-UF simulates advection, deposition, diffusion, and dispersion of particles in the atmosphere. In addition, it incorporates the Dynamic Model for Aerosol Nucleation (DMAN) model (Jung et al., 2010) which uses the Two-Moment Aerosol Sectional (TOMAS) algorithm of Adams and Seinfeld (2002), itself an application to aerosols of a numerical method first developed for cloud microphysics (Tzivion et al., 1987, 1989). The model discretizes particle size into 41 size bins defined by dry mass per particle, with the first 21 bins for particles with D_p < ~100 nm. Dry mass doubles between bins with the lower boundary of the first bing at 3.75×10^{-25} kg per particle. Microphysical processes in the model include coagulation, condensation, and nucleation. Model treatment of coagulation follows that of Adams and Seinfeld (2002). Condensation treatment incorporates the updated model DMANx developed by Patoulias et al. (2015), which simulates condensation of sulfuric acid, ammonia, and organic vapors according to the Volatility Basis Set (VBS)

framework of Donahue et al., (2006). This version of PM-CAMx-UF incorporating DAMNx, however, treats only the condensation, and not the evaporation, of semi-volatile organic vapors. The model uses the ternary H_2SO_4-NH_3-H_2O nucleation parametrization of Napari et al. (2002) with a tuning factor of 10^{-6} to the predicted rate, similar to previous studies that have used this parametrization (Fountoukis et al., 2013; Posner and Pandis, 2015; Westervelt et al., 2014; Yu et al., 2019). Particle species simulated in the model include sulfate, nitrate, ammonium, sodium, chloride, elemental carbon (EC), crustal material, primary organic aerosol (POA) and secondary organic aerosol (SOA) separated into four volatility bins according to the VBS. Multiple studies have applied PM-CAMx-UF at coarser resolutions to areas over North America and Europe (Jung et al. 2010; Posner and Pandis 2015; Patoulias et al. 2015; Fountoukis et al. 2012) with Patoulias et al. (2018) applying the most updated version over Europe.

2.2.2 Simulation period, nested modeling domain, and model settings

We simulate two periods to capture differences between winter and summer: February 1-28, 2017, and July 1-31, 2017, with the first three days of each simulation omitted as model spin-up. Figure 1 shows the modeling domain at 1 km resolution, which we focus on for most of this analysis.

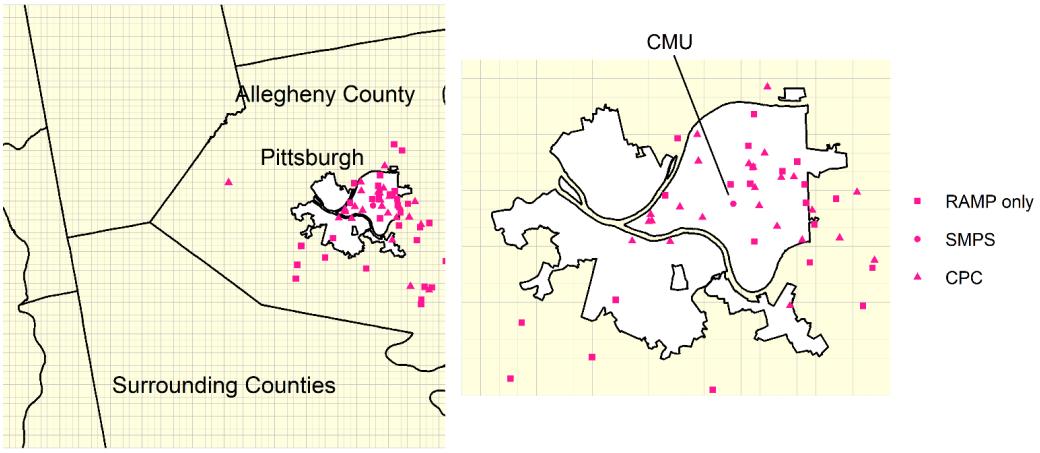

Figure 1
1-km modeling domain with Pittsburgh, Allegheny County and surrounding counties are shown with locations of distributed observation sites available for model evaluation. Every site had CO, NO_2, and $PM_{2.5}$ RAMP observations, with additional sites having CPC and SMPS observations for particle number concentration and size distribution, respectively.

This domain consists of 72 × 72 1-km grid cells covering the entire city of Pittsburgh and

the majority of Allegheny County. Vertically, there are 14 levels extending to approximately 6.7 km on average in February and 7.1 km in July. Surrounding counties include those in southwestern Pennsylvania and neighboring Ohio and West Virginia also gridded at 1-km resolution. We conduct simulations in a one-way nested fashion with coarser resolutions feeding boundary conditions into finer resolutions. These nested domains are the continental United States at 36 km resolution and two successive domains in southwestern Pennsylvania at 12 km and 4 km (Figure 29-31). The default treatment of nucleation described above greatly over-predicted the frequency of nucleation events in the February simulation. Therefore, for February only, we turn off nucleation in the model resulting in better agreement with observations as nucleation events were not observed in Pittsburgh during this time (Saha et al., 2018).

2.2.3 Inputs

2.2.3.1 Meteorology

The Weather Research and Forecasting (WRF) model version 3.6.1 provided meteorological inputs of temperature, wind velocity, water vapor, and vertical diffusivity. The WRF modeling system uses ERA-Interim global climate re-analysis data along with terrestrial data from United States Geological Survey (USGS) and simulates at 12-km resolution. We direct readers to Gilliam and Pleim (2010) for further details.

2.2.3.2 Emissions and particle size distributions

The U.S. Environmental Protection Agency (EPA) National Emissions Inventory (NEI) 2011 projected to 2017 provided emissions for the simulations. We direct the reader to technical support documents for discussion of EPA's process to estimate emissions resolved by sector, chemical species, space and time (U.S. Environmental Protection Agency, 2016). For this study we make two modifications to the default emissions of NEI: (1) we specify particle size distributions to emissions inputs and (2) modify spatial surrogates for on-road traffic emissions and cooking emissions based on more specific location data sources. The default NEI 2011 emissions resolve particle mass emissions into two size categories: fine ($D_p \leq 2.5$ μm) and coarse ($D_p > 2.5$ μm). To distribute these two modes into the 41 size bins required by the model and to convert particle mass emissions to particle number emissions, we apply sector-specific

number size distributions detailed in Table 2 to mass totals from NEI 2011 (Asmi et al., 2011; Ban-weiss et al., 2010; Dennekamp et al., 2001; Elleman and Covert, 2010; Hennigan et al., 2012; Kaltsonoudis et al., 2017). In these conversions, we assume a particle density of 1.8 g cm^{-3} and the size distribution for each sector applies uniformly to all particle species emitted by that sector. Applying an assumed size distribution to the mass emissions estimates from NEI has the effect of converting mass emissions estimates to number emissions estimates. Figure 2 shows the results of this mass-to-number conversion for the entire domain, resolved by simulation month and sector.

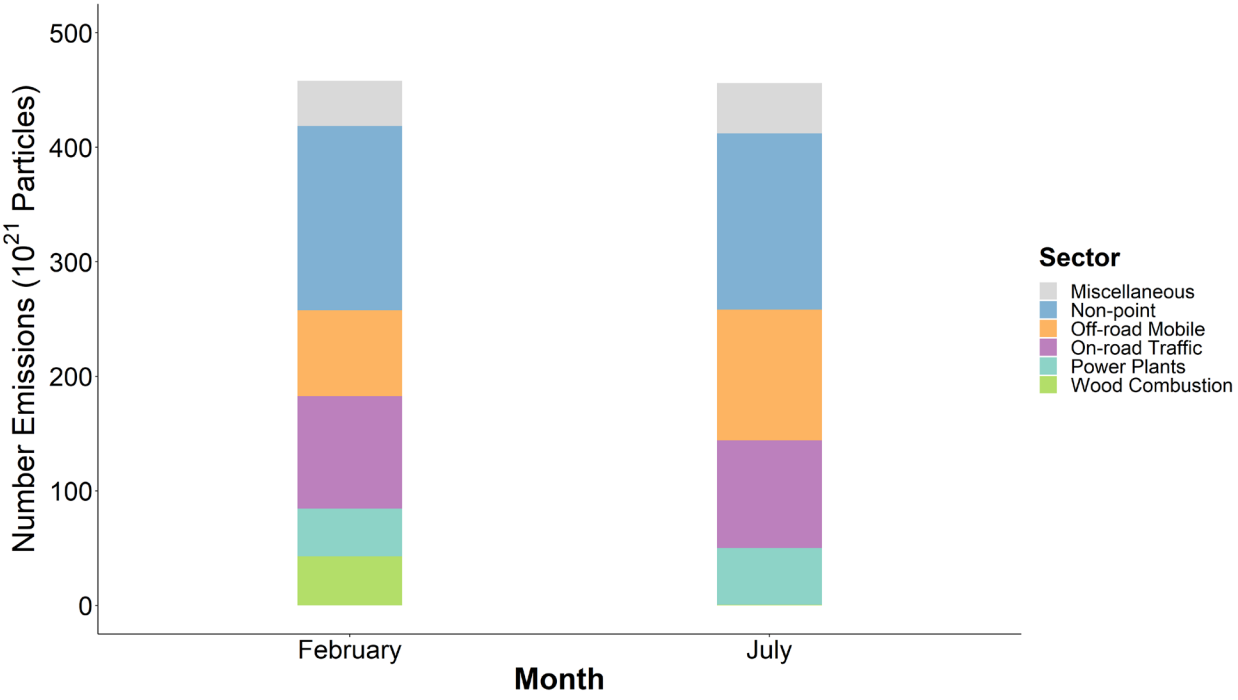

Figure 2
Domain-wide (1-km domain), monthly number emissions totals by sector serve as inputs into the model calculated by applying sector-specific number size distributions to NEI emissions totals. Miscellaneous sources include dust, rail, cooking, marine vessel, industrial and oil and gas sources.

Overall, for both February and July, number emissions are very nearly equal; however, the sectoral distribution differs somewhat. In February, on-road road traffic, off-road mobile, non-point (a combination of stationary fuel combustion, industrial wood combustion, and waste incineration, with natural gas combustion forming 2% of mass emissions but 88% of number emissions in this sector), power plants, and residential wood combustion dominate total number emissions. Miscellaneous sectors include dust, agricultural fire, cooking, oil and gas, marine vessels, rail, and industrial point

sources contribute less than 10% of total number emissions. Meanwhile in July, on-road traffic and non-point sources remain about the same, with increases in off-road mobile sources and power plants offsetting decreased residential wood combustion.

In addition to redistributing mass emissions to number emissions with size distributions, we allocate emissions according to the model grid using spatial surrogates from NEI 2011. However, for cooking emissions, which contribute less than 1% of total number emissions, we allocate emissions according to restaurant density obtained from Google Maps (Google, 2019). For traffic emissions, we modify the EPA-default, temporally static spatial surrogate for on-road traffic by combining it with a traffic model specifically simulated for Pittsburgh (Ma and Qian, 2015). This traffic model simulates traffic counts and speed by hour-of-day (1-24) for weekdays using observations from Pennsylvania Department of Transportation sites throughout Pittsburgh. The model simulates all major and minor roads inside the city, but it consolidates smaller roads with similar speed limits (e.g. neighborhood roads) for computational tractability and accuracy. Consequently, the model captures traffic patterns within the city at higher resolution than patterns outside the city.

To construct the mixed surrogate, we first hold constant the fraction of emissions allocated by the EPA default surrogate only over the grid cells covering Pittsburgh. The EPA default surrogate allocates 19% of on-road traffic emissions to grid cells over the city, while the traffic model allocates 47% of emissions over these same grid cells. Then we reallocate this total emission fraction representing city emissions (19%) using the relative fractions estimated by the traffic model to make the final mixed traffic spatial surrogate.

We also run two additional PM-CAMx-UF simulations with the traffic model and EPA-default spatial surrogates for on-road traffic emissions. Figure 32 shows the change in number emissions for on-road traffic for these surrogates relative to the mixed traffic surrogate. Relative to the mixed spatial surrogate, the traffic model pushes total traffic emissions in the model domain from outside the city into the city. Meanwhile, because EPA-default surrogate is based on road density, it weights emissions over grid cells with larger roads (e.g. highways or arterial roads) than smaller local roads which may see comparable traffic density according to the mixed spatial surrogate.

2.2.4 Sensitivity simulations

To assess the impact of different sources on UFP concentration, we undertake several sector-based zero-out sensitivity simulations for non-point, off-road mobile, on-road traffic, power plants, and residential wood combustion sources (Figure 2). To preserve coagulation sinks and therefore to obtain sector-specific contributions that generally sum to the base case, we apply the procedure used by Posner and Pandis (2015) to zero out the majority of number emissions for a sector while still maintaining the majority of its mass emissions, and therefore, its contribution to the coagulation sink (Pierce and Adams, 2007; Westervelt et al., 2013, 2014). For each sector, we zero-out the emissions in TOMAS/DMAN bins corresponding to approximately 90% of number emissions. Table 2 details the exact percent of number zeroed and mass preserved for each sector. We zero-out emissions for on-road traffic, off-road mobile, non-point, power plants, and residential wood combustion sectors. Furthermore, we conduct an additional sensitivity simulation where we zero-out the natural gas combustion portions of the non-point and power plant sectors. Likewise to quantify the impacts of nucleation in July 2017 (we assume no nucleation in February 2017), we conduct on sensitivity simulation with nucleation turned during this time period.

2.2.5 Observation Network

To evaluate model predictions, we compare simulations to measured data from a network of intraurban sites in Pittsburgh (Figure 1). Up to 81 sites provide a rich dataset for model evaluation and improves upon previous work to simulate UFPs with CTMs, which limit observation sites to handful of sites at interurban scale (Fountoukis et al., 2012; Jung et al., 2010; Patoulias et al., 2018; Posner and Pandis, 2015; Yu et al., 2019) We direct readers to references for detailed descriptions, but briefly summarized available measurements here:

Condensation particle counters (CPC): 30 sites, measuring particle number concentration with $D_p \geq 5$ nm (N_5) in winter 2017 and 2018 (Saha et al., 2019). We use these measurements to evaluate model predictions of N_5. Due to better

data quality and to maximize the number of sites to spatially evaluate model predictions, we compare February 2017 model predictions to seasonal winter averages for sites sampled in January-March 2017, December 2017, and January-March 2018. Each site was sampled for approximately three weeks each during those winter months using 12 water-based CPCs (Aerosol Devices Inc.; MAGIC 200P model) rotated through each site. These instruments did not perform well during summer months, so we do not have summer data. Saha et al. (2019) conclude the three-week sampling period captures seasonal averages of N_5 at each site.

Real-time, Affordable Multi-Pollutant (RAMP) monitors: up to 50 sites measuring a suite of species (CO, $PM_{2.5}$, NO_2) in February and July 2017 and 2018 (Malings et al., 2019; Rose Eilenberg et al., 2020; Tanzer et al., 2019; Zimmerman et al., 2018). For model evaluation, we average observations at each site for each month across both years to maximize number of sites available for comparison. Of available species we focus our analysis on NO_2 as tracer for the spatial distribution of intraurban on-road traffic emissions.

Scanning mobility particle sizer: one site at Carnegie Mellon University (CMU) measuring particle size distribution for particles $D_p > 10$ nm (Saha et al., 2018)

2.3 Results

Figure 3 illustrates predicted, time-averaged N_5 concentrations ($D_p \geq 5$ nm) for February and July 2017.

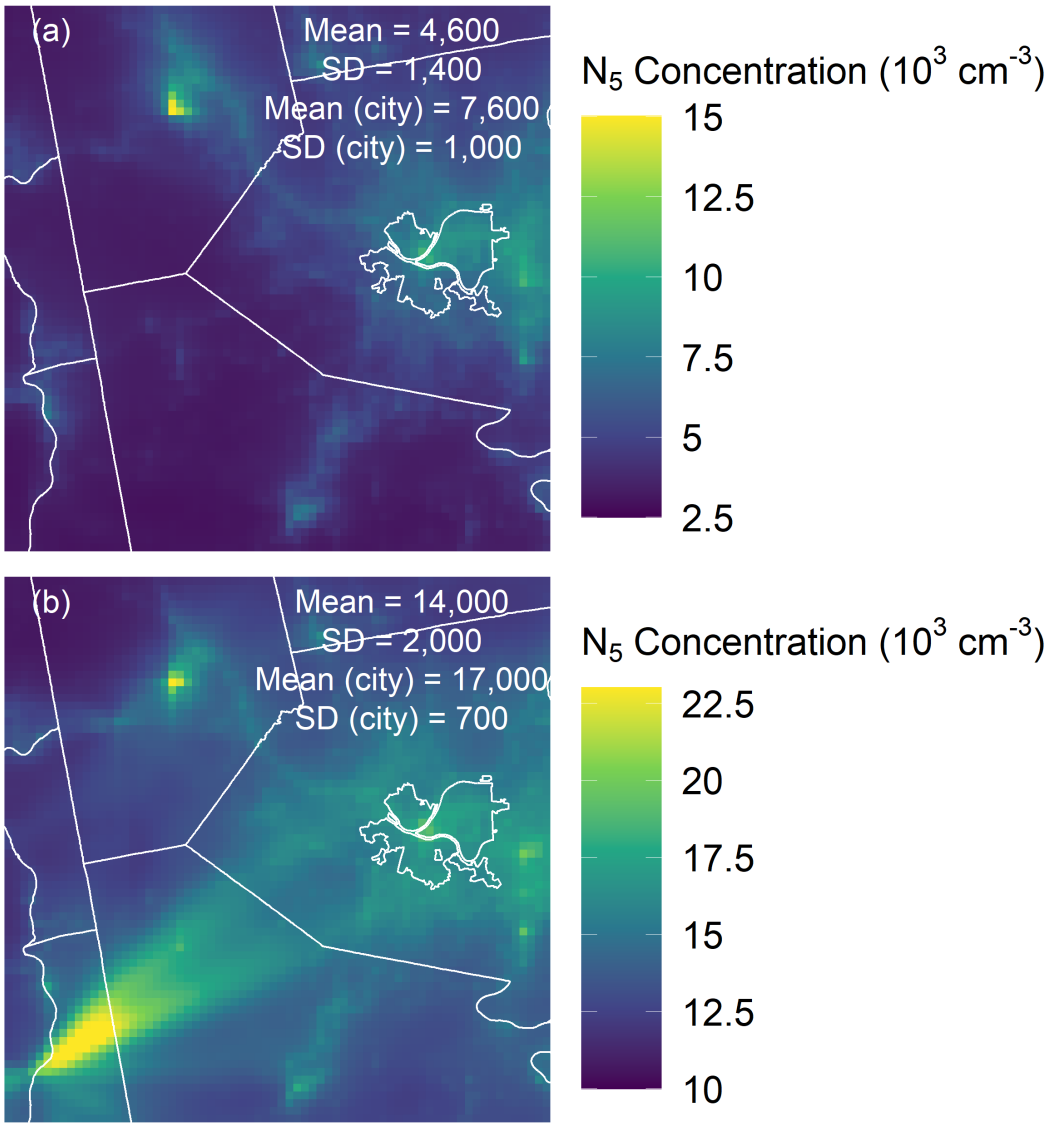

Figure 3
Simulation period-averaged predicted concentrations of N_5 concentration in (a) February 2017 and (b) July 2017 show similar levels of spatial variability, but higher concentrations in July 2017 due to higher regional background (boundary conditions) and regional nucleation. Standard deviations (SD) describe spatial variability.

We use ground-level number concentration to describe UFP burden because UFPs dominate number concentration (~90%) while a small fraction of total $PM_{2.5}$ mass concentration (~10%). In February 2017 (Figure 3a), predicted concentrations average

4,600 cm^{-3} across the 1-km modeling domain, with particle number concentrations increasing 65% to 7,600 cm^{-3} within the city of Pittsburgh, outlined in the middle of the domain. The level of spatial variability however is higher within the city than across the modelling domain, with standard deviations of 1,400 cm^{-3} and 1,000 cm^{-3}, respectively. Concentrations within the city vary with the highest concentrations in the downtown area of the city, a heavily-trafficked area. Elevated concentrations occur within the city, within Allegheny County generally, and along highways extending from the city to surrounding counties. Spatial patterns largely follow the patterns of primary emissions inputs. In the northwest corner of the domain, the model predicts elevated concentrations in a plume emitted by a metal smelter. In July 2017 (Figure 3b), concentrations on average within the city are more than twice as high. In these predictions, an additional power plant plume in the southwest corner of the domain occurs where SO_2 emissions coupled with nucleation increase N_5 concentrations. Like February 2017, the model predicts higher concentrations within the city, Allegheny County, and highways extending to surrounding counties. Primary particle number emissions for both February and July are approximately equal with similar sectoral contributions (Figure 2), and therefore spatial distributions are similar across both months. Likewise, in both months, the change in average predicted N_5 concentrations between the city and the entire modeling domain are about the same (3,000 cm^{-3} in both February and July), implying similar urban-rural spatial differences in both months. Moreover, the predicted intraurban spatial variability in both months is similar, with standard deviation 1,400 cm^{-3} in February and 2,000 cm^{-3} in July.

2.3.1 Spatial and temporal comparisons to observation sites

Figure 4 shows the comparisons of February 2017 model predictions against observations at 30 sites throughout Pittsburgh further detailed in Saha et al. (2019).

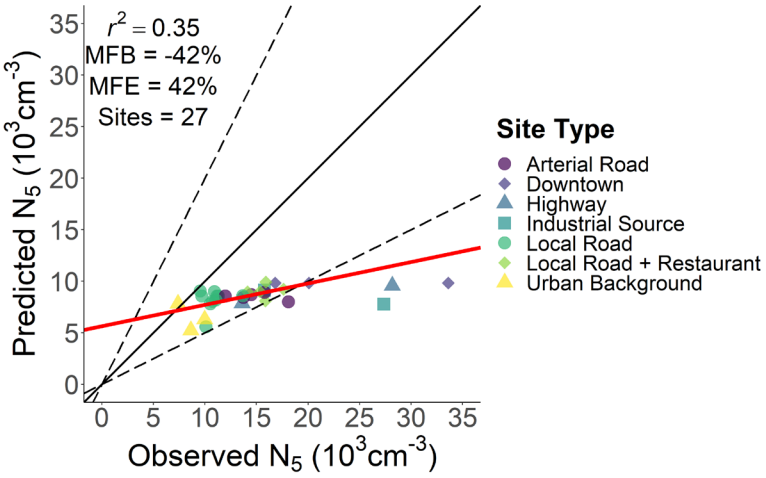

Figure 4
Monthly averaged February 2017 N_5 predictions versus seasonally averaged observed N_5 concentrations from winter 2017 and 2018 (see text). Solid lines represent 1:1, dashed lines are ±50%, and red line is the best fit line for all points except three points to the extreme right.

Each point represents a monthly averaged N_5 concentration prediction at one site plotted against a seasonally averaged (November-February) N_5 concentration observation at the same site. At 27 sites (all but three sites located to the extreme right), the model predicts observed average N_5 concentrations within a factor of two (dashed lines on plot), with r^2 of 0.35, mean fractional bias (MFB) of -42% and mean fractional error (MFE) of 42%. The three extreme sites represent observations highly impacted by sources near the observation site, emissions plumes finer than the 1 km modeling here can resolve. The downtown site is located next to a restaurant vent. The industrial site is located ~500 m directly downwind of Clairton Coke Works, the largest coke manufacturing facility in the United States. The highway site is located ~10 m from the edge of Interstate 376, a large highway connecting Pittsburgh to its eastern suburbs. Within the 27 sites predicted within a factor of two, at 13 sites urban background or local roads influenced concentrations (Saha et al., 2019). At these sites, the model performs well with MFB = -29% and MFE = 30% with points clustered at or below 10,000 cm^{-3}. Meanwhile, at remaining 14 sites local sources or topography influenced concentrations: higher traffic volumes (arterial road or highway), restaurants, street canyons (downtown), or an industrial source. February 2017 predictions show poorer agreement with MFB of -55% and MFE of 55% at these sites. These 14 more polluted sites drive the overall agreement of all 27 sites as indicated by the solid, red line of best

fit in Figure 4 with slope less than one. Overall, Figure 4 suggests that the model reproduces UFP concentrations in the urban background, that it captures intraurban variation in UFP concentrations but tends to underpredict concentration hot spots.

Figure 5 and Figure 6 show diurnal comparisons between model N_5 predictions in February 2017 and seasonally averaged observations for the 27 sites in Figure 4.

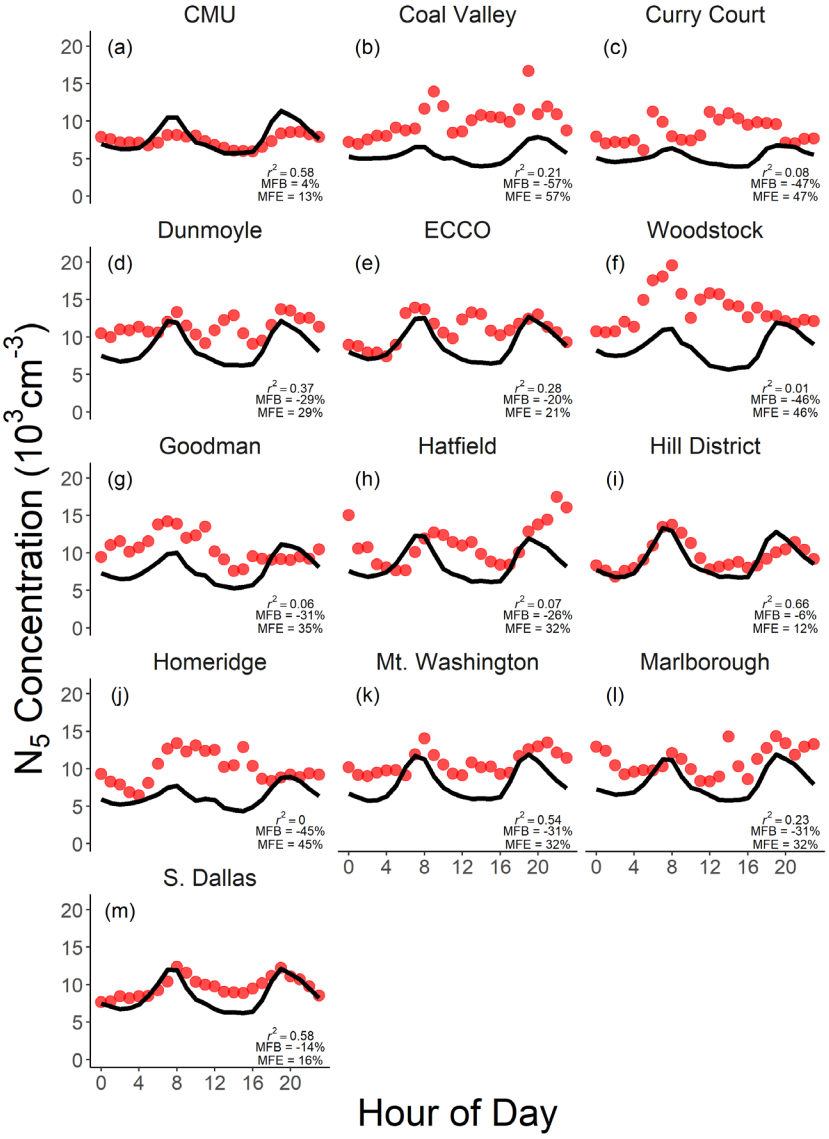

Figure 5
Diurnal averages of February 2017 N_5 model predictions (solid line) and all-winter observed N_5 concentrations (red points) at 13 urban background or local road sites.

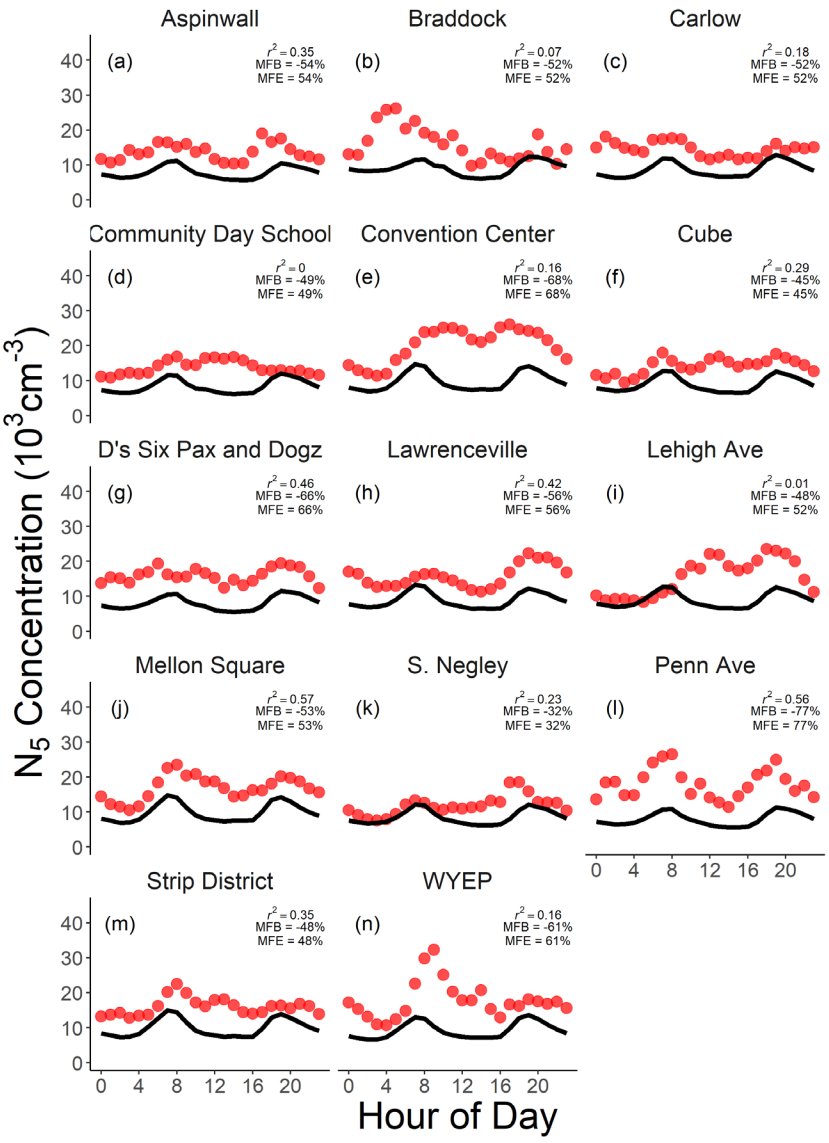

Figure 6
Diurnal averages of February 2017 N_5 model predictions (solid line) and all-winter observed N_5 concentrations (red points) at 14 sites influenced by local sources or topography.

Overall, in both figures we see the model N_5 concentration predictions in solid black lines have visible diurnal peaks compared to the observations in red. Figure 5 shows the 13 local road and urban background sites; Figure 6 shows the 14 remaining sites where local sources or topography influence observations. Due to limited measurements in July 2017, we show temporal evaluations for these simulations in Figure 33. Overall, at six of 13 sites categorized as local road or background, temporal correlation between model predictions and observed N_5 concentrations range between r^2 = 0.28 and r^2 = 0.66 (Figure 5a, d, e, i, k, m). For two of these 13 sites, Coal Valley

and Curry Court (Figure 5b and c), while categorized as local road and urban background sites, respectively, are located near large sources that significant increase concentrations in those areas. Coal Valley is located between two large industrial sources: approximately 1.5 km from Irvin works, a steel manufacturing facility and approximately 3 km away from Clairton Coke Works. Both sources increase N_5 concentrations at those locations and increase sub-1-km variability in concentrations. Likewise, Curry Court is located ~3 km downwind of Pittsburgh International Airport, where emissions increase observed number concentrations (Agarwal et al., 2019; Mazaheri et al., 2009). Aircraft emissions in our emissions inputs are contained within the industrial point source sector and include emissions from aircraft takeoff, landing, and airport operations such as vehicles on the runway (U.S. Environmental Protection Agency, 2016). For the remaining five sites (Figure 5, g, h, j, and l), all are located at residential locations; however, two sites, Hatfield and Marlborough (Figure 5h and l), are in denser residential locations within the city with MFB and MFE values closer to zero. Meanwhile, Woodstock, Homeridge, and Goodman (Figure 5f, g, and j) are in more suburban residential locations have elevated observed N_5 concentrations before evening hours of the day.

Despite consistent underprediction for more polluted sites influenced by local sources or topography in Figure 6, temporally, the model predicts relative diurnal patterns in N_5 concentrations well. At six of 14 sites (Figure 6a, f, g, j, l, and m), r^2 values range between 0.29 and 0.57 much like the local road and urban background sites in Figure 5. All these six sites are less than 50 m from a major roadway, which drives these high temporal correlations, despite other nearby sources such as restaurants at some sites (e.g. Figure 6f, g, and m). Meanwhile, at sites such as Braddock, Convention Center, or Lehigh Ave (Figure 6b, e and i), diurnal correlation degrades with distinct observed elevated concentrations after noon. Here industrial sources, topography, or nearby restaurants, respectively, dominate. At several sites that do not have as high temporal correlation (e.g. Figure 6c, d, h, k, and n), distinct diurnal peaks either in the morning or afternoon show up in both the observations and model predictions.

We provide evaluations of predicted particle number and mass size distribution

against observed size distributions in Figures 40-43. These comparisons show the model predicting number size distribution modes at lower diameters than observations. We also compare estimated daily average $PM_{2.5}$ against four regulatory sites in Figures 44-45 to find the model predicting $PM_{2.5}$ concentrations at arterial road and rural sites well, but like particle number concentration, underpredicting concentrations near industrial sources.

2.3.2 Source apportionment

Figure 7 depicts the source apportionment of time-averaged predicted N_5 concentration spatially averaged over the City of Pittsburgh from February and July 2017 sensitivity simulations.

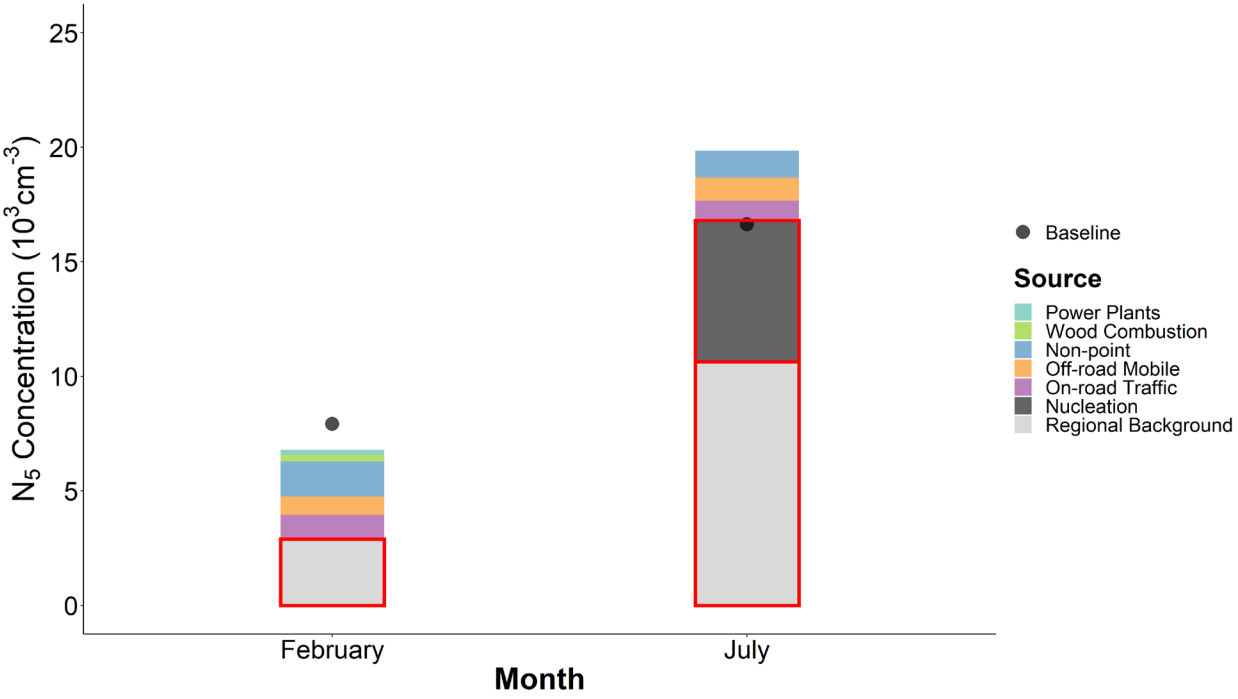

Figure 7
Source apportionment within the City of Pittsburgh sensitivity simulations show on-road traffic, off-road mobile, and non-point sources dominate local UFP concentrations. Red boxes around nucleation and regional background represent non-local sources within the city.

Black points show the baseline mean concentration over the city. Red boxes outline regional, spatially uniform sources as opposed to more spatially variable local sources in the city. To derive this apportionment, we find the difference between the mean predicted N_5 concentration over the city in the baseline simulation and the mean

predicted N_5 concentration over the same area from each zero-out sensitivity simulation. To determine regional background, we find the minimum predicted N_5 concentration from entire modeling domain, assuming boundary conditions largely determine these rural concentrations. For February 2017, this procedure results in a sum (6,800 cm^{-3}) 11% lower than the predicted mean N_5 concentration over the city (7,600 cm^{-3}) due to coagulational losses of particles. Regional background contributes to the plurality of this total (43%), followed by non-point sources (22%), on-road traffic (16%), off-road mobile sources (12%), wood combustion (4%), and power plants (3%). We note that in NEI 2011, the inventory encodes natural gas combustion into both the non-point sector and power plants, so there is a degree of double counting. Natural gas combustion contributes to 88% of non-point sector number emissions and 9% of power plant number emissions. For July 2017, the source apportionment procedure also does not achieve closure with the baseline mean N_5 predictions over Pittsburgh (20,000 cm^{-3} vs. 17,000 cm^{-3}). Regional background once again contributes to the majority of predicted N_5 concentration (54%) followed by nucleation (31%), non-point sources (6%), off-road mobile sources (5%), on-road traffic (4%). Power plants contribute a negligible amount to this first-order, linear source apportionment for July. Comparing across both simulation months, we see nucleation driving much of the difference between seasons through its contribution to in-domain nucleation in July (dark black bar). Likewise, while we do not directly test the contribution of nucleation to out-of-domain concentrations, it does contribute to some portion of regional background (light gray bar). Moreover, when comparing local, intraurban sources, the absolute magnitude of their contributions to N_5 concentration is similar in both months. This similarity is consistent with the similar levels of spatial variability within the city and between the city and suburban and rural areas shown in Figure 3. This is expected given that local emissions sources are comparable in both months (Figure 2).

2.3.3 Evaluation of on-road traffic emissions

According to these simulations, on-road traffic contributes to 16% of predicted mean N_5 concentrations in Pittsburgh in February and 4% in July. Moreover, a fraction of N_5 concentrations attributed to regional background likely comes from on-road traffic outside the modeling domain. Our sensitivity simulations test the effect of different

spatial surrogates for on-road traffic emissions to simulate this source of urban UFPs. Figure 8 compares predicted and observed NO_2, a key tracer for traffic in urban areas, for the baseline and two traffic sensitivity simulations (see section 2.2.4).

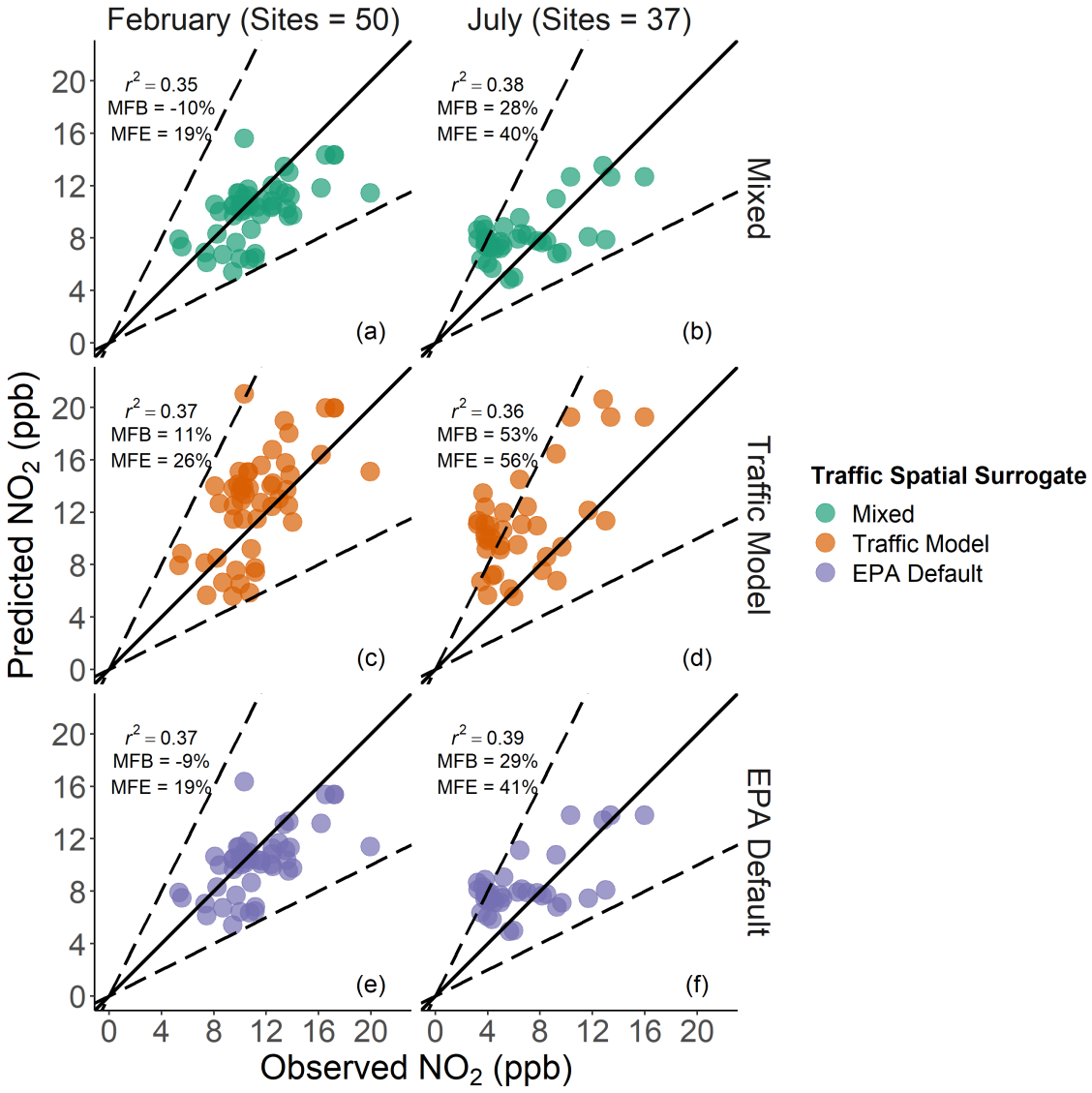

Figure 8
Predicted NO_2 versus observed NO_2 monthly averages at distributed sites in February and July for baseline simulations with mixed traffic spatial surrogates and sensitivity simulations using traffic model and EPA default spatial surrogates for on-road traffic emissions show better agreement in February than July. There is overall similar agreement in NO_2 predictions with the traffic model compared to the default EPA spatial surrogate and the mixed surrogate. Solid lines are 1:1 and dashed lines are ±50%

Each point represents the monthly average value at one of 50 sites in February and 37 sites in July. Spatially, the February 2017 baseline simulation (Figure 8a) reproduces NO_2 concentrations well with r^2 = 0.35, MFB = -10%, and MFE = 19%. The traffic model

and EPA default spatial surrogates (Figure 8c, e) overpredict and underpredict NO_2 concentrations, respectively: r^2 = 0.37, 0.37, MFB = 11%, -9%, and MFE = 26%, 19%. In July meanwhile, baseline simulations predict NO_2 observations at 37 sites (Figure 8b), with MFB = 28%. For July simulations, using the traffic model spatial surrogate results in overprediction between NO_2 predictions and observations, with higher MFB values of 53% (Figure 8b). Using the EPA default spatial surrogate in this month results in similar agreement between NO_2 predictions and observations as the baseline simulation: MFB = 29% and MFE = 41% (Figure 8f).

The traffic model and EPA default traffic spatial surrogates result in similar spatial agreement between predicted and observed NO_2 concentrations compared to the baseline, mixed traffic surrogate model simulation, and this similarity extends to the sensitivity simulation predictions of N_5 concentrations. Figure 9 depicts the predicted and observed N_5 concentrations at the 27 sites shown in Figure 4 in February 2017, but for the simulations with the traffic model (Figure 9a) and EPA default (Figure 9b) spatial surrogates.

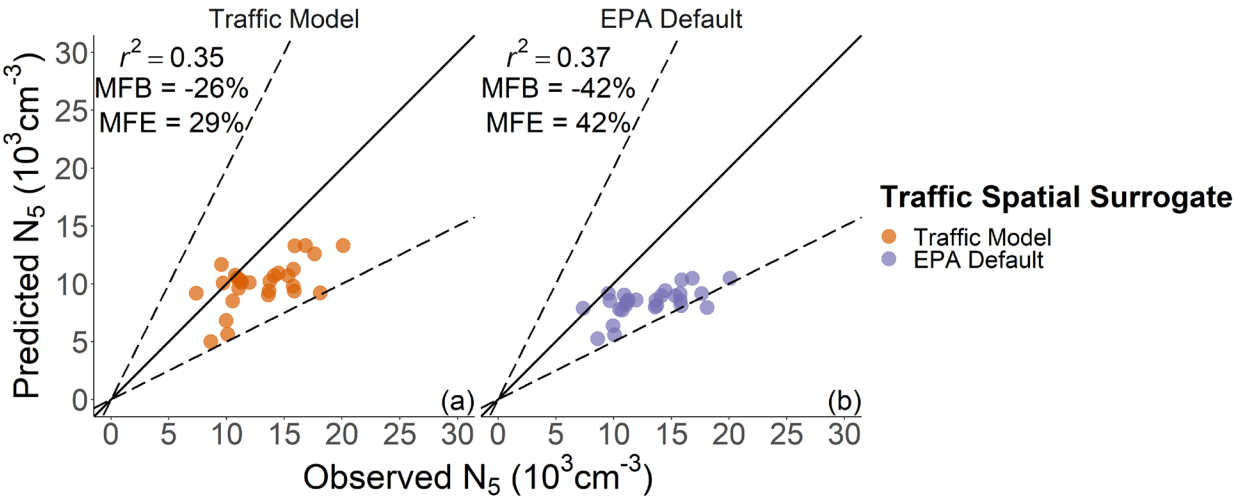

Figure 9
Comparison of predicted N_5 concentrations from mixed and EPA default traffic spatial surrogate simulations against observations shows less predicted spatial variability than baseline simulations with the traffic model spatial surrogate. Extreme observed sites are omitted in this plot.

The three industrial oriented sites in Figure 4 are omitted in this figure. These two surrogates result in similar, r^2 values of 0.35 and 0.37 than the baseline simulation. However, the traffic model spatial surrogate simulation result in better agreement in N_5

concentrations with MFB = -26% and MFE = 29%. The EPA default surrogate results in similar agreement with MFB = -42% and MFE = 43%.

Temporally for February simulation, the traffic model spatial surrogate overpredicts at background and local road sites compared to the mixed and EPA default spatial surrogates, but with similar diurnal correlations. However, at background and local road sites, the traffic model spatial surrogate show higher spikes in concentration during rush hour periods (Figures 34-37).

2.3.4 Modeling resolution and human exposure

To address the question of how well various modeling resolutions captures variability in UFP exposures, we compare outdoor concentrations predicted by different model resolutions (Figure 10), model resolution's effect on reproducing observations (Figure 38), and model resolution on average N_5 concentration over the modeling domain (Figure 39). In Figure 10, the vertical axis shows time-averaged predicted N_5 concentration for February 2017.

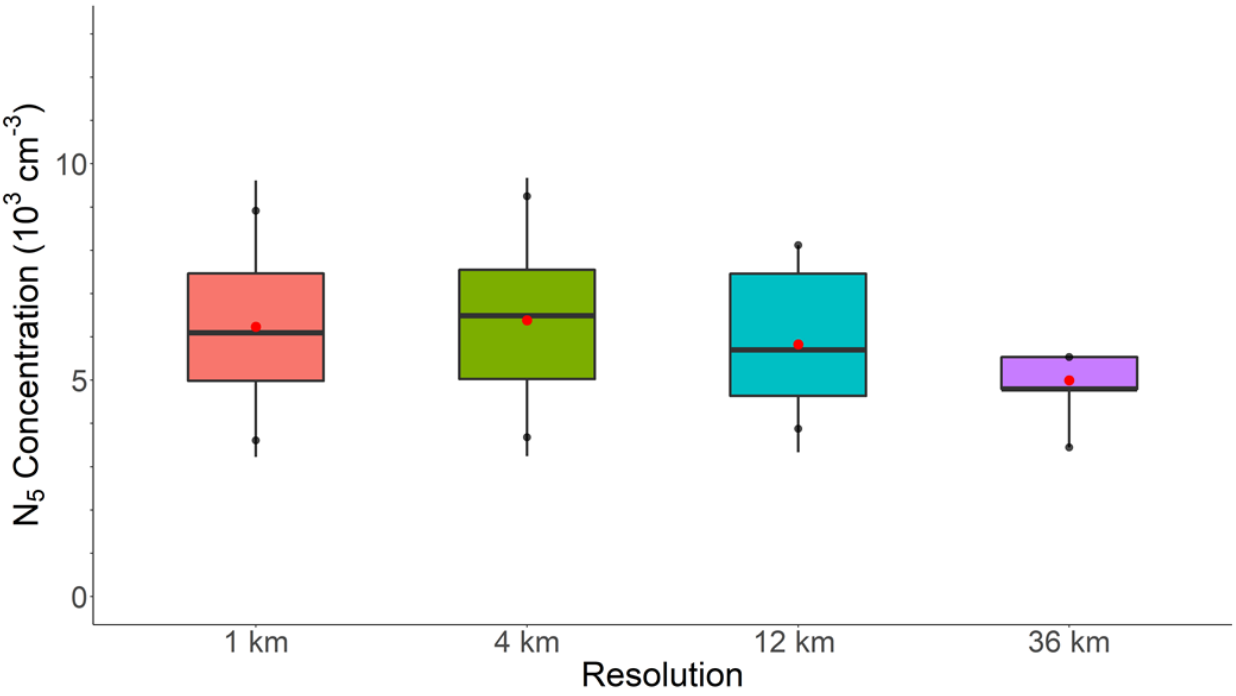

Figure 10
Population-weighted spatial N_5 exposure distributions show 1-km modeling resolution resolves higher exposure variability than 4-km resolution. Whisker endpoints represent 1st and 99th percentiles of population exposure, box ends represent 25th and 75th percentiles population exposure, and center line represents 50th percentile (median) population exposure. Black points show 5th and 95th percentiles and red points are population-weighted mean concentrations.

Each boxplot shown is a population-weighted spatial distribution of UFP exposure using U.S. Census grided population estimates (U.S. Census Bureau, 2017). We show four boxplots representing the different resolutions used to nest the model: 36 km, 12 km, 4 km, and 1 km. The endpoints of the boxplot tails represent the 1st and 99th percentile of exposure. The ends of the boxes represent the 25th and 75th percentiles of exposure, and the solid line in the middle is the 50th percentile (median) exposure. The 1 km simulation resolves more spatial variability, with a 1st-99th percentile range of 3,200-9,600 cm^{-3}. Coarser resolutions quantify similar or less variability with 1st-99th percentile ranges of 3,200-9,700 cm^{-3} (4 km), 3,300-8,100 cm^{-3} (12 km), and 3,400-5,500 cm^{-3} (36 km). Overall, Figure 10 shows that there is considerable variation in UFP concentrations and exposures on the intraurban scale and that, at each step explored here, higher spatial resolution up to 4 km and 1 km resolution is important for resolving the exposures of the upper quartile of the area's population. Figure 39 furthermore shows this lack of spatial resolution from coarser model resolutions. Moreover, Figure 38 shows that coarser model resolutions lower than 1 km are not capable of reproducing observations to the degree seen in Figure 4 with r^2 values lower than 0.05 for all resolutions. It is particularly noteworthy that the r^2 of the model increases from 0.04 to 0.35 as resolution is increased from 4 km to 1 km, highlighting the importance of very high resolution in resolving intraurban UFP concentrations.

2.4 Discussion and Conclusions

This study deployed a state-of-the-science chemical transport model, PM-CAMx-UF, for winter and summer seasons over Pittsburgh at 1-km resolution to simulate UFP concentrations and explore the model's ability to resolve intraurban spatial and temporal variability in UFP concentrations. Model inputs include source-resolved particle number emissions estimated from U.S. EPA NEI particle mass estimates combined with representative particle size distributions and 1-km spatial surrogates. To spatially disaggregate on-road traffic emissions we use predictions from a traffic model based off observed traffic counts and speeds in Pittsburgh and combine them with EPA-default traffic emissions spatial surrogates. We compare model predictions temporally and

spatially to an extensive network of 30 long-term observation sites measuring particle number concentration, and up to 50 sites measuring NO_2 concentrations and $PM_{2.5}$ concentrations. Sensitivity, zero-out simulations assess the source-apportionment of major UFP sources in Pittsburgh. We further evaluate our assumptions about the spatial distribution of on-road traffic emissions inputs by comparing baseline simulation results to simulations using the traffic model only and default EPA spatial surrogates. Lastly, we evaluate the impact of modeling resolution on the variability of predicted UFP human exposure. Combined, these efforts address present shortcomings in using CTMs to quantify UFP exposure and ultimately support efforts to quantify chronic health impacts of UFPs.

Predicted N_5 concentrations are elevated within the city of Pittsburgh, especially near heavily trafficked downtown. Overall, simulation period-averaged predicted concentrations of N_5 in February and July 2017 show the same degree of spatial variability, but overall higher concentrations in July 2017 due to higher regional background (boundary conditions) and nucleation in the domain. Predicted spatial variability, both intraurban and urban-rural, in winter and summer is similar mainly stemming from similar magnitudes and sectoral distribution of primary particle number emissions. Spatially, the model reproduces (within a factor of 2) measurements at 27 sites characterized by urban background and local roads better than those impacted by a local source such as restaurant or topography such as urban street canyons where the model underpredicts.

Mean predicted N_5 concentrations in both summer and winter largely match those reported by Yu et al. (2019) who use a CTM at 4-km model resolution in California and compare to a network of ten interurban sites. The focus of these results is to explain model performance at the intraurban scale and a portion of our performance statistics describe spatial agreement across a network of sites. Yu et al. (2019) however present performance statistics by individual site. An appropriate comparison to these statistics is our performance statistics for temporal evaluations at each site, which range from MFE = 12% to MFE = 66% for 27 sites in February 2017. Yu et al. (2019) report MFE values between 8-38% for the sites evaluated. However, performance reported by Yu et al. (2019) represent comparisons between observed N_7 ($Dp \geq 7$ nm) and predicted

N_{10} (Dp ≥ 10 nm) concentrations and are “best-fit” model results which represent the closest fit within three grid cells of an observation site.

Evaluations at sites impacted by local sources or topography suggests that while the model resolves substantial intraurban variability in UFP concentrations, further intraurban, sub-grid variability exists and is unresolved by the model even at 1 km resolution. Whether the very fine-scale spatial variability in UFP concentrations is important to exposure and health, given that individuals move throughout the city is a different question. Temporally at sites located by roadways, while the model does not agree absolutely with observations, it does reproduce winter average diurnal patterns in N_5 concentrations. This is similar to Yu et al. (2019) who reproduce average December diurnal patterns in observations. Diurnal correlations degrade at sites where other sources such as restaurants, industrial sources, airports, or residential areas influence observations. These degradations along with general underpredictions at these sites furthermore are consistent with sub-grid variability in concentrations not captured by the 1-km model.

Traffic is an important source of intraurban variability in UFP concentrations, and our results show the location of these emissions in model inputs matter to improve model performance for UFP concentration prediction. Spatially, the mixed traffic emissions surrogate combining both traffic model and EPA-default surrogates performs similarly to the EPA-default surrogate only. Meanwhile the traffic model surrogate allocates a greater portion of emissions over the city than the mixed surrogate (Figure 32). This results in the traffic model simulation predictions have poorer absolute agreement at local road and urban background sites than the baseline (mixed) and EPA-default simulations, especially during rush hour peaks where the traffic model predicts higher number concentrations. We see further evidence of the traffic model pushing emissions over the city when comparing NO_2 predictions versus observations at the distributed sites. Its allocation of emissions over the city versus outside the city may compensate for any source of number emissions not captured by the model. In sum, the simulations of the traffic emissions spatial surrogates show that while traffic does explain much of intraurban spatial variability, other sources can also drive variability, especially after accounting for sub-grid variability. Modeling efforts thus must

account for both the relative importance of spatial distribution of on-road traffic emissions inputs and other sources when deploying high-resolution CTMs to simulate UFPs over urban areas.

Furthermore, along with sub-grid concentration variability and traffic emissions spatial patterns, source apportionment analysis shows that other, non-traffic sources of ultrafine particles are just as relevant as traffic in driving urban ultrafine particle concentrations. We use traffic as an indicator for intraurban variability driven by primary emissions, and our attribution of on-road traffic to particle number concentrations (16% in winter, 4% in summer) is also consistent with Saha et al. (2018) who find annual local traffic to contribute ~16% of annual particle number concentration in Pittsburgh in 2016-2017. Our source apportionment simulations suggest non-point sources such as natural gas combustion and restaurants and off-road mobile sources make contributions to N_5 concentrations like that from traffic. Natural gas combustion dominates our non-point source number emissions inputs (88%), so using this sector as proxy for natural gas combustion, our analysis attributes a smaller percentage of N_5 concentration to natural gas combustion (~6-22%) than those found in previous analyses in California (ranging 28-45% for N_{10} in 10 cities) (Yu et al., 2019). Summertime, nationwide source model-based source apportionment for $PM_{0.1}$ likewise find a large source of mass from natural gas combustion in many cities in the United States (Venecek et al., 2019). While Venecek et al. (2019) did not examine Pittsburgh specifically, upwind cities such as Cincinnati, Detroit, and Cleveland, showed much smaller contributions from natural gas to predicted $PM_{0.1}$. Consequently, differing emission mixes between cities modeled in California and Pittsburgh modeled here explain the differing attributions to natural gas combustion. Yu et al. (2019) also found noticeable differences in source apportionment with model resolution, which may be another factor contributing to differences between this work and prior work.

Moreover, source apportionment shows that sources that are spatially homogenous, such as regional background and nucleation, do contribute to absolute UFP concentrations in magnitudes similar to or greater than primary sources like traffic. A substantial portion of our source apportionment attribute concentrations to regional background (43% in February and 54% in July). Moreover, these attributions are lower

than Saha et al. (2018) who attribute more than 75% of average annual observed N_{10} concentrations in Pittsburgh to background values, a combination of both the “true” rural regional background and urban background since the observations were in the middle of the city. Nucleation contributes to a substantial fraction of predicted N_5 concentrations (31%) in July with a higher fraction than those reported by both (Yu et al., 2019) in California, and Saha et al. (2018) in Pittsburgh. This suggests model overprediction due to nucleation and future model improvement to reproduce the substantial decrease in nucleation frequency in Pittsburgh between 2001-2002 and 2016-2017 from SO_2 emissions controls (Saha et al., 2018).

This analysis shows the value-added in resolving UFP human exposure by deploying CTMs at higher 1-km resolution. Previous analyses used CTMs to model UFPs at 4 km resolution. While 1-km modeling resolves similar exposure variability as 4-km modeling, higher resolution model reproduces substantially better the intraurban variability in observations than 4-km modeling. However, these higher resolutions do not resolve sub-1-km variability in observed UFP concentrations in sites impacted by heavy traffic, restaurants, or topography. Resolving the highest percentiles in the exposure distribution requires higher resolution exposure estimates such as empirical land-use regression models which can resolve these sub-1-km variations. However, they are limited by the observations used to develop the models and yield incomplete information on the sources driving urban exposure. These methods must therefore consider covariates for primary sources from traffic and non-traffic. Previous health impacts studies that use empirical models to assign exposure have come to inconclusive results on the impacts of UFPs (Downward et al., 2018; Weichenthal et al., 2017). Given the limitations of both mechanistic and empirical methods to estimate human exposure, future estimates of exposure will most likely need to combine both to construct an aggregate exposure metric for UFPs.

In sum, the use of CTMs to estimate UFP human exposure remains an active area of development. This analysis yields conclusions that a CTM can resolve some of the intraurban spatial variability in UFP concentrations; moreover, CTMs can provide information on source apportionment of UFPs. On-road traffic remains an important source of local, intraurban concentration, but many other sources contribute to

concentrations as well. This is especially relevant because, while a 1 km CTM can resolve more variability in human exposure than coarser model resolutions, it cannot resolve sub-1-km variability that empirical models such as land-use regression. Both traffic and non-traffic sources influence both intraurban variability and this sub-1-km variability. Consequently, future efforts to resolve exposure for chronic UFP health impacts quantifications must account for this variability by accounting for the spatial patterns of various sectors at appropriate resolutions.

3 National policy interventions in current Indian power generation produce disparate, state-level carbon and sulfur emission impacts

3.1 Introduction

India is a growing country with growing energy needs. It is the world's third largest economy (World Bank, 2018a), but per capita GDP remains a fraction of other large economies (World Bank, 2018b). As of 2019, while the Government of India has made considerable progress in delivering electricity to 26 million previously unelectrified households, there is potential to improve quality of electricity supply in the future (Ministry of Power, 2020c). Electricity demand from 2015 could roughly double or triple by 2030 depending on economic growth rates and demand sector composition (Ali, 2018; Spencer and Awasthy, 2019). As the Indian power grid grows, it could exacerbate both local and global environmental challenges: greenhouse gas (GHG) emissions and local and regional air pollution.

Like GDP, India's total GHG emissions rank third in the world (Carbon Brief, 2019; World Resources Institute, 2019). When measured by World Health Organization (WHO) standards for $PM_{2.5}$, suspended particles in the atmosphere less than 2.5 microns in diameter, 99.9% of India's population breathes polluted air (Apte et al., 2015; GBD MAPS Working Group, 2018). This exposure caused by emissions from fossil fuel and biomass combustion led to an estimated 570,000 to 1.1 million premature deaths in India (Conibear et al., 2018; GBD MAPS Working Group, 2018; Ghude et al., 2016; Guo et al., 2018) with premature deaths projected to triple by 2050 if no action is taken to reduce air pollution emissions (GBD MAPS Working Group, 2018).

Indian power generation remains a significant source of GHG emissions and air pollution emissions which lead to premature deaths from $PM_{2.5}$ exposure. Coal-fired power stations form 74% of electricity generation and 55% of installed capacity (Central Electricity Authority, 2019b, 2020a; Centre for Social and Economic Progress, 2019). In addition to contributing to close to 40% of India's GHG emissions (Mohan et al., 2019), Indian coal power stations release uncontrolled $PM_{2.5}$ precursors, sulfur dioxide (SO_2) and nitrogen oxides (NO_X) emissions, which lead to an estimated 7-21% of premature deaths (Apte and Pant, 2019; Conibear et al., 2018; GBD MAPS Working Group, 2018; Guo et al., 2018; Lelieveld et al., 2015).

Planned expansions of coal generation capacity even at lower rates than the past will lead to increases in coal consumption, air pollutant, and GHG emissions (Guttikunda and Jawahar, 2014, 2018; Sahu et al., 2017; Sehgal and Tongia, 2016). However, coal power alone will not meet increased future demand; the Government of India plans to increase renewable generation so that it will constitute 40% of all capacity by 2030 (Government of India, 2015), an increase from approximately 14% non-fossil generation in 2017-2019 (Central Electricity Authority, 2019b; Tongia and Gross, 2019). The growth of non-hydroelectric (non-hydro) renewable generation though in the last decade has largely replaced hydro generation, not thermal generation, on a percentage basis. Thermal (mostly coal) generation has largely stayed constant at approximately 80%, hydro decreased from 15% to 10%, and non-hydro renewables has increase from 4% to 8% (Central Electricity Regulatory Commission, 2018d). This suggests that while capacity additions govern the available fuel mix for generation, how this capacity is operated and dispatched largely determines the actual fuel mix for generation, and consequently air pollutant and GHG emissions.

Previous efforts to analyze Indian power generation with environmental or energy policy relevance generally either lack any treatment of power sector operations and markets or any treatment or air pollutant and GHG emissions. Atmospheric modeling studies have motivated the need for public policy interventions to reduce power sector air pollution emissions, but do not consider how such emissions reductions could occur within the context of Indian power system operations (Gao et al., 2018; GBD MAPS Working Group, 2018; Guttikunda and Jawahar, 2014, 2018). Meanwhile, Indian power system schedule and dispatch modeling studies mainly lack any consideration of air pollutant emissions from power system operations: estimates of actual emissions, internalizing the external social costs imposed from such emissions, or the costs incurred from installing technology to reduce emissions. This includes studies that explicitly analyze increased penetrations of renewable generation, a zero-emission source (Central Electricity Regulatory Commission, 2018a, 2018b; Palchak et al., 2017a, 2017b; Phadke et al., 2016; Spencer et al., 2020). See Appendix B for a detailed summary of previous modeling efforts.

Several analyses (Cropper et al., 2017, 2019; Srinivasan et al., 2018),

specifically examine the costs and avoided $PM_{2.5}$ premature mortality benefits from installing SO_2 control at Indian coal power stations. India has planned stringent sulfur emissions norms (Table 4) for coal power plants, but these are delayed (Ramanathan et al., 2020). These analyses generally find premature mortality benefits of SO_2 control exceed costs but have yet to explore how the Indian electricity sector could operationalize these regulations in the short-term or near-term. Cropper et al., (2019) analyze locational aspects by quantifying the cost and benefits associated with a hypothetical generator with SO_2 control located in eight locations in India. They find net benefits largely scale with population density at a location. Likewise, Cropper et al., (2017) examine the cost-effectiveness (dollars spent per life saved) of flue-gas desulfurization installation in the 2009 Indian coal generation fleet to find that cost-effectiveness varies by plant location. Both Cropper et al., (2019) and Cropper et al. Cropper et al., (2017) assume benchmark, normative plant operations without considering power system operations and dispatch. Srinivasan et al., (2018) lastly quantify the benefits and costs of sulfur control in the 2015 and projected 2030 Indian coal generation fleet to meet the upcoming Indian SO_2 control regulations. They take a generator unit-level, spatially resolved approach where the current and future generation fleet meets electricity demand. However, Srinivasan et al., (2018) do not emphasize how control regulations affect locational aspects of power system dispatch and operations.

To date, only Kumar et al., (2020), Power System Operation Corporation Limited, (2020) and Spencer et al., (2020) use dispatch modeling to mechanistically assess the emissions impacts of altering power dispatch in India. Kumar et al., (2020) find approximately 10% CO_2 emission reductions possibilities between cost minimizing and emissions minimizing dispatch cases; however, they do not consider scenarios for other policies such as emissions regulations or taxes. Meanwhile, POSOCO (Power System Operation Corporation Limited, 2020) finds minimal CO_2 emission reductions of 0.2% for May 2019 with only interstate generators (~20% of total national capacity) economically dispatched. Spencer et al., (2020) model scenarios of the integrating increased variable renewable electricity into the Indian grid in 2030. They find total CO_2 emissions could increase between 3-17% while emissions intensity of electricity could decrease 30-38%

compared to present day. However, they do not consider differences in emissions between states or locations.

Locational aspects remain important for policies pertaining to both carbon emissions and air pollution. With a federal system of government, each state in India largely schedules and dispatches its own power from capacity fuel mixes which vary by state (Safiullah et al., 2017). There are planned market reforms to coordinate and economically dispatch on a limited basis at the national level as opposed to the state level (Power System Operation Corporation Limited, 2020). Moreover, states also deliver power to consumers (Safiullah et al., 2017) and own a plurality of monitored capacity (Ministry of Power, 2020b). With 82% of renewable capacity concentrated in eight of 32 states and territories (Ministry of Power, 2020b), heterogenous capacity fuel mixes among states imply differing emissions impacts from generation and consumption.

In sum, no study has yet mechanistically quantified the expected spatial heterogeneity arising from a federal Indian power sector, i.e. which states emit more or less and from which plants based on the electricity they consume. Moreover, none have explored the potential spatial or state-level differences in emissions from policy interventions in Indian power sector operations. Analyzing current spatial or state-level differences in emissions becomes increasingly relevant as the Indian power sector faces policies on multiple fronts: more stringent sulfur emissions control regulations (Ramanathan et al., 2020), increased penetration of renewable energy (Government of India, 2015), and planned market reforms (Power System Operation Corporation Limited, 2020).

In this paper we develop and present a reduced-order dispatch model of Indian power generation to assess CO_2 and SO_2 emission impacts of policy interventions to address this gap. We focus near-term on the current Indian grid to analyze how policies could induce spatial differences in emissions between states in India. It is the first to present state-level, consumption-based average annual emission factors for India arising from power sector operations. While previous work has used dispatch modeling to simulate Indian power generation (Central Electricity Regulatory Commission, 2018c, 2018b; Kumar et al., 2020; Palchak et al., 2017a; Phadke et al., 2016; Spencer et al.,

2020), this work uses a flexible, computationally simplified method that is both accessible to researchers and policymakers and capable of evaluating policy interventions that affect power sector operations, e.g. greater renewable generation, emissions taxes, emissions regulations, and market reforms like larger load balancing areas. We first evaluate the model's simulations against reported generation data. Then we use the model to simulate several national policy intervention scenarios: stricter sulfur control regulations, progressively increasing carbon taxes, and regional scheduling and dispatch among groups of states.

3.2 Methods

We adopt the approach presented by Deetjen and Azevedo (2019) to develop the reduce-order dispatch model for Indian power generation. Let G_{1h}, G_{2h}, G_{3h}, …, G_{nh} represent a group of n dispatchable, non-renewable generators (i.e. nuclear, hydro, coal, and gas) with capacity G in MW during hour h:

$$(1)\ G_{1h}, G_{2h}, G_{3h}, \cdots, G_{nh}$$

These capacities can be allocated during h to a state s according to fractions f_{nsh}:

$$(2)\ f_{1sh}G_{1h}, f_{2sh}G_{2h}, f_{3sh}G_{3h}, \cdots, f_{nsh}G_{nh}$$

We can order the generators by their variable cost of generation P_{nsh} in ₹/kWh such that

$$(3)\ P_{1sh} \leq P_{2sh} \leq P_{3sh} \leq \cdots \leq P_{nsh}$$

This order $f_{1sh}G_{1h}$, $f_{2sh}G_{2h}$, $f_{3sh}G_{3h}$, …, $f_{nsh}G_{nh}$ represents the merit-order curve of dispatchable, non-renewable generators ordered by variable cost of generation for each hour. State s during hour h has an electricity demand D_{sh} in MWh and non-dispatchable generation (e.g. wind and solar) R_{sh} in MWh. Consequently, to meet net demand D_{sh} - R_{sh} during hour h for state s, the first y generators G_{1h}, G_{2h}, G_{3h}, …, G_{yh} with respective fractions will be dispatched to generate electricity such that:

$$(4)\ \sum_{n=1}^{y} f_{nsh} G_{nh} \leq (D_{sh} - R_{sh}))$$

The model repeats this process for multiple hours and Indian states adjusting available generators with outage information from daily generation reports. We assume no transmission constraints nor any constraints on the ramping or minimum capacity factor capabilities of generators. Likewise, in case the equality condition does not hold in Expression 4, we do not explicitly model interstate electricity transfers to meet any shortfalls in demand. See Appendix B for a detailed discussion of the uncertainty associated with these assumptions.

To compile generators in Expression 1, we combine a publicly available database of all non-variable-renewable generators in India with capacity greater than 25 MW with fossil unit-specific modeled, reported, and calculated net heat rates (Central Electricity Authority, 2015; Ministry of Power, 2020b; Oberschelp et al., 2019) for 2014-2018. We fill in missing heat rates with a log-fit of existing heat rates for units as a function of capacity differing by coal and gas units (Figure 46). To compile variable cost of generation, P_{nsh}, we take differing approaches according to generator fuel type. For coal generators, we calculate production-weighted variable cost of power with the Government of India's coal dispatch database (Coal India, 2019) which reports grade-wise coal amounts sold to individual power stations. We combine these amounts with grade-wise fixed prices of coal from Coal India and state-wise coal transport costs (Coal India, 2018; Kamboj and Tongia, 2018). For plants without any reported sold coal amounts, we fill in using state- and ownership- (central, state, or private) wise median calculated variable cost of power. Calculated variable costs of power for coal units largely match 1:1 to reported variable costs of power from the MERIT India database (Ministry of Power, 2020a) which reports variable cost of generation according to long-term power purchase agreements between generators and states (Figure 47). For gas plants, we use a region-based approach with domestic and imported gas prices and applicable state taxes (Ministry of Petroleum and Natural Gas, 2019; National Thermal Power Corporation, 2017). For nuclear and hydro plants, we assume the reported variable cost of generation in the MERIT India database (Ministry of Power, 2020a).

For intrastate generating plants, 100% of capacity is generally allocated to

respective states, i.e. f_{nsh} = 1; for interstate generation states, f_{nsh} < 1, and capacity allocations to multiple states come from the MERIT India database and capacity allocations from CEA. Our model captures 75-85% of installed capacity based off reported capacity allocations (Central Electricity Authority, 2020b; Ministry of Power, 2020a) (Figure 48).

We estimate net demand D_{sh} - R_{sh} from various sources. We first estimate total hourly demand at the state level by decomposing total daily demand reported at the state level from POSOCO (Power System Operation Corporation Limited, 2018) by state-level diurnal load profiles of demand disaggregated at the monthly level from Energy Analytics Lab (Energy Analytics Lab, 2019). The daily demand reported by state represents the power injected into the state at the state boundary. We estimate average monthly diurnal renewable generation profiles by first disaggregating nationwide renewable generation data for 2018-2019 (Centre for Social and Economic Progress, 2019) to obtain diurnal profiles of renewable generation and then applying these profiles to actual monthly renewable generation for each state from September 2017 to August 2018 (Central Electricity Authority, 2018c) (Figure 49). We estimate net demand for each hour of year for each state by subtracting average monthly diurnal renewable generation from estimated total hourly demand for a given hour.

We structure the model by making SO_2 and CO_2 emission factors as functions of unit heat rate for fossil plants. We assume domestic Indian production-weighted average coal composition (Ministry of Coal, 2018) for all plants and use the mass-balance approach presented by Srinivasan et al., (2018). We assume domestic Indian coal only with no imported coal, which disproportionately is used in handful of coastal locations. For gas plants, we assume standard natural gas for CO_2 emissions (U.S. Energy Information Administration, 2020) and zero SO_2 emissions.

We test a total of eight policies to spatially estimate their impacts on SO_2 and CO_2 emissions (Table 1)

Scenario	Description
State Dispatch (Base Case)	Dispatch plants by individual states with fixed allocations of interstate plants
Sulfur Control	Impose sulfur control variable costs to meet emission regulations
Carbon Tax -10	Impose a CO_2 tax of $10 USD/ton
Carbon Tax - 35	Impose a CO_2 tax of $35 USD/ton
Carbon Tax - 50	Impose a CO_2 tax of $50 USD/ton
Carbon Tax - 100	Impose a CO_2 tax of $100 USD/ton
Sulfur Control + Carbon Tax - 35	Impose sulfur control variable costs with a CO_2 tax of $35 USD/ton
Region Dispatch	Dispatch plants by power region (North, South, East, West, Northeast)

Table 1
Policy scenarios evaluated with the reduced-order model.

Currently dispatch practices in India are hybrid combining pure economic dispatch based on variable cost of generation with heuristics based on historical practices. Heuristic practices vary by state because each state schedules and dispatches its own power with some regional and national coordination (Central Electricity Regulatory Commission, 2018c; Safiullah et al., 2017). These heuristic practices include using hydro capacity during non-monsoon months (generally January through May and November through December) as marginal generators, placing gas generators more expensive than coal generators after this hydro capacity, and dispatching coal and remaining gas generators by merit order. Moreover, hydro reservoirs in India serve other purposes besides power generation, e.g. drinking water, irrigation, flood control, etc. On a diurnal basis, hydro generation highly correlates with net demand (Figure 50) reflecting hydro's load-following nature. Consequently, we structure the model to dispatch power according to increasing variable cost, putting hydro before coal and gas plants. However, to incorporate hydro generation's load-following behavior and to reflect the availability of water in reservoirs, we first constrain daily hydro capacity from reported daily hydro generation. Then we disaggregate that generation to the hourly level according to diurnal profiles for hydro generation (Figure 50). Finally, we compare the capacity available to produce that much amount of electricity for the hour, we scale the available hydro capacity for the hour accordingly to represent the effective hydro capacity available to run at 100% capacity for the hour.

The state dispatch scenario represents the current base case of operations in the

Indian power sector where each state schedules and dispatches its own power. Accordingly, we structure the model to run 32 Indian states and union territories individually with fixed state allocation of interstate generation capacity. The sulfur control scenarios represents the minimal control and costs needed to meet upcoming SO_2 emission regulations in India (Srinivasan et al., 2018). As of December 2019, only 13.75 GW of capacity (~ 5% of monitored capacity) in India have any operational sulfur control (Ramanathan et al., 2020), and we cannot verify if installed control runs regularly due to a lack of publicly available continuous emissions monitoring data. Therefore, for simplicity we assume no sulfur control at any plants in the base case scenario. Assumptions on control technologies and variable costs come from Srinivasan et al., (2018). For this scenario, we first calculate the percentage reduction required for each unit to meet Indian sulfur control regulations. Then we assume the minimal, least cost control technology required to meet that reduction from those presented in Srinivasan et al (Srinivasan et al., 2018). For 368 units totaling 72 GW capacity, we assume dry limestone rejection to reduce sulfur emissions ~60% at cost ₹6,000/ton SO_2 removed ($85/ton). For remaining 279 units totaling 129 GW requiring reductions more than 60% we assume wet flue gas desulfurization at cost ₹7,000/ton SO_2 ($99/ton). These costs only include reagent costs and increase capacity-weighted variable cost of power by 1-2%. All other associated control costs in fixed costs according to Indian regulations; they do not influence dispatch by variable cost of generation (Srinivasan et al., 2018). For the carbon tax scenarios, we assume $1 USD = ₹71 INR, which adds approximately 300% to the average variable cost of coal generation with a $100/ton tax. For the region dispatch scenario, the model dispatches power based on geographical Indian power region by pooling state-level capacities. For each scenario we operate the model at hourly resolution for September 2017 to August 2018 to obtain annual results.

3.3 Results

In Figure 11 we show the annual electricity generation by fuel type for each Indian power regions and for each of our scenarios as well as for reported generation. The state scenario (second column) represents the base case for our simulations. Overall, results for this scenario agree largely with reported generation for most fuel-region generation shares (e.g. coal generation in the northern region, hydro generation

in the eastern generation, etc.) within 30%, except for gas generation in the northern region where gas generation underprediction is 51%. We explain this subsequently in the Discussion. We also show monthly resolved results compared to reported generation for the base case in Figure 51 of the Appendix B, with agreement with reported generation at the monthly resolution largely mirroring agreement at the annual resolution. Likewise, we report state-level comparison of the base case simulation with reported generation for intrastate capacity in Figures 52-56. We compare only intrastate capacity because reported generation from Government of India do not report state-level shares for interstate capacity (see Methods for explanation of interstate versus intrastate capacity). State-level annual comparisons show simulated generation largely agrees with reported generation.

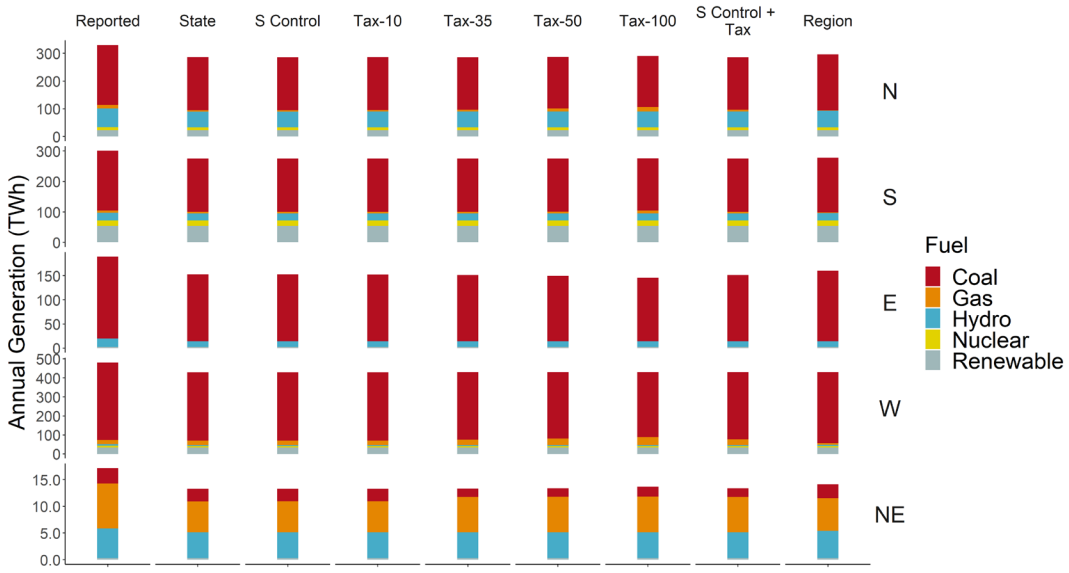

Figure 11
Predicted annual generation in each region from all dispatch scenarios simulated and reported generation.

Progressive carbon taxes of $10, 35, 50 and 100 USD/metric ton CO_2 yield little changes in gross generation mixes. For reference, coal in India today has an implicit carbon tax of under $6/ton CO_2, through a coal cess (tax) of ₹400/ton coal (International Institute for Sustainable Development, 2020). For the $35, $50, and $100 taxes, simulated gas generations increase by 8-175% relative to the base case but still form a small portion of total generation in all regions except the northeast region. This is due to both capacity constraints as well as unavailability of relatively inexpensive gas. Under

the $100 tax, simulated gas generation increases to 6% from 2% in the northern region, from 2% to 4% in the southern region, from 6% to 11 % in the western region, and from 44% to 50% in the northeastern region. Three other scenarios: sulfur control, sulfur control with a $35/ton tax, and regional dispatch yield little changes in overall generation mix compared to the base case.

The lack of significant changes in generation fuel mixes for each scenario also affects overall estimated CO_2 emissions with little changes between each scenario (Figure 57). Due to a lack of directly reported CO_2 emission data, we apply our estimated generator-level emission factors to both reported and simulated generations. The base case scenario estimates nationwide power sector CO_2 emissions to be 22% lower than reported generation. Nationwide, the highest $100 carbon tax reduces emissions by 3% compared to the base case, with progressively higher taxes lowering emissions in all regions except the northeast region. In this region, emissions decrease the most with the $35 tax (7%) and not at higher tax values due to higher predicted intraregional coal dispatched at the highest carbon tax values. Scenarios with sulfur control which account for the small increase in CO_2 emissions from additional energy consumption of control equipment change simulated nationwide emissions by approximately 1%. The region scenario induces the most changes in both nationwide and regional simulated CO_2 emissions. At the national scale, estimated CO_2 emissions increase by 3%, with regional emissions increasing in range between 2-6%. As discussed subsequently, market changes lead to cost savings, not necessarily emissions reductions as locational fuel price differentials outweigh efficiency gains from regional dispatch.

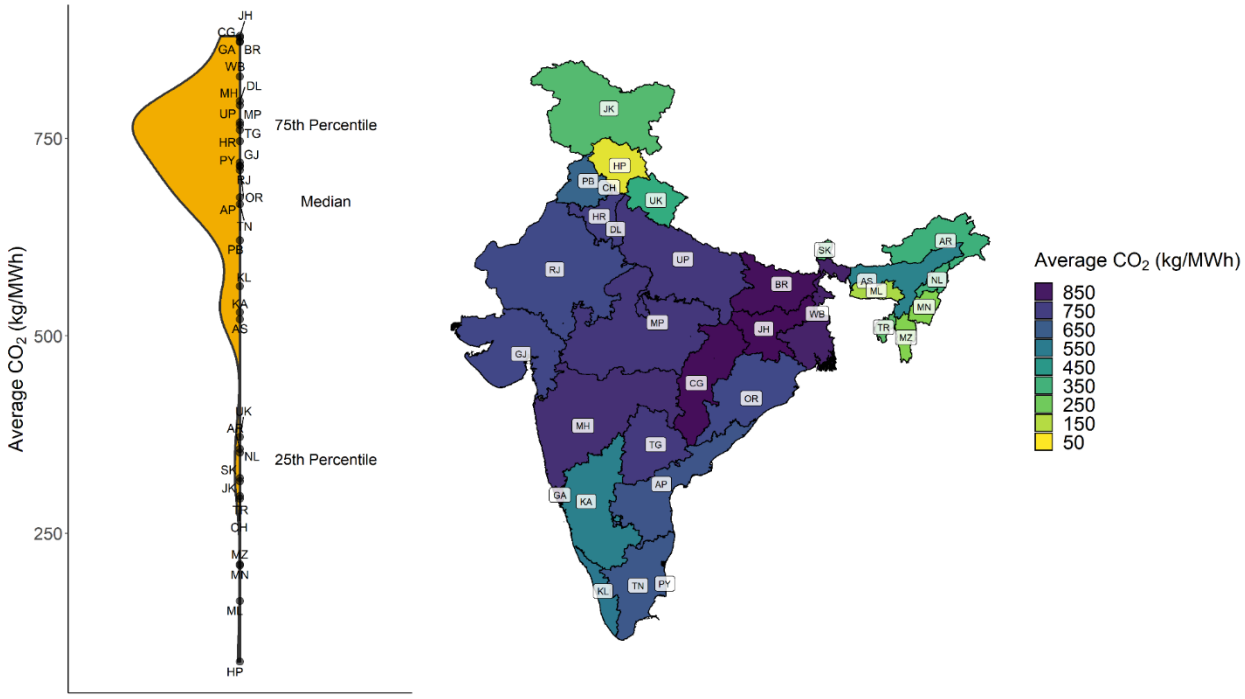

Figure 12
Average annual predicted emission factors for Indian states from the state simulation (base case). Violin plot (left) shows spread of emission factors of electricity consumed in each state (see Table 3 for abbreviations) with density plot of annual demand.

Given the base case's (state dispatch) general agreement with reported generation, we report average consumption-based annual CO_2 emission factors for each state of India in Figure 12. Consumption-based emission factors consider inter-state electricity transfers that production-based emission factors from plants within geographic boundaries would not consider. In Figure 12, the right panel shows the geographic location of each state by its estimated consumption-based emission factor, and the left panel shows the spread of emission factors with a density plot of annual electricity demand. We also present the data underlying this plot in Table 3. Overall, the national generation-weighted average CO_2 emission factor for all states is 711 kg/MWh, but considerable heterogeneity exists (left panel). Two distinct clusters form in the spread of state-level emission factors. At the lower range of state-level emission factors are 11 low annual demand states (~4% of total nationwide demand), primarily Himalayan and Northeastern states, where considerable hydro capacity exists. At the minimum within this group, Himachal Pradesh (HP) reports an average emission factor of 87 kg/MWh with Uttarakhand (UK) at the greatest at 372 kg/MWh. Within this cluster

of low-demand states, those with higher emission factors tend to depend on combination of coal and gas paired with hydro. The second cluster of states are the remaining 21 states simulated, forming 96% of total annual demand. Among this group average annual CO_2 emission factors vary considerably with Assam (AS) and Karnataka (KA) at the lower end of this group (521 kg/MWh and 530 kg/MWh) with the highest emission factor among all states from Jharkhand (879 kg/MWh). While Karnataka, Madhya Pradesh (MP), Tamil Nadu (TN), Maharashtra (MH), Gujarat (GJ), Rajasthan (RJ), Andhra Pradesh (AP) and Telangana (TG) have the highest amounts of renewable capacity, they also use considerable amounts of coal capacity, putting them in the highest cluster of states. We discuss the uncertainty associated with the base case simulation and state-level estimated annual CO_2 emission factors in Appendix B.

To assess differences between states, we report simulated state-level consumption emissions, production emissions, annual demand, and differences in consumption-based emission factors and production-based emission factors (Figure 13). We calculate consumption-based emissions by summing the emissions from interstate and intrastate generation associated with meeting demand for a state.

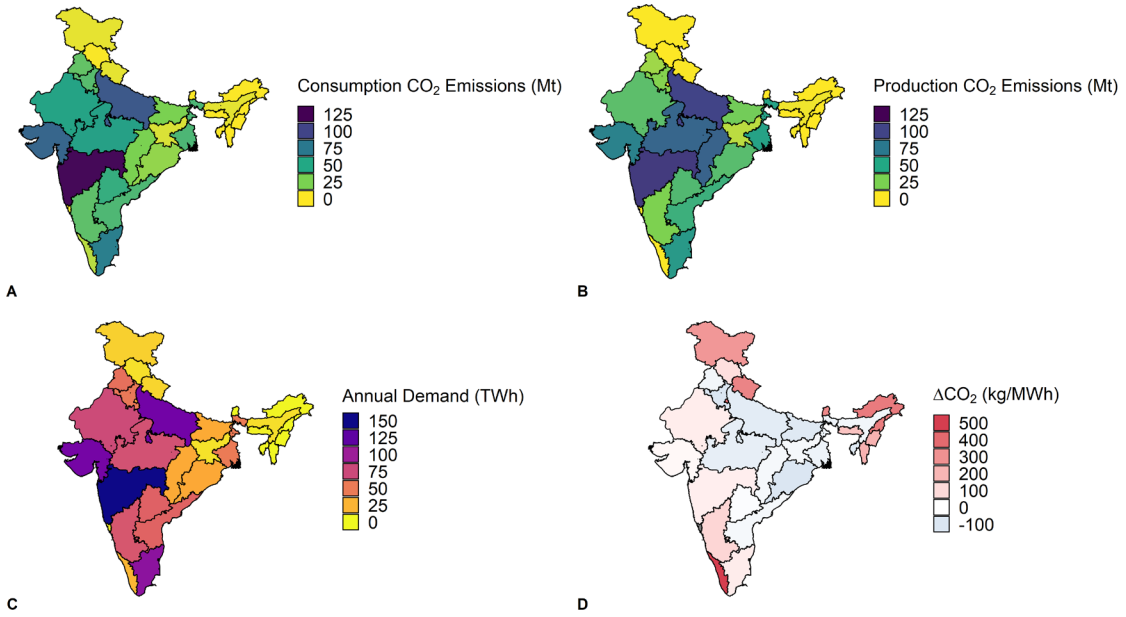

Figure 13
(A) Consumption and (B) production-based simulated total emissions from the Indian power sector by state. Additionally, (C) annual power demand reported and (D) difference in emission factors between consumption-based emission factors and production-based emission factors.

The highest consumption-based emissions occur in Maharashtra (120 Mt), the lowest in Mizoram (MZ, 0.10 Mt) with an average across states at 26 Mt. We calculate production-based emissions by summing the emissions associated with generation within a state's borders only. State-to-state variability in production-based emission (Figure 13b) mirror those for consumption-based emissions; however, several states (e.g. Goa, Manipur, Meghalaya) report zero production-based emissions due to zero-carbon capacity installed in those states. Likewise, Maharashtra reports production-based emission of 104 Mt and average production-based emissions across all states is 26 Mt. The interstate differences in both consumption-based and production-based emissions (Figure 13a, b) mainly arise from differing annual demand by state (Figure 13c). States having the lowest consumption-based emission factors also have the lowest annual demands (e.g. Jammu and Kashmir (JK), Sikkim (SK), Arunachal Pradesh (AR)). Lastly, in Figure 13d we report the difference between consumption-based emission factors for each state (Figure 2) and production-based emission factors. We calculate these latter factors by dividing the total emissions within the geographic boundary of each states by the total generation from generators within the state. This analysis produces distinct differences due to interstate electricity exchanges. For example, in Kerala, while little fossil generation capacity is within the state, the state imports fossil generation from neighboring states, yielding a difference of over 500 kg/MWh between consumption-based and production-based emission factors. A similar pattern holds for a state like Odisha (OR) in the coal belt: its consumption-based emission factor is less than the production-based emission factor, with a difference of 109 kg/MWh.

Figure 14 shows the results of the sulfur control scenario. In Figure 14, overall, we see an 79% decrease in annual nationwide sulfur emissions from 6,100 kt in the base case to 1,300 kt in the sulfur control scenario (Figure 14a). These decreases represent the minimal control needed to meet upcoming Indian SO_2 emission standards for coal generators (Table 4). Likewise, minimal nationwide control yields little change (< 5%) in plant load factor (PLF), i.e. capacity factor of plants (Figure 14b). Only 19 of 162 coal plants dispatched see appreciable changes in PLF with 88% of plants showing no change. These 19 plants sit throughout the country.

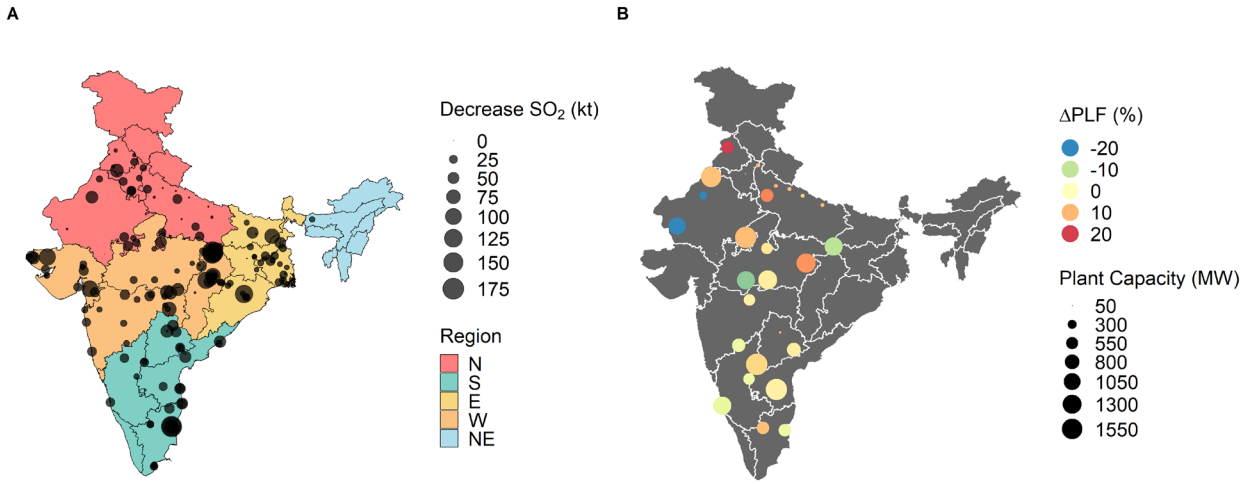

Figure 14
(A) Decrease in SO_2 emissions from implementing minimal sulfur control to meet Indian emissions norms. Decrease is difference in model predictions between the base case, state scenario and the sulfur control scenario. (B) Changes in coal plant load factor (PLF) from sulfur control. Only coal plants with a more than 5% change in PLF are shown.

Figure 15 shows the results of the \$100/ton CO_2 tax scenario. Only 12 states see appreciable decreases (> 5%) in average annual emission factors (Figure 15a): Assam (6% decrease), Gujarat (9%), Kerala (9%) Punjab (10%), Arunachal Pradesh (11%), Meghalaya (11%), Jammu and Kashmir (12%), Manipur (15%), Chandigarh (16%), Nagaland (18%), Mizoram (23%), and Uttarakhand (27%).

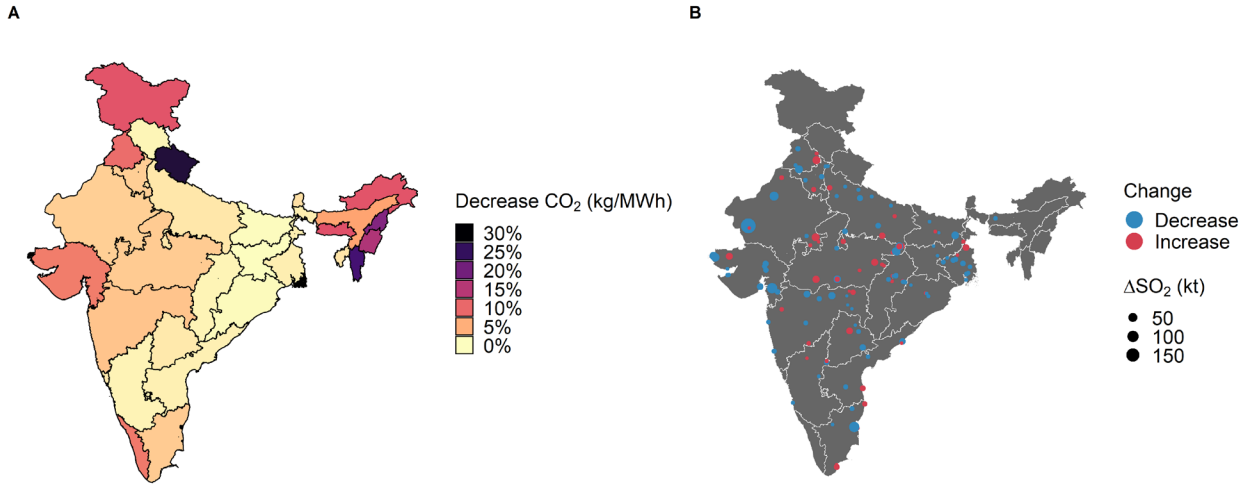

Figure 15
(A) Changes in average annual emission factors by state for a \$100 USD/ton CO_2 tax. (B) Change in SO_2 emissions induced from a \$100 USD/ton CO_2 tax.

These states, accounting for approximately 20% of annual nationwide demand, are generally Himalayan or Northeastern states except for Gujarat, Punjab, and Kerala

which dominate at 16% of total annual demand. Consequently, the annual average nationwide CO_2 emission factor decreases from 711 kg/MWh to 686 kg/MWh, a decrease of 4%. The $100 tax also affects the spatial distribution of SO_2 emissions from plants by decreasing total emissions and concentrating emissions to a fewer number of plants (Figure 15b). Total SO_2 emissions decrease 11% from 6,100 kt to 5,400 kt in this scenario, and 47 plants see increases in SO_2 emissions, 20 see no change, and 95 see decreases in estimated SO_2 emissions. Moreover, the emissions-weighted standard distance of plant emissions with respect to their spatial center of emissions decreases from 769 km in the base case to 740 km in the $100 tax scenario, indicating decreased spatial variability. See Appendix B for a detailed discussion of calculating standard distance. In the other four carbon tax scenarios, similar spatial patterns emerge as the $100 tax scenario (Figure 60).

Figure 16 shows the changes between the regional dispatch scenario and the base case. Regional dispatch increases the average nationwide CO_2 emission factor from 711 kg/MWh to 720 kg/MWh, an increase of approximately 1%.

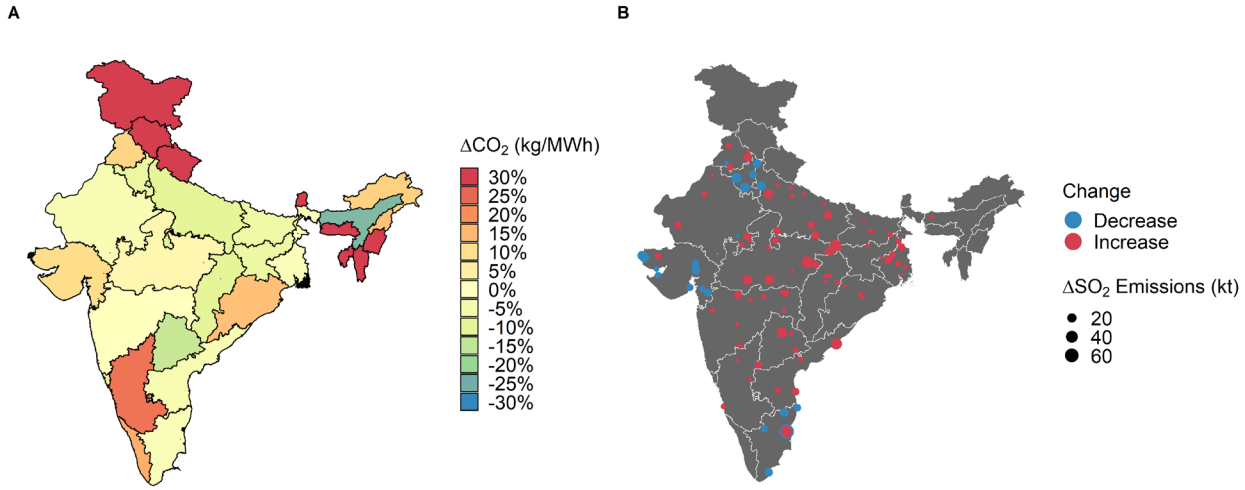

Figure 16
(A) Changes in average annual emission factors by state for regional dispatch (B) Change in SO_2 emissions induced from regional dispatch.

However, the state-level impacts of this regional pooling produces are disparate (Figure 16a) in terms of emission factors. Of 32 states, 13 states see decreases in average emission factors with average percentage decrease of 9%, and 19 states see increases with an average percentage increase of 87% with the highest increases for states with the lowest emission factors in the base case (e.g. Jammu and Kashmir, Himachal

Pradesh, Sikkim). The SO_2 impacts of this simulation show once again SO_2 emissions concentrated in different spatial patterns (Figure 16b). Nationwide SO_2 emissions increase to 6,200 kt in this scenario from the base case scenario, an increase of 2%. The number of plants seeing increases or decreases compared to the base case differ. Of 162 plants, 97 see increases in SO_2 emissions, 31 see decreases, and 34 see no change. In this scenario emissions-weighted standard distance decreases to 740 km from 769 km in the base case. However, clear clusters emerge: plants the furthest away from coal mining areas (e.g. Haryana, Gujarat, and Tamil Nadu) see decreases in SO_2 emissions, while plants closer to mines see increases due to closer plants having lower variable cost with total fuel costs heavily dependent on coal transportation costs.

3.4 Discussion and Conclusions

In this paper we develop and present a reduced-order dispatch model of Indian power generation to assess state-level CO_2 and SO_2 emission impacts of policy interventions. We specifically focus on how policies in the current Indian grid could induce spatial differences in emissions between states in India. We take this approach because Indian power sector operations, capacity, and generation vary by Indian state. Previous analyses have yet to mechanistically quantify which states emit more or less and from which plants, based on the electricity they consume. Increased penetration of renewable energy, the need to control air pollution, and planned market reforms warrant analysis beyond national, aggregate metrics of CO_2 and SO_2 emissions from Indian power generation. We use a flexible, computationally simplified method that is both accessible to researchers and policymakers. We simulate the Indian power sector from September 2017 to August 2018 and evaluate several scenarios: state-level dispatch, sulfur control, CO_2 taxes, and regional dispatch with plants dispatched in order of variable cost. In this section, we discuss the validity of the model by comparing its output to other studies. Then we discuss the CO_2 and SO_2 results and what they reveal about spatial, state-level emissions patterns in the Indian power sector.

Our model scenario of state-level dispatch matches reported generation accurately for most regions and fuel categories. These results qualitatively match Palchak et al. (Palchak et al., 2017a) who report simulations results for 2014; however, they do not report quantitative comparisons of model simulations to observations.

Because the model captures 75-85% of generating capacity (Figure 48) simulated generation is less than reported generation. The model does not capture 100% of generating capacity for two reasons. First, the Government of India data portal we use shows state generation portfolios associated with long-term power purchase agreements (PPA) states have entered with generators. Reporting of these PPAs on the portal varies by state with larger, high demand states reporting better data and not all generators enter PPAs (Ministry of Power, 2020a). Second, states share capacity of interstate generating capacity based on fixed shares from historical demand, but generally up to 85% of a generating unit's capacity is in fixed allocations to states. Capacity not dispatched according to long-term PPAs participate in shorter-term bilateral contracts between states or in short-term spot exchanges. Consequently, our modeling approach and results are consistent with these long-term PPAs that govern 90% of generation in India (Central Electricity Authority, 2020b). This discrepancy also explains where simulations otherwise suggest lack of generation meeting demand; surplus capacity in other states is available to bridge this gap, as has occurred in recent years (see Appendix B for detailed discussion). Furthermore, our approach is similar to Palchak et al. (Palchak et al., 2017a) who do not simulate bilateral exchanges between states. However, our approach differs because 1) our model explicitly considers allocation of centrally owned plants (ISGS) to each respective state, 2) does not consider intrastate, interstate, interregional, or international transmission constraints and 3) the export and import of power with neighboring countries.

Likewise, if we use total CO_2 emissions as a proxy for total generation, our results are consistent with total CO_2 error rates reported by Deetjen and Azevedo (Deetjen and Azevedo, 2019) who develop the reduced-order dispatch method for North American power regions. In this analysis, they find the method reproduces total CO_2 emissions within 20% error, compared to our base case error rate of 22%. Higher data quality and a greater degree of full economic dispatch among North American generators than that of Indian generators yields confidence in the accuracy of this method applied to Indian generators.

To our knowledge, we are the first to present subnational, state-level emission factors for India arising from power sector operations. Our nationwide average emission

factor of 711 kg/MWh largely agree with 2016-2017 estimates of 750 kg/MWh from Soman et al. (Soman et al., 2019), 2019-2020 estimates of 710 kg/MWh from Spencer et al. (Spencer et al., 2020), and 2017-2018 estimates of 820 kg/MWh from Central Electricity Authority (Central Electricity Authority, 2018a). After accounting for uncertainty (Figure 58), our estimated nationwide average CO_2 emission factor ranges between 693 and 721 kg/MWh. Furthermore, total CO_2 emissions estimated from the base case of the model, 820 Mt, are consistent with 920 Mt reported by Central Electricity Authority (Central Electricity Authority, 2018a), more so after accounting for the gap in capacity coverage as described above, which is more likely to be coal-based. In addition to this capacity coverage gap, differences in estimated emission factor and total emissions mainly arise from assumptions about CO_2 emission per unit heat in for coal power stations. Central Electricity Authority (Central Electricity Authority, 2018a) assumes 90 g CO_2/MJ coal with 98% carbon oxidation. This analysis assumes 82 g CO_2/MJ with a 95% oxidation factor based off production-weighted average composition and energy density of domestic Indian coal from Srinivasan et al. (Srinivasan et al., 2018) and Ministry of Coal (Ministry of Coal, 2018).

Minimal interregional electricity exchanges (Palchak et al., 2017a) mean calculation of average annual emission factors at the regional (North, South, East, West, Northeast) level is possible using reported generation and emission factors. However, the lack of easily accessible generation shares for interstate generators mean calculating consumption-based emission factors at the state-level is difficult without some mechanistic understanding of interstate electricity transfers. Our results are consistent with Ryan et al. (Ryan et al., 2016) and de Chalendar et al. (de Chalendar et al., 2019) who both show for the United States that emission factors vary by whether they incorporate electricity exchange across geographic boundaries. Moreover Ryan et al. (Ryan et al., 2016) argue with appropriate uncertainty analysis mechanistic methods such as dispatch models can provide policy-relevant estimates of emission factors not possible with empirical methods using historical data.

Consequently, using generators located with geographic boundaries of states will yield inaccurate results. As seen in Figure 13d, while for some states with the largest demands such as Maharashtra, Tamil Nadu, or Gujarat the difference between

consumption-based and production-based emission factors is less than ±10%, for other states with large demands such as Karnataka or Uttar Pradesh, the difference can be excess of ±10-20%. The difference is most pronounced in states with smaller demand which are more likely to import electricity from neighboring states. This increases their consumption-based emission factors over their production-based emission factors, e.g. Himalayan or Northeastern states. State-level consumption-based emission factors here provide more detailed, accurate information for policy analyses than both national-level emission factors and regional-level factors.

This analysis furthermore quantifies and defines the spatial CO_2 and SO_2 impacts from policy interventions in the current Indian power sector: (1) minimum sulfur control to meet current Indian regulations (2) increasing carbon taxes (3) regionally coordinated dispatch instead of at the state-level. Our results show that despite quite similar aggregate CO_2 emissions and fuel-generation mixes in each scenario compared to the base case (Figure 11), spatial CO_2 and SO_2 patterns differ between scenarios.

For sulfur control, we assume implementation of two control technology options, dry limestone injection or wet flue gas desulfurization, from Srinivasan et al. (Srinivasan et al., 2018), which analyzes an entire suite of possible control technologies. Our base case sulfur emissions estimates (6,100 kt), sulfur control scenario emission (1,300 kt), the percentage reduction (79%), and coal generation-weighted emission factor changes (7.0 kg/MWh to 1.5 kg/MWh) are consistent with previous analyses of sulfur control at Indian power stations. Srinivasan (Srinivasan et al., 2018) report 95% reductions to 650 kt with SO_2 emission factors decreasing from 7.9 kg/MWh to 0.4 kg/MWh with more stringent control under a wider range of control technologies. Likewise previous analyses estimating total SO_2 emissions from the Indian power sector range from 3,500-10,100 kt (Guttikunda and Jawahar, 2018; Li et al., 2017a; Lu et al., 2013a; Oberschelp et al., 2019; Tong et al., 2018). While the capital costs of control technology differ, Srinivasan et al. (Srinivasan et al., 2018) report similar variable costs of operation across all sulfur control technologies analyzed. Consequently, under these assumptions, results from the sulfur control case are less sensitive to the choice of technology than to simply the presence of any technology at a given generator. Our results show most plants see minimal changes in PLF from implementation of sulfur

control, but PLF changes can guide capital investment decisions. Specifically, for plants that see more than 5% decreases in PLF, capital costs may exceed the required PLF to recoup these costs during plant operation. It remains to be seen if Indian regulators allow a pass-through of such costs even in lowered PLF cases. This may impact which plants ultimately do or do not undergo sulfur control installation (Ramanathan et al., 2020). Moreover, we assume all plants implement sulfur control. If policymakers target specific plants in a regional manner, the potential for shifting emissions away from target areas to other areas is possible because of the decentralized manner of power dispatch in India and additional marginal cost of sulfur control, penalizing plants in the dispatch order. Indeed, no clear patterns about plant age, size or location emerge for the plants that do see appreciable changes in PLF in our sulfur control scenario.

According to this analysis, progressively stringent carbon taxes fail to yield significant CO_2 emission reductions in the current Indian grid with fixed generation capacity. As seen in Figure 15a, most states show little changes in CO_2 emissions intensity of their electricity consumption under a CO_2 tax of high $100 per ton. For states that do see changes (e.g. Kerala, Punjab, and Northeastern states), increases in CO_2 compared to the base case scenario occur due to previously expensive gas plants become cheaper than coal plants under a tax. On average in this dispatch analysis, the tax required on a coal generator to achieve parity in variable cost with a gas generator is approximately $66/ton. Consequently, in the current Indian grid, to displace coal generation with gas generation, either a tax imposed must increase to this value, the average variable cost of gas must decrease, or the average cost of coal must increase. Our analysis yields evidence of this increased role of gas generation in Figure 11 and Figure 15b, where we see both an increase in gas generation and a shift in SO_2 emissions from 95 plants where emissions decrease to 47 plants where emissions increase. This decrease in the spatial variability of possible SO_2 emissions shows clear policy relevance because locations of power plant SO_2 emissions impact costs associated with ambient $PM_{2.5}$ (Cropper et al., 2019) as opposed to CO_2, where location of emissions is largely irrelevant to damages, but not control efforts.

Regionally coordinated dispatch slightly increases, approximately 3% and 2%, both SO_2 and CO_2 emissions, respectively, from the Indian power sector with changes

in the spatial patterns of SO_2 emissions. This behavior is consistent with Kumar et al. (Kumar et al., 2020) who find a 10% difference in cost and emissions minimizing scenarios for nationwide dispatch in India. However, changes in state-level emission factors vary as expected by state, especially for states with the lowest emission factors in the base case. Regionally coordinated dispatch furthermore shifts the spatial patterns of SO_2 emissions by shifting emissions from distant plants to plants closer to eastern coal mining regions in Chhattisgarh, Odisha, Jharkhand, Bihar, and West Bengal. Likewise, SO_2 emissions become more spatially disperse with the number plants seeing SO_2 emission increases greater than those seeing decreases. This behavior is consistent with findings from Kamboj and Tongia (Kamboj and Tongia, 2018) who find coal transport costs to predominantly determine the variable cost of electricity for Indian power stations. We use coal transport costs from Kamboj and Tongia (Kamboj and Tongia, 2018). Pooled dispatch across state lines penalizes plants in states with the highest transport costs, e.g. Gujarat, Haryana, and Tamil Nadu. Coupled with increased CO_2 and SO_2 emissions this suggests that in general regionally coordinated dispatch shifts generation to plants in coal-mining areas with lower transport costs. These plants can be less efficient, more polluting than those further away, often a function of age.

We recognize limitations with our estimates of near-term, policy-induced spatial, state-level emissions differences, which derive from the current capacity in the Indian electricity sector. By focusing on the near-term, as opposed to longer-term or future, our results highlight current spatial differences. Of the policy interventions we evaluate, the carbon tax is most sensitive to our assumption of a fixed set of available generation capacity. A carbon tax would likely spur future investment in lower carbon generation capacity in India, lowering both electricity GHG and sulfur emissions over time. Moreover, the other policy scenarios including those we evaluate, sulfur control and regional dispatch, could influence capacity expansion to change the future mix of available generation capacity. However, we hypothesize that spatial, state-level patterns our results illustrate may qualitatively apply to a future Indian grid. Spencer et al (Spencer et al., 2020) find with varying scenarios of increasing renewable generation in the 2030 Indian grid, coal generation could still form at least 50% of national generation, with percentages of hydro and gas generation staying at similar values in 2030 as they

do now. Consequently, with coal potentially playing a significant role in future Indian generation, our results can serve as a basis to test this hypothesis. Future analysis will need to spatially analyze emissions from deploying similar dispatch modeling to hypothetical future Indian grids.

In sum, this analysis presents a reduced-order dispatch model of Indian power generation capable of providing insight into the CO_2 and SO_2 emissions impacts of policy interventions in the current Indian power sector. We quantify the average annual consumption-based CO_2 emission factors of Indian states which provides more detail than regional or national emission factors. Furthermore, these consumption-based factors are different than production-based factors calculated with reported generation and plants located within political boundaries. Implementation of sulfur control to meet upcoming regulations yields evidence that small fraction of plants will see their PLFs change; however, region-focused dispatch coupled with decentralized dispatch in India yield the possibility of SO_2 emissions shifting to other locations. Differences between the average variable cost of coal and the average variable cost of gas along with insufficient gas capacity to displace coal capacity make the current Indian power system insensitive to progressively higher carbon taxes. However, such taxes induce changes in the spatial pattern of SO_2 emissions by decreasing emissions in more plants than those plants seeing increases. This pattern of changes in SO_2 emission patterns reverses for regionally coordinated dispatch versus state-level dispatch with cheaper, less efficient plants near coal mining generating more. We acknowledge limitations with our approach, i.e. mainly that our conclusions apply to today's Indian grid. However, future word may evaluate whether these state-level, spatial emissions patterns hold in a future Indian grid where coal generation will likely still form a large fraction despite increased renewable generation. Our analysis shows that policies that have modest or negligible emissions impacts at the aggregate, national level nonetheless have disparate, state-level, spatial emissions impacts.

4 $PM_{2.5}$ mortality burden of power generation in India under current and future policies

4.1 Introduction

India is the world's third largest emitter of greenhouse gases (GHG) (BP, 2020; Carbon Brief, 2019; World Resources Institute, 2019), with 40% of its emissions coming from coal-dominated power generation(Mohan et al., 2019). Likewise, largely uncontrolled emissions of conventional air pollutants (CAP) sulfur dioxide (SO_2) and nitrogen oxides (NO_X) from Indian power generation contribute to poor ambient air quality in the country. Between 7-21% of the estimated 1.1 million premature deaths in Indian associated with $PM_{2.5}$, solid or liquid particles suspended in the atmosphere, come from power generation (Apte and Pant, 2019; Conibear et al., 2018; Gao et al., 2018; GBD MAPS Working Group, 2018; Guo et al., 2018; Guttikunda and Jawahar, 2014, 2018; Lelieveld et al., 2015). With increasing economic growth, power generation remains a source of GHGs and CAPs poised for growth and consequently control policies (Peng et al., 2020; Venkataraman et al., 2018). The Government of India has targets to increase zero-emission generation to 40% of all power capacity by 2030 (Government of India, 2015) and announced stricter limits on SO_2 and NO_X emissions in 2015.(Ministry of Environment Forest and Climate Change, 2015) Consequently, climate and air pollution control policies for the Indian power sector remain an active area of research due to a sector in flux.

Previous efforts to quantify the premature mortality from Indian power generation under current and future policies largely pair simulations of air quality models with exposure-response functions and mortality rates. Cropper et al., (2021) estimate approximately 78,000 deaths (~9.2% of all $PM_{2.5}$ premature mortality) associated with Indian coal power plants in 2018 with most deaths in the most populous states of Uttar Pradesh and Maharashtra. They estimate annual mortality increases to 112,000 deaths from planned construction of new coal power stations. Gao et al., (2018) likewise estimate 270,000 (~33%) annual deaths associated with Indian power generation, with most deaths in states in the Indo-Gangetic Plain where exposure levels are the highest. Peng et al., (2020) quantify tradeoffs to find failing to enforce emission control regulations at Indian power stations results in 2.5x more deaths in 2040 than failing to

enforce zero-emission energy targets. Overall previous analyses quantifying the impact of power generation have found the sector to be a large contributing sector that will remain important as India meets multiple objectives of development, industrialization, and decarbonization (International Energy Agency, 2021).

However, no study has analyzed control policies within Indian power sector operations accounting for the exchange of electricity between states. Both central government and state governments have federal jurisdiction over the Indian power sector. Moreover, each state individually contracts and schedules generating capacity to meet demand within their borders. Consequently, not only is there state-to-state heterogeneity in power generation impacts on ambient air quality as previous analyses quantify, but also fuel mixes and emissions from the electricity consumed by each state (Power System Operation Corporation Limited, 2020; Safiullah et al., 2017). To analyze premature mortality of policies such as carbon taxes or further integration of wholesale power markets between states, a representative accounting of power sector operations and associated emissions is needed. Likewise quantifying the $PM_{2.5}$ premature mortality embedded in power *consumed* by each state in addition to power *produced* by each state can inform emissions reductions policies at the state-level because states choose which plants where will generate electricity to meet demand.

Here, we feed emissions estimates from reduced-form model of Indian power generation as inputs into a reduced-form air quality model to 1) quantify the $PM_{2.5}$ premature mortality associated with power produce and consumed by each Indian state in 2017-2018 and 2) analyze the impact on $PM_{2.5}$ premature mortality of emission control, market integration, and carbon tax policies in the Indian power sector. Our approach improves upon previous work by accounting for electricity exchanged between states to understand the import and export of air pollution between states as well as power sector operations.

4.2 Methods

We use a reduced-form power sector model and a reduced-form air quality model to quantify $PM_{2.5}$ premature mortality from Indian power generation under current (2017-2018) and future policies. The first, a reduced-form dispatch (production-cost) model estimates the hourly dispatch and generation of power generators in each Indian

state based on electricity demand (Sengupta et al., 2021). States are primarily responsible for procuring and dispatching power based on demand in India, with some regional coordination (Safiullah et al., 2017). For each state, the model orders contracted supply by variable cost from publicly available data (Ministry of Power, 2020a). Then it determines the generating units called to generate by matching the cumulative supply to reported demand, net renewable generation (Central Electricity Authority, 2018c; Energy Analytics Lab, 2019; Power System Operation Corporation Limited, 2018). Output includes explicit hourly generation values for units tied to consumption by each state. We pair simulated generation with estimated emission factors (Oberschelp et al., 2019; Srinivasan et al., 2018) to estimate SO_2, NO_X, and $PM_{2.5}$ emissions from each generating unit. We simulate power generation from September 2017 to August 2018. We do not simulate transmission constraints, but implicitly simulate interstate exchange of electricity with fractional capacity allocations of interstate generating units, consistent with current Indian power sector operations (Ministry of Power, 2020a; Srinivasan et al., 2018). We direct readers section 3.2 and cited papers for further details about the reduced-form dispatch model and estimation of emissions.

We feed our estimates of SO_2, NO_X, and primary $PM_{2.5}$ emissions into a reduced-form air quality model, the Intervention Model for Air Pollution (InMAP) (Gilmore et al., 2019; Tessum et al., 2015, 2017). Previous analyses have used this model to evaluate mortality associated with power sector emissions in the United States (Thind et al., 2019) We use the global version of the model which uses outputs of the GEOS-Chem chemical transport model to approximate steady-state ambient $PM_{2.5}$ concentrations (Thakrar et al., 2021). The reduced-form model uses simplified parametrizations of advection, diffusion, deposition, and chemical reactions based on underlying GEOS-Chem simulations (Hammer et al., 2020). Grid definitions and emissions and meteorology inputs for the underlying GEOS-Chem simulations follow Hammer et al., (2020) who largely use Emissions Database for Global Atmospheric Research (EDGAR) (Crippa et al., 2016) and Modern-era Retrospective Analysis for Research and Applications (MERRA-2) (Gelaro et al., 2017) emissions inputs. However, Global InMAP deviates from this setup by simulating with variable grid cell size based on 0.01º

gridded 2020 global population estimates, increasing spatial resolution (smaller cells) in areas of higher population and population density. Grid cell size varies between 5º × 4º (~500 km at equator) in remote areas to 0.04° × 0.03° (~4 km at equator) in urban areas. Global InMAP takes annual emissions estimates of $PM_{2.5}$ precursors gases to directly estimate annual-average ambient $PM_{2.5}$ concentrations chemical resolved by sulfate, nitrate, ammonium, elemental carbon, and secondary organic components.

We use a similar risk-exposure relationship used in previous analyses (Apte et al., 2015; GBD MAPS Working Group, 2018) to quantify premature mortality attributable ($m_{i,j,power}$) to the power sector (annual deaths from power sector $PM_{2.5}$) and total premature mortality ($m_{i,j,}$ annual deaths from all source $PM_{2.5}$) for each disease endpoint *j* (e.g. heart disease, lung cancer, etc) in each grid cell *i* simulated by InMAP:

$$(1)\ m_{i,j,power} = \frac{PM_{2.5,i,power}}{PM_{2.5,i}} \frac{I_{s,j}}{\overline{RR}_{s,j}} P_i \left[RR_{i,j}\left(PM_{2.5,i}\right) - 1\right]$$

$$(2)\ m_{i,j} = \frac{I_{s,j}}{\overline{RR}_{s,j}} P_i \left[RR_{i,j}\left(PM_{2.5,i}\right) - 1\right]$$

$$(3)\ \overline{RR}_{s,j} = \frac{\sum_{i=1}^{N} P_i \times RR_{i,j}\left(PM_{2.5,i}\right)}{\sum_{i=1}^{N} P_i}$$

Here $I_{s,j}$ is the mortality rate for each disease endpoint (annual deaths per capita from each $PM_{2.5}$-related disease) in each Indian state, *s*, P_i refers to the population in each grid cell *i*, and $RR_{i,j}$ refers to the relative risk of mortality from each disease in each grid cell as a function of annual average concentrations of $PM_{2.5,i}$. We omit subscripts for sex and age for clarity, but all variables except for $PM_{2.5,i}$ vary by sex and age as well. We scale the mortality rates $I_{s,j}$ by a population-weighted average relative risk, $\overline{RR}_{s,j}$ because estimated mortality rates vary by state and not grid cell. However, reported mortality rates for each state do vary by location within each state because mortality rates account for deaths associated with and without $PM_{2.5}$ exposure. Consequently, to account for this variability, we scale mortality rates by a weighted average relative risk of $PM_{2.5}$ exposure (Apte et al., 2015; GBD MAPS Working Group, 2018). This approach differs from several previous analyses (Gao et al., 2018; Guo et al., 2018; Peng et al., 2020) which scale mortality rates by relative risk in each grid cell and not a weighted average of grid cells in each state. Furthermore, we direct readers to previous analyses that derive this fractional attribution approach that quantifies the $PM_{2.5}$ mortality

attributable to power generation by scaling total $PM_{2.5}$ mortality by the portion of $PM_{2.5}$ exposure attributable to power generation (Gao et al., 2018; GBD MAPS Working Group, 2018; Health Effects Institute, 2016).

We use InMAP estimates for the absolute contribution of $PM_{2.5}$ from the power sector, $PM_{2.5,i,power}$ and population, P_i. Because global InMAP takes emissions estimates as perturbations on top of the emissions in its underlying GEOS-Chem simulations, we assume the model's estimates of annual average ambient $PM_{2.5}$ concentrations represent the absolute contribution of $PM_{2.5}$ from the power sector. To account for other sources in $PM_{2.5}$ exposure we use 2018 global grided $PM_{2.5}$ estimates at 0.01º resolution from Hammer et al., (2020) aggregated to the InMAP modeling grid as inputs for $PM_{2.5,i}$. These estimates represent $PM_{2.5}$ from all sources harmonized from satellite measurements, model estimates, and ground measurements. We note the underlying GEOS-Chem simulations are the same in both InMAP and global gridded $PM_{2.5}$ estimates (Thakrar et al., 2021). We obtain mortality rates, I_i, and relative risk curves, $RR(PM_{2.5,i})$ from the Global Burden of Disease (GBD) for six disease endpoints, j: ischemic heart disease, stroke, chronic obstructive pulmonary disease (COPD), lower respiratory infections, lung cancer, and type 2 diabetes. GBD reports relative risk estimates with high and low uncertainty bounds (Global Burden of Disease Collaborative Network, 2021; Indian Council of Medical Research et al., 2017; Pandey et al., 2021). Mortality rates are specific to Indian states split by age (5-year intervals from 0-95+ years), sex (male and female), and disease endpoint (Indian Council of Medical Research et al., 2017).

We run the model in a business as usual (BAU), 2017-2018 case where equation 1 represents the $PM_{2.5}$ mortality attributable to power generation. We also run InMAP to estimate the mortality associated with each Indian state by running the model for each state with only the state's BAU emissions. We take both a (1) a production-oriented view with emissions from plants located within the borders of a state and a (2) consumption-oriented view with emissions from plants supplying power to meet a state's demand. In the latter case, these plants can be within a state or outside a state. We denote the mortality associated with an individual state (production or consumption) as:

$$(3)\ m_{i,j,power,state} = \frac{PM_{2.5,i,power,state}}{PM_{2.5,i}} \frac{I_{s,j}}{\overline{RR}_{s,j}} P_i \left[RR_{i,j}\left(PM_{2.5,i}\right) - 1 \right]$$

Here $PM_{2.5,i,power,state}$ represents the InMAP estimate of $PM_{2.5}$ in a grid cell from the emissions associated with each individual state. Consequently, using equation 3 these simulations quantify the burden of deaths associated either production of electricity within a state or consumption of electricity within a state.

Lastly, we modify inputs to equation 2 to run several policy scenarios (denoted by prime) by modifying total $PM_{2.5}$:

$$(3)\ m'_{i,j} = I_{i,j} P_i \left[1 - \frac{1}{RR\prime_i(PM\prime_{2.5,i})} \right]$$

$$(4)\ PM'_{2.5,i} = PM_{2.5,i} - PM_{2.5,i,power} + PM'_{2.5,i,power}$$

Here $PM_{2.5,i,power}$ are InMAP estimates for BAU power generation $PM_{2.5}$, and $PM_{2.5,i}$ are total PM2.5 exposure estimates from Hammer et al. (2020), $PM'_{2.5,i,power}$ are the InMAP estimates for power generation $PM_{2.5}$ in each scenario, and $m'_{i,j}$ is the total mortality estimate of PM2.5 exposure given changes in exposure from the power generation policy scenario (Hammer et al., 2020). We run a total of eight scenarios across three categories of policies. We refer readers to section 3.2 on the reduced-form model describing each policy scenario in more detail (Sengupta et al., 2021). We first examine sulfur control policies with scenarios quantifying sulfur control to meet current Indian sulfur control regulations and the sulfur control levels with a $35 per metric ton carbon tax. We then examine carbon taxes only at $10, $35, $50, and $100 per metric ton CO_2. Lastly, we examine market integration policies which move away from individual states procuring and dispatching power: dispatching power by geographic region (north, south, east, west, and northeast, see Figure 82), and dispatching power nationally as one market. We estimate the change in mortality, $\Delta m_{i,j,}$ from each policy as:

$$(5)\ \Delta m_{i,j} = m'_{i,j} - m_{i,j}$$

4.3 Results

We show the results of our state-wise attribution of $PM_{2.5}$ premature mortality associated with power generation in India in Figures 17-18. We adopt a similar approach used by (Thind et al., 2019) for attributing electricity generation deaths in the United States. We derive these estimates from our BAU InMAP simulation and

simulations with only BAU emissions associated with power production or consumption in each state. We find that in each grid cell, the sum of the $PM_{2.5}$ estimates of all the state-by-state simulations equals the $PM_{2.5}$ estimate from the BAU simulation, achieving closure with equation 3. We find an annual population-weighted ambient $PM_{2.5}$ concentration of 77 μg m^{-3} and an annual population-weighted fraction attributable to power generation $PM_{2.5}$ concentration of 4.3 μg m^{-3}. In total for 2017-2018, across all grid cells, we estimate that electricity generation is associated with ~71,000 (uncertainty 58,000-82,000) of the annual ~1.1 million (uncertainty 900,000-1.3 million) premature deaths from ambient $PM_{2.5}$ in India. (Figure 61-64). We discuss best estimates without uncertainty ranges for the remaining results presented.

In Figure 17a, we show annual electricity generation deaths from all power generation in India by each state. The data underlying Figure 17a are shown in Figure 64 and Table 5. We find Tamil Nadu in south India to have the highest burden of electricity $PM_{2.5}$ deaths: 18,400 deaths due high sulfur-emitting lignite power plants in the state. This is higher than the next two highest states combined: Maharashtra in western India (8,000 deaths), and West Bengal in eastern India (6,400 deaths). Other large states facing high burdens include Uttar Pradesh (6,100 deaths), Andhra Pradesh (5,200 deaths), and Gujarat (3,800). Small northeastern states (Sikkim, Mizoram, Nagaland, Tripura, Assam, Arunachal Pradesh, Manipur, Meghalaya) and predominantly Himalayan states in north India (Jammu and Kashmir, Himachal Pradesh, Uttarakhand, Delhi, Punjab, and Haryana), face little or no burden from electricity generation deaths (0-700 deaths).

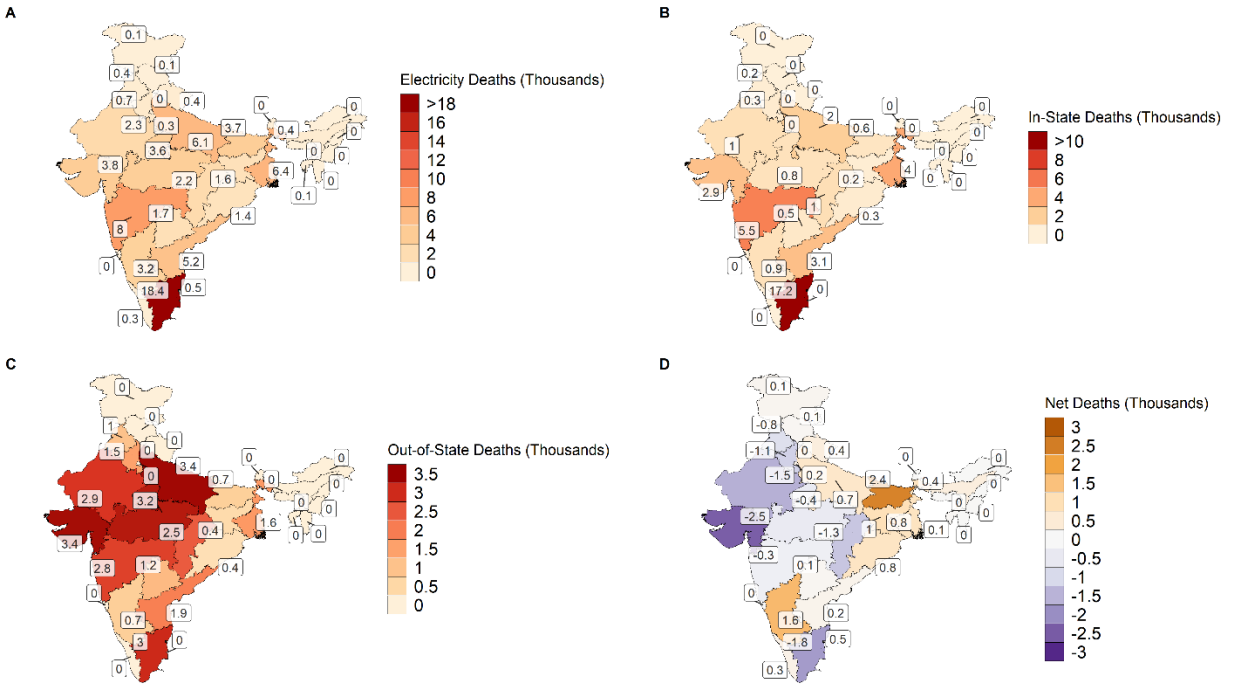

Figure 17
(A) Total $PM_{2.5}$ mortality occurring in a state from all power generation in India. (B) Total attributable $PM_{2.5}$ mortality in each state from power production within that state. (C) Total attributable $PM_{2.5}$ mortality outside each state from power production within that state. (D) Net deaths (A-B-C) in each state associated with power production. Boxed numbers show estimated deaths. Positive numbers mean that a state is a net importer of mortality, and negative numbers mean that a state is a net exporter of mortality to other states.

In Figure 17b, shows annual electricity generation deaths occurring within each state's borders from annual electricity production within that state. Here the highest deaths occur in Tamil Nadu (17,200 deaths) followed by Maharashtra (5,500 deaths), West Bengal (4,000), Andhra Pradesh (3,100 deaths), Gujarat (2,900 deaths), Uttar Pradesh (2,000 deaths), and Chhattisgarh (1,000 deaths). Northeastern states remain relatively unaffected because of few emitting power plants (coal and gas) located within those states. Likewise, north Indian states located in in the Himalayas show low in-state death burdens.

In Figure 17c shows annual electricity generation deaths occurring outside each state's borders from annual electricity production within that state. Here the relative burden of out-of-state deaths differs: Gujarat (3,400 deaths) and Uttar Pradesh (3,400 deaths) both lead in terms of out-of-state deaths from electricity generated within the state. Madhya Pradesh (3,200 deaths), Tamil Nadu (3,000 deaths), Rajasthan (2,900

deaths), Maharashtra (2,800 deaths), Chhattisgarh (2,500 deaths), Andhra Pradesh (1,900 deaths), West Bengal (1,600 deaths), Haryana (1,500 deaths), Telangana (1,200), Punjab (1,000 deaths), and Karnataka (700 deaths) follow them. Once again, northeastern and norther, Himalayan states remain relatively unaffected.

Lastly, Figure 17d shows the unequal mortality burden from electricity production between states in India. To derive these estimates, we first take the mortality burden for each state from all electricity generation in India (Figure 17a) and subtract from it the sum of deaths associated with in-state and out-of-state electricity production for each state (Figure 17b and Figure 17c). If all states shared equal mortality burdens tied to their electricity production, values in Figure 17d would be approximately zero, i.e. the deaths associated with a state's electricity production would be proportional to the state's deaths associated with all electricity generation in India. However, here, distinct spatial patterns emerge, estimates are net negative for states predominately in western, southern, and central India. This means the electricity these states produce is tied to a greater number of deaths than what we would expect if this production were proportional to nationwide electricity deaths ("production death exporters"). That is, the power plants in these states are disproportionately responsible for electricity-associated deaths. For example, electricity production in Gujarat results in 2,500 more total deaths than deaths in Gujarat from overall nationwide, electricity generation. Likewise, other states who produce electricity associated with higher deaths include Tamil Nadu (-1,800 deaths), Rajasthan (-1,500 deaths), Haryana (-1,100 deaths), and Punjab (-800 deaths). Estimates are net positive for states predominately in northern and eastern India, except for one state in the south (Karnataka). This means these states face a disproportionate burden of electricity-associated deaths because they face a higher burden from nationwide electricity-associated deaths than the deaths the deaths associated with electricity produced within these states ("production death importers"). States include Bihar (2,400 deaths), Karnataka (1,600 deaths), Jharkhand (1,000 deaths), West Bengal (800 deaths), Odisha (800 deaths), and Uttar Pradesh (700 deaths).

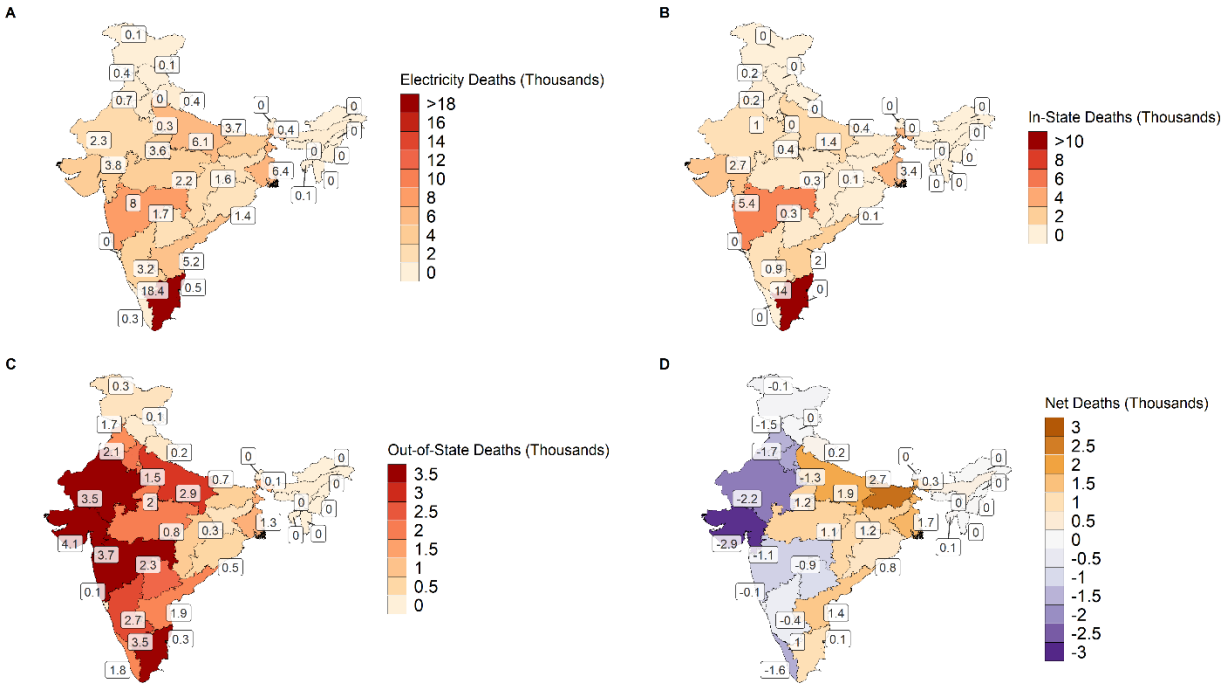

Figure 18
(A) Total attributable $PM_{2.5}$ mortality in each state from all power generation in India. (B) Total attributable $PM_{2.5}$ mortality in each state from power consumption by that state. (C) Total attributable $PM_{2.5}$ mortality outside each state from power consumption by that state. (D) Net deaths (A-B-C) in each state associated with power consumption. Boxed numbers show estimated deaths. Positive numbers mean that a state is a net importer of mortality, and negative numbers mean that a state is a net exporter of mortality to other states.

In an analogous figure to Figure 17, Figure 18b shows annual electricity generation deaths occurring within each state's borders from each respective state's annual power consumption. In Figure 18a, we show the same values as Figure 17a. We present results for each state by consumption because states are responsible for choosing and contracting the plants from which they procure power for their consumers, showing a potential lever for emissions control policies. States can procure power from plants within their borders our outside their borders, so these values incorporate deaths imbedded in electricity imports and exports. Northern, Himalayan states and northeastern states show again the lowest in-state deaths (0-200 deaths). Similar patterns emerge as Figure 18b, with the highest in-state deaths tied to consumption occurring in Tamil Nadu (14,000 deaths), Maharashtra (5,400 deaths), West Bengal (3,400 deaths). However, here Gujarat (2,700 deaths) faces higher in-state deaths than Andhra Pradesh (2,000 deaths) and Uttar Pradesh (1,400).

Figure 18c shows annual electricity generation deaths occurring outside each state's borders from each respective state's annual power consumption. Here clearer geographic patterns emerge where the highest out-of-state deaths occur in western, southern, and northern India, but the lowest out-of-state deaths occur in coal-mining, eastern states. Northeastern areas remain unchanged. Here, the highest out-of-state deaths occur from electricity consumption in Gujarat (4,100 deaths) followed by Maharashtra (3,700 deaths), Tamil Nadu (3,500 deaths), Rajasthan (3,500 deaths), Uttar Pradesh (2,900 deaths), Karnataka (2,600 deaths), and Telangana (2,300 deaths). States in eastern Indian meanwhile see fewer out-of-state deaths: West Bengal (1,300 deaths), Chhattisgarh (800 deaths), Bihar (700 deaths), Odisha (500 deaths), and Jharkhand (300 deaths).

Lastly, Figure 18d shows the unequal mortality burden from electricity consumption between states in India. We derive these estimates in a similar manner as Figure 17d, where we first take the mortality burden for each state from all electricity generation in India (Figure 18a) and subtract from it the sum of deaths associated with in-state and out-of-state electricity consumption for each state (Figure 18b and Figure 18c). Again, if all states shared equal mortality burdens tied to their electricity consumption, values in Figure 18d would be approximately zero, i.e. the deaths associated with a state's electricity consumption would be proportional to the state's deaths associated with all electricity consumption in India. However, here, distinct spatial patterns emerge, estimates are net negative for states predominately in western, southern, and northern India. This means the electricity these states consume is tied to a greater number of deaths than what we would expect if this consumption was proportional to nationwide electricity deaths ("consumption death exporters"). Using Gujarat as an example again, electricity consumption in Gujarat results in 2,900 more total deaths than deaths in Gujarat from overall nationwide, electricity consumption. Likewise, other states who consume electricity associated with higher deaths include Rajasthan (-2,200 deaths), Haryana (-1,700 deaths), Kerala, (-1,600 deaths), Punjab (-1,500 deaths), and Delhi (-1,300 deaths). Estimates are net positive for states predominately in eastern and central India. This means the electricity these states consume is tied to a fewer number of deaths than what we would expect if this

consumption was proportional to nationwide electricity deaths (“consumption death importers”). That is, these states face a disproportionate burden of deaths associated with electricity consumption. States include Bihar (2,700 deaths), Uttar Pradesh (1,900 deaths), West Bengal (1,700 deaths), Andhra Pradesh (1,400 deaths), Madhya Pradesh (1,200 deaths), Jharkhand (1,200 deaths), and Chhattisgarh (1,100 deaths).

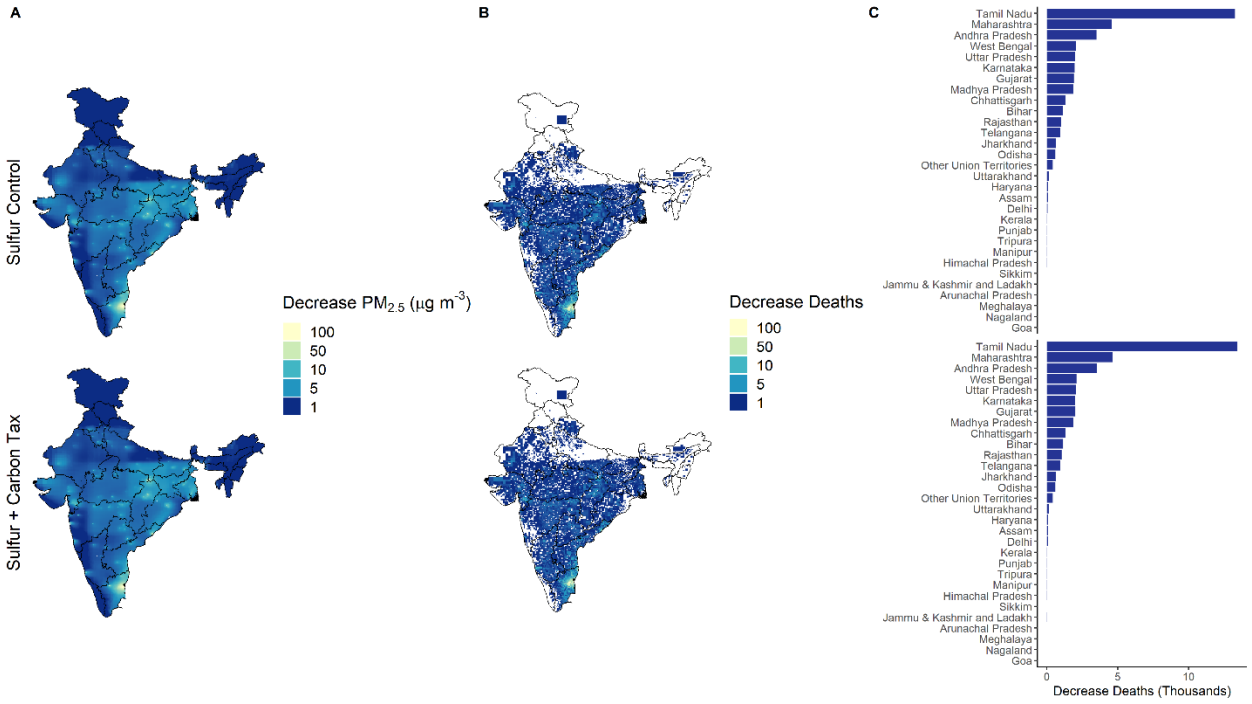

Figure 19
(A) Estimated decreases in $PM_{2.5}$ concentration, (B) decreases in associated mortality and (C) state-wise breakdown of mortality reductions from sulfur control (top panel) and sulfur control and $35/ton carbon tax (bottom panel) policy scenarios.

Figure 19 shows the $PM_{2.5}$ decreases and associated mortality reductions from adopting widespread sulfur control policies in India. The top panel shows results for adopting minimal sulfur control to meet announced, but unimplemented, SO_2 control regulations in India. Figure 14 shows the SO_2 emissions decreases that result in these decreases. We discuss these results in detail as results for SO_2 control regulations with a $35/ton carbon tax (Figure 19, bottom panel) result in very similar mortality reductions as the scenario without the carbon tax. The first column (Figure 19a, top) shows the decrease in estimated ambient $PM_{2.5}$ from implementing sulfur control regulations predicted by InMAP. The estimated annual population-weighted average ambient $PM_{2.5}$ concentration decreases to 73 µg m-3. We see widespread decreases of 1-5 µg m^{-3}

throughout India with highest decreases around plants. In areas around plants, InMAP estimates decreases of between 50-100 μg m^{-3}. Sulfur control causes sulfate $PM_{2.5}$ to decrease, which results in reductions in total annual $PM_{2.5}$ exposure (Figure 19b, top). Consequently, total annual $PM_{2.5}$ mortality decreases ($\sum_j \sum_i \Delta m_{i,j}$) by approximately 42,000 fewer deaths per year. These mortality reductions occur throughout India except in parts of north India, northeastern India, and southwestern India. When looking at the state-wise breakdown of where these reductions (Figure 19c, top), we see Tamil Nadu leads with the most mortality reductions (13,000 deaths), followed by Maharashtra (4,500 deaths), Andhra Pradesh (3,500 deaths), West Bengal (2,100 deaths), Uttar Pradesh (2,000 deaths), Karnataka (2,000 deaths), Gujarat (1,900 deaths), Madhya Pradesh (1,800 deaths), and Chhattisgarh (1,300 deaths).

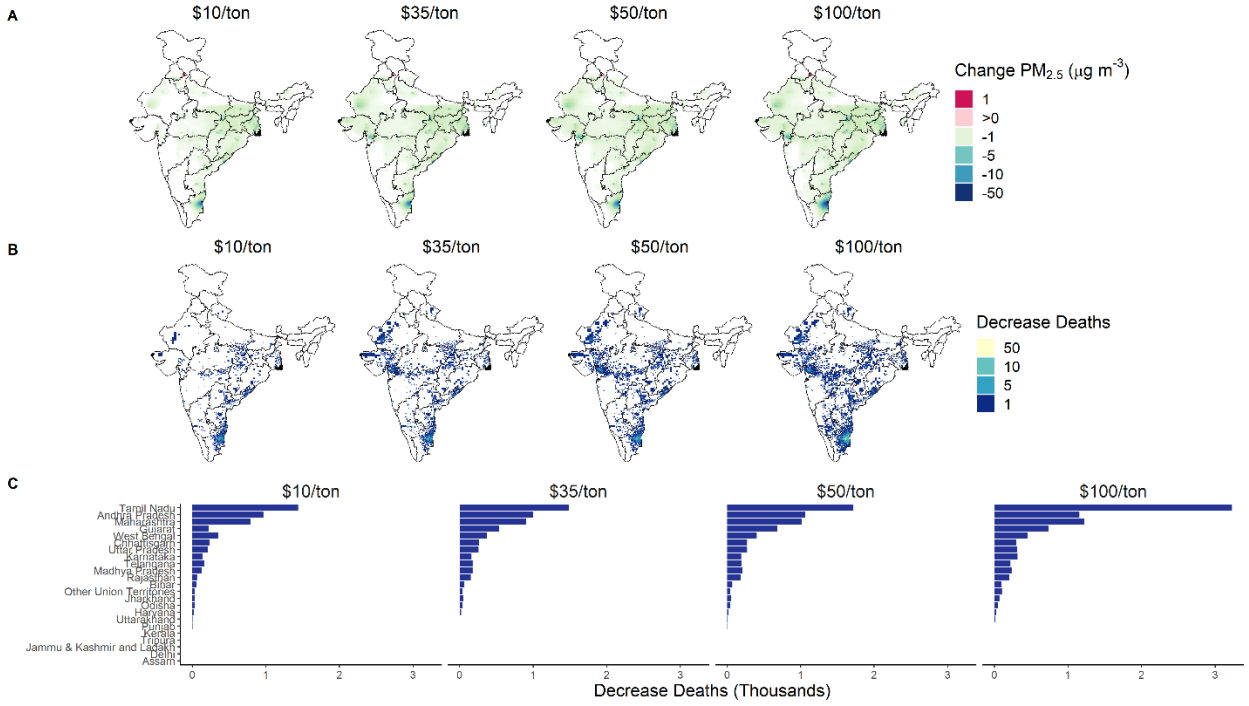

Figure 20
(A) Estimated decreases in $PM_{2.5}$ concentration, (B) decreases in associated mortality, and (C) state-wise breakdown of mortality reductions from progressively increasing carbon taxes on power generation in India. For deaths, only areas that see changes in mortality shown.

Figure 20 shows the $PM_{2.5}$ decreases and associated mortality reductions from imposing carbon taxes from $10/ton to $100/ton on power generation in India. Figure 20a shows the decreases in annual ambient $PM_{2.5}$ concentration from InMAP. Figure 60 and Figure 15 shows the locations of emissions increases and decreases that result in

these concentration changes. Under carbon taxes, emissions decrease at a greater number of less efficient plants and increase at a fewer number of more efficient plants. Higher carbon taxes concentrate emissions further. Consequently, estimated annual population-weighted average ambient $PM_{2.5}$ concentration stays about the same at 75-76 μg m^{-3} in each of these scenarios, with higher carbon taxes decreasing this average. However, we see on average a decrease of ~1 μg m^{-3} predicted by InMAP due to the emissions decreases at plants spread throughout the country. Only an isolated area in north India sees an increase of ~1 μg m^{-3} (Figure 20a). These concentration decreases translate to reductions in annual mortality in several areas throughout the country (Figure 20b). For the $10/ton tax, total annual mortality decreases by approximately 9,400 deaths per year. Decrease in annual mortality number 11,000 deaths, 12,000 deaths, and 14,000 deaths for the $35/ton, $50/ton, and $100/ton taxes, respectively. Several states see the bulk of these decreases in mortality under all carbon taxes (Figure 20c). Here, Tamil Nadu sees the most decreases (1,400-3,200 annual deaths), followed by Andhra Pradesh (1,000-1,200 deaths), Maharashtra (800-1,200 deaths), Gujarat (200-700 deaths), and Chhattisgarh (200-300 deaths).

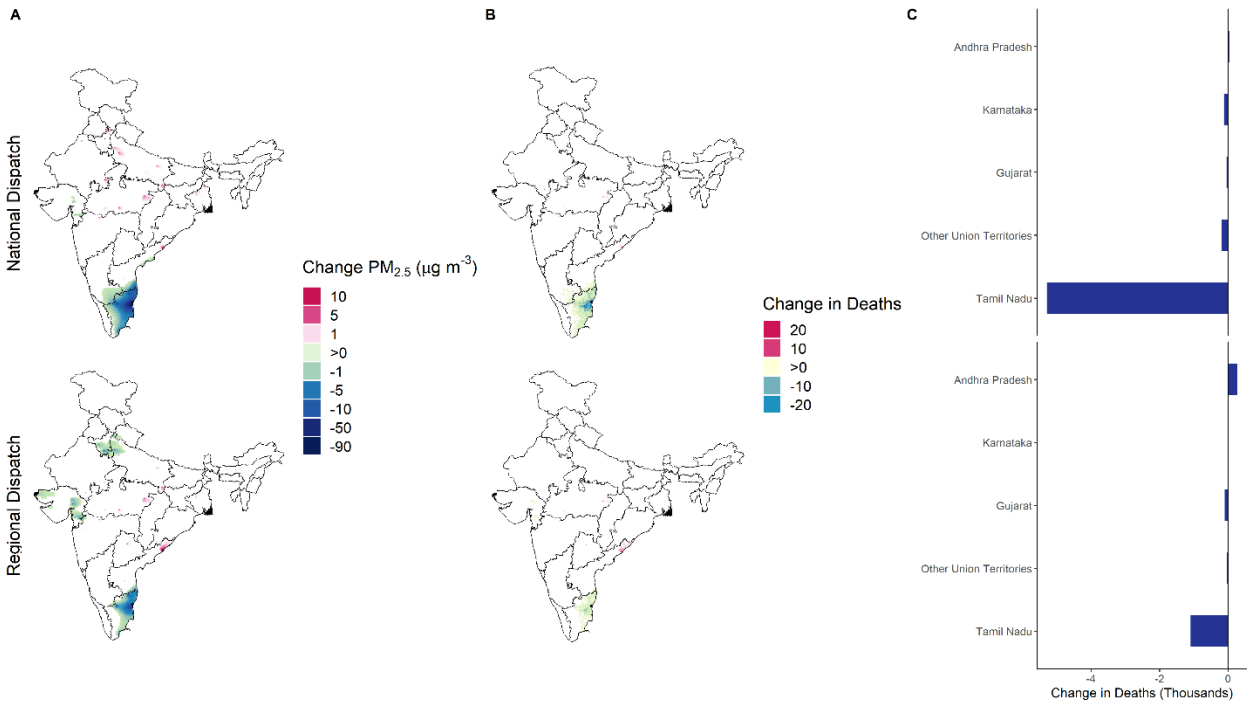

Figure 21
(A) Estimated decreases in $PM_{2.5}$ concentration, (B) decreases in associated mortality, and (C) state-wise

breakdown of mortality reductions from market reform policy scenarios. For deaths, only areas that see changes in mortality shown.

Figure 21 shows the $PM_{2.5}$ decreases and associated mortality reductions from reforming dispatch markets in India. Further integrating dispatch markets in India shifts generation and emissions from plants furthest away in southern, western and northern India to plants in eastern India closes to coal mining areas. The top panel of Figure 21a shows the resulting changes in $PM_{2.5}$ concentration and mortality when all power plants in India participate in a single dispatch order to meet national power demand. Under national dispatch, estimated annual nationwide population-weighted average ambient $PM_{2.5}$ concentration stays approximately the same as state-wise dispatch in current Indian power sector operations at 77 μg m^{-3} The greatest decreases in concentration happen in southern India in Tamil Nadu from emissions reductions at a cluster of high sulfur-emitting lignite power plants. Consequently, under national dispatch which moves power generation away from this cluster, estimated annual ambient $PM_{2.5}$ concentrations decrease by up to 90 μg m^{-3} in southern India. Increases in estimate ambient $PM_{2.5}$ concentration occur in certain areas of north India around plants by up to 14 μg m^{-3}. Translating these concentration changes to changes in mortality, we estimate national dispatch results in approximately 6,900 fewer net total annual deaths compared to state-wise-dispatch (Figure 21b, top). Almost all these mortality reductions occur in Tamil Nadu with negligible mortality increases in Andhra Pradesh from increased concentrations (Figure 21c, top).

The bottom panel of Figure 21 shows estimate changes in $PM_{2.5}$ concentrations and associated mortalities from regional dispatch, i.e. plants participate in merit order by geographic region (north, south, east, west, northeast) instead by each state. Here we see concentration decreases in three different clusters in northern, western, and southern India (Figure 21a, bottom). Figure 16 shows the locations of emissions increases and decreases that result in these concentration changes. Like national dispatch, we see the highest decrease in southern India in Tamil Nadu, but here concentration decreases are at most approximately 32 μg m^{-3}. Other decreases occur in western India in Gujarat, where concentrations decrease by up to 11 μg m^{-3} and in northern India in Haryana, Delhi, and Uttar Pradesh, where concentrations decrease by

up to 12 μg m^{-3}. Concentration increases occur in isolated areas around plants in central and eastern India with the highest increases (32 μg m^{-3}) happening near a coastal plant in Andhra Pradesh. These concentration changes largely yield mostly mortality reductions in southern and western India (Figure 21b bottom panel). The total net mortality reductions from regional dispatch are 1,800 deaths per year. Like the national dispatch scenario, Tamil Nadu sees the most mortality reductions (1,700 deaths) followed by Gujarat (200 deaths). Andhra Pradesh meanwhile sees slight mortality increases of 500 deaths from the increased concentrations at the coastal plant.

4.4 Discussion and Conclusions

In this work we use InMAP, a reduced-complexity air quality model, to evaluate annual $PM_{2.5}$ mortalities associated with electricity production and consumption in India. We evaluate electricity associated mortalities by each Indian state because states are largely responsible for scheduling and dispatching power in India. Moreover, under a federal system, states in India along with the central government share overlapping jurisdiction over power sector policies. Consequently, considerable heterogeneity exists between Indian states in terms of electricity demand, generation fuel mix, and emissions of greenhouse gases and $PM_{2.5}$ precursors. We evaluate this heterogeneity by further resolving the premature mortality embedded in the production and consumption of electricity in each state. Furthermore, we test several policy scenarios including emissions control, carbon taxes and market integration to understand how changes in power sector operations in the current Indian grid affect ambient $PM_{2.5}$ concentrations and associated mortality.

Overall, our baseline 2017-2018 estimates of $PM_{2.5}$ mortality attributable to power generation are consistent with previous estimates. We find approximately 71,000 $PM_{2.5}$ deaths (~6.5% of total $PM_{2.5}$ mortality) attributable to power generation. Most recent 2018 estimates from Cropper et al. (2021) find approximately 113,000 $PM_{2.5}$ deaths (~9.1% of total $PM_{2.5}$ mortality) attributable to the power sector in India, assuming exposure to only outdoor, ambient $PM_{2.5}$ as we have done here. Previous analyses quantifying $PM_{2.5}$ mortality attributable to power generation in India since 2011 find best estimates of 71,000-270,000 deaths with most analyses finding ~100,000 deaths (Apte and Pant, 2019; Conibear et al., 2018; Gao et al., 2018; GBD MAPS Working Group,

2018; Guo et al., 2018; Guttikunda and Jawahar, 2014, 2018; Lelieveld et al., 2015) Estimates differ due to differences in assumptions of emission estimates (from power and non-power sectors), $PM_{2.5}$ exposure estimates predicted by chemical transport models at varying spatial resolutions, and risk-exposure relationships.

Likewise our state wise mortality estimates attributable to power generation are fairly consistent with those from Cropper et al., (2021). Differences arise because we assume higher total emissions from power generation and higher baseline total $PM_{2.5}$ exposure from Hammer et al., (2020) which on balance decrease the fraction of total $PM_{2.5}$ mortality attributable to power generation. Our state-wise breakdowns of total $PM_{2.5}$ mortality from all sources are in closer agreement to those reported Cropper et al. (2021) because despite differences in total $PM_{2.5}$ exposure, both our estimates produce similar relative risk values, i.e. both our analyses end up the on flatter part of the exposure curve at higher concentrations (Global Burden of Disease Collaborative Network, 2021). The largest deviation in state-wise estimates occur in Tamil Nadu, which we estimate to have very high $PM_{2.5}$ concentrations due to a cluster of high sulfur-emitting lignite power plants. While other modeling and empirical, satellite-based analyses have identified this SO_2 emission hotspot (Fioletov et al., 2016; Guo et al., 2018; Li et al., 2017a; Lu et al., 2013b; Srinivasan et al., 2018), our baseline total $PM_{2.5}$ estimates Hammer et al., (2020) do not show this cluster. Consequently, our estimates likely represent an upper bound on impacts from this cluster, and we hypothesize that variability in spatial resolution along with variability in emissions estimates likely drive discrepancies between different analyses. Previous nationwide analyses for the United States quantifying air pollution damages from multiple sectors using chemical transport models have shown the impact of spatial resolution on mortality and damage estimate (Goodkind et al., 2019; Paolella et al., 2018) Consequently this warrants further scrutiny and investigation for India because it is unclear how varying assumptions on source emissions, chemical transport model spatial resolution, and risk-exposure affect the range of estimates for $PM_{2.5}$ mortality source attribution.

Our analysis of net deaths associated with electricity production and consumption in India further show spatial inequities among states with respect to climate and air pollution impacts. In the case of both production and consumption, we

see states in eastern India predominately coal-mining areas with plants that provide the cheapest power near mines (Kamboj and Tongia, 2018) disproportionately face the burden of $PM_{2.5}$ mortality from electricity in India. This difference becomes even more prominent in the consumption case where we see the states that are net death exporters are also those with the highest amounts of renewable capacity and generation (e.g. Gujarat, Rajasthan, Karnataka, Maharashtra, and Telangana). This suggests that as these states have adopted more renewable generation, they have shifted their emitting coal generation to predominately eastern areas, shifting associated $PM_{2.5}$ mortalities as well. As renewable energy continues to grow disproportionately in India in a handful of states and states individually contract for and schedule power, these inequities may grow in the future.

Sulfur control policies to meet currently unimplemented emissions regulations in India show the potential to dramatically decrease $PM_{2.5}$ mortality associated with electricity. We find sulfur control results in widespread mortality decreases in several large Indian states, mainly Tamil Nadu, Maharashtra, Andhra Pradesh, Karnataka, Gujarat, Madhya Pradesh, and West Bengal. Our estimate of approximately 42,000 fewer annual deaths from implementing sulfur control regulations is consistent with Srinivasan et al., (2018) who estimate approximately 30,000 fewer annual deaths, Guttikunda and Jawahar (2018) who estimate 39,000–63,000 fewer annual deaths, and Sugathan et al., (2018) who estimate 45,000 fewer annual deaths. Moreover, our state-wise apportionment of this mortality reductions largely agree with Srinivasan et al., (2018) who find Tamil Nadu seeing the most reductions followed by West Bengal, Maharashtra, Andhra Pradesh, and Uttar Pradesh. The benefits of reductions in $PM_{2.5}$ mortality likely exceed the costs associated implementing stricter power plant emissions regulations in India (Cropper et al., 2017, 2019; Srinivasan et al., 2018), but limited finance has impeded widespread implementation and installation of emission control equipment at Indian power plants. The Government of India has recently announced plans to delay implementation again (Government of India, 2021), and analysis to prioritize installation at plants base prioritization solely on SO_2 concentrations near plants, despite this and other analyses showing the secondary formation of $PM_{2.5}$ from SO_2 oxidation leading to mortality impacts beyond immediate vicinities of plants. While

InMAP predictions of SO_2 and $PM_{2.5}$ concentration attributable to electricity are moderately correlated (r = 0.7) in grid cells with plants, using SO_2 solely as an indicator underestimates the extent of impacts from plants due to transport and oxidation.

Increasing carbon taxes in the current Indian grid reduces emissions at several plants spread throughout the country, which in turn reduces ambient $PM_{2.5}$ concentrations and associated mortality. While carbon taxes do increase emissions at a fewer number of plants, the impact of these increase are not enough to offset estimated decreases. While high carbon taxes will likely spur the longer-term installation of new lower-emitting electricity capacity (outside the focus of this work), our results potentially show the shorter-term induced emissions and associated concentration and mortality changes from operational interventions that make less efficient, costlier, and higher emission plants less likely to run, e.g. greater renewable energy or taxes on health damages. However, fuel transport costs along with efficiency determine variable cost of electricity in India with plants closer to coal mines in eastern states providing cheaper power, even if they are less efficient than plants further away. Peng et al., (2020) find an additional 5,900 to 8,700 more $PM_{2.5}$-related deaths in 2040 from failing to enforce renewable energy targets in India, i.e. additional annual $PM_{2.5}$ deaths from increased electricity generation that would have come from renewables. While Peng at al. (2020) assume stringent pollution control at existing power station in 2040, our results being the same order of magnitude as theirs suggest our results provide an additional line of evidence of what happens to power sector emissions in India in the shorter term when renewable generation increases. Given the complexities in power market contracting and pricing in India, this requires further analyses.

Lastly, market integration policy scenarios show regional and national dispatch decreases emissions, concentrations, associated mortalities in areas furthest away from coal mines in eastern India because these plants have costlier electricity due to higher fuel transportation costs. Like the carbon tax scenarios, these decreases largely offset any impacts from emissions increases at plants from shifting dispatch. Our changes in mortality estimates are likely overestimates because the bulk of changes come from the cluster of high sulfur emitting plants in Tamil Nadu. Because these plants burn lignite from mines nearby, they likely have lower fuel transportation costs (and total variable

cost) than what we assume for all plants in Tamil Nadu. Moreover, the market integration scenarios show that despite emissions increases, associated $PM_{2.5}$ concentrations and mortality do not increase by appreciable amounts. This is consistent with a non-linear risk-exposure relationship for $PM_{2.5}$ mortality where ambient $PM_{2.5}$ concentration in many parts of India are already in ranges where additional exposure does not induce much change in corresponding risk, and consequently mortality.

In sum, this analysis presents the first quantifications of changes in $PM_{2.5}$ and associated mortality from polices that induce changes in power sector operations in India. While much work has focused on the longer-term impacts of capacity expansion and meeting of policy targets in the Indian power sector, we choose to focus on shorter-term impacts to understand how characteristics of power sector operations and heterogeneity between states in India influence the $PM_{2.5}$ mortality burden from power generation. Our results shed light on the spatial patterns in $PM_{2.5}$ mortality burden that will likely exist as long as coal forms a bulk of electricity generation in India.

5 Current and future estimated marginal emission factors for Indian power generation

5.1 Introduction

As the world's third-largest emitter of greenhouse gases (GHG) (BP, 2020; Carbon Brief, 2019; World Resources Institute, 2019), India's current emissions are consequential to global efforts to mitigate climate change and improve air quality. Current per capita emissions remain a fraction of the world average meaning future emissions are similarly consequential (International Energy Agency, 2021). Forty percent of the country's GHG emissions come from its coal-heavy power sector (Mohan et al., 2019), the world's third-largest by generation (BP, 2020). Likewise, uncontrolled sulfur dioxide (SO_2) and nitrogen oxide (NO_2) emissions from Indian power generation contribute to 7-21% of up to 1.1 million premature deaths in India associated with ambient $PM_{2.5}$ pollution, solid or liquid particles suspended in the atmosphere (Apte and Pant, 2019; Conibear et al., 2018; Gao et al., 2018; GBD MAPS Working Group, 2018; Guo et al., 2018; Guttikunda and Jawahar, 2014, 2018; Lelieveld et al., 2015).

Future scenarios point to the power sector as a growing source of GHG emissions and air pollution (International Energy Agency, 2021; Peng et al., 2020; Venkataraman et al., 2018). Expected increases in electricity demand from economic growth drive these emissions increases. Consequently, power generation with its relatively fewer, concentrated sources and growing role, provide policymakers a focus for emissions control policies. The power sector remains a focus of Indian policymakers through the Government of India's 2030 target to increase renewable and other zero-emission capacity to 40% of the country's electricity mix (Government of India, 2015).

Emissions factors from the Indian power grid remain poorly characterized despite its large potential for emissions reductions and size relative to other national grids. These emission factors provide policymakers and analysts a basis to evaluate decarbonization efforts and other interventions. A number of studies have characterized GHG and air pollutant emissions nationally or by individual plants India as well as their impacts on ambient air quality (Cropper et al., 2021; Gao et al., 2018; GBD MAPS Working Group, 2018; Guttikunda and Jawahar, 2014; Lu et al., 2013a; Lu and Streets, 2012; Oberschelp et al., 2019; Tong et al., 2018; Venkataraman et al., 2018). However,

none have characterized emission factors spatially and temporally based on electricity consumption, i.e., the emissions associated with power used in different areas of the country.

Complicating efforts are the lack of widely available continuous emissions monitoring data from Indian power plants and the decentralized, federal system of power scheduling and dispatch in India. Individual states contract with and schedule power from various portfolios of plants owned by central and state governments and the private sector. Moreover, the central government and state governments have overlapping jurisdiction over the Indian power sector. Consequently, not only do fuel mixes and emissions of electricity consumed vary by state, but so do policies governing emissions from the power sector (Power System Operation Corporation Limited, 2020; Safiullah et al., 2017).

While it is possible to characterize the emissions of the Indian power sector spatially and temporally based on generation location using daily reported power generation (Ministry of Power, 2020b), finer sub-daily scale consumption-based estimates require some account of power transfers between states and a diurnal patterns in power consumption. Moreover, currently reported data can only provide estimates of average emission factors, i.e. total emissions divided by total generation, which give an overall estimate of how emission intensive electricity is. However, they are poor estimates of changes in emissions from small changes in electricity demand (Donti et al., 2019; Hawkes, 2010). Instead, marginal emission factors (MEF) are a better representation. These factors estimate the change in emissions from marginal generation, i.e. the electricity generation that increases or decreases to meet a change in demand. These factors provide more accurate assessments especially when analysts or policymakers evaluate interventions that cause changes in electricity demand likely to vary seasonally or time-of-day, e.g. electric vehicles, air conditioning, energy efficiency. Estimating MEF's likewise require sub-daily accounting of diurnal demand and generation patterns because different mixes of generators and fuels may respond to changes in demand depending on season and time-of-day (Siler-Evans et al., 2012).

Dispatch or production-cost models provide one way to address current limitations to characterize Indian power sector emissions factors. These models

simulate scheduling and dispatch of power generators at finer hourly or minute resolution based on power demand (Ryan et al., 2016). Sengupta *et al* (2021) use a reduced-form dispatch model to derive production and consumption-based, 2017-2018 average emission factors for CO_2 and SO_2 from Indian power generation. They find heterogeneity in contracted capacity mixes between states results in differences of up to 26% in average CO_2 emission factors for certain Indian states than estimated by a single national emission factor. However, they do not quantify MEFs.

Previous work has quantified MEFs in the United States, United Kingdom, Canada, and China (Cai et al., 2013; Deetjen and Azevedo, 2019; Donti et al., 2019; Gai et al., 2019; Hawkes, 2010; Li et al., 2017b; Siler-Evans et al., 2012; Thind et al., 2017), but detailed estimates for India remain absent. The only estimate available for India is a single, national operating margin emission estimate for CO_2 (Central Electricity Authority, 2018a) developed as part of the Clean Development Mechanism (CDM) of the United Nations Framework Convention on Climate Change (UNFCC). The CDM is a way for developed countries to offset emissions in developing countries. This value represents the displaced CO_2 emissions for any CDM infrastructure projects, and the United Nations and other international organizations use this value to calculate resulting carbon offsets (United Nations Framework Convention on Climate Change, 2015). Current estimates used in analysis do not adequately reflect subnational variability in marginal emissions from power sector interventions in India. This becomes increasingly relevant as countries around the world set net-zero emissions targets and climate finance efforts look to fund climate mitigation efforts in developing countries such as India.

Consequently, here we use scheduling and dispatch (production cost) models to spatially, temporally, and seasonally quantify CO_2, SO_2, NO_X, and primary (directly emitted) $PM_{2.5}$ MEFs in current (2017-2018) and future Indian power generation (2030-2031). Our MEFs represent the first analysis to characterize a growing and changing Indian power sector. They provide policymakers, analysts, and researchers emission factors more representative of Indian power system operations.

5.2 Methods

We calculate CO_2, SO_2, NO_X, and $PM_{2.5}$ MEFs using two sets of dispatch models: (1) a reduced-form model (Sengupta et al., 2021) developed for Indian power generation to simulate 2017-2018 and (2) a full-form model (Spencer et al., 2020) to simulate 2030-2031. The reduced-form model estimates MEFs based on the decentralized, state-wise dispatch of power in current grid operations. Moreover, the model incorporates current installed capacity mixes and fixed allocations of interstate generating capacity, implicitly modeling the transfer of electricity across state lines through these allocations. Demand estimates derive from daily demand data and monthly, diurnal demand distributions (Energy Analytics Lab, 2019; Power System Operation Corporation Limited, 2018). The full-form dispatch model quantifies 2030-2031 grid operations, along with transmission and generator constraints (Spencer et al., 2020). This model incorporates planned Government of India capacity allocations, especially build-out of increased renewable capacity. It also explicitly simulates the transfer of electricity across state lines and simultaneously optimizes dispatch to meet future estimated power demand.

For each generating unit in the models, we estimate unit-specific emission factors based on fuel combustion analysis using methods presented by Srinivasan *et al* (2018). For the baseline, we assume no SO_2 or NO_X control, and 90% control of $PM_{2.5}$ emissions. We provide further details of both simulations sets in Appendix D, and we direct readers to cited papers for further details.

We calculate MEFs and marginal fuel shares of generation for each state using two methods: linear regression (Donti et al., 2019; Hawkes, 2010; Li et al., 2017b; Siler-Evans et al., 2012; Thind et al., 2017) and differentiation of emissions-generation curves (Deetjen and Azevedo, 2019).

To calculate marginal emission factors using linear regression we first calculate the hour-to-hour (h) change in emissions (E) and generation (G) associated with meeting demand for each state (s) predicted by the dispatch model:

$$\Delta \boldsymbol{E_{s,h}} = \boldsymbol{E_{s,h}} - \boldsymbol{E_{s,h-1}} \text{ (kg)}$$

$$\Delta \boldsymbol{G_{s,h}} = \boldsymbol{G_{s,h}} - \boldsymbol{G_{s,h-1}} \text{ (MWh)}$$

Here $\Delta E_{s,h}$ and $\Delta G_{s,h}$ are marginal emissions and marginal generation, respectively. The marginal emission factor (β_s) in kg/MWh for each state takes the functional form:

$$\Delta \boldsymbol{E_{s,h}} = \boldsymbol{\beta_s} \Delta \boldsymbol{G_{s,h}} + \boldsymbol{\alpha_s} + \boldsymbol{\varepsilon_s}$$

with α_s and ε_s as the regression intercept and error term, respectively. Likewise, to calculate the fractional share of marginal generation by various fuel types (e.g. coal, hydro, renewables, etc) we define the hourly change in generation from each fuel type, *f*:

$$\Delta \boldsymbol{G_{s,h,f}} = \boldsymbol{G_{s,h,f}} - \boldsymbol{G_{s,h-1,f}}$$

The marginal fuel share ($\gamma_{s,f}$) from fuel *f* takes the functional form:

$$\Delta \boldsymbol{G_{s,h,f}} = \boldsymbol{\gamma_{s,f}} \Delta \boldsymbol{G_{s,h}} + \boldsymbol{\alpha_{s,f}} + \boldsymbol{\varepsilon_{s,f}}$$

and $\alpha_{s,f}$ and $\varepsilon_{s,f}$ are regression intercept and error term, respectively. Marginal fuel share quantifies the frequency each fuel type meets marginal generation. Because marginal generation is met by the sum of marginal generation from each fuel type, this implies:

$$\sum_{f} \Delta \boldsymbol{G_{s,h,f}} = \Delta \boldsymbol{G_{s,h}}$$

$$\sum_{f} \boldsymbol{\gamma_{s,f}} = \boldsymbol{1}$$

Each annual model simulation produces approximately 8,760 hours of emissions, generation, and fuel shares for each state. We partition the data for each state into two seasons: monsoon (June-October) and dry (January-May; November-December). For each season, we further divide the data into five demand periods based on time-of-day: morning peak (6:00 AM to 10:00 AM), midday (10:00 AM to 2:00 PM), afternoon (2:00 PM to 6:00 PM), evening peak (6:00 PM to 10:00 PM), and overnight (10:00 PM to 6:00 AM). We define hours in each period based on visual inspection of the average diurnal national demand profile in each season (Centre for Social and Economic Progress, 2019; Parray et al., 2019). Consequently, we have ten marginal emission factors for each state: five for each season (monsoon and dry).

We also calculate MEFs using differentiation of total emission-total generation

curves. While regression-based marginal emission factors show average changes in emissions per unit change in demand for specified time periods, differentiation-based MEFs can show MEFs as a continuous function of demand. We use the method described by Deetjen and Azevedo (2019). First, we order by increasing demand ($d_{s,n}$) the hourly time series of emissions ($E_{s,h}$) and generation ($G_{s,h}$) for each state with n data points. Then, then we take rolling means of emissions and generation with 5% subsets of the data. This constructs the total emissions ($E_{s,total}$)-total generation ($G_{s,total}$) curve for each state. Then we calculate difference quotients of this curve as an approximation of the curve's derivative to estimate MEF as a function of demand:

$$\boldsymbol{MEF}(\boldsymbol{d_{s,n}}) = \frac{\boldsymbol{E_{s,total}}(\boldsymbol{d_{s,n}}) - \boldsymbol{E_{s,total}}(\boldsymbol{d_{s,n-1}})}{\boldsymbol{G_{s,total}}(\boldsymbol{d_{s,n}}) - \boldsymbol{G_{s,total}}(\boldsymbol{d_{s,n-1}})}$$

To construct the MEF-demand curve, we calculate rolling means with 5% subsets of the MEFs calculated by difference quotient. Note $G_{s,total} = d_{s,n}$ because generation meets all demand.

Similarly, we estimate the share of marginal generation of each fuel type MS_f using similar methods. Instead of emissions, we take rolling means of generation from each fuel type, $G_{s,f,total}$:

$$\boldsymbol{MS_f}(\boldsymbol{d_{s,n}}) = \frac{\boldsymbol{G_{s,f,total}}(\boldsymbol{d_{s,n}}) - \boldsymbol{G_{s,f,total}}(\boldsymbol{d_{s,n-1}})}{\boldsymbol{G_{s,total}}(\boldsymbol{d_{s,n}}) - \boldsymbol{G_{s,total}}(\boldsymbol{d_{s,n-1}})}$$

$$\sum_{f} \boldsymbol{MS_f}(\boldsymbol{d_{s,n}}) = \mathbf{1}$$

To explicitly estimate the shares of each generator to each state's demand for the 2030-2031 model, we use the "downstream-looking" power tracing algorithm presented by Bialek (1996). The 2017-2018 reduced-form model explicitly estimates each hour the share of each generator unit supplying electricity to meet demand in each state. The 2030-2031 full-form model on the other hand simulates power flows between states in its optimization to determine which units generate to meet demand at each state. The algorithm of Bialek (1996) assumes perfectly mixed nodes where power flow

out of a state is proportional to power flow into a state from respective sources. It traces power flow for each estimated hour to apportion generation and emissions from each generating unit to each state's demand. This results in an explicit time series of generation and emissions tied to generating unit for each state.

5.3 Results

In Figure 22, we show the time-of-day resolved marginal CO_2 emission factors for dry and monsoon seasons for electricity consumed in each Indian state based on the 2017-2018 reduced form dispatch model (Sengupta et al., 2021).

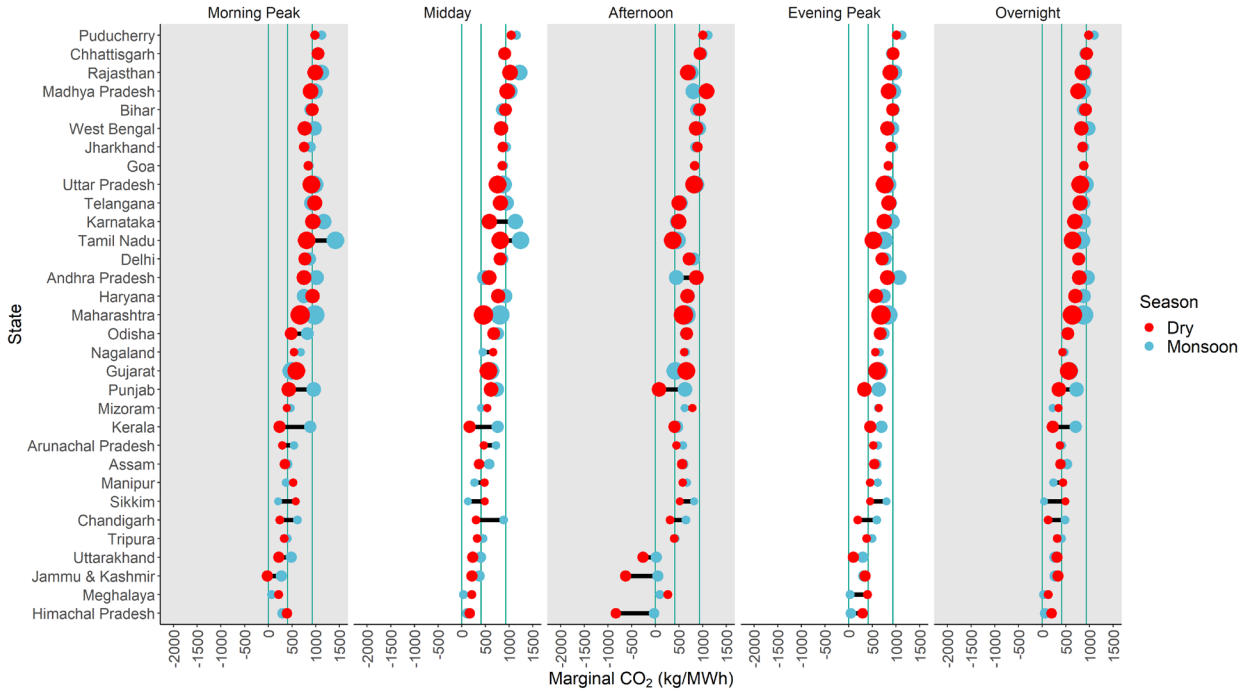

Figure 22
2017-2018 regression-based, marginal CO_2 emission factors for dry and monsoon seasons in each Indian state. Panels separate the time-of-day in each season. Size of dots scale to annual electricity demand in each state. Vertical lines from left to right indicate generation-weighted CO_2 emission factors for zero-emission, gas, and coal generators, respectively.

See Figure 82 for a map of India with states. We present SO_2, NO_X, and $PM_{2.5}$ MEFs for the same time periods in Figure 68, Figure 70, and Figure 72. MEFs for these other pollutants show similar trends as those for CO_2 (due to unit-specific emission factors that are functions of fuel composition) so we focus our presentation on CO_2 MEFs. Size of points scale to annual electricity demand consumed in each state. Vertical lines from left to right show the generation-weighted emission factors of zero-emission, gas, and

coal generators, respectively. Negative marginal emission factors mean emissions *decrease* with increases in marginal power consumption. Tables 7-8 show the data underlying Figure 22 along with regression standard error and coefficients. In general, r^2 values decrease as CO_2 emission factors decrease, indicating the weaker relationship between marginal generation and marginal CO_2 emissions due to increasing hydro and renewable marginal generation.

Marginal emission factors for CO_2 span three orders of magnitude across 32 states. Overall, two broad groups of states emerge in both seasons and all periods: 16 higher emission states with higher electricity demand (larger points) and 16 lower emission states with lower electricity demand (smaller points). There are some exceptions to these general groupings, e.g. Gujarat and Punjab are lower emission but higher demand, and Puducherry and Goa are higher emission but lower demand. For higher emission states Puducherry to Maharashtra (in order from top to bottom in Figure 1), CO_2 MEFs sit around the emission factor line for coal generators (930 kg/MWh) with median 860 kg/MWh across all seasons and times-of-day. For lower emission states, Odisha to Himachal Pradesh CO_2 MEFs sit around the emission factor line for gas generators (410 kg/MWh) and zero-emission generators (0 kg/MWh), with median 460 kg/MWh for all seasons and times-of-day.

In general, we see little seasonal temporal variability in CO_2 MEFs between monsoon and dry seasons with monsoon MEFs slightly higher than dry MEFs. Moreover, lower emission states show more variability than higher emission states. Seasonally, across all times of the day, the median absolute difference between monsoon and dry CO_2 MEFs in 16 lower emission states is 140 kg/MWh. The same value is 100 kg/MWh for the 16 higher emission states.

When analyzing intraday temporal variability, we see similar levels of variability between times of day in both high emission and low emission states across both seasons. Monsoon season sees more time-of-day variability than dry season. Across low emission states, the median time-of-day CO_2 MEF ranges from 420 kg/MWh (overnight) to 620 kg/MWh (evening peak) during monsoon season and 350 kg/MWh (overnight) to 460 kg/MWh (afternoon) during dry season. Likewise, across high emission states, the median time-of-day CO_2 MEF in ranges from 800 kg/MWh

(afternoon) to 980 kg/MWh (morning peak) during monsoon season and 800 kg/MWh (overnight) to 890 kg/MWh (morning peak) during dry season.

Figure 23 shows the frequency at which different fuels form marginal generation in each state and demand period in the dry season for 2017-2018. Here marginal renewable generation includes solar and wind.

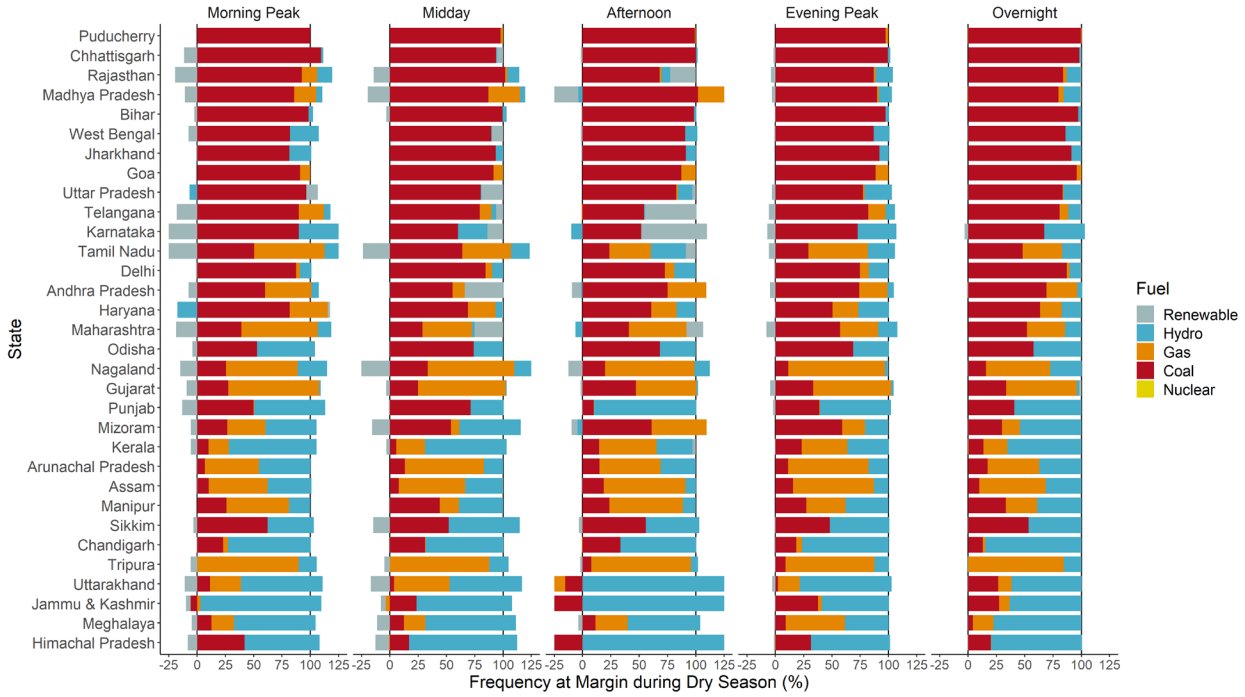

Figure 23
2017-2018 regression-based, marginal fuel frequency for each Indian state during dry season. Negative percentages in each period indicate fuel source generation decreases with increases in marginal power demand in each state, requiring increase in generation from other fuels to meet demand. The sum of each bar is 100%.

In this figure, negative percentages in each period indicate generation from a particular fuel *decreases* with increases in marginal power consumption in each state, requiring increases in generation from other fuels to meet demand. The sum of each bar in Figure 23 is 100%. Because of little inter-seasonal variability, we show the comparable monsoon season estimates in Figure 67.

In the lower emission states (Odisha to Himachal Pradesh), we see more hydro and/or gas marginal generation than coal marginal generation driving lower CO_2 MEFs. In these states, median hydro generation across all states ranges between 31% (afternoon) and 47% (overnight), and marginal gas generation ranges between 16%

(overnight) and 29% (afternoon). Meanwhile dry season marginal coal generation numbers between 19% (afternoon) to 27% (evening peak). We similar trends in monsoon season (Figure 67) with slightly more marginal coal generation than dry season. Overall, these higher percentages of marginal generation from gas and hydro drive lower MEFs in these states.

Oppositely, in high emission states (Puducherry to Maharashtra) coal dominates marginal generation, which drive higher emissions. During the dry season, median coal marginal generation varies between 75% (afternoon) to 87% (morning peak) of the time across these states. Similar patterns emerge during the monsoon season (Figure 67). Moreover, in these higher emission states, median time-of-day marginal hydro generation is higher during the dry season (2-14%) than the monsoon season (3-9%).

However, among higher demand states, considerable renewable marginal generation exists, especially in eight high renewable states: Maharashtra, Gujarat, Tamil Nadu, Madhya Pradesh, Rajasthan, Karnataka, Telangana, and Andhra Pradesh. In these states, during morning peak and midday hours, marginal renewable generation generally falls below zero, ranging from as low as -56% (morning peak hours during monsoon in Tamil Nadu) to -2% (midday hours during monsoon in Telangana). This means that marginal renewable generation decreases during these hours to meet increases in demand. Consequently, other fuels, most likely carbon-emitting gas or coal, must increase marginal generation to meet the increases in demand. Marginal renewable generation largely is greater than zero during afternoon hours in these high renewable states where it ranges between 8% (monsoon season in Madhya Pradesh) to 58% (dry season in Karnataka).

Figure 24 shows the dispatch (merit) order of capacity during the annual maximum hourly demand for the previously mentioned eight high renewable states from the 2017-2018 reduced-form model. The top panel shows the capacity ordered by price (variable cost) in ₹/kWh and the bottom panel shows the emissions intensity of that ordered capacity in kg/MWh. We show the annual maximum hourly demand to show the high capacity amounts available to meet demand in each state.

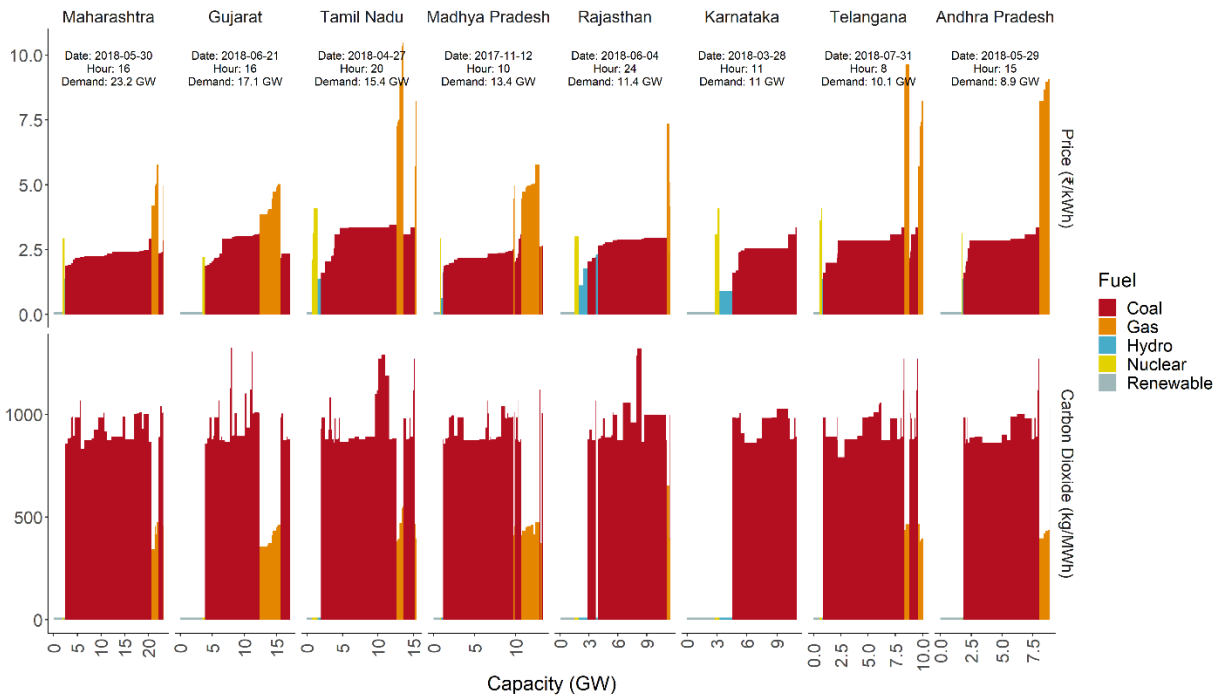

Figure 24
Hourly dispatch (merit) order for maximum hourly demand in eight high renewable states. Top panel shows capacity ordered by variable cost and bottom panel shows CO2 emissions intensity of the same capacity. Capacity is ordered by renewable capacity and nuclear capacity first which are must run. Then hydro, coal, and gas capacity contracted with the state are ordered by variable cost. Lastly, leftover capacity not used by contracted states is ordered at the regional and national level.

We order the capacity by price at three levels: state, regional and national to reflect the three levels of successive dispatch the reduced form dispatch model assumes. Capacity available to the right of the dispatch orders at lower prices than capacity to the left show dispatch at regional and national levels after state level dispatch. Overall coal dominates dispatch in these states, despite high renewable capacity, especially for states where maximum annual demand occurs at during midday or afternoon hours when renewable capacity available is the highest, e.g. Karnataka and Andhra Pradesh. A caveat with these dispatch orders is that renewable and hydro capacity may change from hour to hour and thus contribute to meeting changes in demand. Indeed, the frequency of marginal renewable or hydro generation can be positive or negative during these hours (Figure 23, Figure 67). Thus, the more than one fuel type may meet marginal demand and determine marginal CO_2 emissions. Nonetheless, because coal capacity dominates dispatch order in these states, it meets marginal demand much of the time (Figure 23, Figure 67).

In Figure 25, we show the time-of-day resolved marginal CO_2 emission factors for dry and monsoon seasons for electricity consumed in Indian state based on the 2030-2031 full form dispatch model. Table 9-10 show the data underlying this figure.

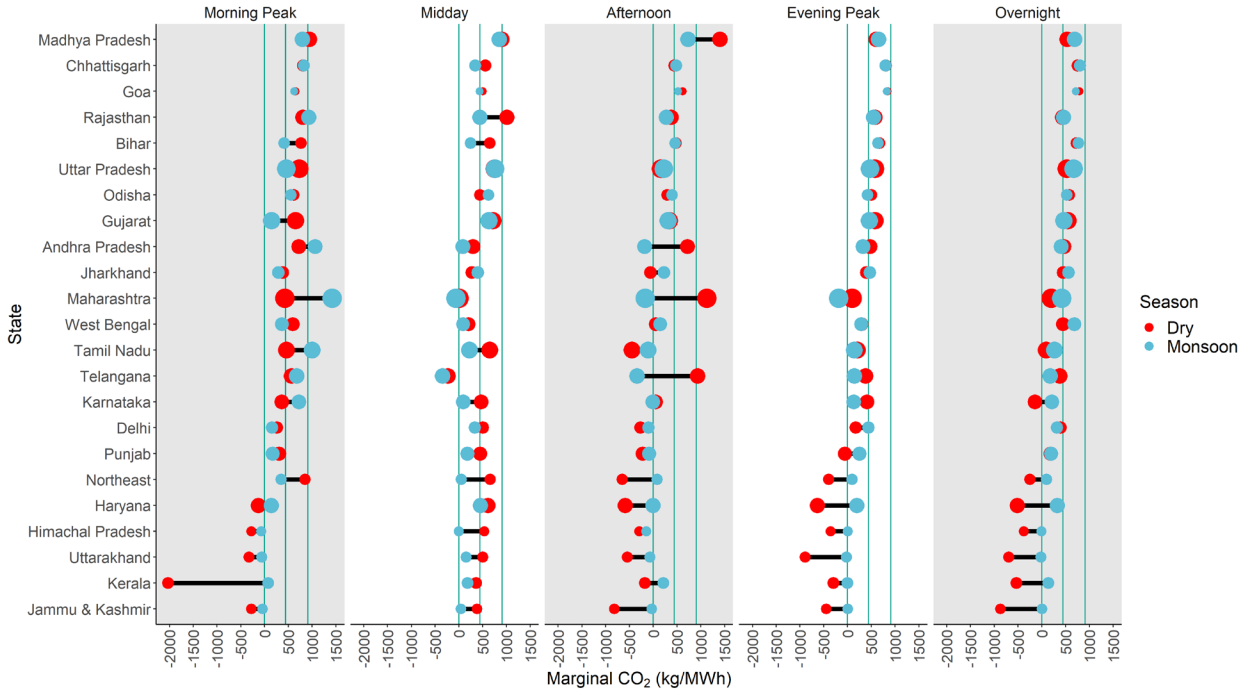

Figure 25
2030-2031 regression-based, marginal CO_2 emission factors for dry and monsoon seasons in each Indian state. Panels separate the time-of-day in each season. Size of dots scale to annual electricity demand in each state. Vertical lines from left to right indicate generation-weighted CO_2 emission factors for zero-emission, gas, and coal generators, respectively.

These future simulations treat the low-demand, northeastern states of Sikkim, Assam, Mizoram, Tripura, Arunachal Pradesh, Nagaland, Manipur, and Meghalaya as one Northeast state. Likewise, these simulations treat territories of Chandigarh in north India and Puducherry in south India as part of neighboring states (Spencer et al., 2020). To simplify comparisons between 2030-2031 and 2017-2018 estimates, we ignore these territories and Northeastern states, which form 1-2% of annual national demand during respective simulation periods. We present SO_2, NO_X, and $PM_{2.5}$ MEFs for the same time period in Figure 69, Figure 71, and Figure 73. Each panel shows same five time-of-day demand periods in each season as Figure 22. Likewise, size of points scale to annual projected electricity demand consumed in each state in 2030-2031. Vertical lines from left to right show the generation-weighted emission factors of zero-emission, gas, and

coal generators, respectively, using estimated generation from the full-form dispatch model.

Figure 25 shows that under 2030-2031 assumptions, estimated marginal CO_2 emission factors are generally lower than those in 2017-2018 but show similar variability between states. Emission factors once against vary across three orders of magnitude between states, with the same, higher emission, higher demand states in 2017-2018 (Chhattisgarh, Rajasthan, Madhya Pradesh, Bihar, West Bengal, Jharkhand, Goa, Uttar Pradesh, Telangana, Karnataka, Tamil Nadu, Delhi, Andhra Pradesh, Haryana, and Maharashtra) having relatively higher emission factors as 2017-2018. In these states, 2030-2031 CO2 MEFs largely sit to the left of the coal generator emission factor line (910 kg/MWh) with median 420 kg/MWh among seasons and times-of-day. For the remaining lower emission, lower demand states in 2017-2017, 2030-2031 marginal CO_2 MEFs decrease further with median 160 kg/MWh.

Furthermore, we see more seasonal variability in both high emission and low emission states in 2030-2031. Like 2017-2018, lower emission states show more difference between dry and monsoon seasons than higher emission states. The median absolute seasonal difference in CO_2 MEFs across all times-of-day in lower emission states increases to 320 kg/MWh in 2030-2031. For higher emission states, this median value increases to 150 kg/MWh.

Under 2030-2031 assumptions we also see more temporal variability between times-of-day in CO_2 MEFs. In low emission states, the median time-of-day CO_2 MEF in both seasons ranges from 20 kg/MWh (afternoon) to 160 kg/MWh (midday) during monsoon season and -330 kg/MWh (evening peak) to 470 kg/MWh (midday) during dry season. Likewise, across high emission states, the median time-of-day CO_2 MEF in ranges from 150 kg/MWh (afternoon) to 680 kg/MWh (morning peak) during monsoon season and 380 kg/MWh (afternoon) to 590 kg/MWh (morning peak) during dry season.

Greater marginal generation from renewables and hydro relative to coal marginal generation explain lower, more temporally variable CO_2 MEFs in 2030-2031 for both higher and emission and lower emission states. In Figure 26, we show an analogous figure to Figure 23 where we show the frequency of marginal generation from each fuel type for the 2030-2031 dry season. We show the same plot for monsoon season in

Figure 26
2030-2031 regression-based, marginal fuel frequency for each Indian state during dry season. Negative percentages in each period indicate fuel source generation decreases with increases in marginal power demand in each state, requiring increase in generation from other fuels to meet demand. The sum of each bar is 100%.

Figure 74 where similar trends emerge. Here we see marginal renewable generation predominately during midday and afternoon hours. Across all states, median marginal renewable generation frequency numbers 40% and 37% during midday and afternoon dry seasons hours, respectively. During morning peak, evening peak and overnight hours, it numbers -5%, 5%, and 6% respectively. Marginal hydro generation meanwhile dominates during evening peak and overnight hours with median 57% and 47% respectively, across all states. Lastly, marginal coal generation is the highest in most states during all times-of-day except afternoon hours, when median frequency across all states decreases to 5%. During other times-of-day median frequency ranges between 32-62%.

There is a 1:1 relation between decreasing CO_2 marginal emission intensities and increasing non-emitting marginal generation, i.e., increased hourly generation to meet new hourly load. However, the relationship between increased average zero-emission generation and marginal CO_2 emission factors is not as direct because

average non-emitting generation may not change when there is an increase or decrease in electricity demand. We explore this relationship in Figure 27.

Figure 27 shows marginal CO_2 emissions in each demand period against average percent zero emission generation (renewables, hydro and nuclear), in dry and monsoon seasons, for both 2017-2018 and 2030-2031.

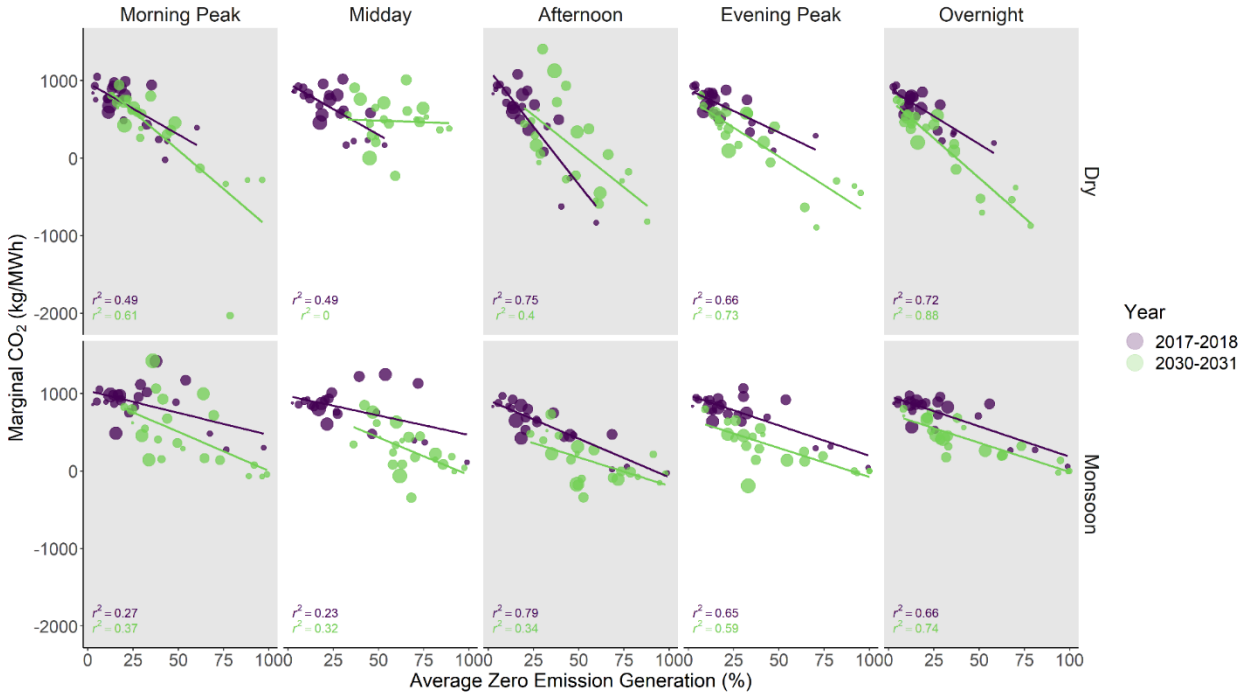

Figure 27
Marginal CO_2 emissions versus average zero emission (hydro, renewables, and nuclear) generation in each demand period in dry and monsoon seasons for 2017-2018 and 2030-2031. Each dot represents one state and the size of dots scales to annual demand for each state. Lines are lines of best fit.

Each dot represents a state, and size of dots scale to annual demand in each simulation period. Lines are lines of best fit.

In the dry season in 2017-2018 (violet points, top panel Figure 27), average zero-emission generation shares and marginal CO_2 emission factors are the most correlated during afternoon and overnight periods with r^2 values 0.75 and 0.72, respectively. During evening peak periods, correlation decreases to r^2 = 0.66. The relationship weakens the most during morning peak and midday periods when r^2 values decrease to 0.49 in both periods.

In 2030-2031 dry season, during all periods except midday afternoon, the relationship strengthens (green points, top panel Figure 27). Increasing average zero

emission generation is associated with decreasing marginal CO_2 emission factors. During morning peak, evening peak, and overnight hours, r^2 values increase to 0.61, 0.73, and 0.88, respectively. In midday and afternoon hours, r^2 in 2030-2031 however decreases to 0.00 and 0.4, respectively.

In the monsoon season in 2017-2018 (violet points, bottom panel Figure 27), increasing average zero-emission generation is most correlated with decreasing marginal emission factors during afternoon and overnight hours, r^2 = 0.79, 0.66, respectively. During morning peak, midday, and evening peak hours, r^2 = 0.27, 0.23, and 0.65, respectively.

In the 2030-2031 monsoon season (green points, bottom panel Figure 27), correlation increases in all periods except afternoon and evening peak hours. Morning peak sees r^2 = 0.37, midday sees r^2 = 0.32, and overnight r^2 = 0.74. However, during afternoon and evening periods correlation decreases, r^2 = 0.34 and 0.59, respectively.

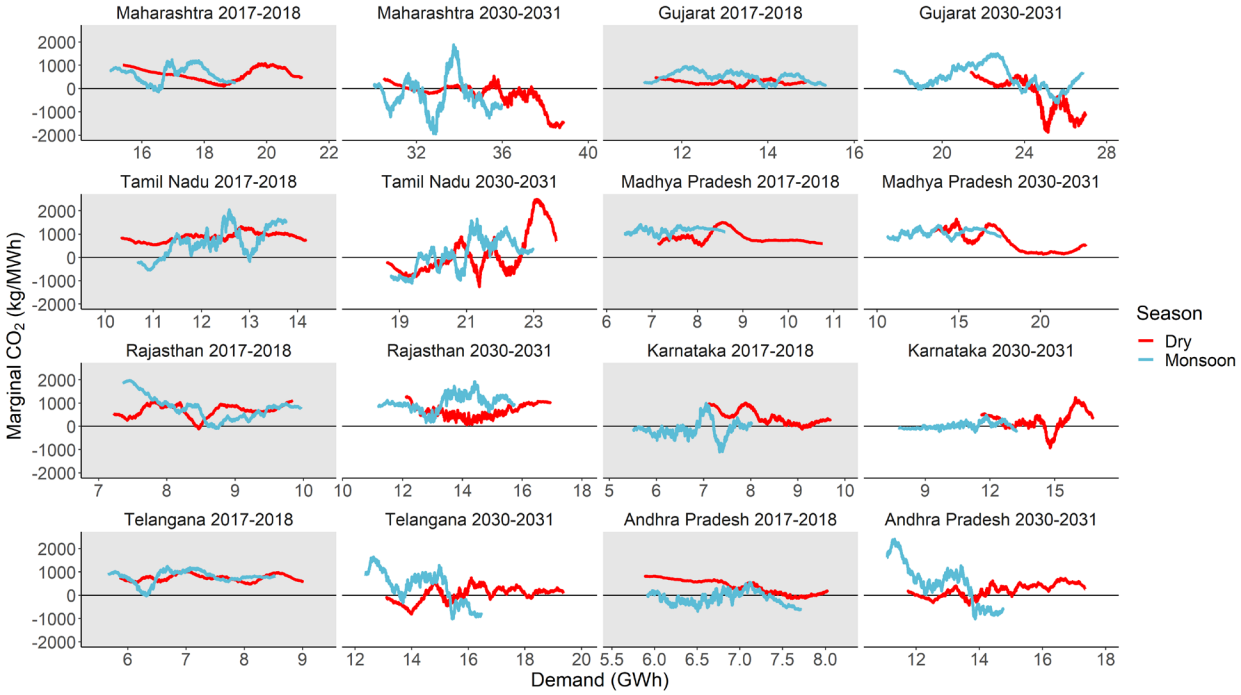

Figure 28
2017-2018 and 2030-2031 dry and monsoon season marginal CO_2 emission factors as a function of demand in eight high variable renewable energy (solar, wind) states. In 2017-2018, these eight states collectively form 85% of all variable renewable energy generation. In 2030-2031, these eight states collectively form 60% of all variable renewable energy generation.

Figure 28 shows marginal CO_2 emission factors as functions of electricity demand for both dry and monsoon seasons for 2017-2018 and 2030-2031. We illustrate eight high renewable capacity states with collectively generate 85% of annual renewable generation in 2017-2018 and 60% in 2030-2031. We show similar curves for SO_2, NO_X, and $PM_{2.5}$ in Figures 79-81. We order states by decreasing electricity demand, i.e. Maharashtra has highest demand, and Andhra Pradesh has lowest demand. In all states except Maharashtra, Madhya Pradesh, and Karnataka, we see significant overlap in electricity demand between seasons, indicating little difference in demand between seasons. Emission factors differ by season and vary as function of demand, increasing and decreasing depending on demand conditions. For example, in Maharashtra during dry season, between 14.7 and 18.6 GWh, CO_2 marginal emission factors decrease from 1014 to 99 kg/MWh, but then increase at loads greater than 18.6 GWh. For these same demand range in the monsoon period, marginal CO_2 emission factors oscillate between -147 and 1240 kg/MWh. These differences stem from differences in renewable and coal marginal generation as function of demand illustrated in Figures 75-76.

In 2030-2031, we see higher electricity demand in line with future demand assumptions for 2030-2031 simulations. Gujarat, Karnataka, and Madhya Pradesh show seasonal differences in demand with less overlap in demand between curves for each season. Overall, we see much more intra-seasonal and inter-seasonal variability in MEFs. For example, in Gujarat dry season marginal CO_2 emissions vary between -1880 and 701 kg/MWh between electricity demand 21.4 GWh and 27 GWh. Likewise, in the monsoon season in Gujarat, marginal CO_2 emissions vary between -625 and 1500 kg/MWh while demand spans 17.7 GWh to 26.9 GWh. Greater amounts of renewable generation at the margin and at different demand levels cause this variability (Figure 77-Figure 78).

5.4 Discussion and Conclusions

In this analysis we use dispatch models to quantify the spatial and temporal patterns of marginal CO_2, SO_2, NO_X, and $PM_{2.5}$ emission factors in current and future Indian power generation. These emission factors are based on power consumed in each state because our estimates account for imports and exports between states. Due

to a lack of readily available continuous emissions monitoring data or sub-daily power generation data, no analysis has well quantified from which states, during which seasons, and during which hours of the day Indian power generation emits due to changes in demand. Moreover, given increasing shares of renewable energy and increasing power demand from economic growth, no analysis has quantified potential emissions intensities of the Indian grid in the future. This analysis is especially relevant because policy efforts to decarbonize Indian power generation happen at both central and state-levels so subnational estimates provide more accurate emission intensities than commonly used national estimates. Consequently, our estimates are useful to policymakers, analysts, or researchers who may seek to quantify the emissions impacts of new interventions of electricity demand, e.g. electric vehicles, air conditioning, or energy efficiency. The MEFs presented here are more representative than average emission factors of the various types of generation meeting demand during different seasons and times-of-day.

In the current, 2017-2018 Indian grid CO_2 MEFs vary considerably across states. Despite renewables and hydro decreasing MEFs in lower emission, lower demand states, coal dominates marginal generation and emissions in higher emission, higher demand states. Further inspection of the merit order under which we simulate plants to generate shows the dominance of coal at the margin. Even in the high renewable energy states we illustrate, where the merit order would fluctuate due to change renewable and hydro generation throughout the day, coal still forms the bulk of the available capacity throughout the day. Consequently, coal individually or in combination with other fuels forms the bulk of marginal generation.

Furthermore, while we see little seasonal differences in CO_2 MEFs in the current Indian grid, slightly increased MEFs during monsoon season than the dry season is consistent with current operation of hydro generating units in India. Because of increased rainfall during the monsoon, operators use hydro generation as baseload capacity during this season. During the dry season when there are further constraints on the amount of water available to generate electricity, e.g. irrigation, drinking water, etc., hydro units are more likely to act as peaking plants that ramp up and down quickly. Our analysis shows higher marginal hydro generation during the dry season. Thus,

hydro plants play a greater role in meeting marginal demand and decrease marginal emissions during dryer months.

Our analysis shows that incorporation of greater shares of renewable energy by 2030 in line with the Government of India's targets will increase the likelihood that renewable generation meets marginal demand, decreasing median CO_2 MEFs across all states by approximately a factor of two. Higher marginal renewable generation (mostly from solar) during the middle of the day drive this potential future decrease. Moreover, this is consistent with CO_2 MEFs from the United States where marginal CO_2 emissions decrease with increasing marginal wind generation during the middle of the day (Thind et al., 2017).

A future Indian grid with more renewables will also show more variability in marginal emissions estimates, both seasonally and between hours of the day. Median absolute seasonal difference increases by approximately a factor of two. Likewise, time-of-day variability increases: differences between lowest and highest median time-of-day MEFs increases by up to a factor of approximately four. Nonetheless, under projected capacity expansions to 2030, coal generation will still form a sizable portion of marginal generation during times other than the middle of the day especially in larger, higher demand states. This results in higher marginal emissions during these times of the day.

Comparing current and future estimates, we show stronger relationships between greater shares of average zero emission generation (mostly renewables) and lower marginal emission factors. This implies that long-term policy targets to increase renewable generation do have short-term impacts on emissions from new additional loads. Less emissions-intensive generation is more likely to meet these new loads which may not be uniformly spread across all seasons and times-of-day.

Analyzing marginal emissions as a function of current and future demand assumptions in high renewable states indicate variability and non-monotonic relationships between demand and marginal emissions. This is consistent with the increased variability in regression-based MEFs we see from increased marginal renewable generation. Moreover, while all states see increases in demand from 2017-2018 to 2030-2031, no clear patterns emerge on whether marginal emissions from future demand are distinctly lower than those from current demand. For example, in

Madhya Pradesh, 2030-2031 marginal emissions-demand curves show comparable emission intensity as those for 2017-2018. On the other hand, Telangana shows decreases in dry seasons for both modeling periods. A limitation with estimating marginal emissions as a function of demand is that these curves remove the temporal aspect associated with demand at different levels by ordering demand of different hours as a continuous series of data.

We identify two limitations to this analysis: the lack of observed continuous emissions monitoring data to compare our 2017-2018 emissions estimates, and assumptions about installed capacity, demand, and market structure in our 2030-2031 estimates. We discuss the 2017-2018 model simulation's ability to capture temporal and spatial trends with comparisons to reported generation data in Appendix D. Overall, the reduced-form model captures spatial and temporal trends in generation well, with weakest agreement during monsoon season when uncertainty from renewable generation decreases performance. This increases uncertainty in our MEF estimates, but is consistent with previous estimates from the United States of grids with marginal renewable generation (Li et al., 2017b; Thind et al., 2017) and high marginal gas generation (Siler-Evans et al., 2012). Indeed our estimates for the lowest MEFs are the most uncertain with low regression r^2 values and wide standard errors (see Table 7-Table 10). However, this is consistent with limitations from regression-based MEFs: because we regress changes in emissions against change in generation, if a particular generation sources has zero emissions, the correlation between emissions changes and generation changes weakens.

Another limitation of this analysis stem from our 2030-2031 estimates, which assume increased electricity demand, capacity expansion from all fuels to meet this demand, transmission capacity expansion, and further integrated power markets between states in India and the absence of current decentralized state-wise dispatch. This means the future 2030-2031 India grid analyzed here has more ability than the current 2017-2018 grid to transfer power between states having heterogenous electricity mixes. Consequently, our 2030-2031 estimates likely characterize an upper bound in terms of the MEF decreases we see between 2017-2018 and 2030-2031 estimate. Greater electricity sharing between states is incumbent upon policy reforms and

increased transmission capacity. These estimates show an Indian grid with higher renewable generation, but several exogenous factors such as economic growth and access to capital to finance capacity and transmission expansion will likely determine the Indian electricity fuel mix in 2030. Moreover, the speed of current policy efforts to coordinate dispatch (Power System Operation Corporation Limited, 2020) between states in India will determine how the Indian power system will adopt the centralized dispatch simulated by the full-form model. If states stay fragmented in their scheduling decisions, then zero-emission energy is less likely to move to emissions intensive states.

In conclusion, we present first-ever spatially and temporally resolved marginal CO_2, SO_2, NO_X and $PM_{2.5}$ emission factors for current and future Indian power generation. Our results are broadly applicable to energy researchers, policy analysts and decision makers when evaluating any interventions that change power demand in India. Given the country's growing power demand, expansion of renewable generating capacity, and state-level heterogeneity in fuel mixes and power sector operations, a detailed evaluation of emissions from new loads is critical to understanding emissions trajectories for India. Moreover, as both developed and developing countries look to net-zero targets to reduce climate-warming emissions, MEFs presented here provide once piece of information to accurately assess policies to meet these targets.

6 Conclusion

This thesis explored the interactions between air pollution, climate, and energy across a developed country, the United States, and a developing country, India. In the United States, we use high-resolution chemical transport models to understand the variability and sources of urban ultrafine particles within Pittsburgh. We find that high resolution simulations can resolve variability and attribute urban UFP concentrations to sources. However, considerable variability at finer spatial resolutions still exists. Empirical models capable of resolving this finer spatial variability will likely need to pair with mechanistic models in future work to full resolve UFP exposure and consequently constrain health effects quantifications for UFPs.

In India, we analyze power generation, a sector crucial to India's energy transition as well as global air quality and climate change. Due to the Indian power sector's size and importance in efforts to improve air quality and mitigate climate change, we present quantifications of the sector's air pollution and climate impacts at higher spatial and temporal resolution than previous analyses. Crucial to this added granularity are India's states, which act as underappreciated nodes of energy and environmental decision making in the country. We quantify the emissions impacts associated with each state's power production and consumption under current and future policy scenarios to find considerable differences between high renewable energy states in southern and western India, coal-mining states in central and eastern India, and hydro-rich states in northeastern India and the Himalayas. These differences likewise extend to the mortality associated with emissions from power generation in India. Coal generation underscores this variability between states, many times inducing differences in emissions and associated mortality. As renewable energy grows in the Indian power sector, it will add an additional of variability in emissions between states, times-of-day, and seasons. Ultimately the added granularity we resolve here can inform policy efforts by provide more accurate values characterizing the air quality and climate impacts of the Indian power sector.

7 References

Abbafati, C., Abbas, K. M., Abbasi-Kangevari, M., Abd-Allah, F., Abdelalim, A., Abdollahi, M., Abdollahpour, I., Abegaz, K. H., Abolhassani, H., Aboyans, V., Abreu, L. G., Abrigo, M. R. M., Abualhasan, A., Abu-Raddad, L. J., Abushouk, A. I., Adabi, M., Adekanmbi, V., Adeoye, A. M., Adetokunboh, O. O., Adham, D., Advani, S. M., Afshin, A., Agarwal, G., Aghamir, S. M. K., Agrawal, A., Ahmad, T., Ahmadi, K., Ahmadi, M., Ahmadieh, H., Ahmed, M. B., Akalu, T. Y., Akinyemi, R. O., Akinyemiju, T., Akombi, B., Akunna, C. J., Alahdab, F., Al-Aly, Z., Alam, K., Alam, S., Alam, T., Alanezi, F. M., Alanzi, T. M., Alemu, B. W., Alhabib, K. F., Ali, M., Ali, S., Alicandro, G., Alinia, C., Alipour, V., Alizade, H., Aljunid, S. M., Alla, F., Allebeck, P., Almasi-Hashiani, A., Al-Mekhlafi, H. M., Alonso, J., Altirkawi, K. A., Amini-Rarani, M., Amiri, F., Amugsi, D. A., Ancuceanu, R., Anderlini, D., Anderson, J. A., Andrei, C. L., Andrei, T., Angus, C., Anjomshoa, M., Ansari, F., Ansari-Moghaddam, A., Antonazzo, I. C., Antonio, C. A. T., Antony, C. M., Antriyandarti, E., Anvari, D., Anwer, R., Appiah, S. C. Y., Arabloo, J., Arab-Zozani, M., Aravkin, A. Y., Ariani, F., Armoon, B., Ärnlöv, J., Arzani, A., Asadi-Aliabadi, M., Asadi-Pooya, A. A., Ashbaugh, C., Assmus, M., Atafar, Z., Atnafu, D. D., Atout, M. M. d. W., Ausloos, F., Ausloos, M., Ayala Quintanilla, B. P., Ayano, G., Ayanore, M. A., Azari, S., Azarian, G., Azene, Z. N., Badawi, A., et al.: Global burden of 87 risk factors in 204 countries and territories, 1990–2019: a systematic analysis for the Global Burden of Disease Study 2019, Lancet, 396(10258), 1223–1249, doi:10.1016/S0140-6736(20)30752-2, 2020.

Adams, P. J. and Seinfeld, J. H.: Predicting global aerosol size distributions in general circulation models, J. Geophys. Res. Atmos., 107(19), 1–23, doi:10.1029/2001JD001010, 2002.

Agarwal, A., Speth, R. L., Fritz, T. M., Jacob, S. D., Rindlisbacher, T., Iovinelli, R., Owen, B., Miake-Lye, R. C., Sabnis, J. S. and Barrett, S. R. H.: SCOPE11 Method for Estimating Aircraft Black Carbon Mass and Particle Number Emissions, Environ. Sci. Technol., 53(3), 1364–1373, doi:10.1021/acs.est.8b04060, 2019.

Ali, S.: Indian electricity demand How much, by whom, and under what conditions?, New Delhi. [online] Available from: https://www.brookings.edu/research/the-future-of-indian-electricity-demand-how-much-by-whom-and-under-what-conditions/, 2018.

Apte, J. S. and Pant, P.: Toward cleaner air for a billion Indians, Proc. Natl. Acad. Sci., 201905458, doi:10.1073/pnas.1905458116, 2019.

Apte, J. S., Marshall, J. D., Cohen, A. J. and Brauer, M.: Addressing Global Mortality from Ambient PM 2.5, Environ. Sci. Technol., 49(13), 8057–8066, doi:10.1021/acs.est.5b01236, 2015.

Asmi, A., Wiedensohler, A., Laj, P., Fjaeraa, A., Sellegri, K., Birmili, W., Weingartner, E. and Baltensperger, U.: and Physics Number size distributions and seasonality of submicron particles in Europe 2008 – 2009, , 5505–5538, doi:10.5194/acp-11-5505-2011, 2011.

Baldauf, R. W., Devlin, R. B., Gehr, P., Giannelli, R., Hassett-sipple, B., Jung, H., Martini, G., Mcdonald, J., Sacks, J. D. and Walker, K.: Ultrafine Particle Metrics and Research Considerations : Review

of the 2015 UFP Workshop, , (December 2012), 1–21, doi:10.3390/ijerph13111054, 2016.

Ban-weiss, G. A., Lunden, M. M., Kirchstetter, T. W. and Harley, R. A.: Size-resolved particle number and volume emission factors for on-road gasoline and diesel motor vehicles, J. Aerosol Sci., 41(1), 5–12, doi:10.1016/j.jaerosci.2009.08.001, 2010.

Bialek, J.: Tracing the flow of electricity, IEE Proc. - Gener. Transm. Distrib., 143(4), 313, doi:10.1049/ip-gtd:19960461, 1996.

Blair, N., Diorio, N., Freeman, J., Gilman, P., Janzou, S., Neises, T. W. and Wagner, M. J.: System Advisor Model (SAM) General Description, , (NREL/TP-6A20-70414) [online] Available from: https://www.nrel.gov/docs/fy18osti/70414.pdf, 2018.

BP: Statistical Review of World Energy. [online] Available from: https://www.bp.com/content/dam/bp/business-sites/en/global/corporate/pdfs/energy-economics/statistical-review/bp-stats-review-2020-full-report.pdf, 2020.

Brown, T., Hörsch, J. and Schlachtberger, D.: PyPSA: Python for Power System Analysis, J. Open Res. Softw., 6, doi:10.5334/jors.188, 2018.

Cai, W., Wang, C., Jin, Z. and Chen, J.: Quantifying baseline emission factors of air pollutants in China's regional power grids, Environ. Sci. Technol., 47(8), 3590–3597, doi:10.1021/es304915q, 2013.

Carbon Brief: The Carbon Brief Profile: India, [online] Available from: https://www.carbonbrief.org/the-carbon-brief-profile-india, 2019.

Central Electricity Authority: Annual Performance of Review of Thermal Power Stations 2014-15, New Delhi., 2015.

Central Electricity Authority: CO2 Baseline Database for the Indian Power Sector, New Delhi, India. [online] Available from: http://www.cea.nic.in/reports/others/thermal/tpece/cdm_co2/user_guide_ver14.pdf, 2018a.

Central Electricity Authority: National Electricity Plan - Volume I: Generation, New Delhi., 2018b.

Central Electricity Authority: Renewable Energy Generation Data, 2018c.

Central Electricity Authority: All India Electricity Statistics: General Review 2019., 2019a.

Central Electricity Authority: Annual Generation Programme 2019-20. [online] Available from: http://cea.nic.in/reports/others/god/opm/generation19_20.pdf, 2019b.

Central Electricity Authority: Flexible Operation of Thermal Power Plant for Integration, New Delhi., 2019c.

Central Electricity Authority: Executive Summary on Power Sector May 2020, New Delhi., 2020a.

Central Electricity Authority: Power Allocation from Central Sector, [online] Available from: http://www.cea.nic.in/monthlypowersupply.html, 2020b.

Central Electricity Regulatory Commission: Consultation Paper On Security Constrained Economic Despatch of Inter State Generating Stations pan India., 2018a.

Central Electricity Regulatory Commission: Discussion Paper on Market Based Economic Dispatch of Electricity : Re-designing of Day-ahead Market (DAM) in India., 2018b.

Central Electricity Regulatory Commission: Discussion Paper on Re-designing Real Time Electricity

Markets in India., 2018c.
Central Electricity Regulatory Commission: Report on Short-term Power Market in India : 2017-19, 2018d.
Centre for Social and Economic Progress: Centre for Social and Economic Progress Electricity and Carbon Tracker, [online] Available from: https://carbontracker.in/, 2019.
de Chalendar, J. A., Taggart, J. and Benson, S. M.: Tracking emissions in the US electricity system, Proc. Natl. Acad. Sci. U. S. A., 116(51), 25497–25502, doi:10.1073/pnas.1912950116, 2019.
Coal India: Price Notification, Kolkata, India. [online] Available from: https://www.coalindia.in/DesktopModules/DocumentList/documents/Price_Notification_dated_08.01.2018_effective_from_0000_Hrs_of_09.01.2018_09012018.pdf, 2018.
Coal India: Koyla Grahak Seva, [online] Available from: https://elib.cmpdi.co.in/SEVA/index.php (Accessed 24 February 2020), 2019.
Cohen, A. J., Brauer, M., Burnett, R., Anderson, H. R., Frostad, J., Estep, K., Balakrishnan, K., Brunekreef, B., Dandona, L., Dandona, R., Feigin, V., Freedman, G., Hubbell, B., Jobling, A., Kan, H., Knibbs, L., Liu, Y., Martin, R., Morawska, L., Pope, C. A., Shin, H., Straif, K., Shaddick, G., Thomas, M., van Dingenen, R., van Donkelaar, A., Vos, T., Murray, C. J. L. and Forouzanfar, M. H.: Estimates and 25-year trends of the global burden of disease attributable to ambient air pollution: an analysis of data from the Global Burden of Diseases Study 2015, Lancet, 389(10082), 1907–1918, doi:10.1016/S0140-6736(17)30505-6, 2017.
Conibear, L., Butt, E. W., Knote, C., Arnold, S. R. and Spracklen, D. V.: Stringent Emission Control Policies Can Provide Large Improvements in Air Quality and Public Health in India, GeoHealth, 2(7), 196–211, doi:10.1029/2018gh000139, 2018.
Crippa, M., Janssens-Maenhout, G., Dentener, F., Guizzardi, D., Sindelarova, K., Muntean, M., Van Dingenen, R. and Granier, C.: Forty years of improvements in European air quality: Regional policy-industry interactions with global impacts, Atmos. Chem. Phys., 16(6), 3825–3841, doi:10.5194/acp-16-3825-2016, 2016.
Cropper, M., Cui, R., Guttikunda, S., Hultman, N., Jawahar, P., Park, Y., Yao, X. and Song, X. P.: The mortality impacts of current and planned coal-fired power plants in India, Proc. Natl. Acad. Sci. U. S. A., 118(5), 1–7, doi:10.1073/pnas.2017936118, 2021.
Cropper, M. L., Guttikunda, S., Jawahar, P., Malik, K. and Partridge, I.: Costs and Benefits of Installing Flue-Gas Desulfurization Units at Coal-Fired Power Plants in India, in Disease Control Priorities, Third Edition (Volume 7): Injury Prevention and Environmental Health, pp. 239–248, The World Bank., 2017.
Cropper, M. L., Guttikunda, S., Jawahar, P., Lazri, Z., Malik, K., Song, X. P. and Yao, X.: Applying Benefit-Cost Analysis to Air Pollution Control in the Indian Power Sector, J. Benefit-Cost Anal., 10(May), 185–205, doi:10.1017/bca.2018.27, 2019.
Deetjen, T. A. and Azevedo, I. L.: Reduced-Order Dispatch Model for Simulating Marginal Emissions Factors for the United States Power Sector, Environ. Sci. Technol., 53(17), 10506–10513,

doi:10.1021/acs.est.9b02500, 2019.

Dennekamp, M., Howarth, S., Dick, C. A. J., Cherrie, J. W., Donaldson, K. and Seaton, A.: Ultrafine particles and nitrogen oxides generated by gas and electric cooking Ultrafine particles and nitrogen oxides generated by gas and electric cooking, Occup. Environ. Med., 58(2), 511–516, doi:10.1136/oem.58.8.511, 2001.

Dockery, D. W., Pope, C. A., Xu, X., Spengler, J. D., Ware, J. H., Fay, M. E., Ferris, B. G. and Speizer, F. E.: An Association between Air Pollution and Mortality in Six U.S. Cities, N. Engl. J. Med., 329(24), 1753–1759, doi:10.1056/NEJM199312093292401, 1993.

Donahue, N. M., Robinson, A. L., Stanier, C. O. and Pandis, S. N.: Coupled partitioning, dilution, and chemical aging of semivolatile organics, Environ. Sci. Technol., 40(8), 2635–2643, doi:10.1021/es052297c, 2006.

Donti, P. L., Kolter, J. Z. and Azevedo, I. L.: How Much Are We Saving after All? Characterizing the Effects of Commonly Varying Assumptions on Emissions and Damage Estimates in PJM, Environ. Sci. Technol., 53(16), 9905–9914, doi:10.1021/acs.est.8b06586, 2019.

Downward, G. S., van Nunen, E. J. H. M., Kerckhoffs, J., Vineis, P., Brunekreef, B., Boer, J. M. A., Messier, K. P., Roy, A., Verschuren, W. M. M., van der Schouw, Y. T., Sluijs, I., Gulliver, J., Hoek, G. and Vermeulen, R.: Long-Term Exposure to Ultrafine Particles and Incidence of Cardiovascular and Cerebrovascular Disease in a Prospective Study of a Dutch Cohort, Environ. Health Perspect., 126(12), 127007, doi:10.1289/EHP3047, 2018.

Elleman, R. A. and Covert, D. S.: Aerosol size distribution modeling with the Community Multiscale Air Quality modeling system in the Pacific Northwest : 3 . Size distribution of particles emitted into a mesoscale model, , 115, 1–14, doi:10.1029/2009JD012401, 2010.

Energy Analytics Lab: Average System Load Profile, Kanpur, India. [online] Available from: https://eal.iitk.ac.in/download/system_load_profile.php, 2019.

Environ: User's guide to the comprehensive air quality model with extensions (CAMx), version 4.02, Novato, CA. [online] Available from: http://www.camx.com/, 2003.

Fioletov, V. E., McLinden, C. A., Krotkov, N., Li, C., Joiner, J., Theys, N., Carn, S. and Moran, M. D.: A global catalogue of large SO2 sources and emissions derived from the Ozone Monitoring Instrument, Atmos. Chem. Phys., 16(18), 11497–11519, doi:10.5194/acp-16-11497-2016, 2016.

Fountoukis, C., Riipinen, I., Denier Van Der Gon, H. A. C., Charalampidis, P. E., Pilinis, C., Wiedensohler, A., O 'dowd, C., Putaud, J. P., Moerman, M. and Pandis, S. N.: Simulating ultrafine particle formation in Europe using a regional CTM: contribution of primary emissions versus secondary formation to aerosol number concentrations, Atmos. Chem. Phys. Atmos. Chem. Phys., 12, 8663–8677, doi:10.5194/acp-12-8663-2012, 2012.

Fountoukis, C., Koraj, D., Denier van der Gon, H. A. C., Charalampidis, P. E., Pilinis, C. and Pandis, S. N.: Impact of grid resolution on the predicted fine PM by a regional 3-D chemical transport model, Atmos. Environ., 68, 24–32, doi:10.1016/j.atmosenv.2012.11.008, 2013.

Gai, Y., Wang, A., Pereira, L., Hatzopoulou, M. and Posen, I. D.: Marginal Greenhouse Gas Emissions of Ontario's Electricity System and the Implications of Electric Vehicle Charging, Environ. Sci. Technol., 53(13), 7903–7912, doi:10.1021/acs.est.9b01519, 2019.

Gao, M., Beig, G., Song, S., Zhang, H., Hu, J., Ying, Q., Liang, F., Liu, Y., Wang, H., Lu, X., Zhu, T., Carmichael, G. R., Nielsen, C. P. and McElroy, M. B.: The impact of power generation emissions on ambient PM2.5 pollution and human health in China and India, Environ. Int., 121(June), 250–259, doi:10.1016/j.envint.2018.09.015, 2018.

Gaydos, T. M., Pinder, R., Koo, B., Fahey, K. M., Yarwood, G. and Pandis, S. N.: Development and application of a three-dimensional aerosol chemical transport model, PMCAMx, Atmos. Environ., 41(12), 2594–2611, doi:10.1016/j.atmosenv.2006.11.034, 2007.

GBD MAPS Working Group: Burden of Disease Attributable to Major Air Pollution Sources in India, Boston., 2018.

Gelaro, R., McCarty, W., Suárez, M. J., Todling, R., Molod, A., Takacs, L., Randles, C. A., Darmenov, A., Bosilovich, M. G., Reichle, R., Wargan, K., Coy, L., Cullather, R., Draper, C., Akella, S., Buchard, V., Conaty, A., da Silva, A. M., Gu, W., Kim, G. K., Koster, R., Lucchesi, R., Merkova, D., Nielsen, J. E., Partyka, G., Pawson, S., Putman, W., Rienecker, M., Schubert, S. D., Sienkiewicz, M. and Zhao, B.: The modern-era retrospective analysis for research and applications, version 2 (MERRA-2), J. Clim., 30(14), 5419–5454, doi:10.1175/JCLI-D-16-0758.1, 2017.

Ghude, S. D., Chate, D. M., Jena, C., Beig, G., Kumar, R., Barth, M. C., Pfister, G. G., Fadnavis, S. and Pithani, P.: Premature mortality in India due to PM 2.5 and ozone exposure, Geophys. Res. Lett., 43(9), 4650–4658, doi:10.1002/2016GL068949, 2016.

Gilliam, R. C. and Pleim, J. E.: Performance Assessment of New Land Surface and Planetary Boundary Layer Physics in the WRF-ARW, J. Appl. Meteorol. Climatol., 49(4), 760–774, doi:10.1175/2009JAMC2126.1, 2010.

Gilmore, E. A., Heo, J., Muller, N. Z., Tessum, C. W., Hill, J., Marshall, J. and Adams, P. J.: An inter-comparison of air quality social cost estimates from reduced-complexity models, Environ. Res. Lett., 2, 1–2, doi:10.1088/1748-9326/ab1ab5, 2019.

Global Burden of Disease Collaborative Network: Global Burden of Disease Study 2019 (GBD 2019) Particulate Matter Risk Curves, Seattle. [online] Available from: https://doi.org/10.6069/KHWH-2703, 2021.

Goodkind, A. L., Tessum, C. W., Coggins, J. S., Hill, J. D. and Marshall, J. D.: Fine-scale damage estimates of particulate matter air pollution reveal opportunities for location-specific mitigation of emissions, Proc. Natl. Acad. Sci. U. S. A., 116(18), 8775–8780, doi:10.1073/pnas.1816102116, 2019.

Google: Google Maps Platform Documentation, [online] Available from: https://developers.google.com/maps/documentation/, 2019.

Government of India: India's Intended Nationally Determined Contribution. [online] Available from:

http://www4.unfccc.int/submissions/INDC/Published Documents/India/1/INDIA INDC TO UNFCCC.pdf, 2015.

Government of India: Gazette of India CG-DL-E-01042021-226335., 2021.

Guo, H., Kota, S. H., Chen, K., Sahu, S. K., Hu, J., Ying, Q., Wang, Y. and Zhang, H.: Source contributions and potential reductions to health effects of particulate matter in India, Atmos. Chem. Phys., 18(20), 15219–15229, doi:10.5194/acp-18-15219-2018, 2018.

Guttikunda, S. K. and Jawahar, P.: Atmospheric emissions and pollution from the coal-fired thermal power plants in India, Atmos. Environ., 92, 449–460, doi:10.1016/j.atmosenv.2014.04.057, 2014.

Guttikunda, S. K. and Jawahar, P.: Evaluation of Particulate Pollution and Health Impacts from Planned Expansion of Coal-Fired Thermal Power Plants in India Using WRF-CAMx Modeling System, Aerosol Air Qual. Res., 18(12), 3187–3202, doi:10.4209/aaqr.2018.04.0134, 2018.

Hammer, M. S., Van Donkelaar, A., Li, C., Lyapustin, A., Sayer, A. M., Hsu, N. C., Levy, R. C., Garay, M. J., Kalashnikova, O. V., Kahn, R. A., Brauer, M., Apte, J. S., Henze, D. K., Zhang, L., Zhang, Q., Ford, B., Pierce, J. R. and Martin, R. V.: Global Estimates and Long-Term Trends of Fine Particulate Matter Concentrations (1998-2018), Environ. Sci. Technol., 54(13), 7879–7890, doi:10.1021/acs.est.0c01764, 2020.

Hawkes, A. D.: Estimating marginal CO2 emissions rates for national electricity systems, Energy Policy, 38(10), 5977–5987, doi:10.1016/j.enpol.2010.05.053, 2010.

Health Effects Institute: Special Report 20 Burden of Disease Attributable to Coal-Burning and Other Major Sources of Air Pollution in China, Boston, MA., 2016.

HEI Review Panel: Understanding the Health Effects of Ambient Ultrafine Particles, Heal. Eff. Inst., (January), 122 [online] Available from: http://pubs.healtheffects.org/view.php?id=394, 2013.

Hennigan, C. J., Westervelt, D. M., Riipinen, I., Engelhart, G. J., Lee, T., Jr, J. L. C., Pandis, S. N., Adams, P. J. and Robinson, A. L.: New particle formation and growth in biomass burning plumes : An important source of cloud condensation nuclei, , 39, 1–5, doi:10.1029/2012GL050930, 2012.

Hoek, G., Brunekreef, B., Goldbohm, S., Fischer, P. and Van Den Brandt, P. A.: Association between mortality and indicators of traffic-related air pollution in the Netherlands: A cohort study, Lancet, 360(9341), 1203–1209, doi:10.1016/S0140-6736(02)11280-3, 2002.

Hoek, G., Krishnan, R. M., Beelen, R., Peters, A., Ostro, B., Brunekreef, B. and Kaufman, J. D.: Long-term air pollution exposure and cardio- respiratory mortality: a review, Environ. Heal., 12(1), 43, doi:10.1186/1476-069X-12-43, 2013.

Hoffmann, B., Moebus, S., Möhlenkamp, S., Stang, A., Lehmann, N., Dragano, N., Schmermund, A., Memmesheimer, M., Mann, K., Erbel, R. and Jöckel, K. H.: Residential exposure to traffic is associated with coronary atherosclerosis, Circulation, 116(5), 489–496, doi:10.1161/CIRCULATIONAHA.107.693622, 2007.

Indian Council of Medical Research, Public Health Foundation of India and Institute for Health Metrics and Evaluation: GBD India Compare Data Visualization, New Delhi., 2017.

Institute, H. E.: State of Global Air 2020, Boston, MA., 2020.

International Energy Agency: India Energy Outlook 2021. [online] Available from: http://www.worldenergyoutlook.org/media/weowebsite/2015/IndiaEnergyOutlook_WEO2015.pdf, 2021.

International Institute for Sustainable Development: The Evolution of the Clean Energy Cess on Coal Production in India. [online] Available from: https://www.iisd.org/sites/default/files/publications/stories-g20-india-en.pdf, 2020.

Jung, J. G., Fountoukis, C., Adams, P. J. and Pandis, S. N.: Simulation of in situ ultrafine particle formation in the eastern United States using PMCAMx-UF, J. Geophys. Res. Atmos., 115(3), D03203, doi:10.1029/2009JD012313, 2010.

Kaltsonoudis, C., Kostenidou, E., Louvaris, E., Psichoudaki, M., Tsiligiannis, E., Florou, K., Liangou, A. and Pandis, S. N.: Characterization of fresh and aged organic aerosol emissions from meat charbroiling, , 7143–7155, 2017.

Kamboj, P. and Tongia, R.: Indian Railways and Coal: An Unsustainable Interdependency, New Delhi, India., 2018.

Karner, A. A., Eisinger, D. S. and Niemeier, D. E. B. A.: Near-Roadway Air Quality : Synthesizing the Findings from Real-World Data, Environ. Sci. Technol., 44(14), 5334–5344, doi:10.1021/es100008x, 2010.

Karydis, V. A., Tsimpidi, A. P. and Pandis, S. N.: Evaluation of a three-dimensional chemical transport model (PMCAMx) in the eastern United States for all four seasons, J. Geophys. Res., 112(D14), D14211, doi:10.1029/2006JD007890, 2007.

Kreyling, W. G., Semmler-Behnke, M. and Mo?ller, W.: Ultrafine particle - Lung interactions: Does size matter?, J. Aerosol Med. Depos. Clear. Eff. Lung, 19(1), 74–83, doi:10.1089/jam.2006.19.74, 2006.

Kumar, P., Banerjee, R. and Mishra, T.: A framework for analyzing trade-offs in cost and emissions in power sector, Energy, 195, 116949, doi:10.1016/j.energy.2020.116949, 2020.

Laden, F., Schwartz, J., Speizer, F. E. and Dockery, D. W.: Reduction in fine particulate air pollution and mortality: Extended follow-up of the Harvard Six Cities Study, Am. J. Respir. Crit. Care Med., 173(6), 667–672, doi:10.1164/rccm.200503-443OC, 2006.

Lanki, T., Pekkanen, J., Aalto, P., Elosua, R., Berglind, N., D'Ippoliti, D., Kulmala, M., Nyberg, F., Peters, A., Picciotto, S., Salomaa, V., Sunyer, J., Tiittanen, P., Von Klot, S. and Forastiere, F.: Associations of traffic related air pollutants with hospitalisation for first acute myocardial infarction: The HEAPSS study, Occup. Environ. Med., 63(12), 844–851, doi:10.1136/oem.2005.023911, 2006.

Laumbach, R. J., Rich, D. Q., Gandhi, S., Amorosa, L., Schneider, S., Zhang, J., Ohman-Strickland, P., Gong, J., Lelyanov, O. and Kipen, H. M.: Acute Changes in Heart Rate Variability in Subjects With Diabetes Following a Highway Traffic Exposure, J. Occup. Environ. Med., 52(3), 324–331,

doi:10.1097/JOM.0b013e3181d241fa, 2010.

Lelieveld, J., Evans, J. S., Fnais, M., Giannadaki, D. and Pozzer, A.: The contribution of outdoor air pollution sources to premature mortality on a global scale, Nature, 525(7569), 367–371, doi:10.1038/nature15371, 2015.

Li, C., McLinden, C., Fioletov, V., Krotkov, N., Carn, S., Joiner, J., Streets, D., He, H., Ren, X., Li, Z. and Dickerson, R. R.: India Is Overtaking China as the World's Largest Emitter of Anthropogenic Sulfur Dioxide, Sci. Rep., 7(1), 14304, doi:10.1038/s41598-017-14639-8, 2017a.

Li, M., Smith, T. M., Yang, Y. and Wilson, E. J.: Marginal Emission Factors Considering Renewables: A Case Study of the U.S. Midcontinent Independent System Operator (MISO) System, Environ. Sci. Technol., 51(19), 11215–11223, doi:10.1021/acs.est.7b00034, 2017b.

Lipsett, M. J., Ostro, B. D., Reynolds, P., Goldberg, D., Hertz, A., Jerrett, M., Smith, D. F., Garcia, C., Chang, E. T. and Bernstein, L.: Long-term exposure to air pollution and cardiorespiratory disease in the California teachers study cohort, Am. J. Respir. Crit. Care Med., 184(7), 828–835, doi:10.1164/rccm.201012-2082OC, 2011.

Lu, Z. and Streets, D. G.: Increase in NOx emissions from indian thermal power plants during 1996-2010: Unit-based inventories and multisatellite observations, Environ. Sci. Technol., 46(14), 7463–7470, doi:10.1021/es300831w, 2012.

Lu, Z., Streets, D. G., Foy, B. De and Krotkov, N. A.: Ozone Monitoring Instrument Observations of Interannual Increases in SO 2 Emissions from Indian Coal-Fired Power Plants during 2005 − 2012, , doi:10.1021/es4039648, 2013a.

Lu, Z., Streets, D. G., De Foy, B. and Krotkov, N. A.: Ozone monitoring instrument observations of interannual increases in SO2 emissions from Indian coal-fired power plants during 2005-2012, Environ. Sci. Technol., 47(24), 13993–14000, doi:10.1021/es4039648, 2013b.

Ma, W. and Qian, S.: Traffic impact of the Greenfield Bridge closure (AM Peak)., 2015.

Malings, C., Tanzer, R., Hauryliuk, A., Kumar, S. P. N., Zimmerman, N., Kara, L. B. and Presto, A. A.: Development of a general calibration model and long-term performance evaluation of low-cost sensors for air pollutant gas monitoring, Atmos. Meas. Tech., 12(2), 903–920, doi:10.5194/amt-12-903-2019, 2019.

Mazaheri, M., Johnson, G. R. and Morawska, L.: Particle and Gaseous Emissions from Commercial Aircraft at Each Stage of the Landing and Takeoff Cycle, Environ. Sci. Technol., 43(2), 441–446, doi:10.1021/es8013985, 2009.

McCreanor, J., Cullinan, P., Nieuwenhuijsen, M. J., Stewart-Evans, J., Malliarou, E., Jarup, L., Harrington, R., Svartengren, M., Han, I.-K., Ohman-Strickland, P., Chung, K. F. and Zhang, J.: Respiratory Effects of Exposure to Diesel Traffic in Persons with Asthma, N. Engl. J. Med., 357(23), 2348–2358, doi:10.1056/NEJMoa071535, 2007.

Ministry of Coal: Provisional Coal Statistics 2017-2018, Kolkata, India. [online] Available from: file:///C:/Users/sseng/Downloads/ProvisionalCoalStat2017-18.pdf, 2018.

Ministry of Environment Forest and Climate Change: Gazette of India REGD. NO. D. L.-33004/99., 2015.

Ministry of Petroleum and Natural Gas: State/UT-wise Sales Tax Rates Applicable on Crude Oil, Natural Gas and Select Major Petroleum Products As on 1 April, 2018, [online] Available from: https://data.gov.in/resources/stateut-wise-sales-tax-rates-applicable-crude-oil-natural-gas-and-select-major-petroleum (Accessed 24 February 2020), 2019.

Ministry of Power: Merit Order Despatch of Electricity for Rejuvenation of Income and Transparency (MERIT), [online] Available from: http://meritindia.in/, 2020a.

Ministry of Power: National Power Portal, [online] Available from: https://npp.gov.in/publishedReports (Accessed 24 February 2020b), 2020.

Ministry of Power: Pradhan Mantri Sahaj Bijli Har Ghar Yojana, [online] Available from: https://saubhagya.gov.in/, 2020c.

Mitchell, A.: The ESRI Guide to GIS Analysis, Volume 2, ESRI Press., 2005.

Mohan, R. R., Dharmala, N., Ramakrishnan, M., Kumar, P. and Bose, A.: Greenhouse Gas Emission Estimates from the Energy Sector in India at the Sub-national Level (Version/edition 2.0), New Delhi. [online] Available from: http://www.ghgplatform-india.org/methodology-electricityenergy-sector, 2019.

Napari, I., Noppel, M., Vehkamaki, H. and Kulmala, M.: Parametrization of ternary nucleation rates for H2SO4-NH3-H2O vapors, J. Geophys. Res. Atmos., 107(19), 2–7, doi:10.1029/2002JD002132, 2002.

National Thermal Power Corporation: Delivered Cost of Gas, 2017.

Oberschelp, C., Pfister, S., Raptis, C. E. and Hellweg, S.: Global emission hotspots of coal power generation, Nat. Sustain., 2(2), 113–121, doi:10.1038/s41893-019-0221-6, 2019.

Ohlwein, S., Kappeler, R., Kutlar Joss, M., Künzli, N. and Hoffmann, B.: Health effects of ultrafine particles: a systematic literature review update of epidemiological evidence, Int. J. Public Health, 7(Hei 2013), doi:10.1007/s00038-019-01202-7, 2019.

Ostro, B., Hu, J., Goldberg, D., Reynolds, P., Hertz, A., Bernstein, L. and Kleeman, M. J.: Associations of mortality with long-term exposures to fine and ultrafine particles, species and sources: results from the california teachers study cohort., Environ. Health Perspect., 123(6), 549–56, doi:10.1289/ehp.1408565, 2015.

Palchak, D., Cochran, J., Ehlen, A., McBennett, B., Milligan, M., Chernyakhoviskiy, I., Deshmukh, R., Abhyankar, N., Soonee, S. K., Narasimhan, S. R., Joshi, M. and Sreedharan, P.: Greening the Grid: Pathways to Integrate 175 Gigawatts of Renewable Energy Into India’s Electric Grid: Vol I., 2017a.

Palchak, D., Cochran, J., Ehlen, A., McBennett, B., Milligan, M., Chernyakhoviskiy, I., Deshmukh, R., Abhyankar, N., Soonee, S. K., Narasimhan, S. R., Joshi, M. and Sreedharan, P.: Greening the Grid: Pathways to Integrate 175 Gigawatts of Renewable Energy Into India’s Electric Grid: Vol II., 2017b.

Pandey, A., Brauer, M., Cropper, M. L., Balakrishnan, K., Mathur, P., Dey, S., Turkgulu, B., Kumar, G. A., Khare, M., Beig, G., Gupta, T., Krishnankutty, R. P., Causey, K., Cohen, A. J., Bhargava, S., Aggarwal, A. N., Agrawal, A., Awasthi, S., Bennitt, F., Bhagwat, S., Bhanumati, P., Burkart, K., Chakma, J. K., Chiles, T. C., Chowdhury, S., Christopher, D. J., Dey, S., Fisher, S., Fraumeni, B., Fuller, R., Ghoshal, A. G., Golechha, M. J., Gupta, P. C., Gupta, R., Gupta, R., Gupta, S., Guttikunda, S., Hanrahan, D., Harikrishnan, S., Jeemon, P., Joshi, T. K., Kant, R., Kant, S., Kaur, T., Koul, P. A., Kumar, P., Kumar, R., Larson, S. L., Lodha, R., Madhipatla, K. K., Mahesh, P. A., Malhotra, R., Managi, S., Martin, K., Mathai, M., Mathew, J. L., Mehrotra, R., Mohan, B. V. M., Mohan, V., Mukhopadhyay, S., Mutreja, P., Naik, N., Nair, S., Pandian, J. D., Pant, P., Perianayagam, A., Prabhakaran, D., Prabhakaran, P., Rath, G. K., Ravi, S., Roy, A., Sabde, Y. D., Salvi, S., Sambandam, S., Sharma, B., Sharma, M., Sharma, S., Sharma, R. S., Shrivastava, A., Singh, S., Singh, V., Smith, R., Stanaway, J. D., Taghian, G., Tandon, N., Thakur, J. S., Thomas, N. J., Toteja, G. S., Varghese, C. M., Venkataraman, C., Venugopal, K. N., Walker, K. D., Watson, A. Y., Wozniak, S., Xavier, D., Yadama, G. N., Yadav, G., Shukla, D. K., Bekedam, H. J., et al.: Health and economic impact of air pollution in the states of India: the Global Burden of Disease Study 2019, Lancet Planet. Heal., 5(1), e25–e38, doi:10.1016/S2542-5196(20)30298-9, 2021.

Paolella, D. A., Tessum, C. W., Adams, P. J., Apte, J. S., Chambliss, S., Hill, J., Muller, N. Z. and Marshall, J. D.: Effect of Model Spatial Resolution on Estimates of Fine Particulate Matter Exposure and Exposure Disparities in the United States, Environ. Sci. Technol. Lett., 5(7), 436–441, doi:10.1021/acs.estlett.8b00279, 2018.

Parray, M. T., Dalal, U. and Tongia, R.: Brookings India Electricity and Carbon Tracker. [online] Available from: https://www.brookings.edu/research/insights-from-the-brookings-india-electricity-and-carbon-tracker/, 2019.

Patoulias, D., Riipinen, I. and Pandis, S. N.: The role of organic condensation on ultrafine particle growth during nucleation events, Atmos. Chem. Phys., 15(11), 2259, doi:10.5194/acp-15-6337-2015, 2015.

Patoulias, D., Fountoukis, C., Riipinen, I., Asmi, A., Kulmala, M. and Pandis, S. N.: Simulation of the size-composition distribution of atmospheric nanoparticles over Europe, Atmos. Chem. Phys., 18(18), 13639–13654, doi:10.5194/acp-18-13639-2018, 2018.

Peng, W., Dai, H., Guo, H., Purohit, P., Urpelainen, J., Wagner, F., Wu, Y. and Zhang, H.: The Critical Role of Policy Enforcement in Achieving Health, Air Quality, and Climate Benefits from India's Clean Electricity Transition, Environ. Sci. Technol., doi:10.1021/acs.est.0c01622, 2020.

Peters, A., von Klot, S., Heier, M., Trentinaglia, I., Hörmann, A., Wichmann, H. E. and Löwel, H.: Exposure to Traffic and the Onset of Myocardial Infarction, N. Engl. J. Med., 351(17), 1721–1730, doi:10.1056/NEJMoa040203, 2004.

Phadke, A., Abhyankar, N. and Deshmukh, R.: Techno-Economic Assessment of Integrating 175GW of

Renewable Energy into the Indian Grid by 2022., 2016.

Pierce, J. R. and Adams, P. J.: Efficiency of cloud condensation nuclei formation from ultrafine particles, Atmos. Chem. Phys., 7, 1367–1379, doi:10.5194/acpd-6-10991-2006, 2007.

Pope, C. A., Burnett, R. T., Thun, M. J., Calle, E. E., Krewski, D. and Thurston, G. D.: to Fine Particulate Air Pollution, J. Am. Med. Assoc., 287(9), 1132–1141, doi:10.1001/jama.287.9.1132, 2002.

Posner, L. N. and Pandis, S. N.: Sources of ultrafine particles in the Eastern United States, Atmos. Environ., 111, 103–112, doi:10.1016/j.atmosenv.2015.03.033, 2015.

Power System Operation Corporation Limited: Daily Power Supply Position Report, New Delhi, India. [online] Available from: https://posoco.in/reports/daily-reports/, 2018.

Power System Operation Corporation Limited: Security Constrained Economic Dispatch of Inter-state Generating Stations pan-India: Detailed Feedback Report on Pilot, New Delhi., 2020.

Ramanathan, S., Arora, S. and Trivedi, V.: Coal-Based Power Norms: Where do we stand today?, New Delhi. [online] Available from: https://www.cseindia.org/coal-based-power-norms-coal-based-10125, 2020.

Rose Eilenberg, S., Subramanian, R., Malings, C., Hauryliuk, A., Presto, A. A. and Robinson, A. L.: Using a network of lower-cost monitors to identify the influence of modifiable factors driving spatial patterns in fine particulate matter concentrations in an urban environment, J. Expo. Sci. Environ. Epidemiol., 30(6), 949–961, doi:10.1038/s41370-020-0255-x, 2020.

Ryan, N. A., Johnson, J. X. and Keoleian, G. A.: Comparative Assessment of Models and Methods to Calculate Grid Electricity Emissions, Environ. Sci. Technol., 50(17), 8937–8953, doi:10.1021/acs.est.5b05216, 2016.

Safiullah, H., Hug, G. and Tongia, R.: Design of load balancing mechanism for Indian electricity markets, Energy Syst., 8(2), 309–350, doi:10.1007/s12667-016-0199-3, 2017.

Saha, P. K., Robinson, E. S., Shah, R. U., Apte, J. S., Robinson, A. L. and Presto, A. A.: Reduced Ultrafine Particle Concentration in Urban Air : Changes in Nucleation and Anthropogenic Emissions, , doi:10.1021/acs.est.8b00910, 2018.

Saha, P. K., Zimmerman, N., Malings, C., Hauryliuk, A., Li, Z., Snell, L., Subramanian, R., Lipsky, E., Apte, J. S., Robinson, A. L. and Presto, A. A.: Quantifying high-resolution spatial variations and local source impacts of urban ultrafine particle concentrations, Sci. Total Environ., 655, 473–481, doi:10.1016/j.scitotenv.2018.11.197, 2019.

Sahu, S. K., Ohara, T. and Beig, G.: The role of coal technology in redefining India’s climate change agents and other pollutants, Environ. Res. Lett., 12(10), doi:10.1088/1748-9326/aa814a, 2017.

Sehgal, A. and Tongia, R.: Coal Requirement in 2020 : A Bottom-up Analysis., 2016.

Sengupta, S., Deetjen, T. A., Kumboj, P., D’Souza, S., Adams, P. J., Tongia, R. and Azevedo, I. L.: National Policy Interventions in Current Indian Power Generation Produce Disparate, State-Level Carbon and Sulfur Emission Impacts., 2021.

Siler-Evans, K., Azevedo, I. L. and Morgan, M. G.: Marginal emissions factors for the U.S. electricity

system, Environ. Sci. Technol., 46(9), 4742–4748, doi:10.1021/es300145v, 2012.

Soman, A., Ganesan, K. and Kaur, H.: India's Electric Vehicle Transition, , (October), 2019.

Spencer, T. and Awasthy, A.: Analysing and Projecting Indian Electricity Demand to 2030, New Delhi. [online] Available from: https://www.teriin.org/sites/default/files/2019-02/Analysing and Projecting Indian Electricity Demand to 2030.pdf, 2019.

Spencer, T., Rodrigues, N., Pachouri, R., Thakre, S. and Renjith, G.: Renewable Power Pathways: Modelling the Integration of Wind and Solar in India by 2030, New Delhi., 2020.

Srinivasan, S., Roshna, N., Guttikunda, S., Kanudia, A., Saif, S. and Asundi, J.: Benefit Cost Analysis of Emissions Standards for Coal-Based Thermal Power Plants in India, Bangalore. [online] Available from: (CSTEP-Report-2018-06), 2018.

Sugathan, A., Bhangale, R., Kansal, V. and Hulke, U.: How can Indian power plants cost-effectively meet the new sulfur emission standards? Policy evaluation using marginal abatement cost-curves, Energy Policy, 121(June), 124–137, doi:10.1016/j.enpol.2018.06.008, 2018.

Tanzer, R., Malings, C., Hauryliuk, A., Subramanian, R. and Presto, A. A.: Demonstration of a Low-Cost Multi-Pollutant Network to Quantify Intra-Urban Spatial Variations in Air Pollutant Source Impacts and to Evaluate Environmental Justice, Int. J. Environ. Res. Public Health, 16(14), 2523, doi:10.3390/ijerph16142523, 2019.

Tessum, C. W., Hill, J. D. and Marshall, J. D.: InMAP: a new model for air pollution interventions, Geosci. Model Dev. Discuss., 8(10), 9281–9321, doi:10.5194/gmdd-8-9281-2015, 2015.

Tessum, C. W., Hill, J. D. and Marshall, J. D.: InMAP: A model for air pollution interventions, edited by J. A. Añel, PLoS One, 12(4), e0176131, doi:10.1371/journal.pone.0176131, 2017.

Thakrar, S. K., Tessum, C. W., Apte, J. S., Balasubramanian, S., Millet, D. B., Pandis, S. N., Marshall, J. D. and Hill, J. D.: Global, high-resolution, reduced-complexity air quality modeling using InMAP (Intervention Model for Air Pollution), ChemRxiv [online] Available from: https://doi.org/10.26434/chemrxiv.14330375.v1, 2021.

Thind, M. P. S., Wilson, E. J., Azevedo, I. L. and Marshall, J. D.: Marginal Emissions Factors for Electricity Generation in the Midcontinent ISO, Environ. Sci. Technol., 51(24), 14445–14452, doi:10.1021/acs.est.7b03047, 2017.

Thind, M. P. S., Tessum, C. W., Azevedo, I. L. and Marshall, J. D.: Fine Particulate Air Pollution from Electricity Generation in the US: Health Impacts by Race, Income, and Geography, Environ. Sci. Technol., 53(23), 14010–14019, doi:10.1021/acs.est.9b02527, 2019.

Tong, D., Zhang, Q., Davis, S. J., Liu, F., Zheng, B., Geng, G., Xue, T., Li, M., Hong, C., Lu, Z., Streets, D. G., Guan, D. and He, K.: Targeted emission reductions from global super-polluting power plant units, Nat. Sustain., 1(1), 59–68, doi:10.1038/s41893-017-0003-y, 2018.

Tongia, R. and Gross, S.: Coal in India: Adjusting to transition, , (March) [online] Available from: https://www.brookings.edu/wp-content/uploads/2019/03/Tongia_and_Gross_2019_Coal_In_India_Adjusting_To_Transition.pdf,

2019.

Tzivion, S., Feingold, G. and Levin, Z.: An Efficient Numerical Solution to the Stochastic Collection Equation, J. Atmos. Sci., 44(21), 3139–3149, doi:10.1175/1520-0469(1987)044<3139:AENSTT>2.0.CO;2, 1987.

Tzivion, S., Feingold, G. and Levin, Z.: The Evolution of Raindrop Spectra. Part II: Collisional Collection/Breakup and Evaporation in a Rainshaft, J. Atmos. Sci., 46(21), 3312–3328, doi:10.1175/1520-0469(1989)046<3312:TEORSP>2.0.CO;2, 1989.

U.S. Census Bureau: TIGER / Line Shapefiles Technical Documentation. [online] Available from: https://www.census.gov/geo/maps-data/data/pdfs/tiger/tgrshp2012/TGRSHP2012_TechDoc.pdf, 2017.

U.S. Energy Information Administration: How much carbon dioxide is produced when different fuels are burned?, [online] Available from: https://www.eia.gov/tools/faqs/faq.php?id=73&t=11, 2020.

U.S. Environmental Protection Agency: Technical Support Document (TSD) Preparation of Emissions Inventories for the Version 6.3 , 2011 Emissions Modeling Platform. [online] Available from: https://www.epa.gov/sites/production/files/2016-09/documents/2011v6_3_2017_emismod_tsd_aug2016_final.pdf, 2016.

U.S. EPA: The Emissions & Generation Resource Integrated Database (eGRID) Technical Support Document, US Environ. Prot. Agency, 2018.

United Nations Framework Convention on Climate Change: Methodological Tool: Tool to calculate the emission factor for an electricity system., 2015.

Venecek, M. A., Yu, X. and Kleeman, M. J.: Predicted ultrafine particulate matter source contribution across the continental United States during summertime air pollution events, Atmos. Chem. Phys., 19(14), 9399–9412, doi:10.5194/acp-19-9399-2019, 2019.

Venkataraman, C., Brauer, M., Tibrewal, K., Sadavarte, P., Ma, Q., Cohen, A., Chaliyakunnel, S., Frostad, J., Klimont, Z., Martin, R. V., Millet, D. B., Philip, S., Walker, K. and Wang, S.: Source influence on emission pathways and ambient PM2.5 pollution over India (2015–2050), Atmos. Chem. Phys., 18(11), 8017–8039, doi:10.5194/acp-18-8017-2018, 2018.

Wang, J., Xing, J., Mathur, R., Pleim, J. E., Wang, S., Hogrefe, C., Gan, C.-M., Wong, D. C. and Hao, J.: Historical Trends in PM 2.5 -Related Premature Mortality during 1990–2010 across the Northern Hemisphere, Environ. Health Perspect., 125(3), 400–408, doi:10.1289/EHP298, 2017.

Weichenthal, S., Kulka, R., Dubeau, A., Martin, C., Wang, D. and Dales, R.: Traffic-related air pollution and acute changes in heart rate variability and respiratory function in urban cyclists, Environ. Health Perspect., 119(10), 1373–1378, doi:10.1289/ehp.1003321, 2011.

Weichenthal, S., Bai, L., Hatzopoulou, M., Van Ryswyk, K., Kwong, J. C., Jerrett, M., van Donkelaar, A., Martin, R. V., Burnett, R. T., Lu, H. and Chen, H.: Long-term exposure to ambient ultrafine particles and respiratory disease incidence in in Toronto, Canada: a cohort study, Environ. Heal., 16(1), 64, doi:10.1186/s12940-017-0276-7, 2017.

Westervelt, D. M., Pierce, J. R., Riipinen, I., Trivitayanurak, W., Hamed, A., Kulmala, M., Laaksonen, A., Decesari, S. and Adams, P. J.: Formation and growth of nucleated particles into cloud condensation nuclei: Model-measurement comparison, Atmos. Chem. Phys., 13(15), 7645–7663, doi:10.5194/acp-13-7645-2013, 2013.

Westervelt, D. M., Pierce, J. R. and Adams, P. J.: Analysis of feedbacks between nucleation rate, survival probability and cloud condensation nuclei formation, Atmos. Chem. Phys., 14(11), 5577–5597, doi:10.5194/acp-14-5577-2014, 2014.

World Bank: GDP, PPP (current international $), [online] Available from: https://data.worldbank.org/indicator/ny.gdp.mktp.pp.cd, 2018a.

World Bank: GDP per capita, PPP (current international $), [online] Available from: https://data.worldbank.org/indicator/NY.GDP.PCAP.PP.CD, 2018b.

World Resources Institute: CAIT Climate Data Explorer, [online] Available from: http://cait.wri.org/, 2019.

Yu, X., Venecek, M., Kumar, A., Hu, J., Tanrikulu, S., Soon, S. T., Tran, C., Fairley, D. and Kleeman, M. J.: Regional sources of airborne ultrafine particle number and mass concentrations in California, Atmos. Chem. Phys., 19(23), 14677–14702, doi:10.5194/acp-19-14677-2019, 2019.

Zhang, Y., West, J. J., Mathur, R., Xing, J., Hogrefe, C., Roselle, S. J., Bash, J. O., Pleim, J. E., Gan, C.-M. and Wong, D. C.: Long-term trends in the ambient PM2.5- and O3-related mortality burdens in the United States under emission reductions from 1990 to 2010, Atmos. Chem. Phys., 18(20), 15003–15016, doi:10.5194/acp-18-15003-2018, 2018.

Zimmerman, N., Presto, A. A., Kumar, S. P. N., Gu, J., Hauryliuk, A., Robinson, E. S., Robinson, A. L. and Subramanian, R.: A machine learning calibration model using random forests to improve sensor performance for lower-cost air quality monitoring, , 291–313, 2018.

Zuurbier, M., Hoek, G., Oldenwening, M., Meliefste, K., Krop, E., van den Hazel, P. and Brunekreef, B.: In-traffic air pollution exposure and CC16, blood coagulation, and inflammation markers in healthy adults, Environ. Health Perspect., 119(10), 1384–1389, doi:10.1289/ehp.1003151, 2011.

8 Appendix A

Sector	Size Distribution	Reference	Number Emissions Zeroed Out	Mass Emissions Preserved
Dust	100% dust	Asmi et al. (2011)	-	-
Agricultural Fire	100% biomass	Hennigan et al. (2012)	-	-
Marine Vessels	100% diesel	Ban-Weiss et al. (2010)	-	-
Cooking	100% meat cooking	Kaltsonoudis et al. (2017)	-	-
Non-Point	95% biomass + 2% natural gas combustion + 1 % diesel + 2% coal	Hennigan et al. (2012), Dennekamp et al. (2001), Ban-Weiss et al. (2010), Elleman and Covert (2010)	90%	98%
Off-Road Mobile	55% diesel + 45% gasoline	Ban-Weiss et al. (2010)	92%	86%
Oil & Gas	100% diesel	Ban-Weiss et al. (2010)	-	-
On-Road Traffic	52% diesel + 48% gasoline	Ban-Weiss et al. (2010)	93%	86%
Oil & Gas Point	100% diesel	Ban-Weiss et al. (2010)	-	-
Power Plants	99.7% coal + 0.3% natural gas	Elleman and Covert (2010), Dennekamp et al. (2001)	91%	92%
Industrial Point	100% diesel	Ban-Weiss et al. (2010)	-	-
Rail	100% diesel	Ban-Weiss et al. (2010)	-	-
Residential Wood Combustion	100% biomass	Hennigan et al. (2012)	92%	59%

Table 2
Size distributions applied to convert mass emissions to number emissions along with sensitivity zero out values.

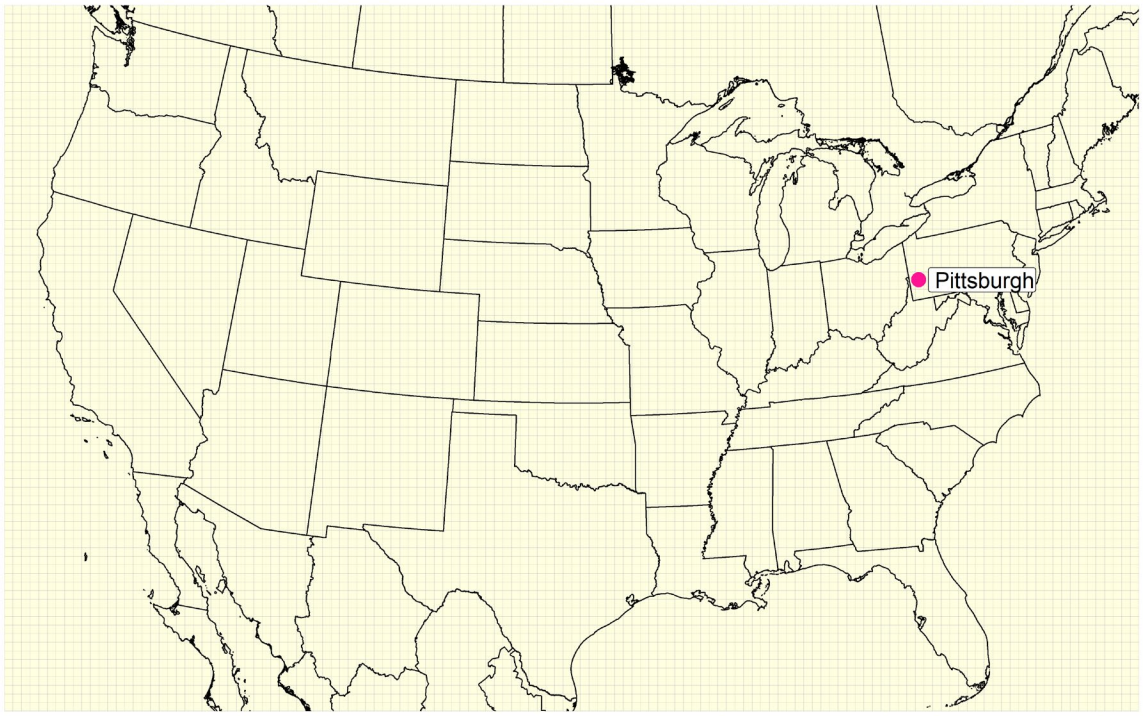

Figure 29
36-km resolution modeling domain over the continental United States with the location of Pittsburgh.

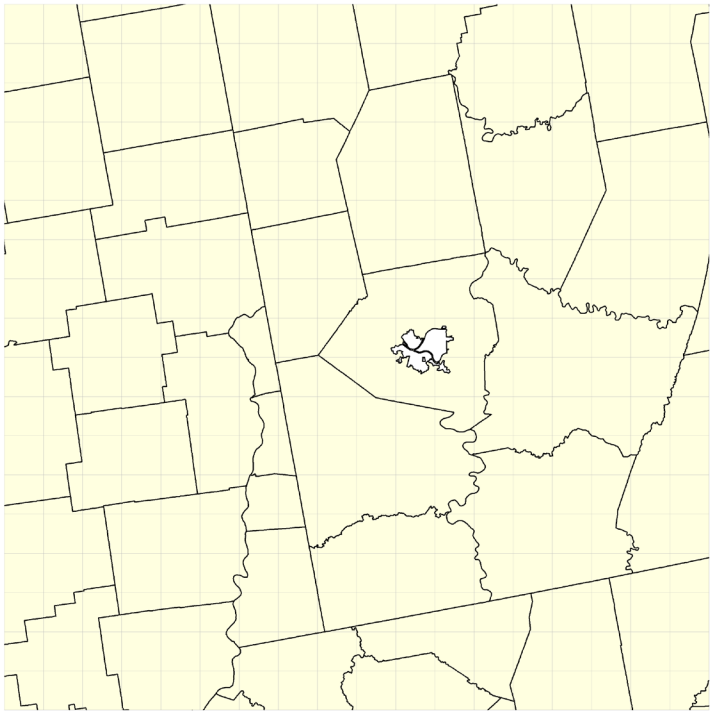

Figure 30
12-km modeling domain over southwestern Pennsylvania with location of Pittsburgh noted in center.

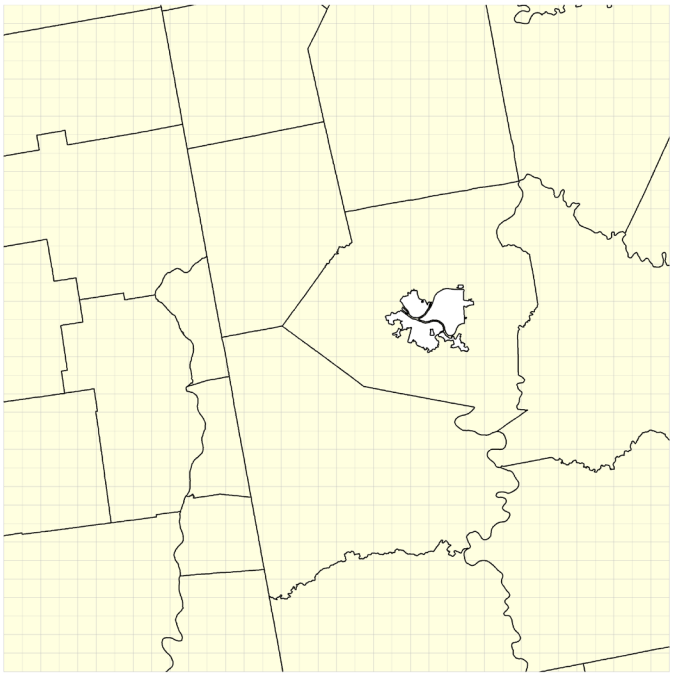

Figure 31
4-km modeling domain over southwestern Pennsylvania with location of Pittsburgh noted in center.

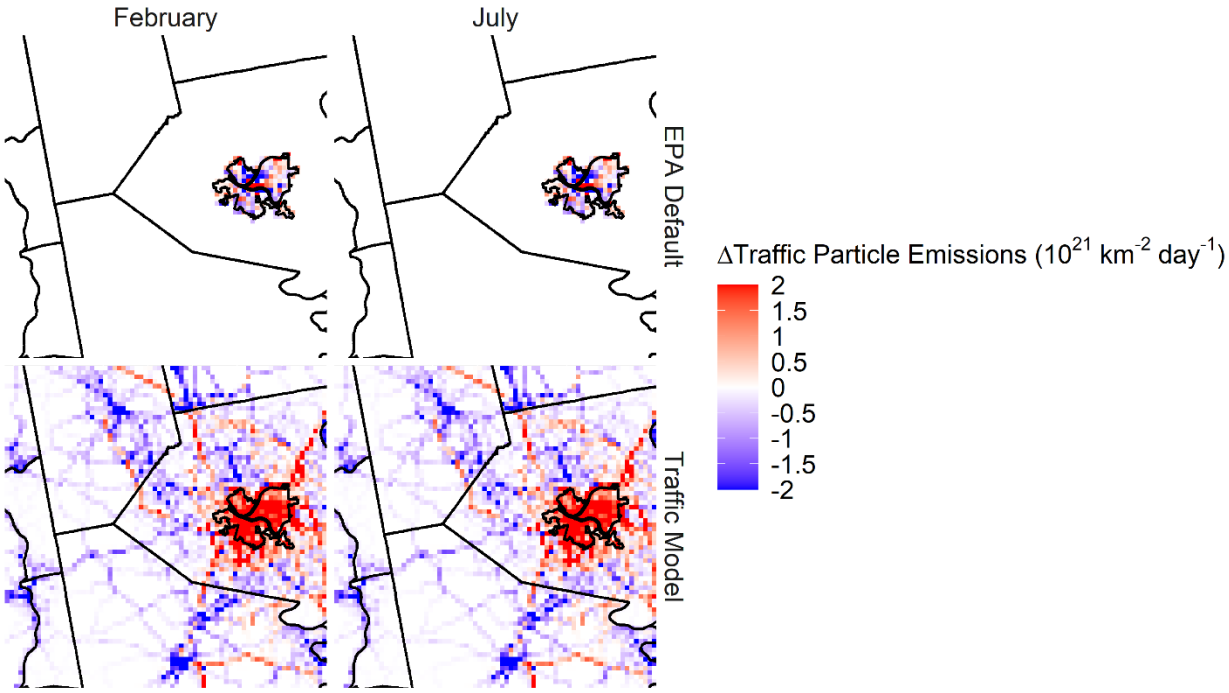

Figure 32
Change in on-road traffic number emissions for the EPA-default and traffic model on-road traffic emission spatial surrogate relative to the traffic model.

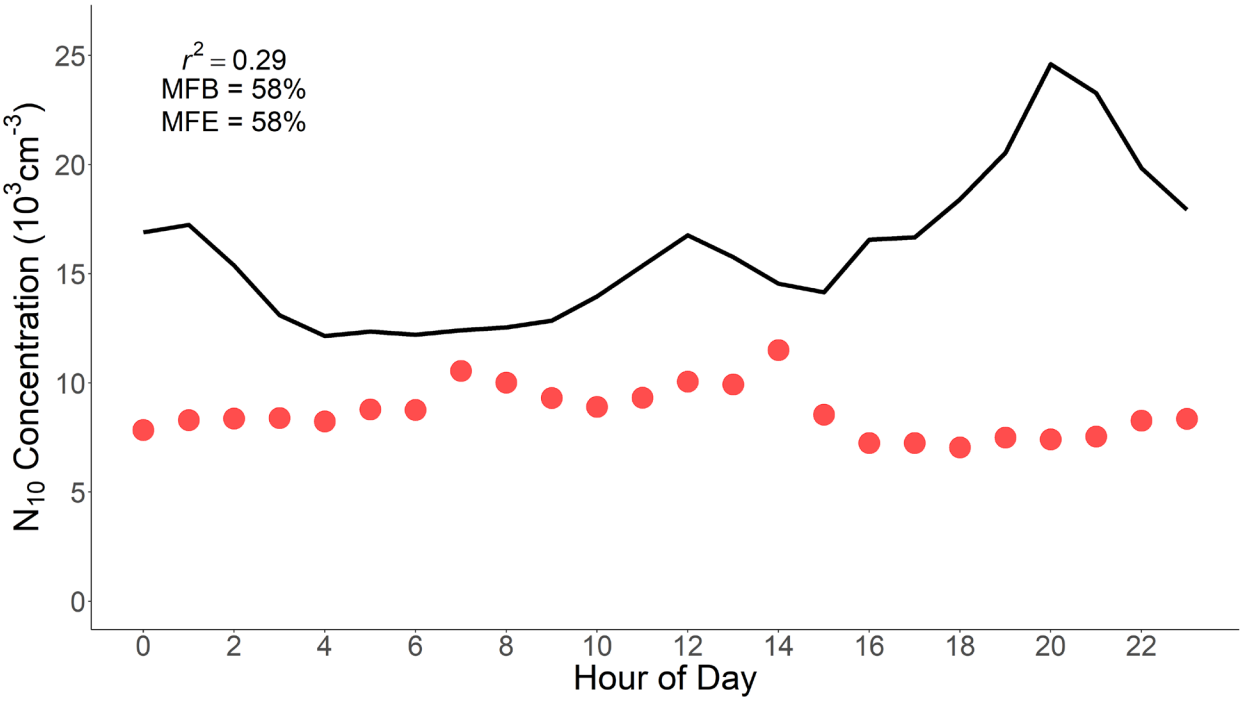

Figure 33
Diurnal averages of July 2017 N_{10} model predictions (solid line) and N_{10} observations at Carnegie Mellon University (red points).

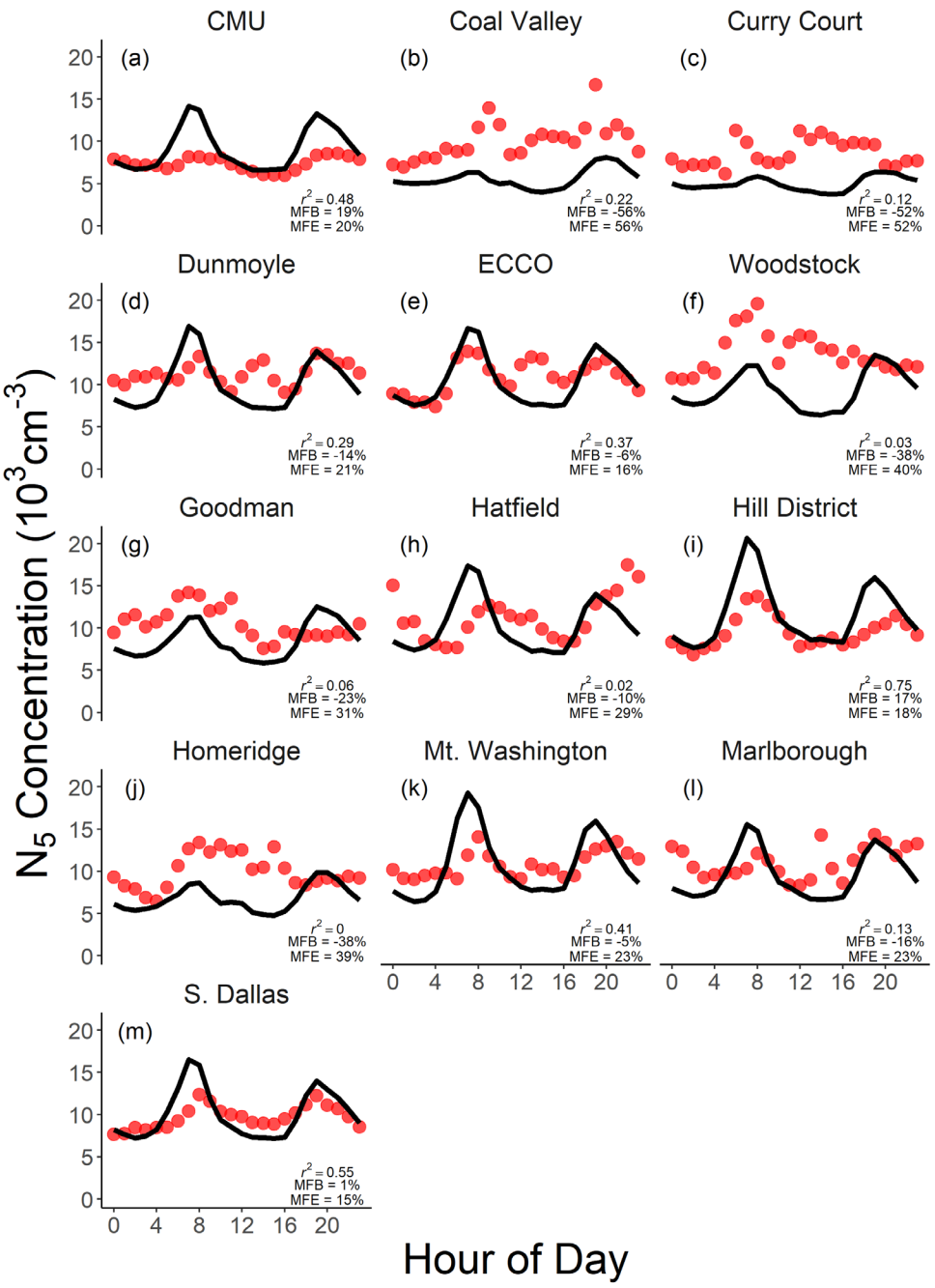

Figure 34
Diurnal averages of February 2017 N_5 model predictions (solid line) and all-winter observed N_5 concentrations (red points) at 13 urban background or local road sites using the traffic model on-road traffic emissions spatial surrogate. Sites are the same sites as **Figure 5**.

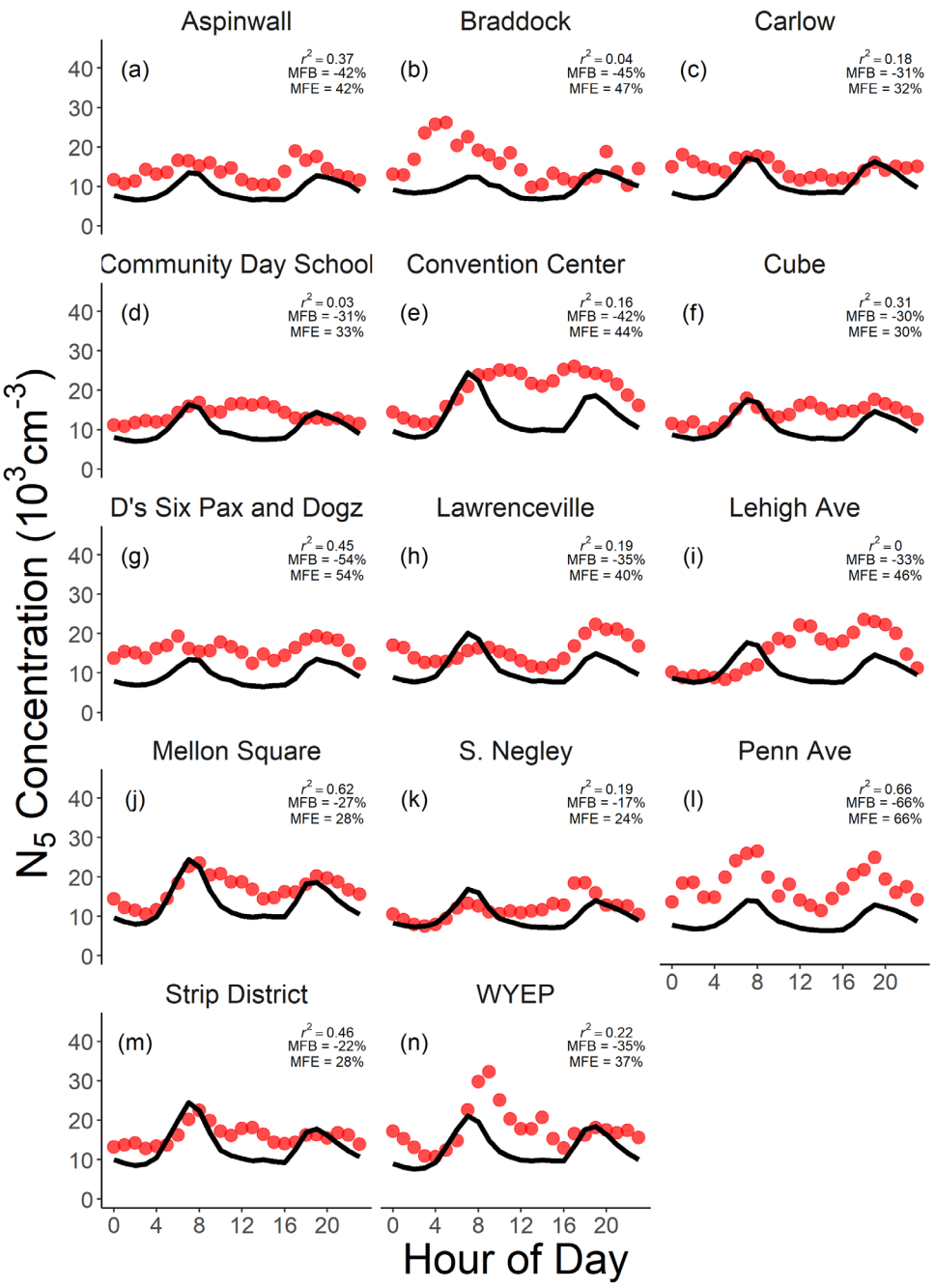

Figure 35
Diurnal averages of February 2017 N_5 model predictions (solid line) and all-winter observed N_5 concentrations (red points) at 14 influenced by local sources or topography using the mixed on-road traffic emissions spatial surrogate. Sites are the same sites as **Figure 6**.

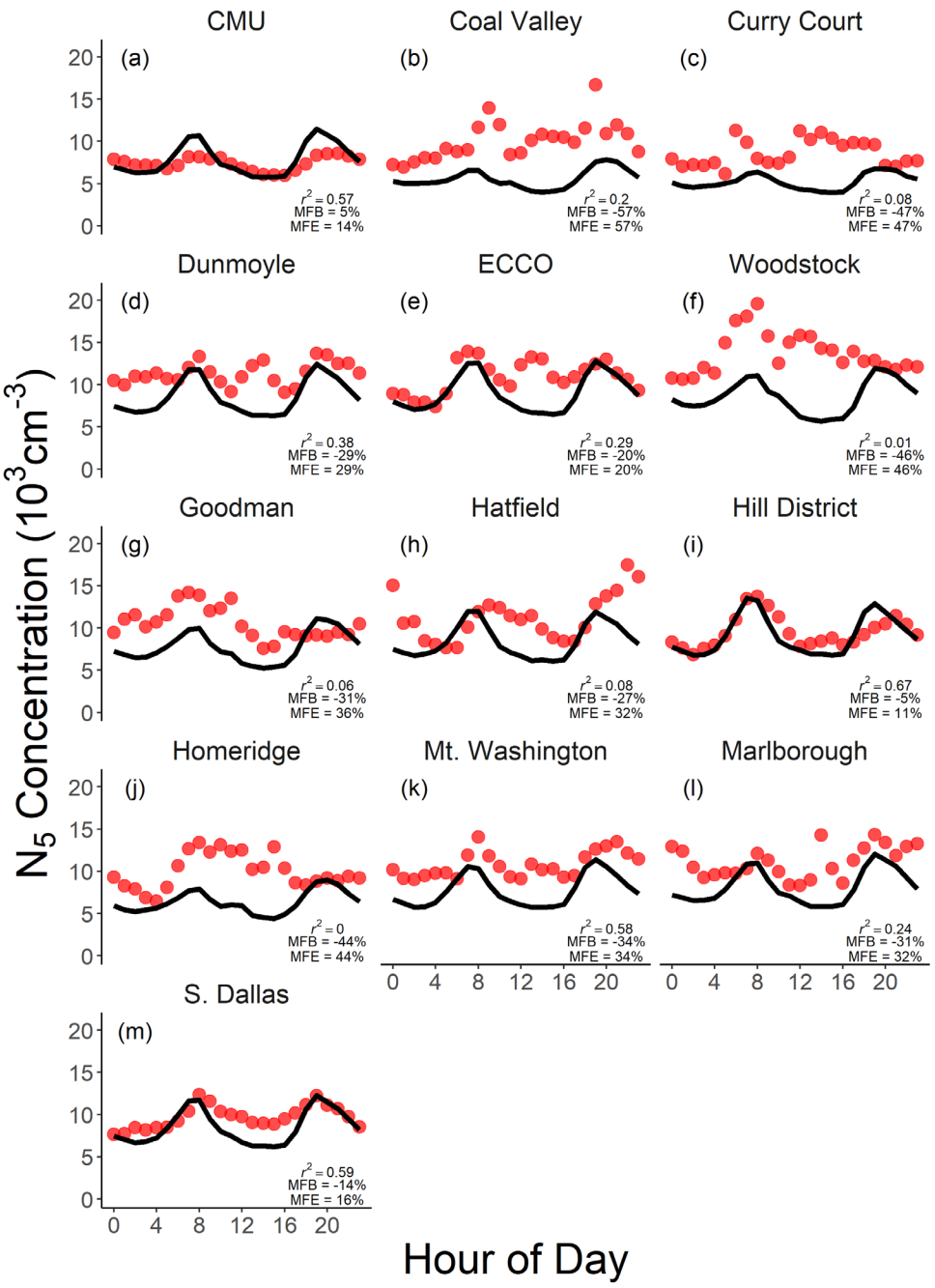

Figure 36
Diurnal averages of February 2017 N_5 model predictions (solid line) and all-winter observed N_5 concentrations (red points) at 13 urban background or local road sites using the EPA-default on-road traffic emissions spatial surrogate. Sites are the same sites as **Figure 5**.

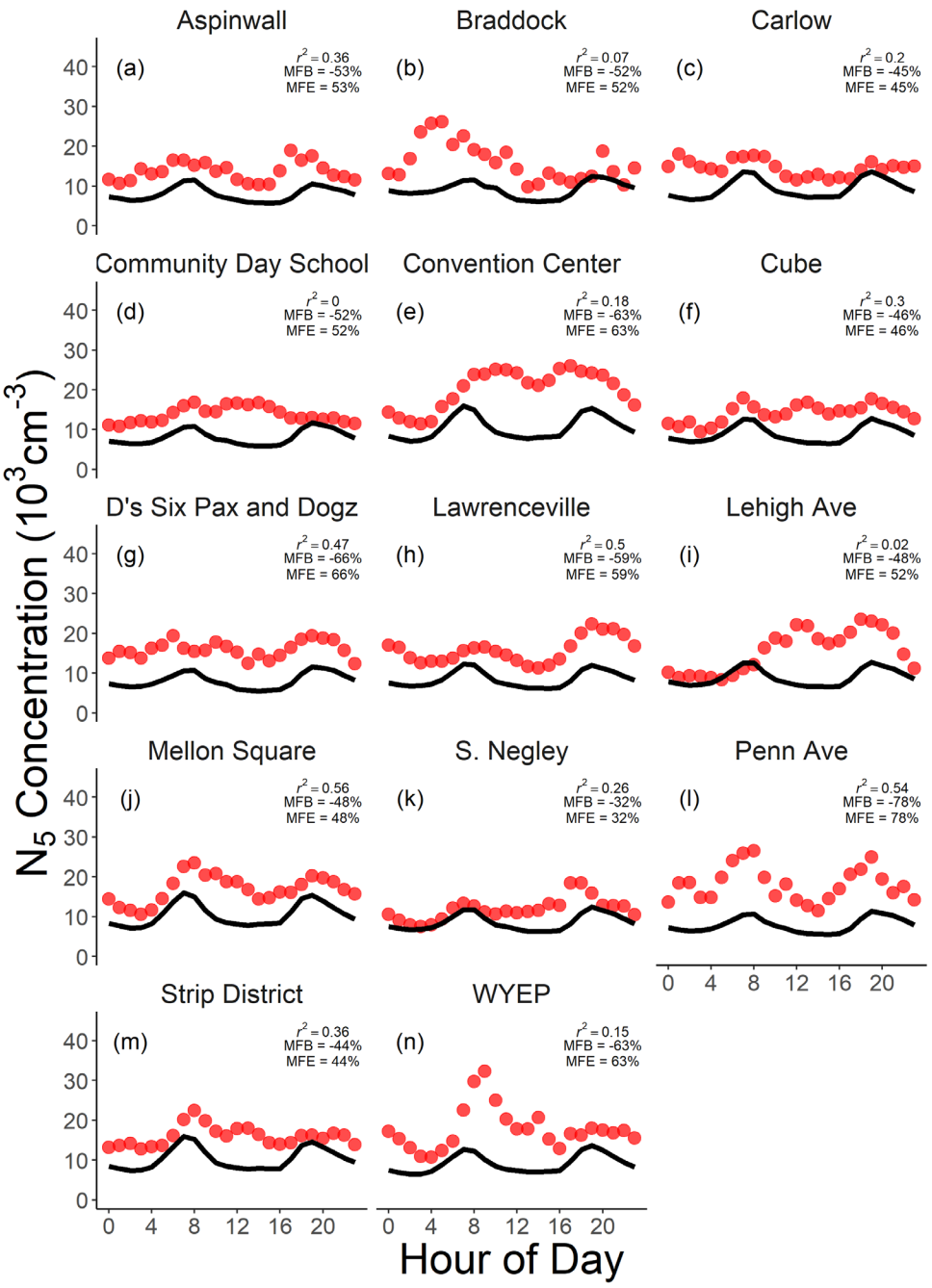

Figure 37
Diurnal averages of February 2017 N_5 model predictions (solid line) and all-winter observed N_5 concentrations (red points) at 14 influenced by local sources or topography using the EPA-default on-road traffic emissions spatial surrogate. Sites are the same sites as **Figure 6**.

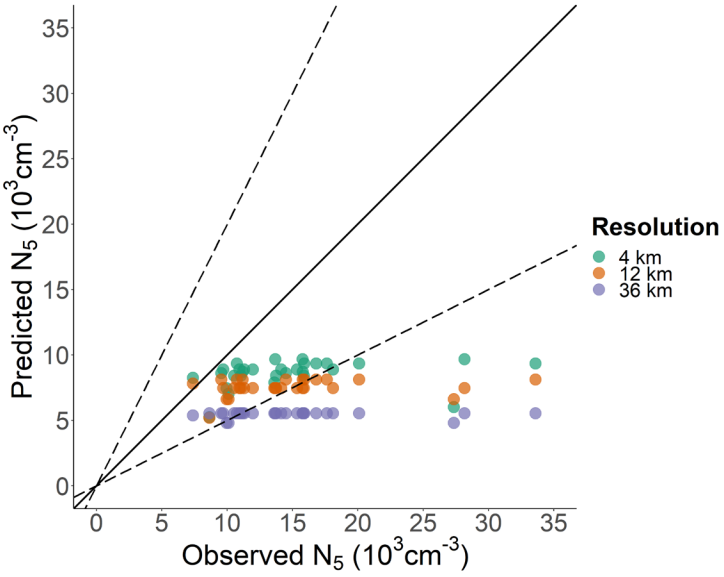

Figure 38
Monthly averaged predicted February 2017 N_5 concentrations versus seasonally averaged observed Winter 2017, 2018 N_5 concentrations at coarser model resolutions show these resolutions are not capable of capturing the spatial variability in observations as well as the 1-km resolution. Solid lines represent 1:1 and dashed lines are ±50%.

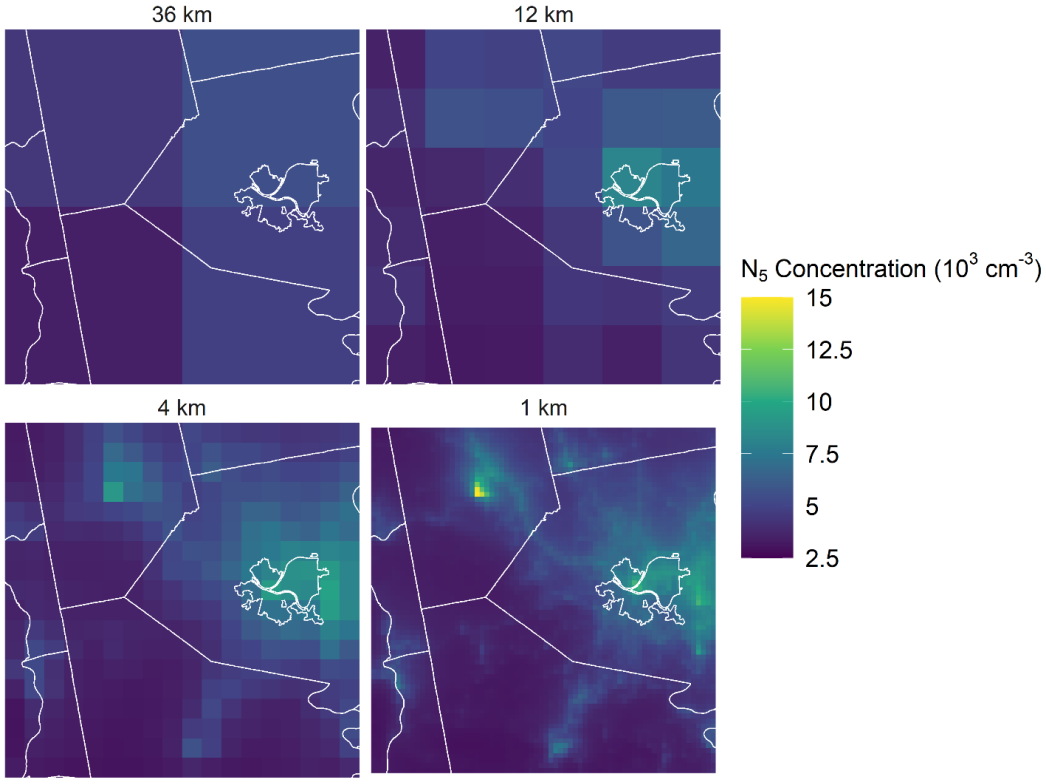

Figure 39
Predicted time-averaged N5 concentration in February 2017 for different modeling resolutions.

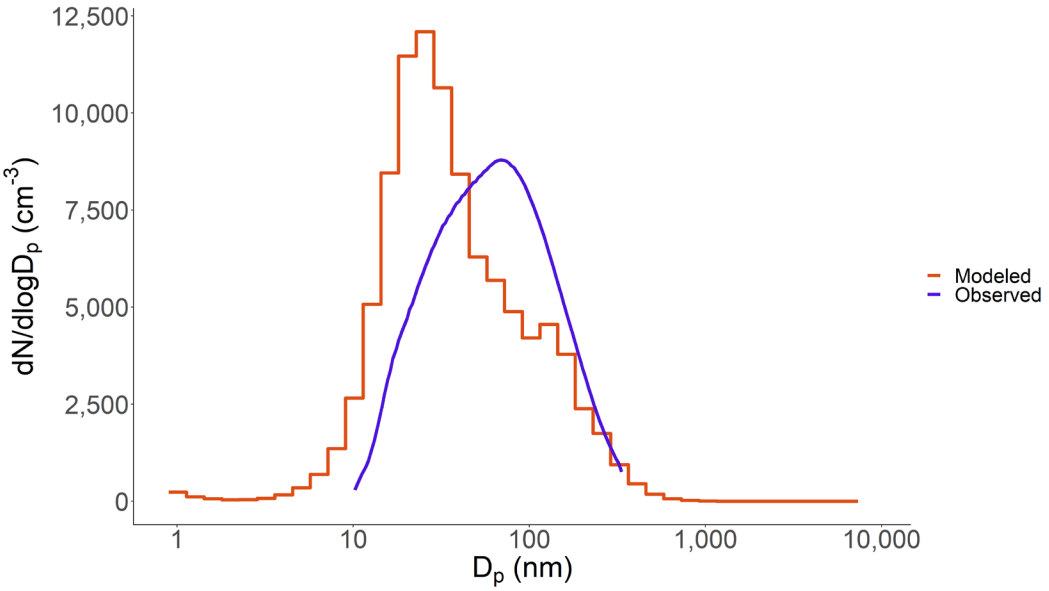

Figure 40
Number size distribution at the CMU site for February 2017.

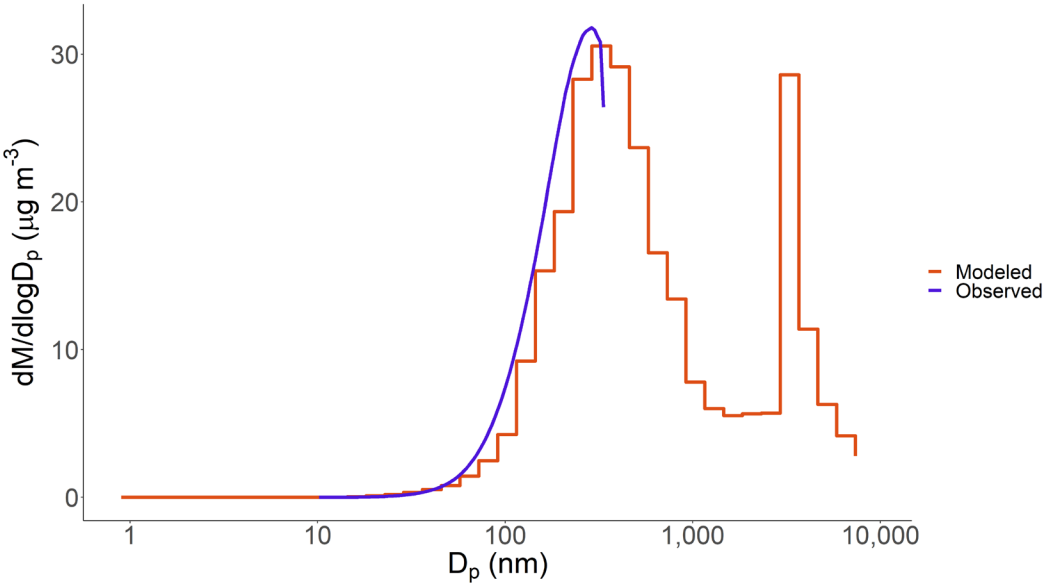

Figure 41
Mass size distribution at the CMU site for February 2017 assuming particle density 1.8 g cm^{-3}

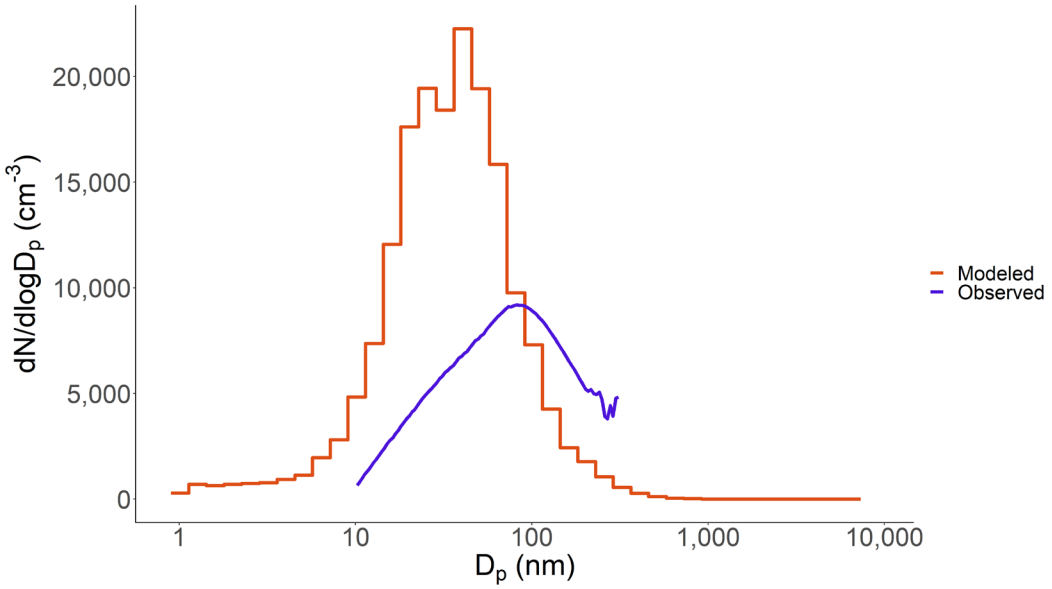

Figure 42
Number size distribution at the CMU site for July 2017.

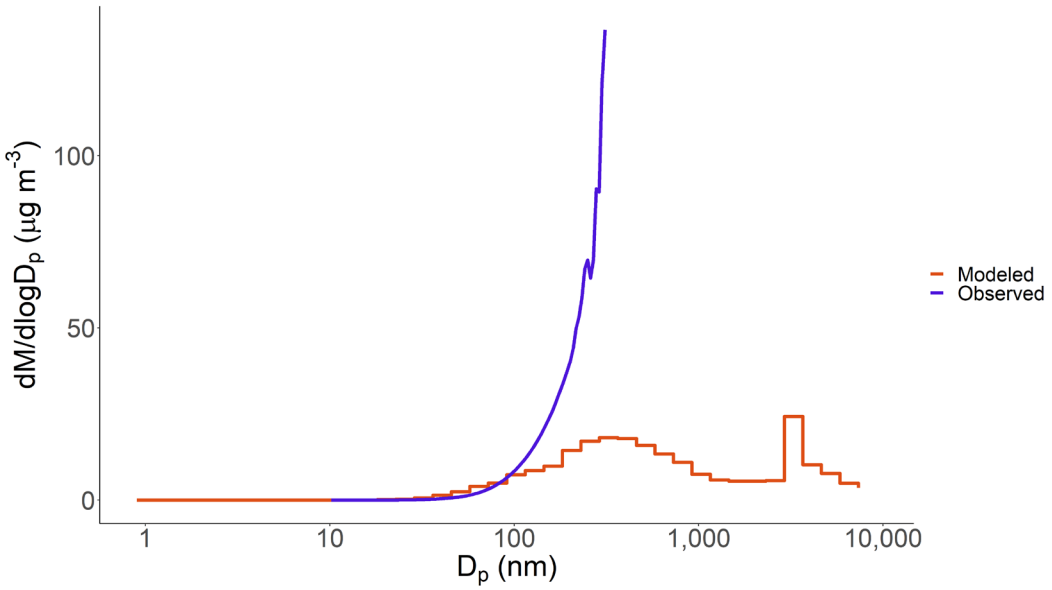

Figure 43
Mass size distribution at the CMU site for July 2017 assuming particle density 1.8 g cm^{-3}

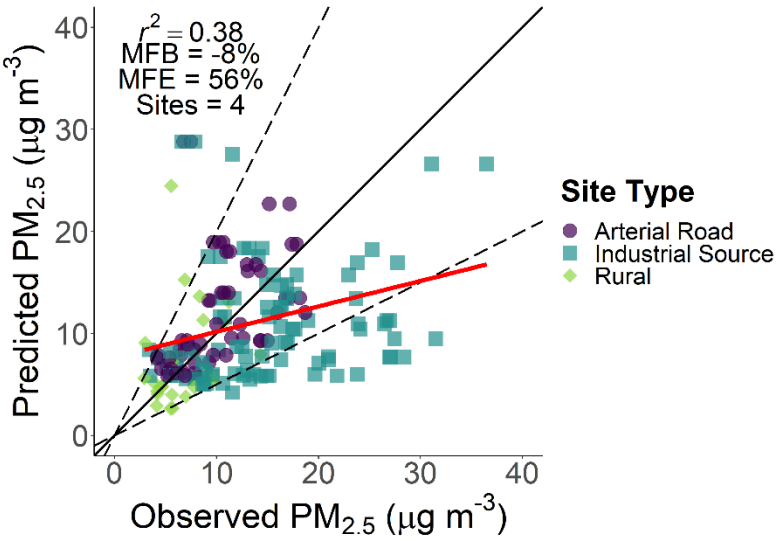

Figure 44
Daily averaged predicted February 2017 $PM_{2.5}$ concentrations versus observed $PM_{2.5}$ concentrations from February 2017. Solid lines represent 1:1, dashed lines are ±50%, and red line is the best fit line for all points.

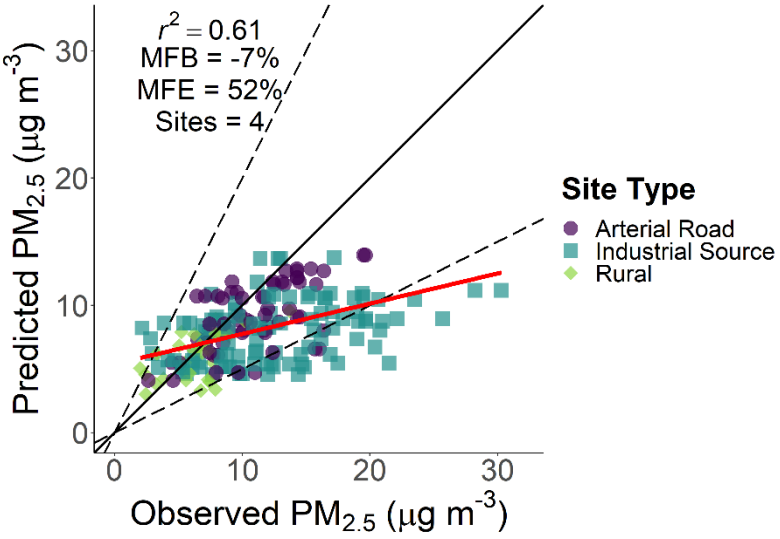

Figure 45
Daily averaged predicted July 2017 $PM_{2.5}$ concentrations versus observed $PM_{2.5}$ concentrations from February 2017. Solid lines represent 1:1, dashed lines are ±50%, and red line is the best fit line for all points.

9 Appendix B

Previous efforts to model Indian power sector operations

Previous efforts to model the Indian power sector have largely focused on the cost savings from economic dispatch of plants in the future. To analyze the impacts of impending market reforms, the Central Electricity Regulatory Commission (CERC) has simulated the scheduling and dispatch of centrally owned power stations based on variable cost (Central Electricity Regulatory Commission, 2018c, 2018b). Further modeling efforts from the Power System Operation Corporation of India (POSOCO), the nationwide power system operator, where power from centrally owned power stations only (~20% of installed capacity) would be pooled and dispatched according to least variable cost yield the possibility of savings of ₹2.4 crore per day (~$350,000 per day or ~1.3% in production costs) compared to the current practice of siloed procurement and no uniform market clearing price (Central Electricity Regulatory Commission, 2018a). Further analysis from POSOCO on economic dispatch of interstate stations yield similar estimates of economic dispatch of interstate stations: reduction in ~1.5% in production costs (Power System Operation Corporation Limited, 2020). Recent modeling by Palchak et al. (Palchak et al., 2017a) analyzing the future integration of 175 GW of renewable capacity into the Indian grid, in line with the Government of India's policy goals, show the possibility of reduction in annual costs of ₹6,300 crore ($980 million) from greater pooling and economic dispatch of both state-owned and centrally owned power stations. This along with the explicit goals of greater renewable generation suggests the possibility of GHG and air pollutant emissions reductions from operational changes to the Indian power sector; however Palchak et al. (Palchak et al., 2017a) do not consider emissions impacts of the power systems they simulate. Likewise, in a companion study to Palchak et al. (Palchak et al., 2017a), Palchak et al. (Palchak et al., 2017b) present sub-national variability with results for several Indian states, but no emissions impacts for each state. Similar efforts from Phadke et al. (Phadke et al., 2016) present regional level capacity expansion and dispatch modeling for India to assess integrating greater amounts of renewable energy into the Indian grid. These efforts conclude that 175 GW renewables will lead to marginal increases (~4%) in wholesale electricity price, but Phadke et al. (Phadke et al., 2016) do not explicitly

consider the environmental benefits of greater renewables.

Indian power stations impact on ambient air quality and premature mortality

Atmospheric modeling studies have quantified the specific health impacts of the Indian coal power stations. While quantifications are approximately the same order of magnitude, they differ due to modeling assumptions and data inputs. Guttikunda and Jawahar (Guttikunda and Jawahar, 2014) model the emissions of coal power stations using an atmospheric chemical transport model and $PM_{2.5}$ exposure relationships to find between 80,000 to 115,000 premature deaths attributed coal power stations in 2011-2012. Despite only considering emissions from coal power stations and no other sources such as vehicles in their model, these estimates compare similarly to those in analyses from the Global Burden of Disease, which found approximately 82,000 premature deaths from coal power stations (GBD MAPS Working Group, 2018). Recent estimates from Gao et al. (Gao et al., 2018) estimate approximately 300,000 premature deaths from power generation in India. Subsequent modeling from Guttikunda and Jawahar (Guttikunda and Jawahar, 2018) specifically look at the application of flue gas desulfurization in Indian coal power stations to meet Indian SO_2 emissions regulations. They show reductions in attributable premature deaths between 39,000 and 63,000 in 2017, with higher reductions as coal power generation expands to 2030.

Wholesale Indian electricity market structure

Over 90% of wholesale power transactions in India happen through relatively inflexible long-term power purchase agreements. Generally, distribution companies schedule and dispatch power from generators according to the companies' respective portfolios of long-term (typically 25-year) contracts. Not all distribution companies have contracts with all generators (especially those owned by state governments) and when reporting their schedules to power system operators, distribution companies need not report the variable cost of the power they plan to purchase. This market structure with no market clearing prices of power, where wholesale power buyers and sellers operate in silos, leaves the possibility of distribution companies procuring higher priced power when available cheaper options exist (Central Electricity Regulatory Commission, 2018c, 2018b, 2018a). The central government, state governments, or private producers own generators; however, generally generators owned by the central

government or private producers send power across state lines, with each state having an allocation of total capacity from each of these respective interstate generating stations (ISGS) (Safiullah et al., 2017).

Uncertainty in simulated generation, estimated SO_2 emissions, and estimated state annual CO_2 emission factors

With the incorporated capacity allocations (Figure 48), we calculate the percentage annual demand met for each state from model predictions (Table 3). We do not explicitly model interstate electricity transfers, but model estimates implicitly incorporate interstate generator capacity allocations to each state. Consequently, for certain hours for certain states, demand is not met with simulated generation. To ensure consistency, we calculate these generation shortfalls for each hour and each state and find that unused capacity in the model will meet these shortfalls for most hours simulated if we explicitly assume interstate electricity transfers occur. For 131 hours (1.1%) of 8,640 simulated (360 days), unused capacity would still not meet generation shortfall even after assuming interstate electricity transfers. Of these 131 hours, the maximum hourly generation shortfall was 4.1 GWh, which capacity not incorporated into the model (Figure 48) could meet.

Unmet state demand from simulated generation would also affect estimated plant-level SO_2 emissions. To assess the uncertainty associated with estimated SO_2 emissions, we first find the nationwide, annual total unmet demand for each scenario, approximately 3% of nationwide, annual total demand in the state-wise dispatch scenarios and 0.7% in the region-wise dispatch scenarios. Then we reorder model-estimated annual plant load factor (PLF), i.e. capacity factor, of each plant in order of decreasing PLF to find which plants are more likely to be dispatched to meet this annual unmet demand. Plants would meet this unmet demand through estimated remaining generation capacity. This bounding exercise resulted in approximately 3% increase in nationwide, annual SO_2 emissions in the state-wise dispatch scenarios and 0.7% in the region-wise dispatch scenario, corresponding to the percentage shortfalls in annual demand. The relative spatial patterns of plant emissions remain similar with an emissions-weighted standard distance decreasing to 763 km from 768 km (see Appendix B on quantifying spatial distribution of emissions estimates); however, 42

plants see annual SO_2 emission increases of up to 20%.

While the model is self-consistent with interstate electricity transfers, the estimated average annual emission factors for each state (Figure 12; Table S1) would vary according to how much of annual demand simulated generation meets. To assess this variability, we present minimum-maximum ranges of average annual emission factors for each state in Figure 56. For these ranges, we assume either zero-carbon generation sources or average coal generation (~1,100 kg CO_2/MWh) meets the generation shortfall for each state to calculate the minimum and maximum average annual emission factors, respectively. Demand met for each state varies between 78% (Jharkhand) to 98-100% for multiple states (e.g. Maharashtra, Karnataka, etc.). This uncertainty estimation shows the average emission factors vary the most for eight states: Himachal Pradesh, Chandigarh, Jammu and Kashmir, Assam, Odisha, Haryana, Bihar, and Jharkhand, which collectively form 14% of total annual demand. This uncertainty estimation results in a nationwide average emission factor, ranging from 693 kg/MWh to 721 kg/MWh compared to the model estimate of 711 kg/MWh.

Coal ramping and minimum capacity constraints

Typical full-complexity dispatch models incorporate constraints on minimum capacity and ramping of coal generators. Coal generators do not operate below a certain percentage of their nameplate capacity, a technical minimum officially regulated at 55% in India (Central Electricity Authority, 2019c). This requires a constraint which we do not incorporate in our reduced-complexity model. Likewise, coal generators have a limit on hourly rate of change in electricity they can generate, typically 1% nameplate capacity per minute (Central Electricity Authority, 2019c), which we also do not explicitly incorporate in our model. We estimate how frequently the model violates these constraints in simulations. Sixty-two of 556 coal units, 22 GW capacity (15% allocated capacity) violate a 55% technical minimum constraint more than 5% of the time, with the Chhabra-4 unit violating the constraint the most frequently at 24% of the time (Figure 59a). Likewise, 11 of 556 coal units, 3.4 GW (2% allocated capacity), violate a ±1% ramp rate constraint more than 5% of the time with Chhabra-3 violating the constraint most frequently at 13% of the time (Figure 59b). In addition to leading to small shifts between plants, any additional ramping beyond today's existing cycling is also likely to

result in higher emissions due to heat rate penalties, as well as impacts on NO_x emissions (sulfur emissions being largely dependent on fuel throughput).

Quantifying spatial distribution of emissions estimates

To quantify the spatial distribution of SO_2 emissions from plants in each scenario we use the emissions-weighted standard distance, SD_w (Mitchell, 2005). This metric is analogous to emissions-weighted standard deviation.

(1) $$SD_w = \sqrt{\frac{\sum_{i=1}^{n} e_i(x_i - \bar{X}_w)^2}{\sum_i^n e_i} + \frac{\sum_{i=1}^{n} e_i(y_i - \bar{Y}_w)^2}{\sum_i^n e_i}}$$

Here, n is the number of plants, e_i is the annual emissions from each plant estimated by each scenario, and (x_i, y_i) is the location of the plant in space. X_w and Y_w are the emissions-weighted center of plants:

(2) $$(\bar{X}_w, \bar{Y}_w) = \left(\frac{\sum_{i=1}^{n} e_i x_i}{\sum_i^n e_i}, \frac{\sum_{i=1}^{n} e_i y_i}{\sum_i^n e_i}\right)$$

A lower SD_w indicates decreased spatial variability either through a lower scatter of points, emissions hotspots, or both.

State or Union Territory	Abbreviation	Average CO_2 Emission Factor (kg/MWh)	Annual Demand (TWh)	Percentage Annual Demand	Percentage Annual Demand Met
Himachal Pradesh	HP	87	9.2	0.8%	79%
Meghalaya	ML	164	1.9	0.2%	99%
Manipur	MN	209	0.8	0.1%	100%
Mizoram	MZ	211	0.5	0.04%	100%
Chandigarh	CH	294	1.5	0.1%	89%
Tripura	TR	297	1.4	0.1%	100%
Jammu & Kashmir	JK	316	14.8	1.3%	87%
Sikkim	SK	320	0.5	0.04%	100%
Nagaland	NL	352	0.8	0.1%	99%
Arunachal Pradesh	AR	357	0.8	0.1%	98%
Uttarakhand	UK	372	13.3	1.1%	99%
Assam	AS	521	9.3	0.8%	91%
Karnataka*	KA	530	66.7	5.6%	98%
Kerala	KL	563	23.8	2.0%	99%
Punjab	PB	621	53.8	4.5%	97%
Tamil Nadu*	TN	667	106.3	9.0%	98%
Andhra Pradesh*	AP	675	59.6	5.0%	100%
Rajasthan*	RJ	710	73.5	6.2%	100%
Odisha	OR	714	29.1	2.5%	87%
Puducherry	PY	716	2.6	0.2%	100%
Gujarat*	GJ	719	113.9	9.6%	99%
Haryana	HR	746	50.7	4.3%	92%
Telangana*	TG	760	61.4	5.2%	99%
Uttar Pradesh	UP	767	116.5	9.8%	99%
Madhya Pradesh*	MP	770	69.5	5.9%	99%
Maharashtra*	MH	792	153.8	13.0%	100%
Delhi	DL	797	31.5	2.7%	98%
West Bengal	WB	828	49.8	4.2%	97%
Bihar	BR	872	28.0	2.4%	80%
Goa	GA	873	3.5	0.3%	99%
Chhattisgarh	CG	878	28.3	2.4%	97%
Jharkhand	JH	879	8.3	0.7%	78%

Table 3
State abbreviations, annual CO_2 emission factors, annual demand, percentage annual demand and percentage annual demand met with simulated generation. Asterisks denote high renewable state

Installation Period	Unit Capacity (MW)	SO_2 Standard (mg/Nm^3)
Before 2003	< 500	600
	≥ 500	200
2003-2016	< 500	600
	≥ 500	200
2017-Present	All Units	100

Table 4
Upcoming SO_2 emission standards for Indian coal power stations from Srinivasan et al. (Srinivasan et al., 2018) at normal temperature and pressure: 0º C and 1 atm pressure.

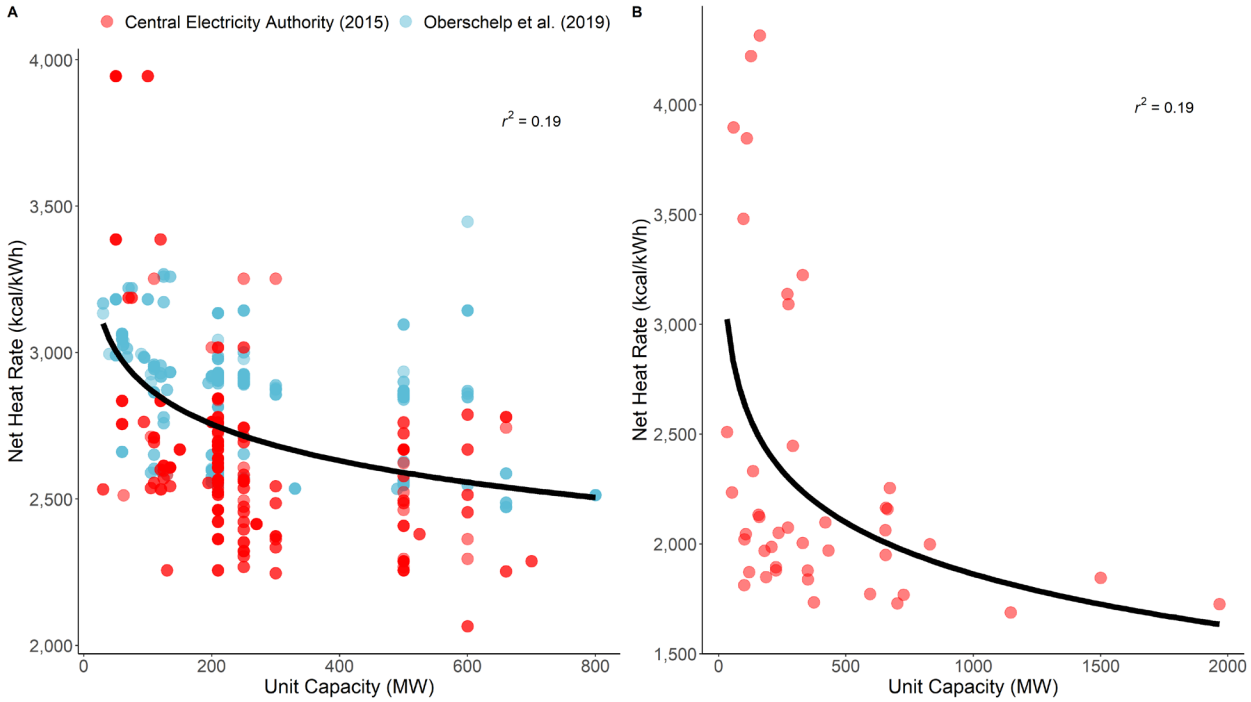

Figure 46
Coal unit-wise heat rate-capacity relationship using data from Central Electricity Authority (Central Electricity Authority, 2015) and Oberschelp et al. (Oberschelp et al., 2019) (A). Gas unit-wise heat rate-capacity relationship using gas consumption data from Ministry of Power (Ministry of Power, 2020b) (B).

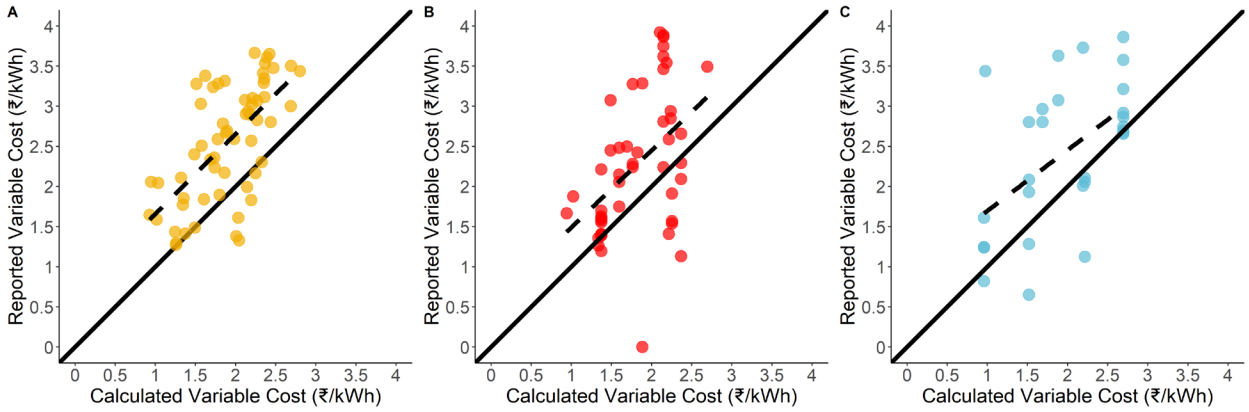

Figure 47
Unadjusted comparison of calculated variable cost of power using data on coal dispatched to individual plants (Coal India, 2019) and transport costs (Kamboj and Tongia, 2018) to reported variable cost from Government of India MERIT database (Ministry of Power, 2020a) with lines of best fit (dashed) and 1:1 line (solid). Each point represents annual average of grade-weighted monthly prices at one coal plant. First, we compare plants in the coal purchase data to those in the MERIT database (A). Then for any missing plants not in the coal purchase data, we fill in with state-sector-wise medians of calculated coal prices plus transport costs (B). Then for any remaining plants without calculated variable cost, we fill in with state-wise medians of calculated coal prices plus transport costs (C). We calculate variable cost of power to verify reported MERIT database prices and adjust calculated variable cost of power by ₹0.66/kWh to close gap between lines of best fit and 1:1 line.

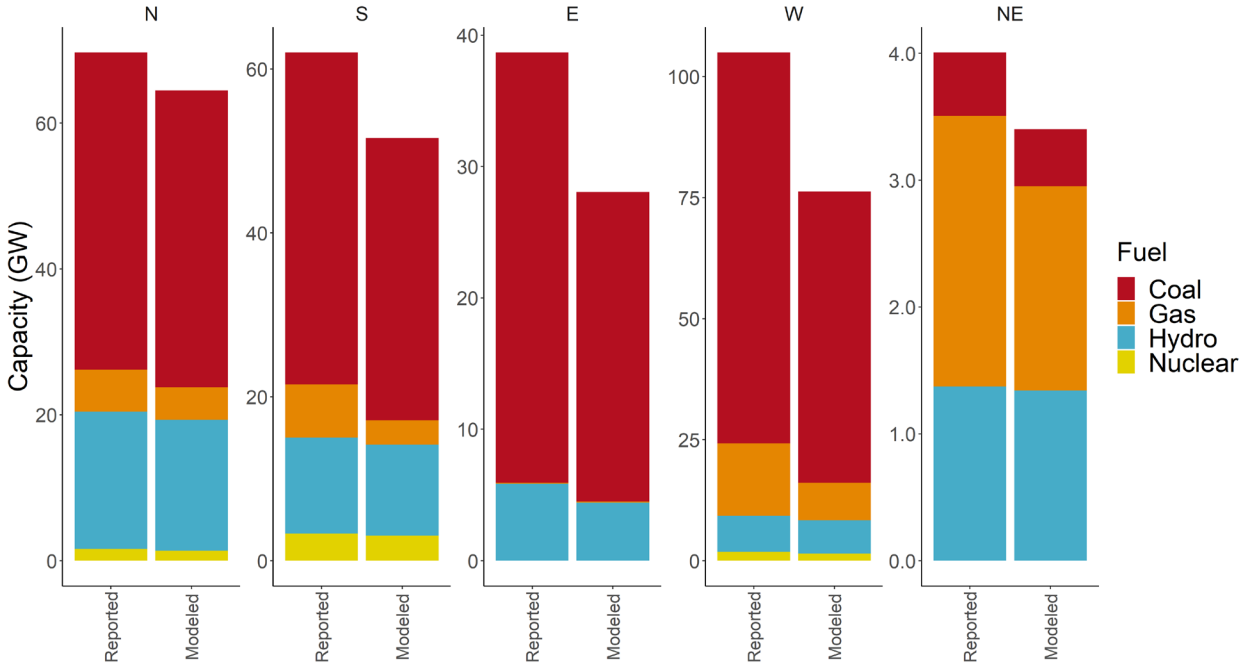

Figure 48
Reported, monitored capacity from Government of India generation reports and capacity incorporated into model from dashboard of long-term power contracts for each state. Reported, monitored capacity is less than total installed capacity (Ministry of Power, 2020a).

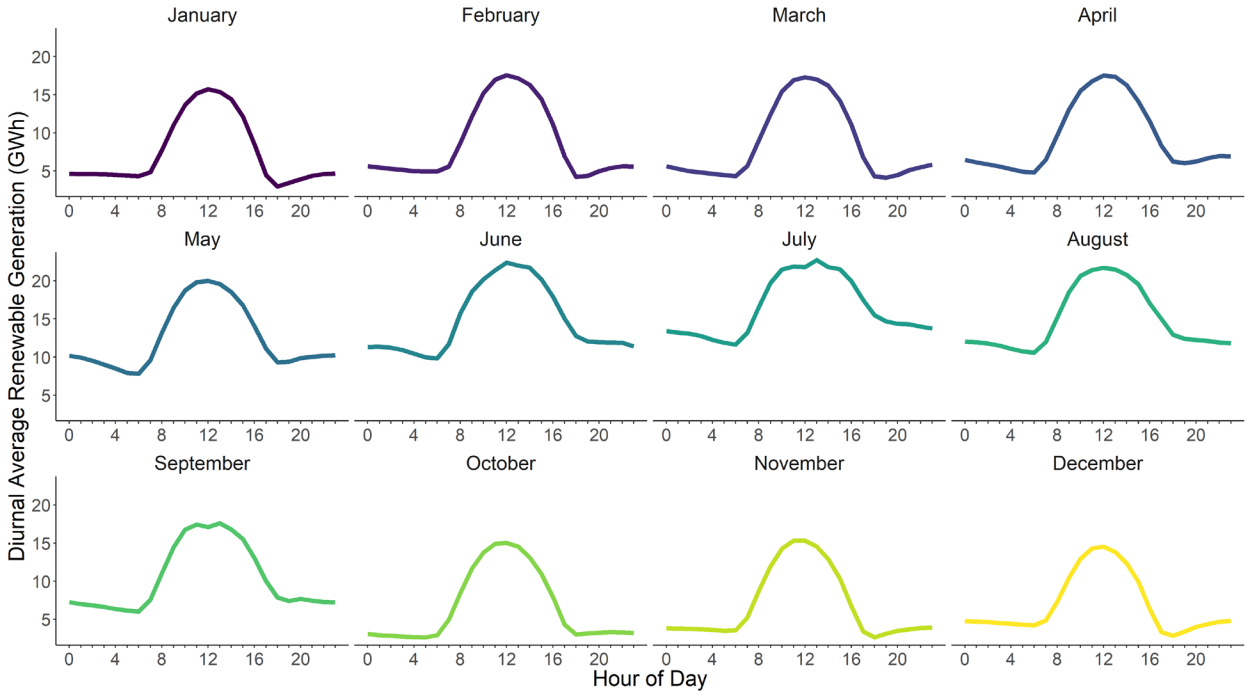

Figure 49
Diurnal national renewable generation profiles for each month from Brookings India Electricity and Carbon Tracker (Centre for Social and Economic Progress, 2019) used to temporally disaggregate reported monthly renewable generation for each state and calculate net demand.

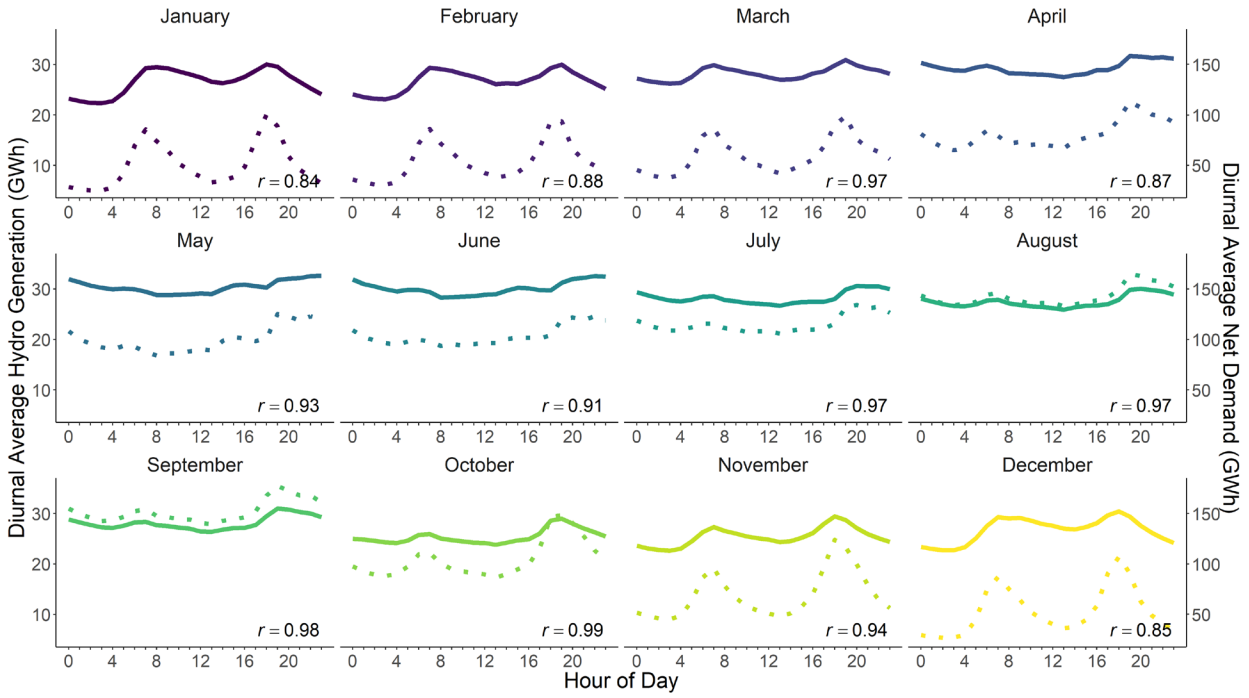

Figure 50
Diurnal average national hydro generation (dotted line) and average net demand (solid line) from Brookings India Electricity and Carbon Tracker (Centre for Social and Economic Progress, 2019) used to constrain hydro capacity.

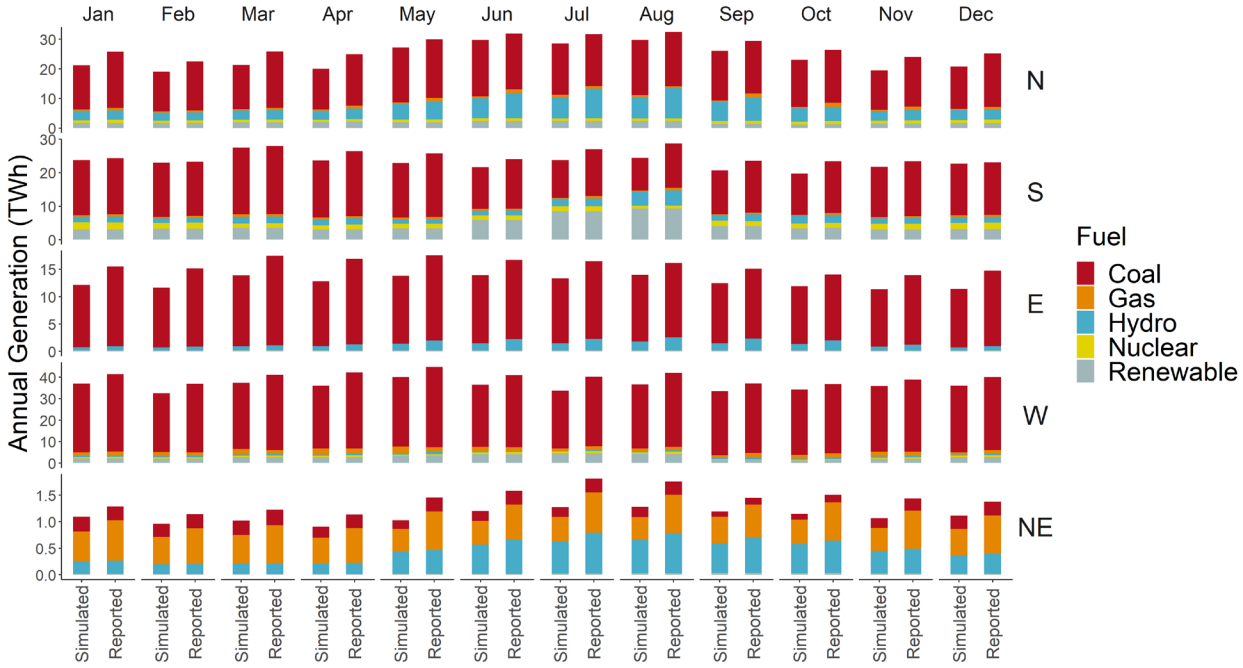

Figure 51
Monthly simulated and reported generations for the state scenario (base case) separated by Indian power region.

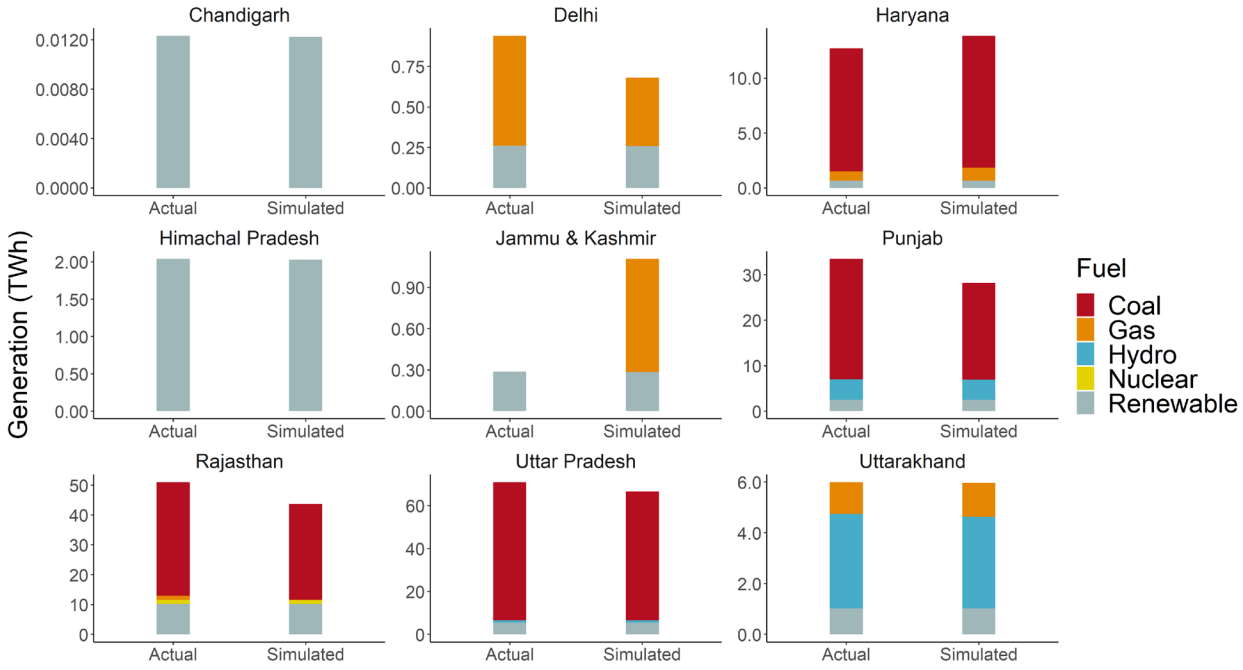

Figure 52
State-level reported and base case simulated generation for intrastate capacity for the Northern region.

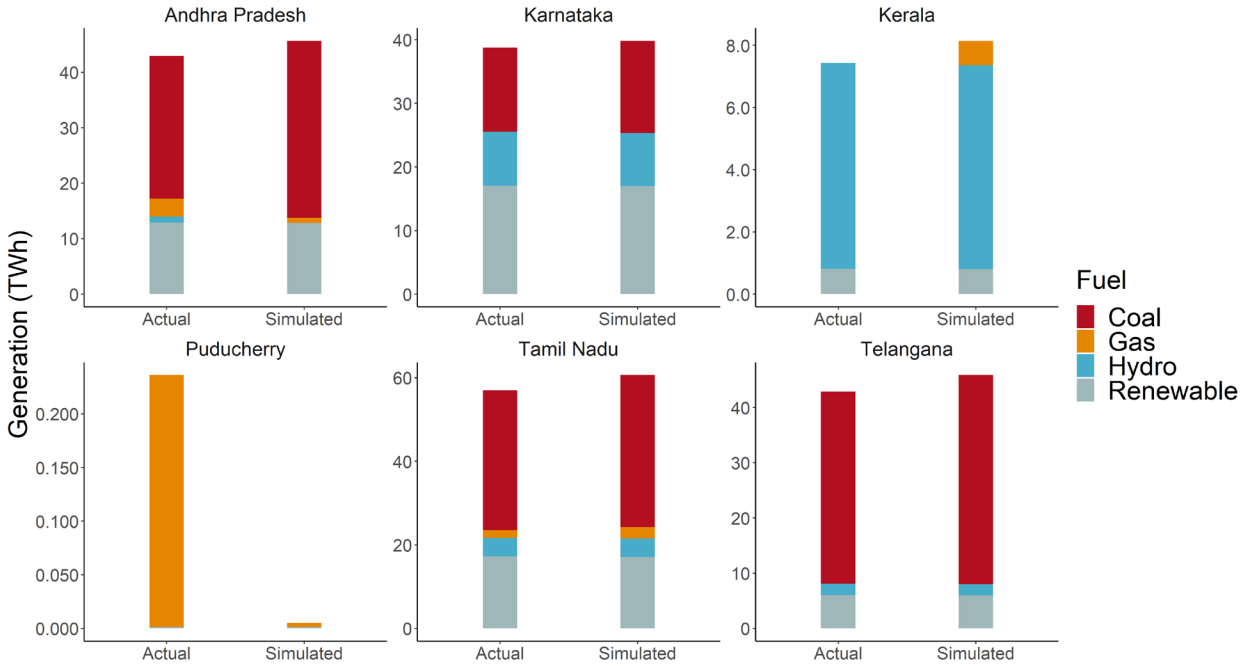

Figure 53
State-level reported and base case simulated generation for intrastate capacity for the Southern region.

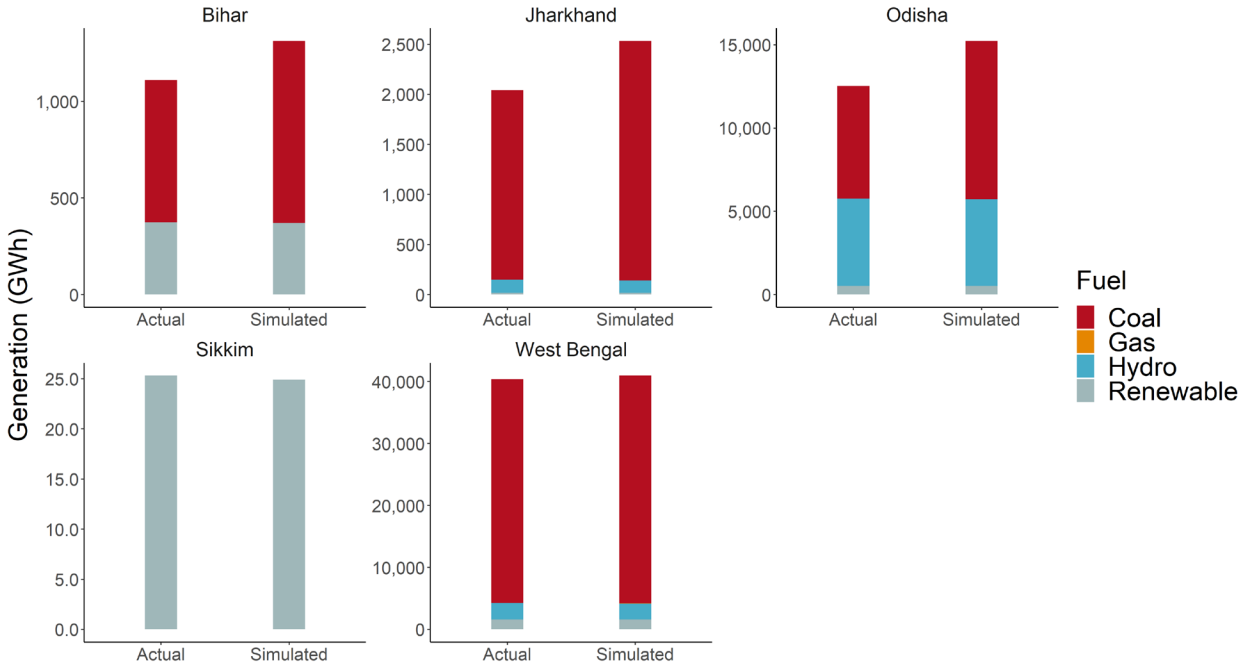

Figure 54
State-level reported and base case simulated generation for intrastate capacity for the Eastern region.

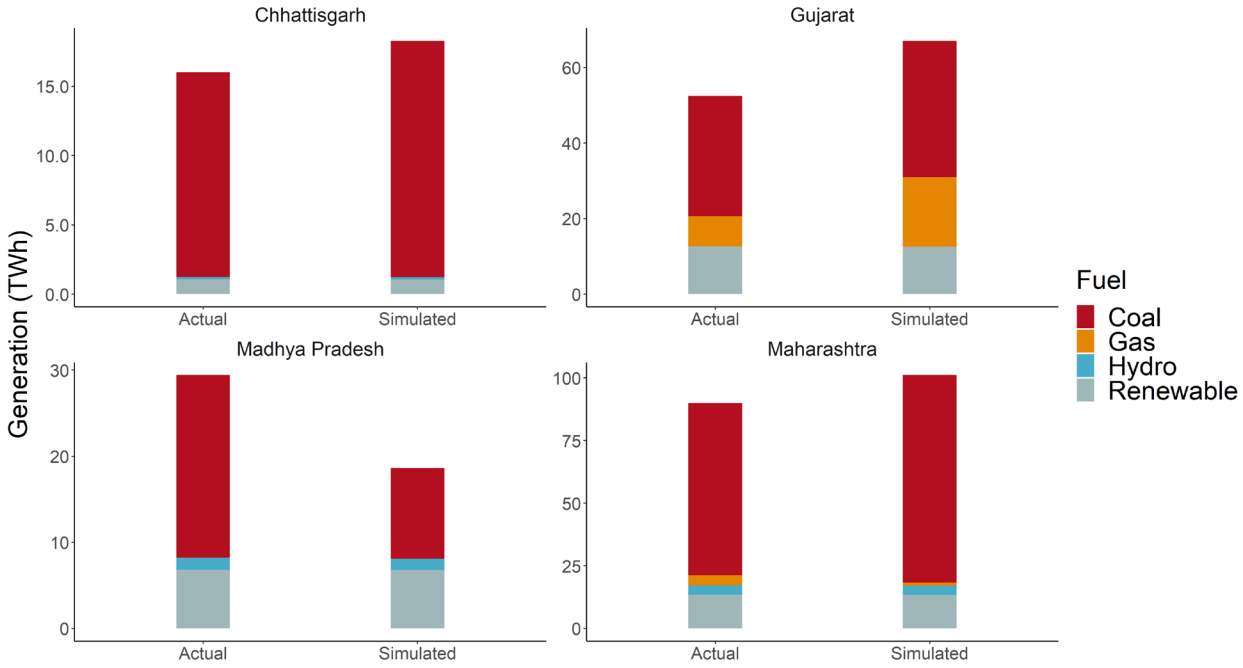

Figure 55
State-level reported and base case simulated generation for intrastate capacity for the Western region.

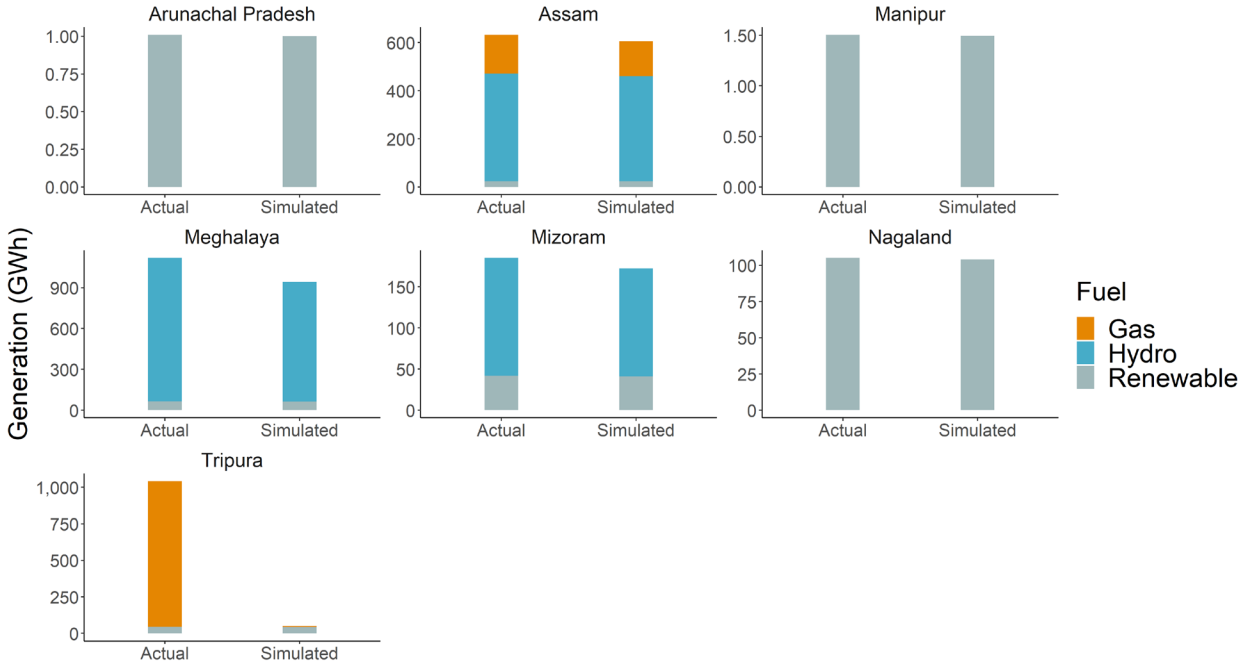

Figure 56
State-level reported and base case simulated generation for intrastate capacity for the Northeastern region.

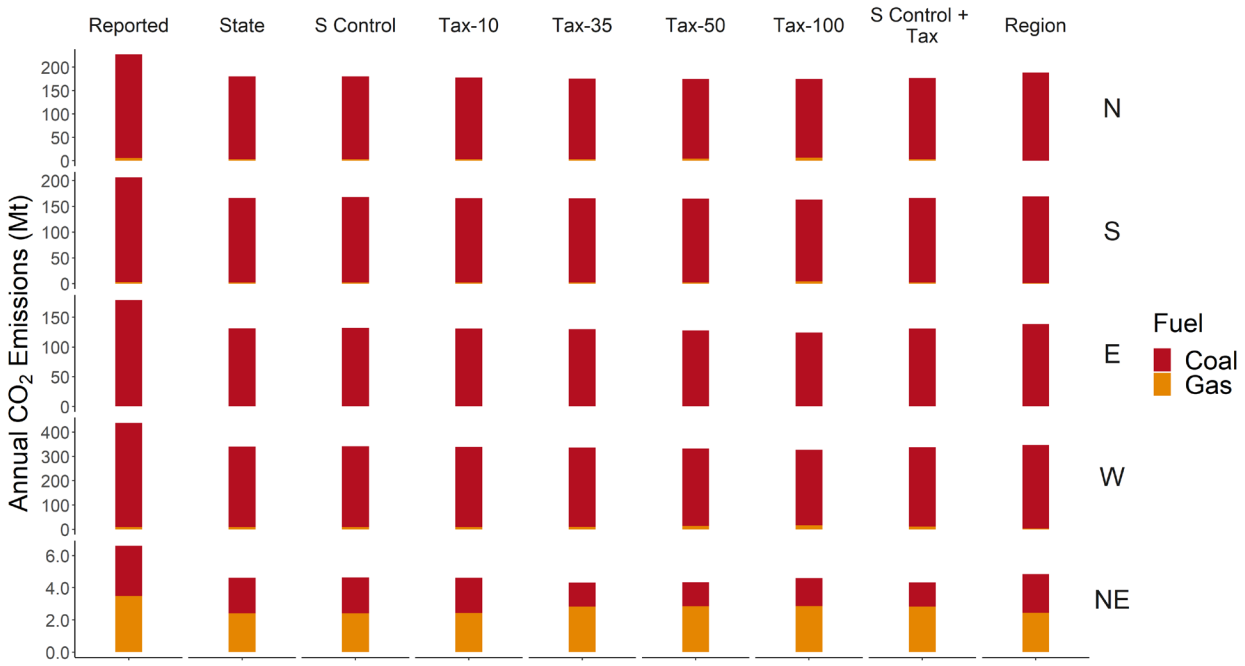

Figure 57
Estimated annual CO_2 emissions from reported and simulated generation for each scenario.

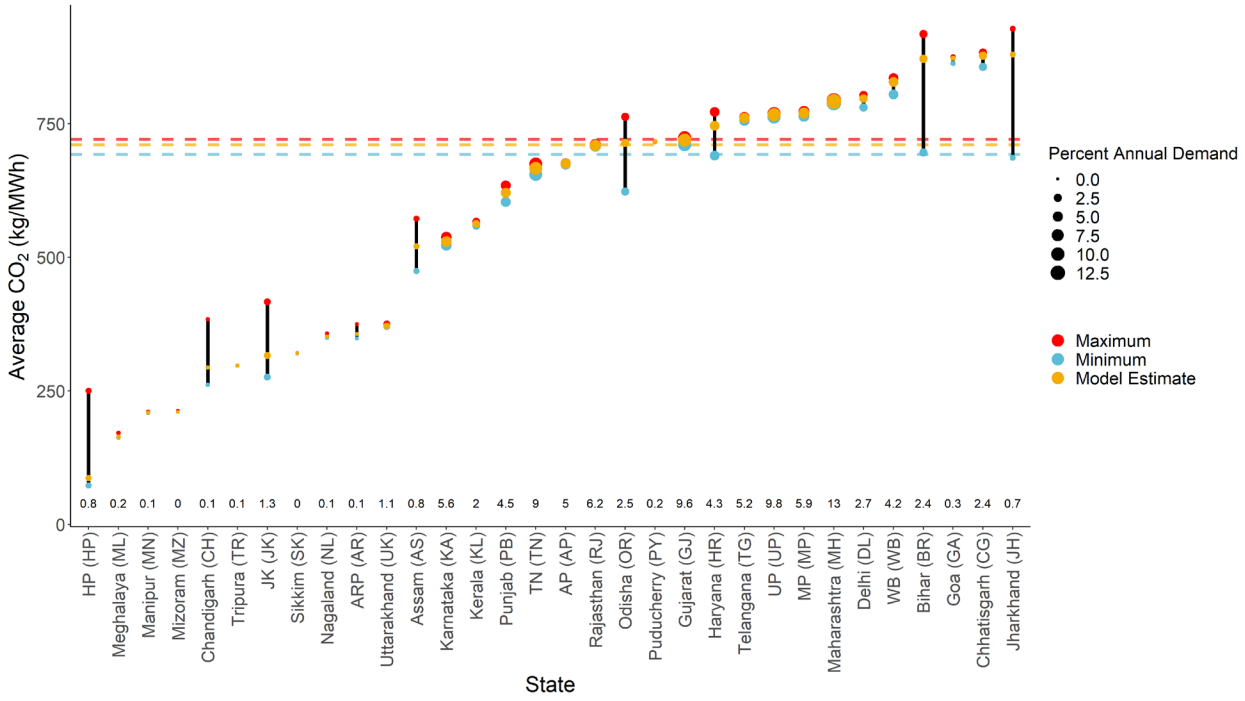

Figure 58
Uncertainty ranges for state average CO2 emission factors assuming zero-carbon generation sources (minimum) or average Indian coal generation (maximum) meet demand not met by simulated generation. Percentage of total annual demand in the bottom row and dot sizes are proportional to percentage annual demand. Dashed lines show nationwide average.

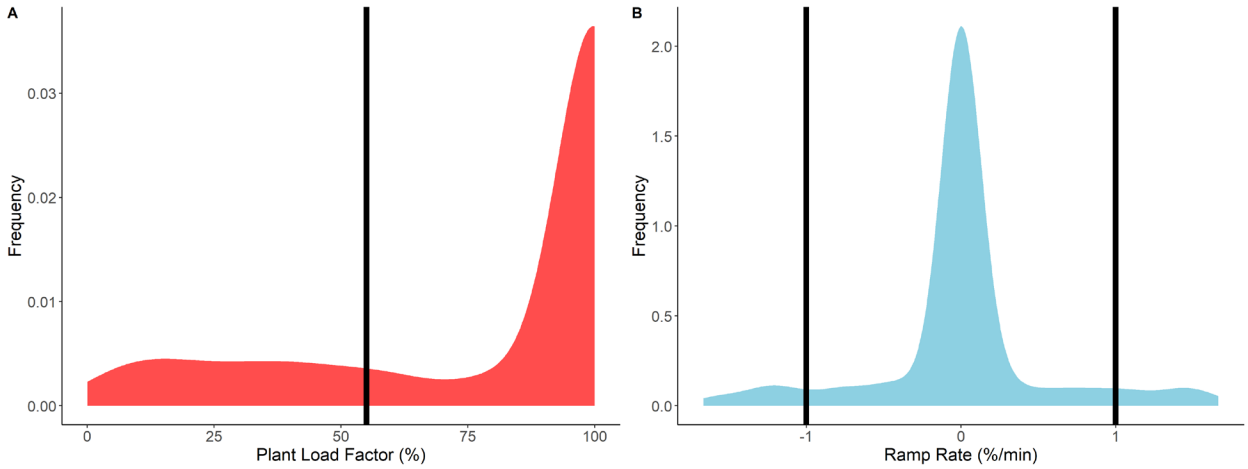

Figure 59
Frequency of plant load factor of Chhabra-4 (250 MW), unit with highest fraction of time under technical minimum capacity, 24% (A) and frequency of ramping rate of Chhabra-3 (250 MW), unit with highest fraction of time with ramp rate exceeding ±1% /min, 13% (B).

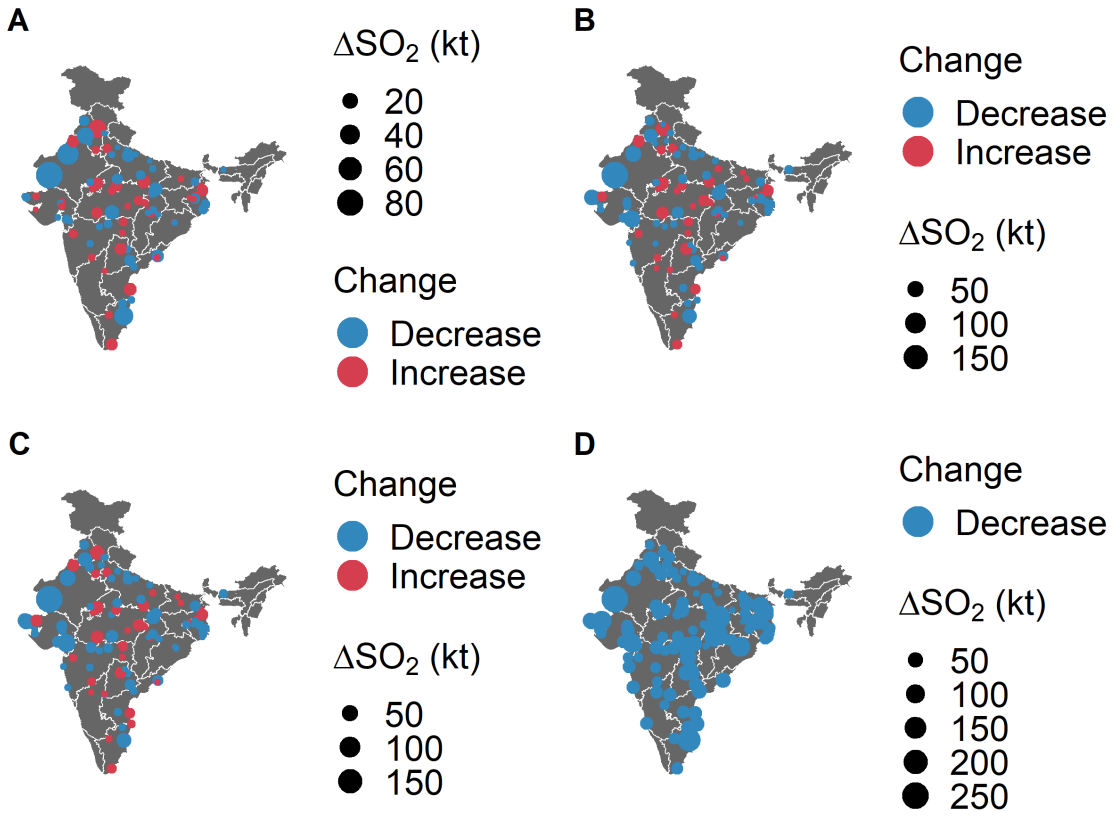

Figure 60
Change in SO_2 emissions induced from a \$10/ton CO_2 tax with emissions-weighted standard distance 760 km (A). Change in SO_2 emissions induced from a \$35/ton CO_2 tax with emissions-weighted standard distance 748 km (B). Change in SO_2 emissions induced from a \$50/ton CO_2 tax with emissions-weighted standard distance 746 km (C). Change in SO_2 emissions induced from a \$35/ton CO_2 tax and uniform

sulfur control with emissions-weighted standard distance 728 km (D)

10 Appendix C

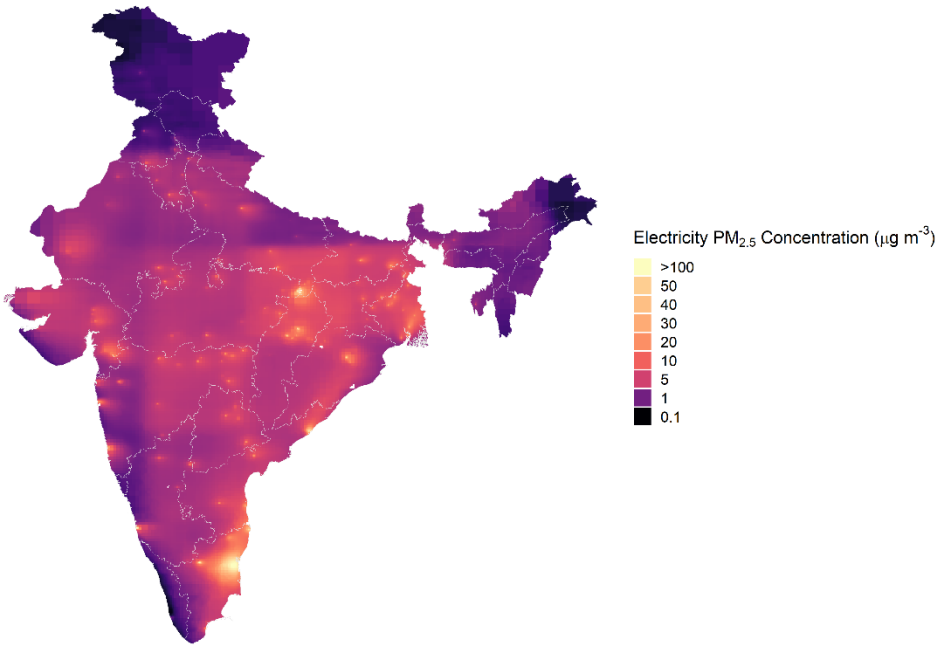

Figure 61
InMAP-estimated $PM_{2.5}$ concentrations attributable to emissions from power generation.

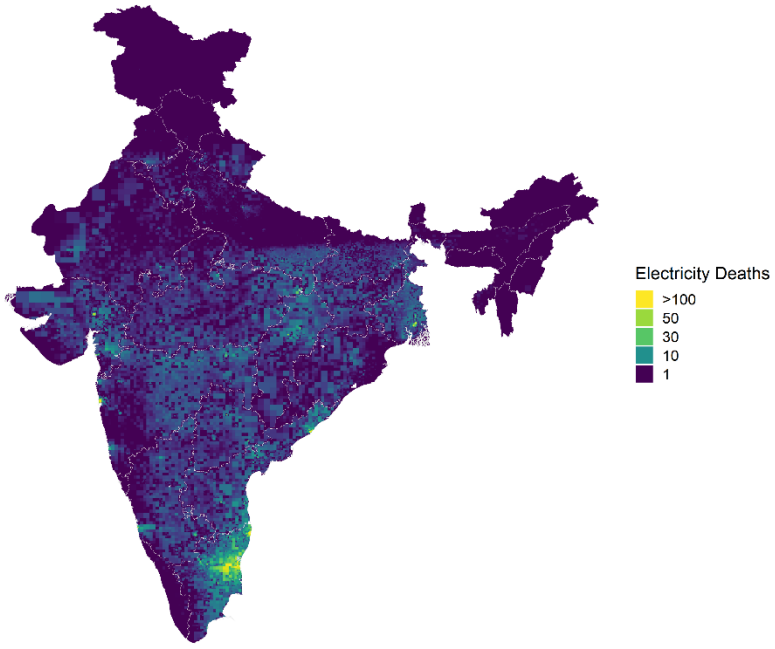

Figure 62
Estimated $PM_{2.5}$ mortality attributable to electricity generation.

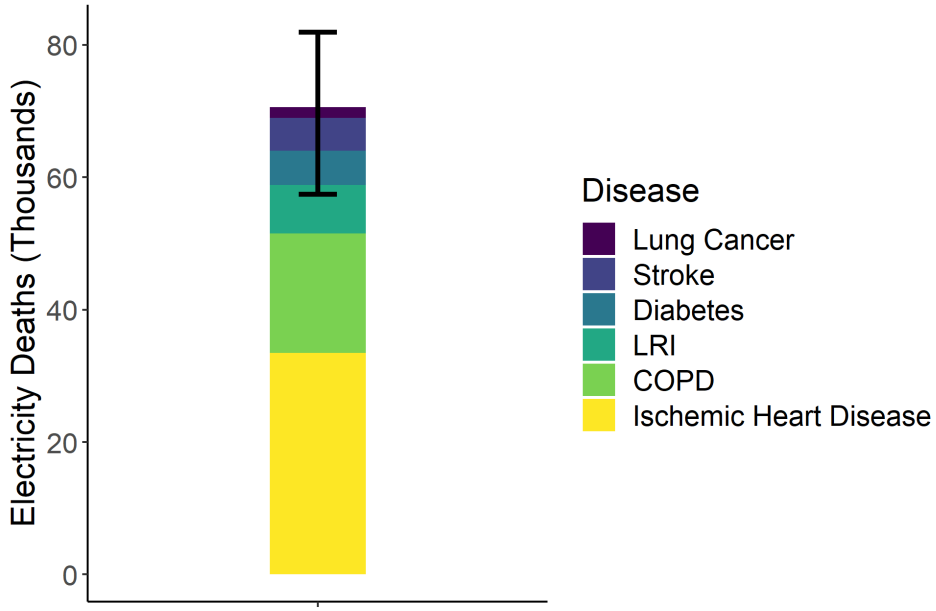

Figure 63
Total estimate mortality attributable to electricity generation broken up by disease endpoint.

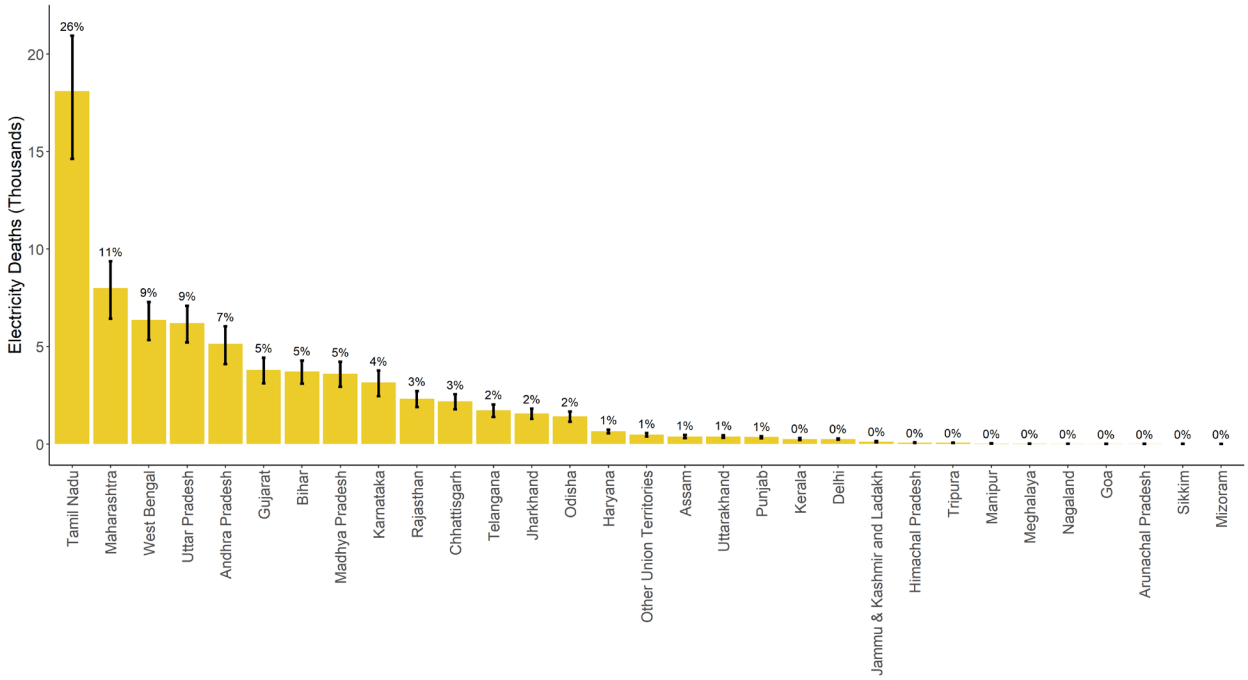

Figure 64
State-wise mortality burden from all electricity generation. Percentages show fraction of total national deaths attributable to electricity generation.

State or Union Territory	Electricity $PM_{2.5}$ deaths	Low Estimate	High Estimate
Tamil Nadu	18088	14626	20933
Maharashtra	7999	6421	9370
West Bengal	6374	5332	7283
Uttar Pradesh	6197	5209	7096
Andhra Pradesh	5144	4108	6038
Gujarat	3814	3111	4427
Bihar	3733	3108	4282
Madhya Pradesh	3613	2941	4218
Karnataka	3166	2467	3769
Rajasthan	2324	1901	2717
Chhattisgarh	2190	1779	2554
Telangana	1742	1396	2040
Jharkhand	1568	1290	1815
Odisha	1420	1138	1670
Haryana	656	555	744
Other Union Territories	487	393	566
Assam	399	317	472
Uttarakhand	396	320	464
Punjab	364	305	412
Kerala	263	207	312
Delhi	256	216	290
Jammu & Kashmir and Ladakh	125	97	149
Himachal Pradesh	71	56	84
Tripura	68	55	78
Manipur	35	27	43
Meghalaya	30	24	36
Nagaland	17	13	21
Goa	15	11	18
Arunachal Pradesh	12	9	15
Sikkim	11	8	14
Mizoram	9	7	11

Table 5
Best, high and low estimates of nationwide, electricity-associated $PM_{2.5}$ death burdens for each Indian state

11 Appendix D

2017-2018 Reduced-form dispatch model

The 2017-2018 reduced-form model (Sengupta et al., 2021) is based off similar methods developed for U.S. power generation (Deetjen and Azevedo, 2019). This model creates a supply curve of available generating capacity by first ordering generating units by variable cost of power (fuel and fuel transport costs (Coal India, 2018, 2019; Kamboj and Tongia, 2018; National Thermal Power Corporation, 2017) and then summing cumulatively to find generating capacity available at or below variable cost of power for each unit. It then takes net demand for the hour (electricity demand minus renewable generation) and chooses generators whose cumulative sum based on the supply curve meets net demand. This is equivalent to minimizing the hourly total system cost of electricity to meet net demand. This method assumes no other constraints or costs including those from transmission, generator ramp limits, or startup costs.

The reduced-form model simulates each hour between September 2017 to August 2018 using all dispatchable generators (coal, gas, nuclear and hydro) based on inventories of power plants in India from daily generation reports with outages (Ministry of Power, 2020b). Table S1 shows the fuel-wise capacity incorporated in the reduced-form model. Sengupta *et al* (2021) structure the model as individual models for each Indian state to mirror the decentralized manner of Indian power dispatch. Each state self-schedules generators to meet demand based on a portfolio of long-term power purchase agreements (PPA) entered by the state. The reduced-form model incorporates this reported capacity tied into PPAs (Central Electricity Authority, 2020b; Ministry of Power, 2020a), which govern 90%+ generation in India (Central Electricity Regulatory Commission, 2018a, 2018b, 2018c). Note that 2017-2018 reduced-form model does not include all installed capacity but only those modeled from reported capacity in long-term contracts (Ministry of Power, 2020a). Likewise, it allocates intrastate capacity (owned by state governments) 100% to each respective state, and interstate capacity (owned by central government and private sector) to beneficiary states by reported fractional capacity allocations < 100% (Central Electricity Authority, 2020b). To reflect season constraints on hydro, the model constrains hydro capacity

available in each hour using reported hydro generation by plant (Ministry of Power, 2020b) and diurnal hydro generation profiles for each month (Centre for Social and Economic Progress, 2019).

Inputs for demand come from reported daily demand (Power System Operation Corporation Limited, 2018) disaggregated by diurnal monthly demand profiles (Energy Analytics Lab, 2019). We pair these demand values with monthly reported renewable generation for each state (Central Electricity Authority, 2018c) disaggregated by diurnal renewable generation profiles for each month (Centre for Social and Economic Progress, 2019) to estimate net demand.

To estimate emissions associated with simulated generation, the reduced-form models use CO_2, SO_2, NO_X and $PM_{2.5}$ emission factors for each generating unit estimated by heat rate (Central Electricity Authority, 2015; Oberschelp et al., 2019) and weighted-average Indian coal composition (Ministry of Coal, 2018; Srinivasan et al., 2018). We assume no sulfur or NO_X control at coal power stations, but 90% control of $PM_{2.5}$ emissions. For gas plants, we assume zero sulfur and PM2.5 emissions, and a constant NO_X emission factor of 2.95 kg/MWh from U.S. EPA (2018).

The model presented by Sengupta *et al* (2021) only simulates each individual state, implicitly modeling interstate electricity transfers through fractional allocations of interstate generation capacity. This method results in approximately 3% annual national demand (varying by hour and state) not met due to idle capacity. Idle capacity is contracted capacity in state not being available to an outside state should the model determine it is not needed to meet demand within the state. For example, if 60% of a 500 MW unit is only needed to satisfy demand in a contracted state, the remaining 40% (200 MW) would not generate. This 40% would likely participate in bilateral exchanges with other states or short term power market (Central Electricity Regulatory Commission, 2018c, 2018b). To simulate this interstate exchange of power and to meet the 3% shortfall in annual demand, we rerun the reduced-form model each hour at regional and national levels by ordering leftover capacity by variable cost and dispatching accordingly to meet unmet net demand. This procedure results in 4 of 8,592 simulated (seven days throughout the year do not have reported demand data) with unmet net demand anywhere in the country. The highest deficit in generation among

these hours was 1.0 GWh, easily met by capacity not incorporated into the model.

2030-2031 Full-form dispatch model

The 2030-2031 full-form model (Spencer et al., 2020) uses open-source Python for Power System Analysis (PyPSA) (Brown et al., 2018) customized for India, PyPSA-India. Spencer *et al* (2020) configure PyPSA-India to be a unit commitment and dispatch model which finds the combination of generators that minimizes total system costs to meet demand in an hour. There are additional constraints and costs on generator minima, ramp rates, startup and transmission included in this optimization. Additionally, PyPSA-India accounts for generator outages probabilistically by defining the likelihood a generator is out in each hour, based on historical data and interviews with Indian power sector experts.

The full-form model simulates April 2030 to March 2031 generator capacity mixes exogenously defined by the National Electricity Plan developed by the Government of India (Central Electricity Authority, 2018b). These generators have marginal costs from similar reported and estimated sources as the reduced-form model (Ministry of Power, 2020a) The capacity mixes shown in Table S1 shows differences in the full-form model from the reduced-form model in thermal capacity (50%) as well as differences in hydro (100%), renewables (380%) in line with Government of India targets to expand non-fossil capacity by 2030 (Government of India, 2015). The model assumes integrated markets, that is capacity anywhere in the country can meet demand anywhere assuming sufficient transmission. This contrasts with the fragmented, decentralized way the Indian power system currently operates, and incorporated into the reduced-form model. Like the reduced-form model, the model enforces daily constraints on hydro generation to reflect seasonal water availability. To produce renewable generation

The full-form model estimates future 2030-2031 electricity demand by assuming the same rates of demand growth in each state from 2008 to 2017, projecting out to 2030. It uses renewable capacity sited by estimates of resource potential, and pairs these with renewable generation profiles estimated by National Renewable Energy Laboratory's System Advisory Model (Blair et al., 2018).

To estimate emissions associated with simulate generation from the full-form model, we take a similar as the reduced-form model. Where reported heat rates were

not available for new units, we estimate their heat rates based off a log fit of heat rates versus capacity from existing plants in our data set.

Comparisons of 2017-2018 model simulation estimates to reported generation data

Figure S1 shows the time series of national, annual CO_2 emissions (Figure 1a), SO_2 emissions (Figure 1b), NO_X emissions (Figure 1c), $PM_{2.5}$ emissions (Figure 1d), and annual demand (Figure 1e) as predicted by our 2017-2018 model and those reported by Carbon Tracker (Centre for Social and Economic Progress, 2019). Modeled values span September 2017 to August 2018. Observed values span November 2018 to October 2018 due to unavailability of reported generation before this time. Publicly available emissions data from plants are not available in India, so we infer emission from reported generation by applying generation-weighted emission factors to reported data. Each point represents an hourly value, and the solid lines are rolling 24-hour averages. We plot time series and compare to reported values to evaluate the model's ability to capture general temporal trends. The gray shaded region (June-October) spans monsoon months we assume. The remaining (January-May, November-December) months are dry months. Overall, modeled and observed hourly CO_2 emissions correlate annually, with $r = 0.61$, with higher correlation during dry months, $r = 0.73$, than monsoon months, $r = 0.37$. Similar correlations emerge for SO_2 emissions, annually ($r = 0.64$), and seasonally (dry $r = 0.7$, monsoon $r = 0.41$). Similar patterns emerge for NO_X emissions (annual $r = 0.61$, dry $r = 0.73$, monsoon $r = 0.37$) and $PM_{2.5}$ emissions (annual $r = 0.58$, dry $r = 0.73$, monsoon $r = 0.33$). Observed demand and demand assumed by the model likewise correlate, annually ($r = 0.82$) and seasonally (dry $r = 0.9$, monsoon $r = 0.66$), despite representing separate years. In Figure S2, we further evaluate reduced-order dispatch model performance by comparing estimated fractions of annual generation located within a state (in-state) and outside a state (out-of-state) against those reported in official statistics (Central Electricity Authority, 2019a). We find root mean square error (RMSE) of 0.16 and mean absolute error (MAE) of 0.11 for out-of-state generation fractions among all states.

Fuel	2017-2018 Reduced-Form Model	2030-2031 Full-Form Model

	(GW)	(GW)
Coal + Lignite	159	263*
Gas	17	
Hydro	42	84
Renewables (solar, wind, biomass, waste)	71	341
Nuclear	6	17

Table 6
Capacities by fuel type in reduced-form and full-form models
*reported as thermal: coal, gas and lignite combined, majority of which is coal

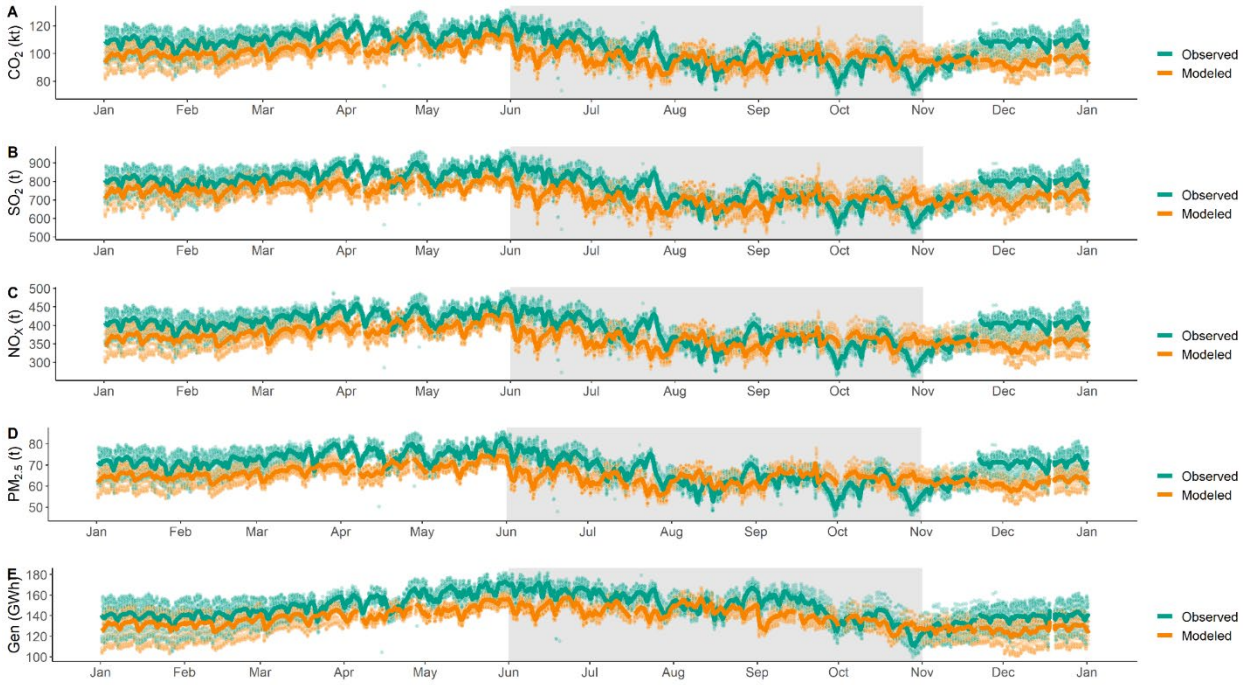

Figure 65
Annual comparisons of national observed and 2017-2018 modeled CO_2 emissions (A), SO_2 emissions (B), NO_X emissions (C), $PM_{2.5}$ emissions (D), and electricity generation (E). Observed values are from Brookings India Carbon Tracker (Nov 2018-Oct 2019), and modeled values are from reduced-order dispatch model (September 2017-August 2018). Each point is an hourly value, and solid line is a rolling 24-hour average. Gray shaded region are monsoon months: June-October.

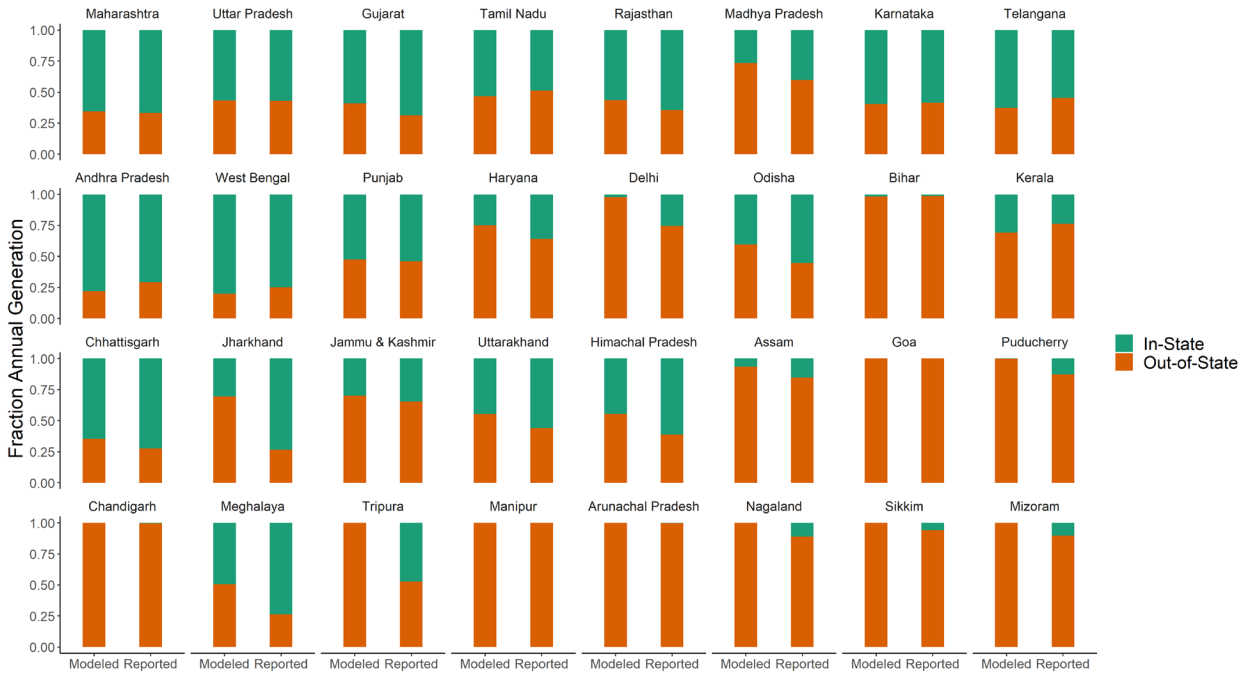

Figure 66
In-state and out-of-state modeled and reported fractions of annual generation for each Indian state. Modeled fractions come from reduced-order dispatch model, and reported fractions come from Central Electricity Authority (2019). States are in order of largest to smallest annual demand.

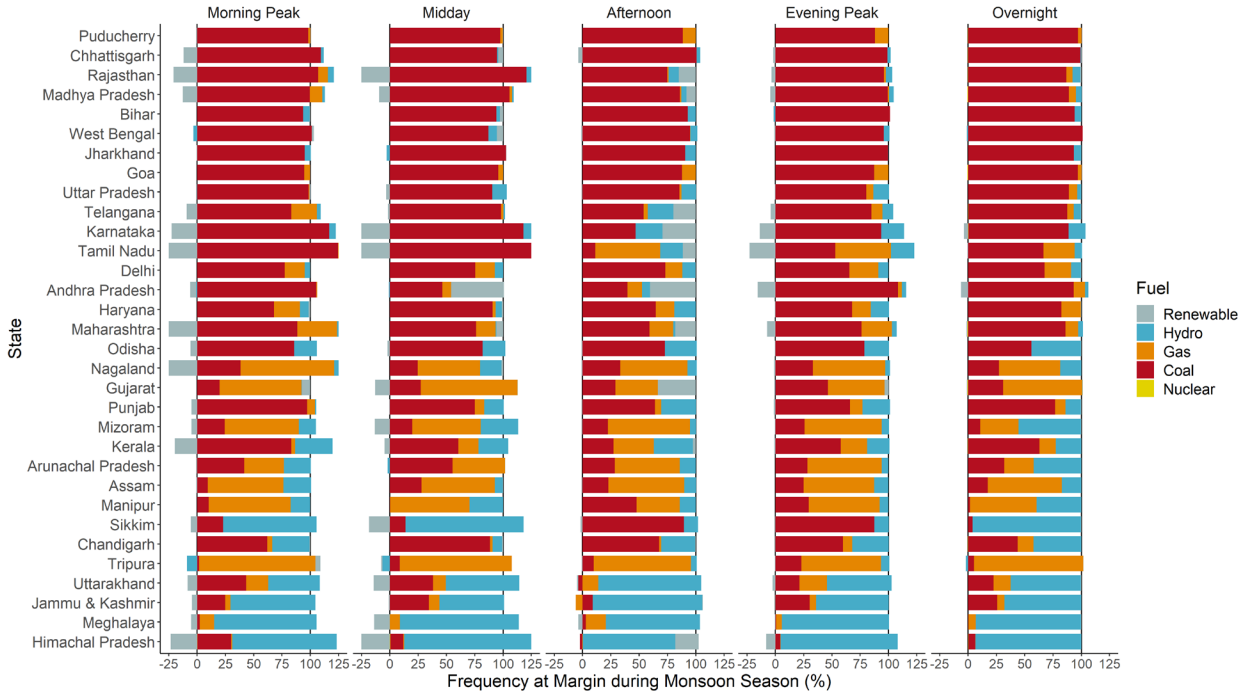

Figure 67
2017-2018 regression-based, marginal fuel frequency for each Indian state during monsoon season. Negative percentages in each period indicate fuel source generation decreases with increases in unit power consumption in each state, requiring increases in generation from other fuels to meet marginal demand. The sum of each bar is 100%

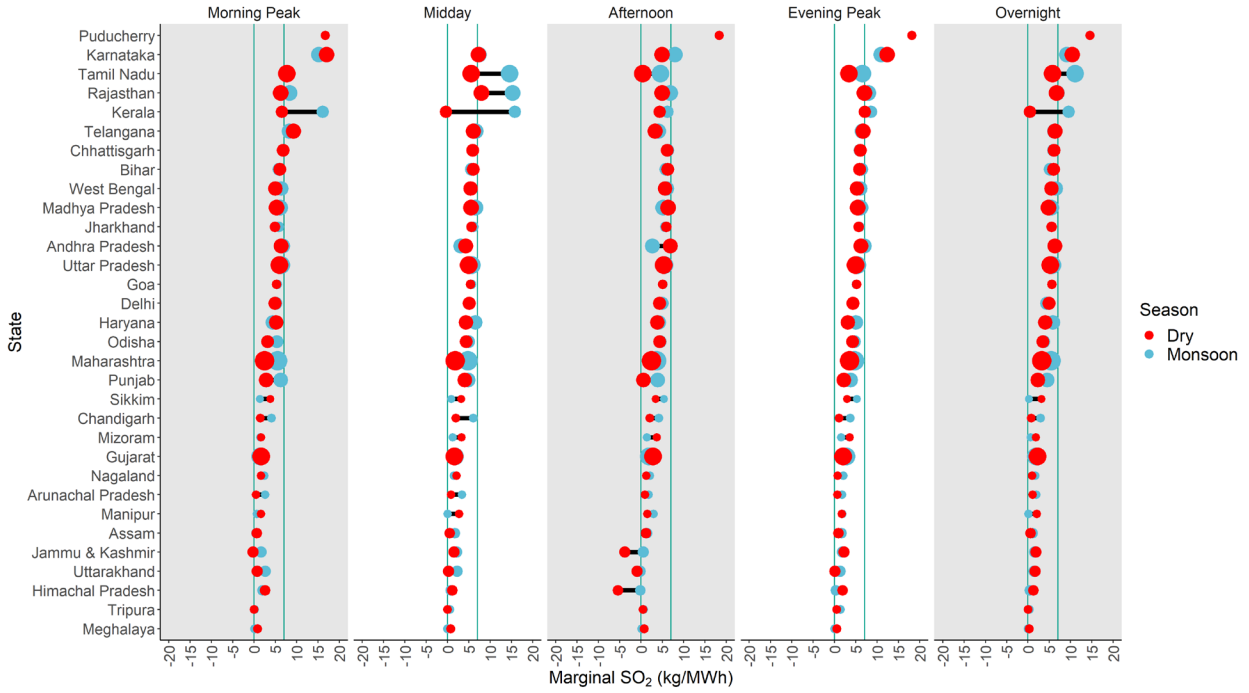

Figure 68
2017-2018 marginal SO_2 emission factors for dry and monsoon seasons. Panels separate the time-of-day in each season. Size of dots scale to annual electricity demand in each state. Vertical lines from left to right indicate generation-weighted SO_2 emission factors for gas and coal generators, respectively.

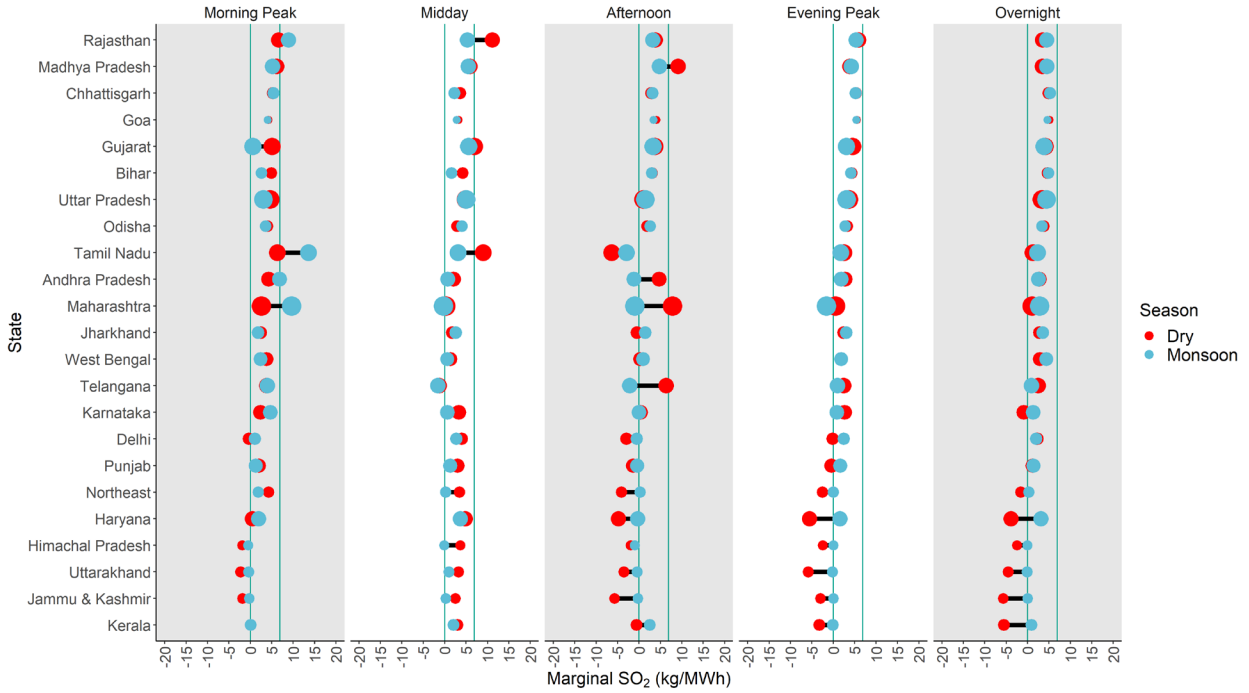

Figure 69
2030-2031 marginal SO_2 emission factors for dry and monsoon seasons Panels separate the time-of-day in each season. Size of dots scale to annual electricity demand in each state. Vertical lines from left to right indicate generation-weighted SO_2 emission factors for gas and coal generators, respectively.

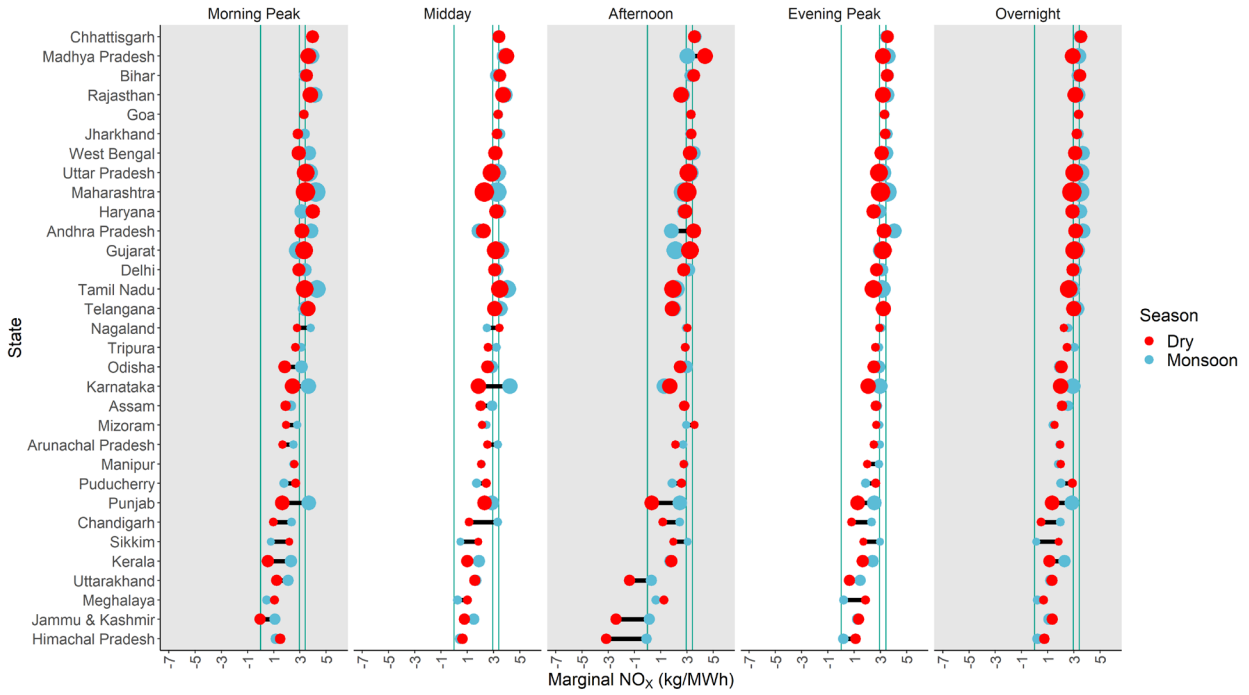

Figure 70
2017-2018, marginal NO_X emission factors for dry and monsoon seasons. Panels separate the time-of-day in each season. Size of dots scale to annual electricity demand in each state. Vertical lines from left to right indicate generation-weighted NO_X emission factors for gas and coal generators, respectively.

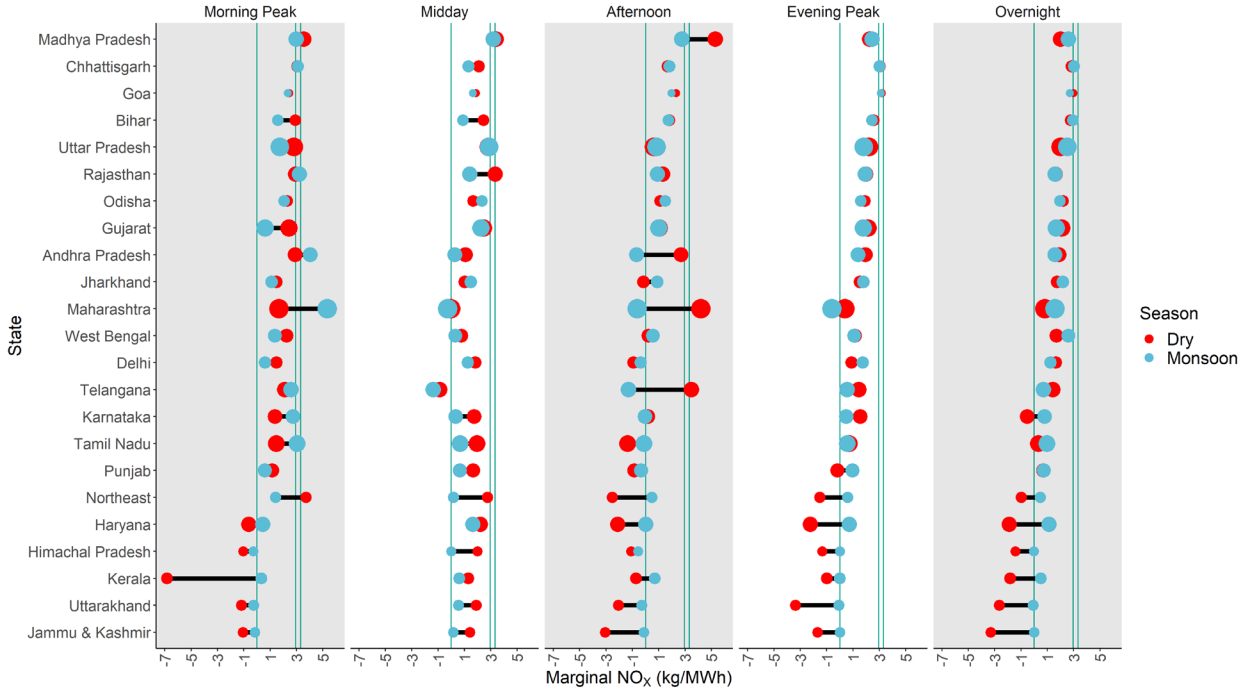

Figure 71
2030-2031 marginal NO_X emission factors for dry and monsoon seasons. Panels separate the time-of-day in each season. Size of dots scale to annual electricity demand in each state. Vertical lines from left to right indicate generation-weighted NO_X emission factors for gas and coal generators, respectively.

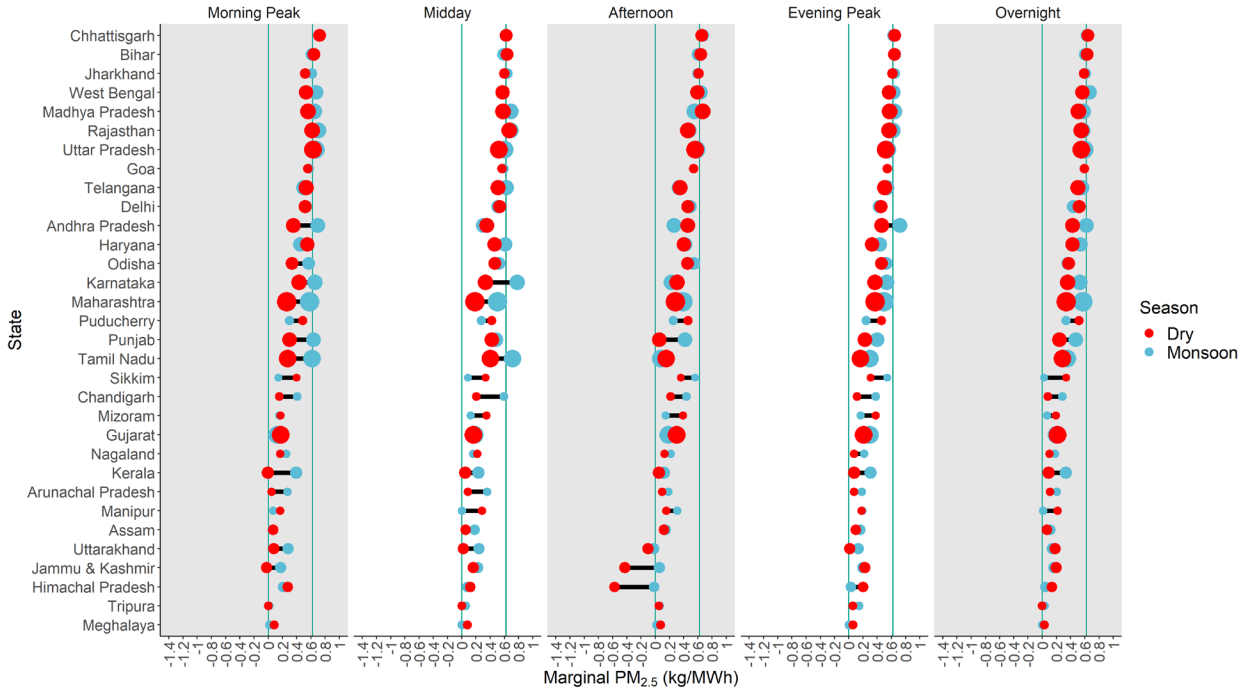

Figure 72
2017-2018 marginal $PM_{2.5}$ emission factors for dry and monsoon seasons. Panels separate the time-of-day in each season. Size of dots scale to annual electricity demand in each state. Vertical lines from left to right indicate generation-weighted $PM_{2.5}$ emission factors for gas and coal generators, respectively.

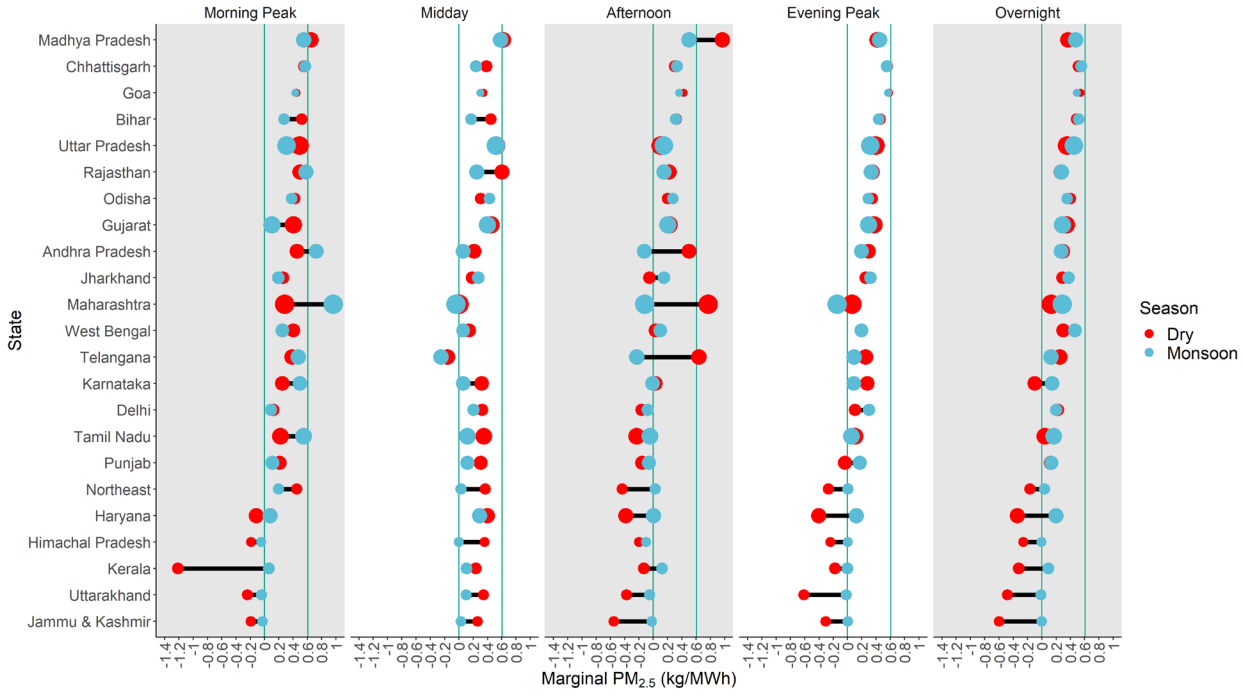

Figure 73
2030-2031 marginal $PM_{2.5}$ emission factors for dry and monsoon seasons. Panels separate the time-of-day in each season. Size of dots scale to annual electricity demand in each state. Vertical lines from left to right indicate generation-weighted $PM_{2.5}$ emission factors for gas and coal generators, respectively.

Table 7

	Morning Peak		Midday		Afternoon		Evening Peak		Overnight	
State	MEF CO_2 ± 2σ	r^2	MEF CO_2 ± 2σ	r^2	MEF CO_2 ± 2σ	r^2	MEF CO_2 ± 2σ	r^2	MEF CO_2 ± 2σ	r^2
Puducherry	1020 ± 11	0.99	1056 ± 10	0.99	1106 ± 10	0.99	1027 ± 10	0.99	1046 ± 11	0.99
Chhattisgarh	1049 ± 11	0.98	909 ± 12	0.96	946 ± 11	0.97	940 ± 5	0.99	936 ± 4	0.99
Rajasthan	988 ± 12	0.97	1019 ± 45	0.71	688 ± 36	0.63	876 ± 10	0.98	850 ± 5	0.99
Madhya Pradesh	892 ± 15	0.95	956 ± 27	0.86	1081 ± 29	0.87	841 ± 10	0.97	755 ± 8	0.95
Bihar	929 ± 9	0.98	925 ± 10	0.98	937 ± 6	0.99	927 ± 11	0.97	918 ± 8	0.97
West Bengal	770 ± 21	0.86	833 ± 6	0.99	863 ± 7	0.99	820 ± 13	0.95	826 ± 14	0.89
Jharkhand	752 ± 25	0.81	865 ± 18	0.92	888 ± 13	0.96	886 ± 17	0.93	852 ± 12	0.92
Goa	840 ± 14	0.95	855 ± 20	0.90	831 ± 11	0.96	835 ± 10	0.97	876 ± 4	0.99
Uttar Pradesh	910 ± 11	0.97	754 ± 25	0.81	819 ± 13	0.95	759 ± 14	0.94	799 ± 8	0.96
Telangana	977 ± 13	0.96	814 ± 50	0.56	502 ± 50	0.33	848 ± 16	0.93	801 ± 9	0.95
Karnataka	943 ± 31	0.82	584 ± 93	0.16	497 ± 99	0.11	753 ± 27	0.79	689 ± 30	0.56
Tamil Nadu	810 ± 29	0.79	813 ± 76	0.36	371 ± 72	0.11	521 ± 28	0.62	643 ± 13	0.85
Delhi	769 ± 9	0.97	810 ± 8	0.98	715 ± 11	0.95	702 ± 13	0.93	769 ± 5	0.98
Andhra Pradesh	756 ± 46	0.56	576 ± 37	0.54	870 ± 33	0.77	819 ± 15	0.93	785 ± 13	0.90
Haryana	937 ± 25	0.87	770 ± 23	0.85	680 ± 15	0.91	575 ± 16	0.86	700 ± 12	0.89
Maharashtra	672 ± 24	0.78	458 ± 21	0.70	594 ± 28	0.68	683 ± 23	0.81	634 ± 13	0.85
Odisha	486 ± 26	0.63	675 ± 16	0.89	663 ± 17	0.88	665 ± 31	0.69	542 ± 25	0.52
Nagaland	543 ± 37	0.51	659 ± 29	0.71	611 ± 32	0.64	561 ± 33	0.59	425 ± 11	0.78
Gujarat	592 ± 20	0.80	559 ± 24	0.73	653 ± 32	0.66	597 ± 16	0.87	559 ± 14	0.78
Punjab	432 ± 35	0.43	614 ± 23	0.78	80 ± 51	0.01	331 ± 29	0.39	352 ± 13	0.63
Mizoram	391 ± 25	0.54	540 ± 44	0.42	788 ± 89	0.28	636 ± 80	0.23	347 ± 17	0.51
Kerala	238 ± 89	0.03	167 ± 43	0.07	407 ± 41	0.32	457 ± 31	0.51	222 ± 19	0.24
Arunachal Pradesh	291 ± 24	0.41	462 ± 48	0.31	444 ± 26	0.58	517 ± 38	0.47	370 ± 22	0.40
Assam	346 ± 15	0.71	366 ± 27	0.46	567 ± 12	0.91	539 ± 20	0.77	382 ± 12	0.71
Manipur	526 ± 16	0.85	480 ± 23	0.68	575 ± 18	0.83	452 ± 70	0.17	437 ± 10	0.82
Sikkim	577 ± 24	0.74	486 ± 50	0.31	519 ± 56	0.29	448 ± 76	0.14	487 ± 13	0.76
Chandigarh	244 ± 39	0.16	302 ± 52	0.14	313 ± 49	0.16	193 ± 55	0.06	126 ± 16	0.14
Tripura	335 ± 4	0.96	328 ± 9	0.85	401 ± 9	0.91	378 ± 14	0.77	315 ± 5	0.92
Uttarakhand	222 ± 19	0.40	230 ± 14	0.57	-257 ± 44	0.14	97 ± 46	0.02	310 ± 22	0.32
Jammu & Kashmir	-22 ± 75	0.00	217 ± 60	0.06	-626 ± 90	0.19	348 ± 69	0.11	335 ± 29	0.24
Meghalaya	217 ± 27	0.24	211 ± 35	0.15	263 ± 42	0.16	393 ± 69	0.13	125 ± 18	0.10
Himachal Pradesh	394 ± 34	0.39	168 ± 41	0.08	-834 ± 102	0.24	290 ± 80	0.06	197 ± 26	0.12

2017-2018 dry season regression-based, marginal CO_2 emission factors with regression fit parameters for each Indian state.

Chhattisgarh	1050 ± 51	0.74	904 ± 21	0.93	966 ± 18	0.95	920 ± 10	0.98	920 ± 9	0.97
Rajasthan	1116 ± 32	0.89	1220 ± 58	0.75	748 ± 23	0.88	961 ± 10	0.98	891 ± 9	0.97
Madhya Pradesh	983 ± 31	0.87	1010 ± 25	0.91	800 ± 31	0.82	937 ± 7	0.99	861 ± 19	0.87
Bihar	896 ± 19	0.94	858 ± 84	0.42	876 ± 17	0.94	945 ± 19	0.94	867 ± 22	0.83
West Bengal	980 ± 23	0.92	834 ± 28	0.86	923 ± 9	0.99	917 ± 7	0.99	978 ± 15	0.94
Jharkhand	889 ± 80	0.45	929 ± 71	0.53	845 ± 26	0.88	932 ± 21	0.93	882 ± 33	0.71
Goa	856 ± 12	0.97	877 ± 15	0.96	833 ± 9	0.98	836 ± 9	0.98	875 ± 6	0.98
Uttar Pradesh	974 ± 13	0.97	870 ± 23	0.91	846 ± 8	0.99	817 ± 13	0.96	902 ± 16	0.91
Telangana	912 ± 18	0.94	938 ± 34	0.84	529 ± 53	0.40	856 ± 21	0.92	858 ± 15	0.92
Karnataka	1171 ± 56	0.75	1131 ± 113	0.40	473 ± 73	0.22	919 ± 12	0.98	867 ± 19	0.87
Tamil Nadu	1417 ± 109	0.53	1245 ± 106	0.48	460 ± 224	0.03	747 ± 37	0.73	827 ± 20	0.85
Delhi	870 ± 17	0.95	847 ± 21	0.92	810 ± 28	0.85	771 ± 16	0.94	776 ± 16	0.89
Andhra Pradesh	1018 ± 191	0.16	480 ± 49	0.39	443 ± 41	0.44	1067 ± 16	0.97	956 ± 18	0.90
Haryana	753 ± 39	0.71	916 ± 92	0.40	686 ± 23	0.86	734 ± 28	0.82	879 ± 37	0.66
Maharashtra	981 ± 63	0.62	803 ± 31	0.82	650 ± 38	0.67	826 ± 21	0.92	871 ± 12	0.94
Odisha	827 ± 43	0.72	761 ± 41	0.70	661 ± 35	0.71	730 ± 19	0.91	530 ± 48	0.29
Nagaland	685 ± 57	0.49	440 ± 11	0.92	643 ± 15	0.92	656 ± 12	0.96	469 ± 18	0.69
Gujarat	486 ± 34	0.58	605 ± 31	0.72	422 ± 31	0.55	637 ± 20	0.87	568 ± 21	0.71
Punjab	955 ± 53	0.68	735 ± 35	0.75	629 ± 52	0.50	633 ± 43	0.59	725 ± 20	0.82
Mizoram	474 ± 22	0.76	408 ± 28	0.59	619 ± 15	0.92	621 ± 17	0.90	226 ± 13	0.52
Kerala	888 ± 40	0.77	757 ± 54	0.57	463 ± 28	0.64	694 ± 20	0.89	707 ± 21	0.80
Arunachal Pradesh	540 ± 38	0.58	718 ± 49	0.59	584 ± 12	0.94	616 ± 12	0.95	415 ± 41	0.26
Assam	399 ± 46	0.34	575 ± 49	0.48	586 ± 19	0.86	581 ± 28	0.75	523 ± 36	0.42
Manipur	370 ± 14	0.83	266 ± 13	0.73	666 ± 22	0.86	609 ± 25	0.80	238 ± 12	0.56
Sikkim	204 ± 29	0.25	126 ± 34	0.09	818 ± 20	0.92	799 ± 23	0.89	35 ± 13	0.02
Chandigarh	617 ± 61	0.41	883 ± 109	0.31	646 ± 41	0.62	591 ± 40	0.60	481 ± 31	0.45
Tripura	400 ± 16	0.81	453 ± 27	0.65	421 ± 8	0.94	493 ± 14	0.90	412 ± 12	0.79
Uttarakhand	483 ± 35	0.56	396 ± 48	0.32	24 ± 46	0.00	295 ± 37	0.30	269 ± 33	0.19
Jammu & Kashmir	274 ± 47	0.19	371 ± 59	0.21	54 ± 38	0.01	316 ± 29	0.44	272 ± 23	0.31
Meghalaya	70 ± 18	0.09	34 ± 18	0.02	95 ± 24	0.09	28 ± 17	0.02	27 ± 18	0.01
Himachal Pradesh	301 ± 34	0.35	114 ± 34	0.08	-25 ± 17	0.02	44 ± 19	0.03	61 ± 15	0.05

Table 8

	Morning Peak		Midday		Afternoon		Evening Peak		Overnight	
State	MEF CO_2 ± 2σ	r^2	MEF CO_2 ± 2σ	r^2	MEF CO_2 ± 2σ	r^2	MEF CO_2 ± 2σ	r^2	MEF CO_2 ± 2σ	r^2
Madhya Pradesh	945 ± 23	0.89	905 ± 63	0.49	1406 ± 106	0.46	602 ± 34	0.6	530 ± 32	0.39
Chhattisgarh	807 ± 55	0.50	555 ± 77	0.20	440 ± 53	0.25	804 ± 19	0.89	749 ± 22	0.73
Goa	648 ± 35	0.62	498 ± 53	0.29	618 ± 49	0.42	842 ± 12	0.96	790 ± 13	0.90
Rajasthan	799 ± 29	0.78	1009 ± 93	0.36	377 ± 105	0.06	575 ± 31	0.62	431 ± 19	0.54
Bihar	763 ± 63	0.41	647 ± 73	0.27	476 ± 24	0.65	672 ± 32	0.68	721 ± 24	0.68
Uttar Pradesh	731 ± 43	0.58	758 ± 59	0.44	165 ± 64	0.03	579 ± 25	0.71	527 ± 27	0.48
Odisha	610 ± 54	0.37	441 ± 79	0.13	290 ± 47	0.15	501 ± 37	0.46	578 ± 33	0.43

2017-2018 monsoon season regression-based, marginal CO_2 emission factors with regression fit parameters for each Indian state.

State	Morning Peak		Midday		Afternoon		Evening Peak		Overnight	
	MEF CO_2 ± 2σ	r^2	MEF CO_2 ± 2σ	r^2	MEF CO_2 ± 2σ	r^2	MEF CO_2 ± 2σ	r^2	MEF CO_2 ± 2σ	r^2
Gujarat	650 ± 103	0.14	714 ± 143	0.10	336 ± 125	0.03	577 ± 40	0.50	547 ± 56	0.18
Madhya Pradesh	794 ± 108	0.26	850 ± 84	0.40	750 ± 96	0.27	852 ± 39	0.69	887 ± 50	0.38
Andhra Pradesh	710 ± 77	0.29	296 ± 130	0.03	721 ± 130	0.12	471 ± 42	0.38	465 ± 27	0.41
Chhattisgarh	824 ± 164	0.14	345 ± 150	0.03	480 ± 69	0.24	797 ± 31	0.81	802 ± 49	0.46
Jharkhand	382 ± 110	0.05	271 ± 85	0.05	-58 ± 98	0.00	391 ± 92	0.08	443 ± 85	0.06
Goa	621 ± 64	0.38	432 ± 96	0.12	521 ± 66	0.29	821 ± 18	0.93	713 ± 18	0.84
Maharashtra	422 ± 134	0.05	0 ± 113	0.00	1124 ± 122	0.28	94 ± 87	0.01	200 ± 50	0.04
Rajasthan	928 ± 97	0.37	436 ± 101	0.11	273 ± 83	0.07	546 ± 36	0.6	454 ± 34	0.36
West Bengal	504 ± 97	0.15	206 ± 63	0.05	54 ± 38	0.01	294 ± 65	0.09	445 ± 47	0.17
Bihar	407 ± 89	0.12	299 ± 92	0.04	456 ± 37	0.90	638 ± 16	0.91	767 ± 22	0.80
Tamil Nadu	455 ± 95	0.10	645 ± 163	0.07	-451 ± 180	0.03	206 ± 65	0.04	91 ± 44	0.01
Telangana	566 ± 63	0.28	-229 ± 122	0.02	933 ± 138	0.18	378 ± 57	0.17	376 ± 36	0.21
Karnataka	360 ± 132	0.03	468 ± 112	0.08	46 ± 116	0.00	407 ± 41	0.32	-144 ± 80	0.01
Delhi	262 ± 66	0.07	502 ± 55	0.28	-271 ± 101	0.03	171 ± 82	0.02	392 ± 28	0.31
Punjab	306 ± 60	0.11	442 ± 64	0.18	-227 ± 101	0.02	-56 ± 53	0.01	181 ± 32	0.07
Northeast	849 ± 161	0.12	659 ± 91	0.20	-654 ± 115	0.13	-397 ± 219	0.02	-251 ± 87	0.02
Haryana	-132 ± 180	0.00	607 ± 89	0.18	-589 ± 128	0.09	-636 ± 113	0.13	-519 ± 86	0.08
Himachal Pradesh	-281 ± 73	0.06	530 ± 59	0.27	-293 ± 177	0.01	-358 ± 81	0.08	-380 ± 45	0.15
Uttarakhand	-332 ± 92	0.06	500 ± 51	0.31	-548 ± 177	0.04	-894 ± 169	0.12	-701 ± 94	0.12
Kerala	-2032 ± 283	0.20	364 ± 97	0.06	-177 ± 172	0.00	-296 ± 91	0.05	-536 ± 115	0.05
Jammu & Kashmir	-284 ± 207	0.01	378 ± 97	0.07	-820 ± 320	0.03	-449 ± 166	0.03	-873 ± 159	0.07

2030-2031 dry season regression-based, marginal CO_2 emission factors with regression fit parameters for each Indian state.

Table 9

Uttar Pradesh	458 ± 77	0.19	760 ± 80	0.37	221 ± 71	0.06	475 ± 27	0.68	667 ± 34	0.56
Odisha	547 ± 95	0.18	617 ± 140	0.11	395 ± 56	0.25	419 ± 33	0.51	518 ± 47	0.28
Gujarat	145 ± 145	0.01	630 ± 150	0.1	310 ± 135	0.03	457 ± 64	0.25	458 ± 49	0.23
Andhra Pradesh	1063 ± 188	0.17	83 ± 117	0.00	-179 ± 159	0.01	325 ± 45	0.25	408 ± 47	0.2
Jharkhand	289 ± 119	0.04	393 ± 109	0.08	226 ± 87	0.04	470 ± 36	0.53	559 ± 53	0.27
Maharashtra	1420 ± 231	0.20	-65 ± 171	0.00	-171 ± 173	0.01	-191 ± 79	0.04	418 ± 54	0.17
West Bengal	362 ± 71	0.15	86 ± 111	0.00	147 ± 41	0.08	287 ± 36	0.29	686 ± 56	0.33
Tamil Nadu	997 ± 162	0.20	222 ± 69	0.06	-108 ± 218	0.00	142 ± 47	0.06	266 ± 32	0.18
Telangana	676 ± 108	0.20	-344 ± 178	0.02	-339 ± 129	0.04	144 ± 52	0.05	179 ± 51	0.04
Karnataka	720 ± 125	0.18	87 ± 56	0.02	-14 ± 87	0.00	128 ± 24	0.15	209 ± 33	0.12
Delhi	154 ± 68	0.03	335 ± 66	0.14	-99 ± 105	0.01	442 ± 57	0.28	317 ± 48	0.13
Punjab	165 ± 104	0.02	177 ± 76	0.03	-88 ± 91	0.01	248 ± 40	0.20	194 ± 33	0.10
Northeast	348 ± 206	0.02	52 ± 196	0.00	83 ± 91	0.01	97 ± 33	0.05	97 ± 42	0.02
Haryana	140 ± 153	0.01	448 ± 102	0.11	-5 ± 125	0.00	194 ± 45	0.11	322 ± 61	0.08
Himachal Pradesh	-71 ± 68	0.01	-6 ± 73	0.00	-150 ± 89	0.02	2 ± 3	0.00	-8 ± 11	0.00
Uttarakhand	-65 ± 136	0.00	147 ± 65	0.03	-74 ± 137	0.00	-26 ± 63	0.00	-20 ± 66	0.00
Kerala	76 ± 178	0.00	183 ± 93	0.02	213 ± 102	0.03	-2 ± 27	0.00	137 ± 28	0.07
Jammu & Kashmir	-43 ± 61	0.00	41 ± 50	0.00	-35 ± 103	0.00	0 ± 1	0.00	-1 ± 6	0.00

2030-2031 monsoon season regression-based, marginal CO_2 emission factors with regression fit parameters for each Indian state.

Table 10

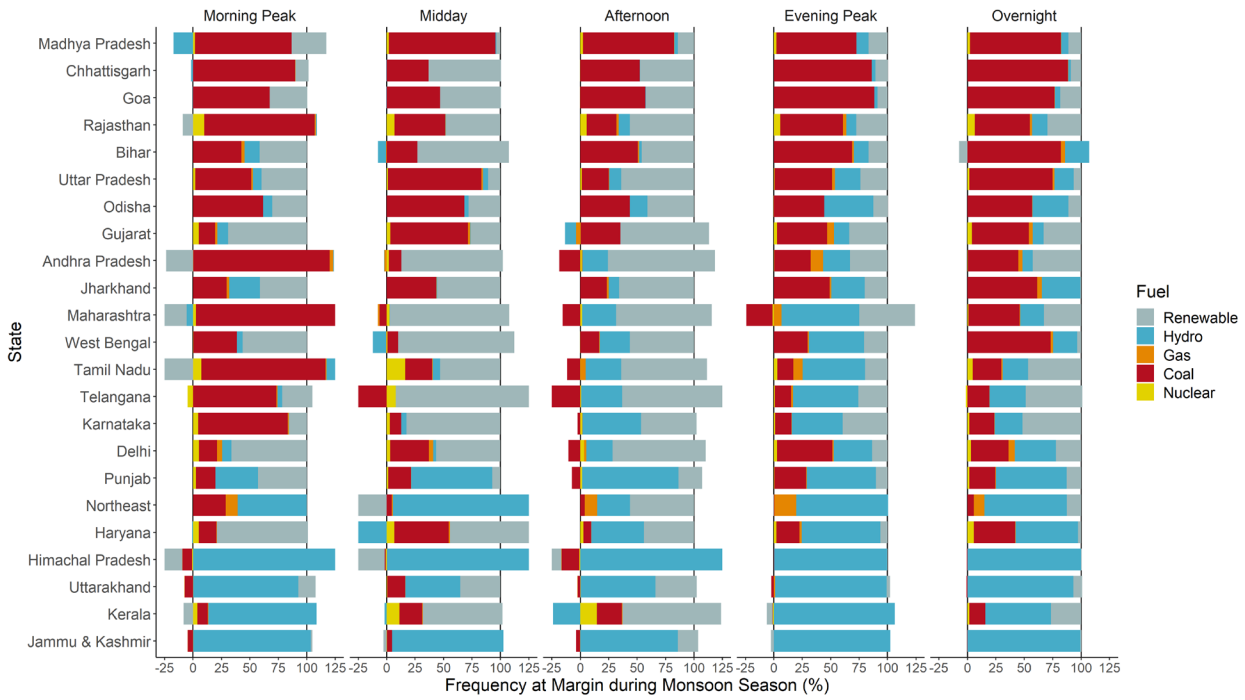

Figure 74
2030-2031 regression-based, marginal fuel frequency for each Indian state during monsoon season. Negative percentages in each period indicate fuel source generation decreases with increases in marginal power demand in each state, requiring increase in generation from other fuels to meet demand. The sum of each bar is 100%.

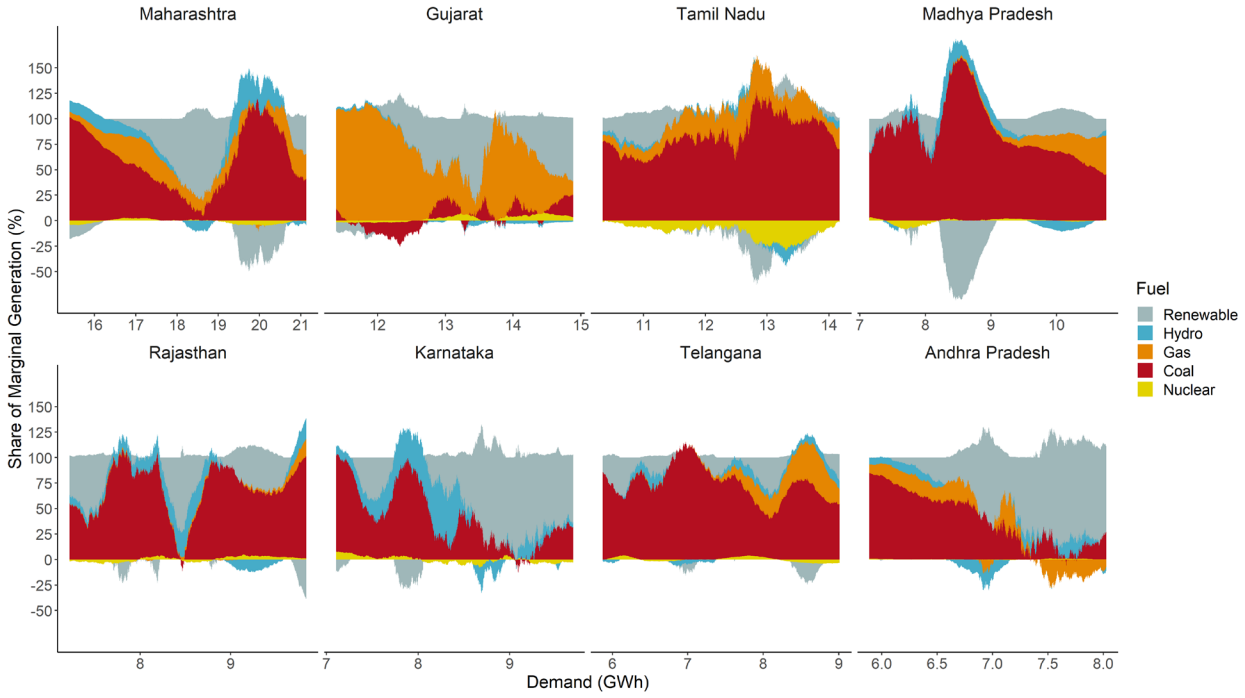

Figure 75
2017-2018 dry season marginal fuel shares as functions of demand in eight high variable renewable energy (solar, wind) states.

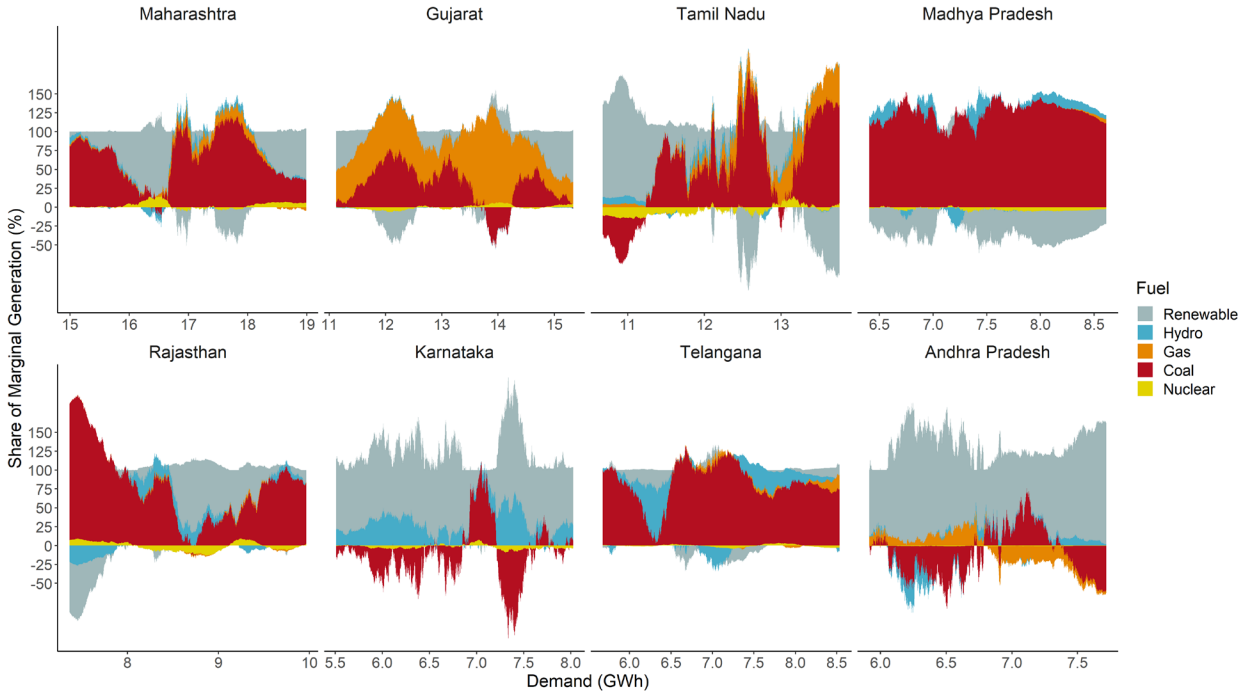

Figure 76
2017-2018 monsoon season marginal fuel shares as functions of demand in eight high variable renewable energy (solar, wind) states.

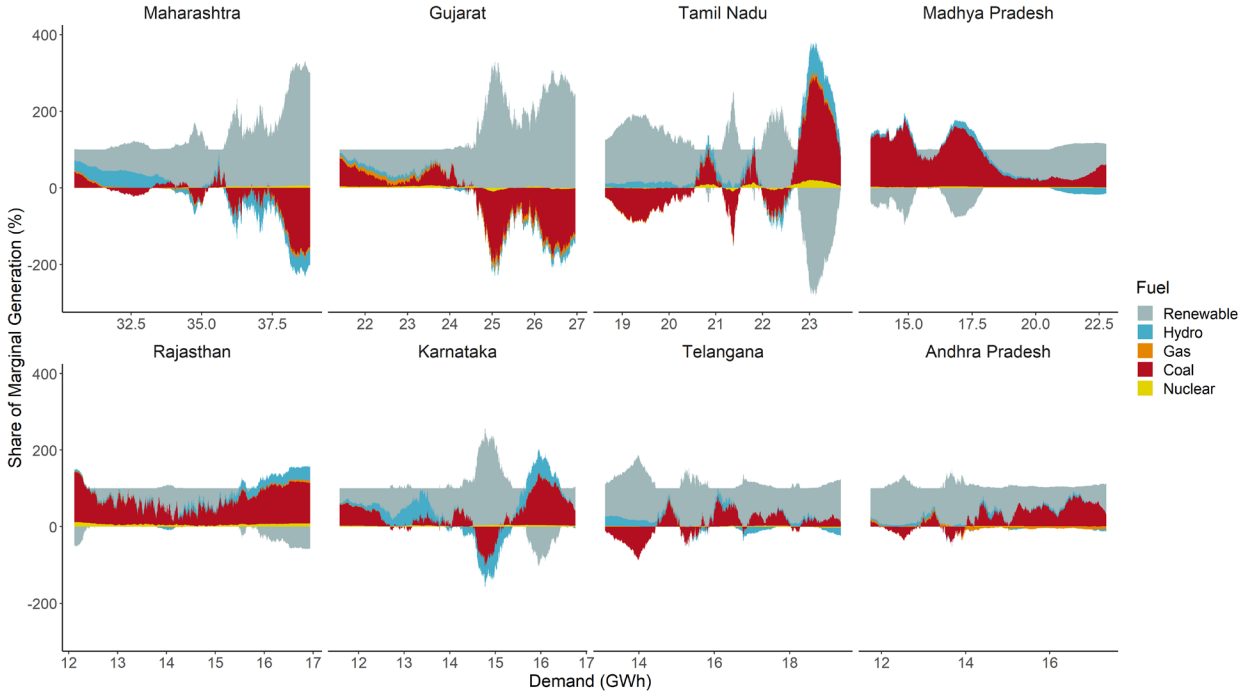

Figure 77
2030-2031 dry season marginal fuel shares as functions of demand in eight high variable renewable energy (solar, wind) states.

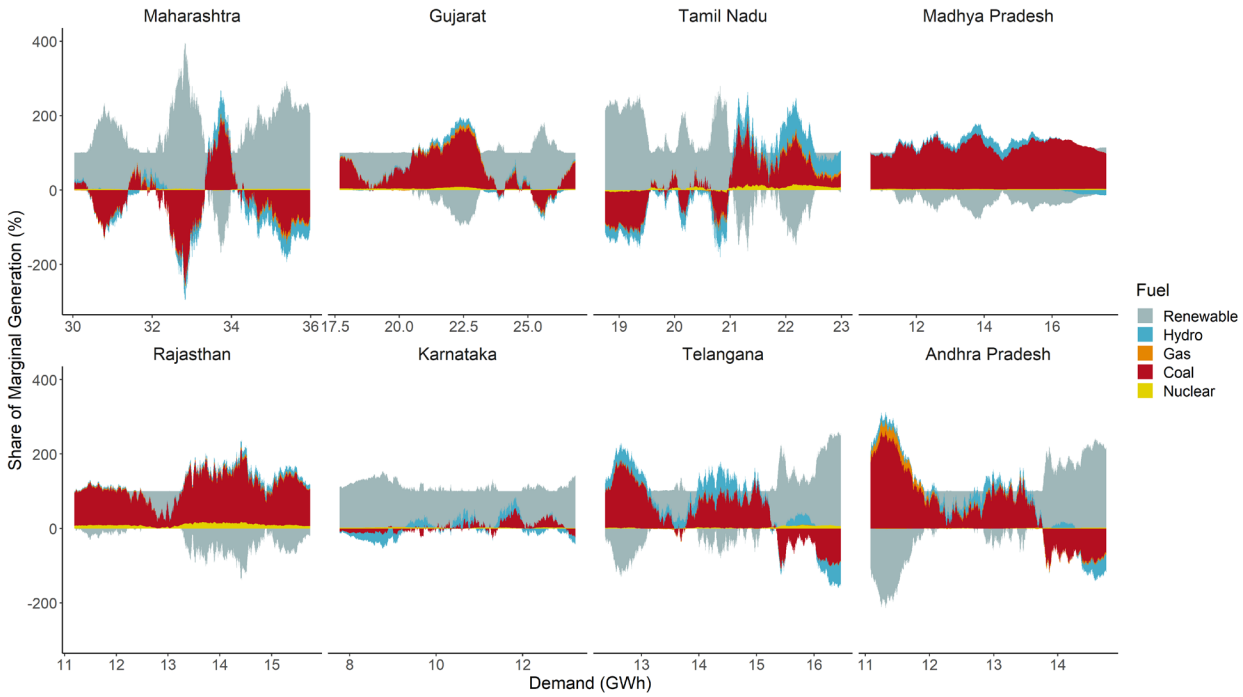

Figure 78
2030-2031 monsoon season marginal fuel shares as functions of demand in eight high variable renewable energy (solar, wind) states.

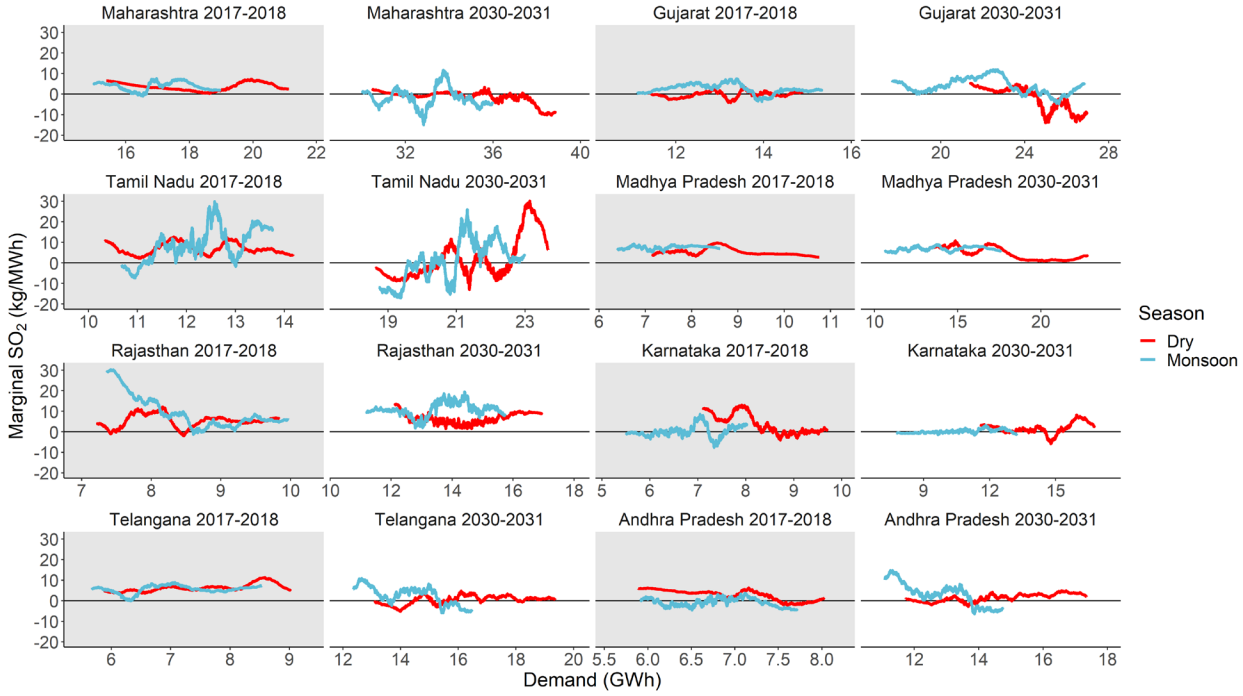

Figure 79
2017-2018 and 2030-2031 dry and monsoon season marginal SO_2 emission factors as a function of demand in eight high variable renewable energy (solar, wind) states.

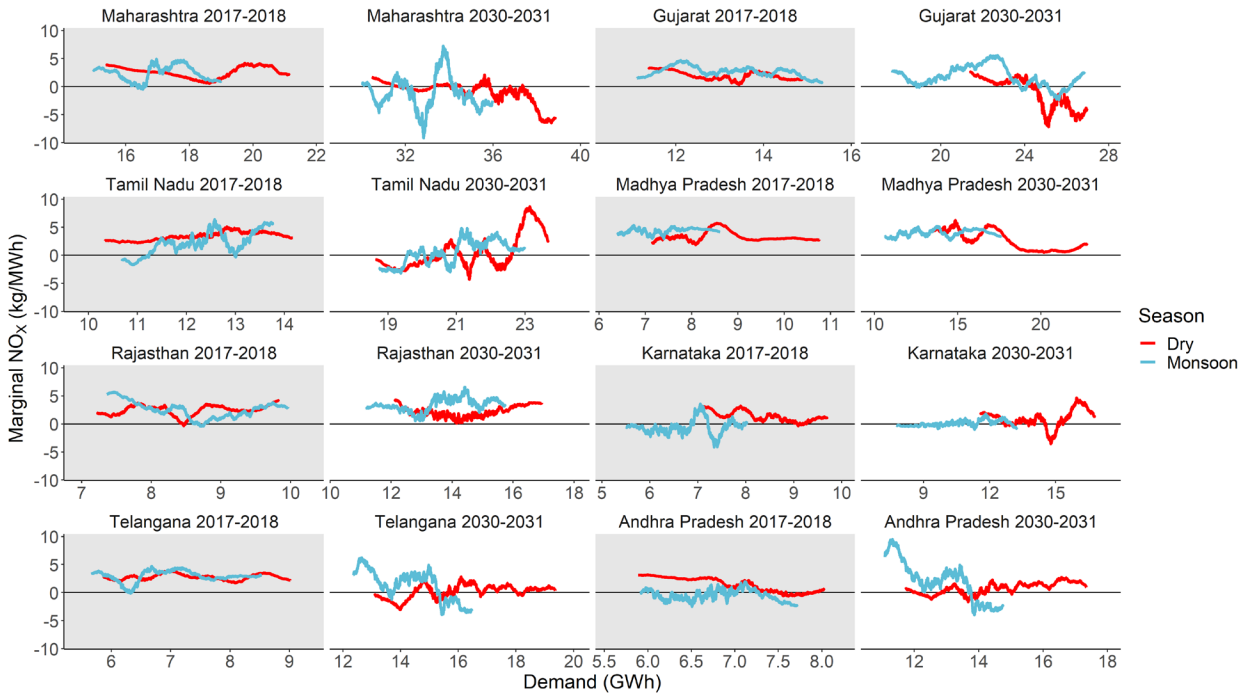

Figure 80
2017-2018 and 2030-2031 dry and monsoon season marginal NO_X emission factors as a function of demand in eight high variable renewable energy (solar, wind) states.

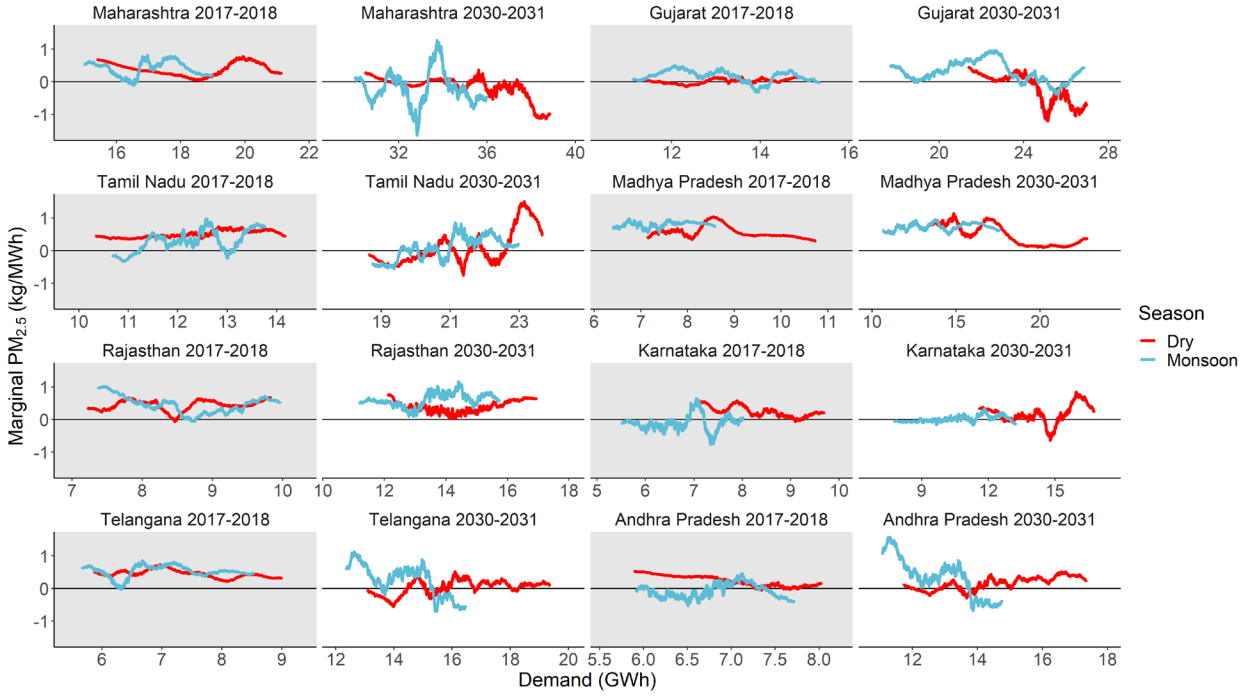

Figure 81
Figure S17. 2017-2018 and 2030-2031 dry and monsoon season marginal $PM_{2.5}$ emission factors as a function of demand in eight high variable renewable energy (solar, wind) states.

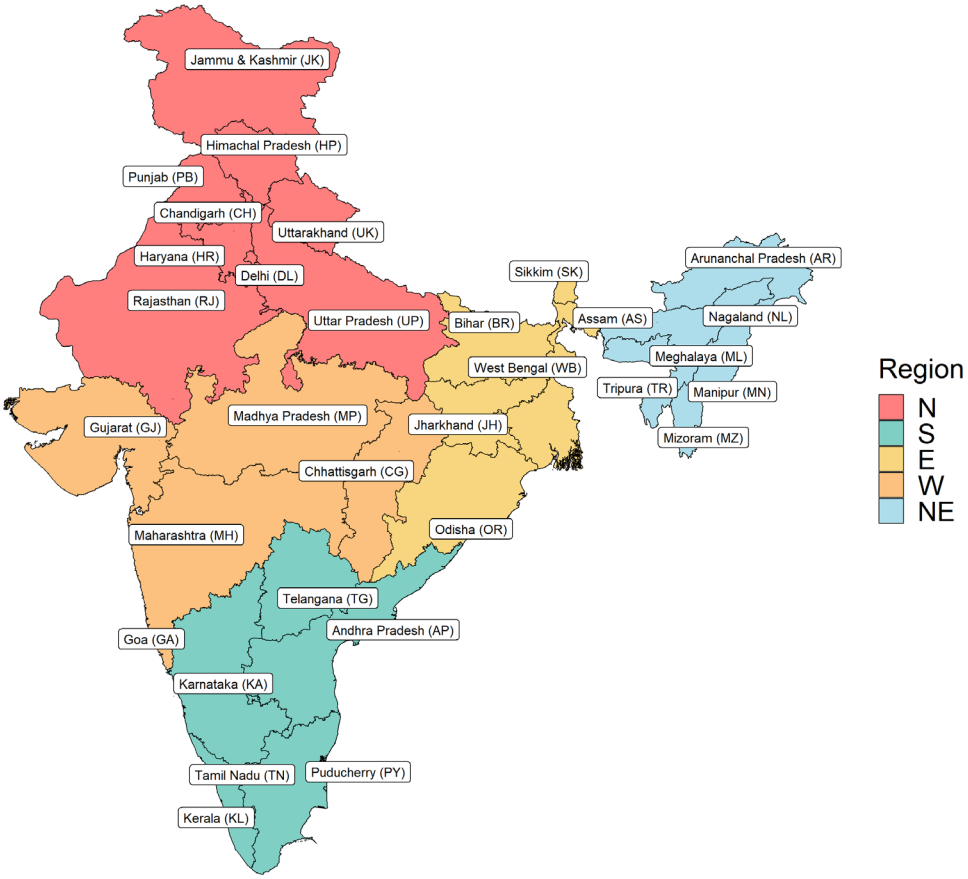

Figure 82
Map of India with states and state abbreviations.